ฟลูออเรสเซนต์โพรบสำหรับดีกลูโคสและเบต้ากลูโคซิเดส ที่มีพื้นฐานเป็นแอนทราควิโนนอิมิดาโซลฟลูออโรฟอร์

นายกฤติธี วรรณจักร

วิทยานิพนธ์นี้เป็นส่วนหนึ่งของการศึกษาตามหลักสูตรปริญญาวิทยาศาสตรมหาบัณฑิต
สาขาวิชาเคมี ภาควิชาเคมี
คณะวิทยาศาสตร์ จุฬาลงกรณ์มหาวิทยาลัย
ปีการศึกษา 2553

FLUORESCENCE PROBE FOR D-GLUCOSE AND β-GLUCOSIDASE BASED ON ANTHRAQUINONE IMIDAZOLE FLUOROPHORES

Mr. Krittithi Wannajuk

A Thesis Submitted in Partial Fulfillment of the Requirements
for the Degree of Master of Science Program in Chemistry
Department of Chemistry
Faculty of Science
Chulalongkorn University
Academic Year 2010

Thesis Title	FLUORESCENCE PROBE FOR D-GLUCOSE AND β-GLUCOSIDASE BASED ON ANTHRAQUINONE IMIDAZOLE FLUOROPHORES
By	Mr. Krittithi Wannajuk
Field of Study	Chemistry
Thesis Advisor	Assistant Professor Boosayarat Tomapatanaget, Ph.D.

Accepted by the Faculty of Science, Chulalongkorn University in Partial Fulfillment of the Requirements for the Master's Degree

……Dean of the Faculty of Science
(Professor Supot Hannongbua, Dr.rer.nat.)

THESIS COMMITTEE

…….. Chairman
(Assistant Professor Warinthorn Chavasiri, Ph.D.)

……..……. Thesis Advisor
(Assistant Professor Boosayarat Tomapatanaget, Ph.D.)

…….. Examiner
(Professor Thawatchai Tuntulani, Ph.D.)

…….. Examiner
(Sumrit Wacharasindhu, Ph.D.)

…….. External Examiner
(Chomchai Suksai, Ph.D.)

กฤติธี วรรณจักร : ฟลูออเรสเซนต์โพรบสำหรับดีกลูโคสและเบต้ากลูโคซิเดส ที่มีพื้นฐานเป็นแอนทราควิโนนอิมิดาโซลฟลูออโรฟอร์. (FLUORESCENCE PROBE FOR D-GLUCOSE AND β-GLUCOSIDASE BASED ON ANTHRAQUINONE IMIDAZOLE FLUOROPHORES) อ. ที่ปรึกษาวิทยานิพนธ์หลัก: ผศ.ดร.บุษยรัตน์ ธรรมพัฒนกิจ, 177 หน้า.

ได้สังเคราะห์เซ็นเซอร์ที่เป็นอนุพันธ์ของแอนทราควิโนนอิมิดาโซลและกรดโบโรนิก หรือ หมู่ไกลโคไซด์ อันดับแรกได้นำอนุพันธ์ของแอนทราควิโนนและกรดโบโรนิก (OB และ PB) มาศึกษาสมบัติในการเป็นเซ็นเซอร์ในการตรวจวัดน้ำตาลกลูโคสในระบบการตรวจวัดด้วยเอนไซม์ ในระบบนี้ได้ใช้เอนไซม์กลูโคสออกซิเดสซึ่งทำงานโดยเกิดปฏิกิริยากับกลูโคสและออกซิเจนให้ผลิตภัณฑ์ คือ กรดกลูโคอิกและไฮโดรเจนเปอร์ออกไซด์ โดยไฮโดรเจนเปอร์ออกไซด์สามารถเกิดปฏิกิริยากับกรดโบโลนิกในเซ็นเซอร์แล้วเปลี่ยนเป็นหมู่ไฮดรอกซิลในโมเลกุล OB ซึ่งจะทำให้สัญญาณฟลูออเรสเซนต์ลดลง ข้อดีของเซ็นเซอร์ที่ใช้ในกระบวนการนี้คือความจำเพาะเจาะจงกับน้ำตาลกลูโคสเท่านั้น และได้ทำการศึกษากลไกการเกิดปฏิกิริยาของเอนไซม์นี้กับ OB โดยคำนวณหาค่าคงที่มิชาเอลิสเมมเทน ได้เท่ากับ 0.174 มิลลิโมลาร์ ซึ่งแสดงว่า OB สามารถเกิดปฏิริยาได้ดีกับเอนไซท์กลูโคส ออกซิเดส และได้คำนวณขีดจำกัดต่ำสุดในการตรวจวัดน้ำตาลในช่วงความเข้มข้นเท่ากับ 0.08-0.42 มิลลิโมลาร์ ได้ขีดจำกัดต่ำสุดเท่ากับ 0.0114 มิลลิโมลาร์ นอกจากนี้ได้นำอนุพันธ์ของแอนทราควิโนนและหมู่ไกลโคไซด์ (OAG และ PAG) ที่มีแอนทราควิโนนเป็นหน่วยให้สัญญาณและหมู่ไกลโคไซด์เป็นหน่วยที่เกิดปฏิกิริยากับเอนไซม์กลูโคซิเดส มาใช้ในการตรวจวัดเอนไซม์เบต้ากลูโคซิเดสโดยเทคนิคฟลูออเรสเซนต์ โดยจะเกิดการลดลงของสัญญาณฟลูออเรสเซนต์ของ PAG เมื่อเติมเอนไซม์เบต้ากลูโคซิเดสลงไปโดยจะเกิดการหลุดของเบต้ากลูโคสที่ติดอยู่ในเซ็นเซอร์ PAG และได้นำ PAG ไปพัฒนาในการตรวจวัดโดยการนำไปใช้ในระบบ ไมเซลล์โดยใช้ CTAB เพื่อช่วยให้สัญญาณฟลูออเรสเซนต์สูงขึ้นและลดสัญญาณรบกวนที่มาจากเบต้ากลูโคซิเดส นอกจากนี้ได้นำ PAG มาประยุกต์ใช้ในการตรวจวัดเอนไซม์ในระบบของอนุภาคนาโนของเซอร์แฟคแทนต์/แลนทาไนด์ จากผลการทดลองพบว่า สามารถเพิ่มสัญญาณของ PAG ได้ในระบบอนุภาคนาโนและมีการเปลี่ยนแปลงของสัญญาณได้มากเมื่อมีการเติมเอนไซม์ลงไปในระบบ จากผลทดลองนี้เป็นการพัฒนาระบบฟลูออเรสเซนต์ ให้มีความว่องไวสูงในการตรวจวัดเอนไซม์เบต้ากลูโคซิเดส ซึ่งมีการใช้เป็นตัวรายงานเกี่ยวกับเอนไซม์กันอย่างแพร่หลาย

ภาควิชา……..…เคมี……ลายมือชื่อนิสิต.....

สาขาวิชา…….เคมี……ลายมือชื่ออ.ที่ปรึกษาวิทยานิพนธ์หลัก.....

ปีการศึกษา……2553……..

5172210823 : MAJOR CHEMISTRY
KEYWORDS : ENZYMATIC PROBE / FLUOROGENIC COMPOUND / D-GLUCOSE / BETA-GLUCOSIDASE / LANTHANIDE NANOPARTICLES

KRITTITHI WANNAJUK: FLUORESCENCE PROBE FOR D-GLUCOSE AND *β*-GLUCOSIDASE BASED ON ANTHRAQUINONE IMIDAZOLE FLUOROPHORES. ADVISOR: ASST. PROF. BOOSAYARAT TOMAPATANAGET, Ph.D., 177 pp.

The anthaquinone derivatives containing boronic acid or glycoside as an active site were synthesized and characterized by spectroscopy. We have developed the boronic anthaquinone based sensors (**OB** and **PB**) for glucose sensing by the enzymatic probe system with glucose oxidase. Actually, the glucose oxidase can react with glucose and oxygen to generate the gluconic acid and hydrogen peroxide. In consistent with our hypothesis, the generated H_2O_2 can convert the boronic moiety of sensors to be hydroxyl group resulting in the fluorescence quenching of sensor **OB**. The advantage of this sensor is that it can detect glucose specifically. The kinetic of this process measured by Michaelis-Menten constant (K_m) provided the K_m values of 0.174 mM, indicating that **OB** exhibits a higher affinity for glucose oxidase. The limit of detection (LOD) of glucose for **OB** evaluated in the range of 0.08-0.42 mM of glucose by the spectrofluorometry was 0.0114 mM.

Moreover, the glycoside anthaquinone based sensors (**OAG** and **PAG**) bearing the anthraquinone as a sensory unit and glucoside as a active site were synthesized to detect *β*-glucosidase. After adding *β*-glucosidase, the fluorescence decreases of **PAG** were observed due to the cleavage of *O*-glucoside. The results showed that **PAG** can be a sensor for determining *β*-glucosidase in enzymatic probe system with the observation of fluorescence change. To improve the sensitivity of **PAG** for *β*-glucosidase sensing, we have applied **PAG** in the micellar system using CTAB as surfactant for enzymatic probe. This micellar system could reduce background signal from *β*-glucosidase and enhance the emission signal of **PAG**. Therefore, **PAG** in the micellar system can serve as a high potential for the *β*-glucosidase sensing. Finally, we tried to apply **PAG** in surfactant/lanthanide nanoparticles. The results also exhibited the enhancement of emission band of **PAG** in lanthanide nanoparticles and after adding *β*-glucosidase, the fluorescence intensity of **PAG** was significantly quenched. All approaches are exemplified by their application to develop a novel and highly sensitive fluorescence probe for *β*-glucosidase, which is widely used as the reporter of enzymes.

Department : Chemistry Student's Signature .....

Field of Study : Chemistry Advisor's Signature .....

Academic Year : 2010

ACKNOWLEDGMENTS

I wish to express my deepest appreciation to my adnisor Asst. Prof. Dr. Boosayarat Tomapatanaget for their guidance, kindnesses, suggestions and supports throughout my master career. In addition, I wish to thank Asst. Prof. Dr. Warinthorn Chavasiri, Prof. Dr. Thawatchai Tuntulani, Dr. Sumrit Wacharasindhu and Dr. Chomchai Suksai for their valuable comments and suggestions as thesis committee and thesis examiner.

I would like to acknowledge the financial support for my study from National Center of Excellence for Petroleum, Petrochemical, and Advanced Materials (NCE-PPAM) and Fund of Faculty of Science (RES-A1B1-24). I gratefully acknowledge the Thailand Research Fund, Commission on Higher Education and Chulalongkorn University (RMU5380003 and RTA5300083) and THE 90th ANNIVERSARY OF CHULALONGKORN UNIVERSITY FUND (Ratchadaphiseksomphot Endowment Fund) for research support. In addition, this accomplishment could not occur without the support from Chulalongkorn University. Special thanks are due to Dr. Matinee Jamkratoke, Miss Sornkrit Marbumrung and all members of Supramolecular Chemistry Research Unit at Department of Chemistry, Chulalongkorn Unitversity for their kindnesses, encouragement and supports.

Finally, I would like to express my deepest gratitude to my parent and my sisters, for their love, care, kindness, encouragement and other supports throughout my life.

CONTENTS

Page

CHAPTER III EXPERIMENTAL

Page

Page

Page

Page

Page

Page

LIST OF TABLES

page

LIST OF FIGURES

page

page

page

page

page

page

page

page

page

page

page

LIST OF SCHEMES

page

LIST OF ABBREVATIONS

eq	Equation
^{1}H-NMR	Proton nuclear magnetic resonance
^{13}C-NMR	Carbon nuclear magnetic resonance
Hz	Hertz
J	Coupling constant
s, d, t, m	Splitting patterns of ^{1}H-NMR (singlet, doublet, triplet, multiplet)
δ	Chemical shift
m/z	Mass per charge ratio
L	Litre
M	Molar
µ	Micro
β	Beta
n	Nano
ppm	Part per million
m	Minute
h	Hour
SEM	Scanning electron microscopy
TEM	Transmission electron microscopy
V	Volt
Φ_{fl}	Fluorescence quantum yield
CTAB	Cetyltrimethylammonium bromide
SDS	Sodium dodecyl sulfate
TX-100	Triton X-100
^{o}C	Degree Celsius

CHAPTER I

INTRODUCTION

1.1 Fluorescence spectroscopy techniques

Fluorescence spectroscopy, one of the most informative and sensitive analytical techniques, has played and continues to play key roles in modern research. Indeed, unraveling the inner workings of biomolecules, cells and organisms relied on the development of fluorescence-based tools. As many of the players in these sophisticated interactions and exceedingly complex systems are not inherently emissive, researchers have relied on synthesizing fluorescent analogs of the building blocks found in biological macromolecules. These are the constituents of the cell surface and cell membrane, as well as proteins and nucleic acids.

Any spectroscopy-based technique is associated with inherent sensitivity traits and time-scale features, which are dependent on the fundamental nature of the transitions involved. Optical excitation of a chromophore generates the Franck-Condon state extremely rapidly (within 10^{-15} s). The efficiency of this process is related to the chromophore's absorption cross-section (σ), which is proportional to its extinction coefficient (ε). Vibrational relaxation (within 10^{-12}-10^{-10} s) quickly populates the lowest vibronic state of the chromophore's excited state (**Figure 1.1**) [1]. This relaxation process, generating the emissive state, accounts for the lower emission energy of a chromophore compared with its excitation energy (Stokes shift). Typical organic chromophores reside in their excited state for a period of (0.5-20) × 10^{-9} s. The excited state lifetime reflects the sum of the various radiative and nonradiative processes that the excited chromophore undergoes in decaying back to the ground state (τ_0). The fraction responsible for emitting a photon, or the fluorescence lifetime (τ), reflects the emission quantum yield of the chromophores ($Q = \Phi = \tau/\tau_0$). In some studies, the brightness ($\varepsilon\Phi$) of a fluorophore is reported, which is the product of the molar absorptivity (ε) and the fluorescence quantum yield (Φ). This becomes useful when comparing the utility of two fluorophores with similar fluorescence quantum yields but very different molar absorptivities.

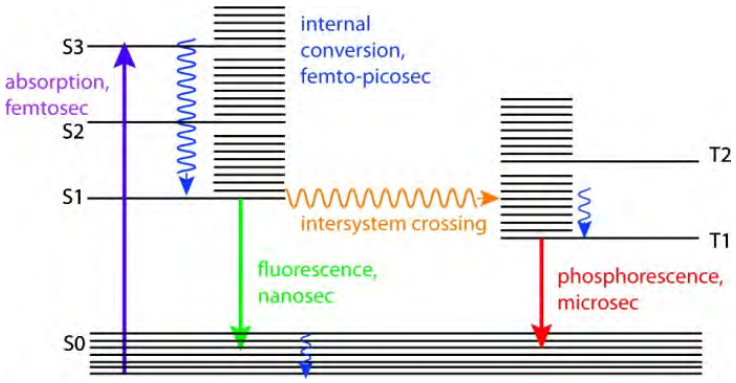

Figure 1.1 Jablonski diagram and a time scale of photophysical processes for organic molecules

Fluorescence based techniques are commonly appreciated for their versatility and sensitivity (up to a 1000-fold higher than absorption spectrophotometry). Creative probe design can provide chromophores with appropriate excitation and emission wavelengths, while minimizing interference by other emissive cellular constituents. Selective excitation coupled to the sensitivity of many chromophores to various environmental parameters (pH, polarity, viscosity, presence of quenchers, etc.) makes molecular fluorescence an extremely effective tool for in *vitro* biophysical and biochemical analyses, as well as in *vivo* cellular imaging, capable of providing spatial and temporal information [1-3].

1.2 Photophysics of fluorescent sensors

1.2.1 Photoinduced electron transfer (PeT)

In the simplest cases, emission of a photon, fluorescence, follows HOMO to LUMO excitation of an electron in a molecule. Where this emission is efficient, the molecule may be termed a fluorophore. Vibrational deactivation of the excited state prior to emission usually gives rise to a “Stokes shift” in that the wavelength of the emitted radiation is less than that of the exciting radiation [4]. Various other interactions may also modify the emission process, and these are of considerable importance in regard to analytical applications of fluorescence.

Thus, when a lone pair electron is located in an orbital of the fluorophore itself or an adjacent molecule and the energy of this orbital lies between those of the HOMO and LUMO, efficient electron transfer of one electron of the pair to the hole in the HOMO created by light absorption may occur, followed by transfer of the initially excited electron to the lone pair orbital. Such PeT provides a mechanism for nonradiative deactivation of the excited state (**Figure 1.2**), leading to a decrease in emission intensity or “quenching” of the fluorescence [5-9].

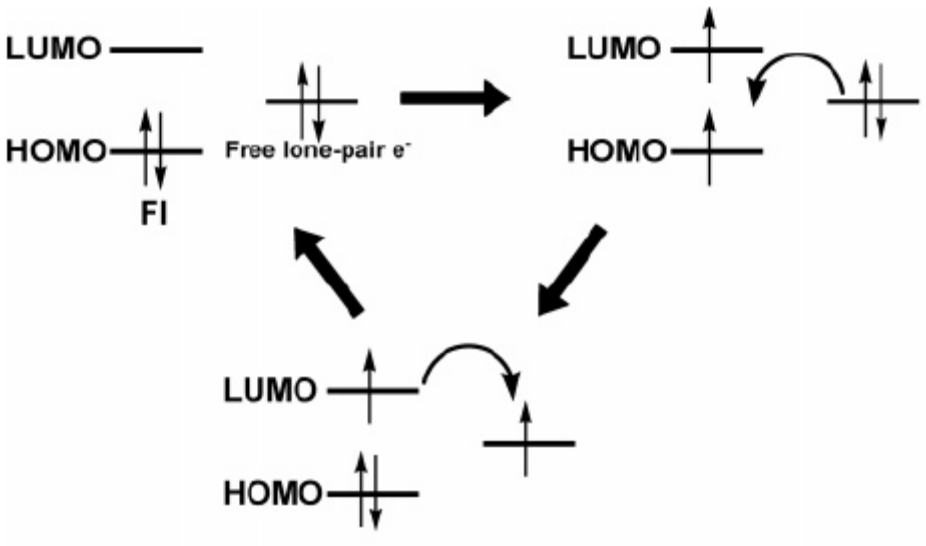

Figure 1.2 Mechanisms for PeT systems

1.2.2 Photoinduced Charge Transfer (PCT)

Electronic excitation necessarily involves some degree of charge transfer, but in fluorophores containing both electron-withdrawing and electron-donating substituents, this charge transfer may occur over long distances and be associated with major dipole moment changes, making the process particularly sensitive to the microenvironment of the fluorophore. Thus, it can be expected that cations or anions in close interaction with the donor or the acceptor moiety will change the photophysical properties of the fluorophore [10-12]. Upon, for example, cation complexation of an electron donor group within a fluorophore, the electron-donating character of the donor group will be reduced. The resulting reduction of conjugation causes a blue shift of the absorption spectrum together with a decrease of the molar absorptivity. In contrast, metal ion binding to the acceptor group enhances its electron-withdrawing character, and the absorption spectrum is thus red-shifted with an increase in molar absorptivity (**Figure 1.3**) [13]. The fluorescence spectra should be shifted in the same direction as the absorption spectra, and in addition to these shifts, changes in the quantum yields and lifetimes can be observed. All these photophysical effects are obviously dependent on the charge and the size of the cation, and therefore, some selectivity is expected [14]. [15-24]

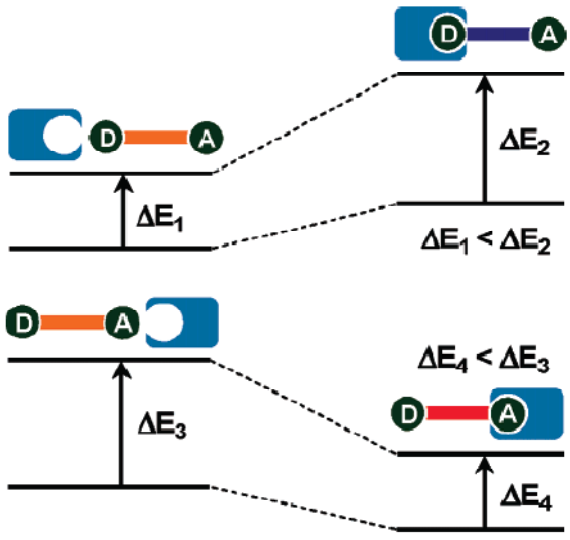

Figure 1.3 Mechanisms for PCT systems

1.3 Michaelis–Menten kinetics

The catalytic activity of enzymes has long been understood in terms of the Michaelis-Menten mechanism [15-22]: a substrate S binds reversibly with an enzyme E to form an enzyme-substrate complex ES that undergoes unimolecular decomposition to form a product P, regenerating the original enzyme E via E^0.

$$E + S \underset{k_{-1}}{\overset{k_1}{\rightleftarrows}} ES \overset{k_2}{\rightarrow} E^0 + P \quad : \quad E^0 \overset{\delta}{\rightarrow} E \qquad \textit{eq 1}$$

The rate of product formation V has a hyperbolic dependence on the substrate concentration [S], i.e., $v = k_2[E]_T[S]/([S] + K_m)$, where $K_m = (k_{-1} + k_2)/k_1$ and $[E]_T$ is the total enzyme concentration. This rate expression, the Michaelis-Menten equation, provides a highly satisfactory description of ensemble averaged enzyme kinetics. The Michaelis-Menten mechanism for the enzymatic conversion of substrate S to product P by enzyme E is described in *eq 1*. The rate equations for the concentrations of the chemical species in the first reaction are therefore given by

$$\frac{d[E]}{dt} = -k_1[E][S] + k_{-1}[ES] \qquad \textit{eq 2}$$

$$\frac{d[ES]}{dt} = k_1[E][S] - (k_{-1} + k_2)[ES] \qquad \textit{eq 3}$$

$$\frac{d[E^0]}{dt} = \frac{d[P]}{dt} = k_2[ES] \qquad \textit{eq 4}$$

Where *t* is the elapsed time from the onset of an ensemble averaged experiment. The initial conditions are [ES] = 0 and $[E^0] = 0$ at *t* = 0. At early times, when very little substrate has been converted to product, the second reaction in *eq 1* can be neglected. Because both [E] and [S] are time dependent, *eq 2-4* are nonlinear differential equations and cannot be solved exactly. However, an approximate solution for v = d[P]/dt can be obtained if the concentration of the complex, [ES], is assumed to reach a steady state shortly after the onset of the reaction. This steady-state

approximation corresponds to the condition d[ES]/dt = 0, and its application to *eq 2-4* is easily shown to lead to the classic Michaelis-Menten equation [23-24].

$$v = \frac{v_{max}[S]}{[S] + K_m} \qquad eq\ 5$$

Where V_{max}, defined as $V_{max} = k_2[E]T$, with $[E]T = [E] + [ES]$ the total enzyme concentration, is the reaction velocity at saturating substrate concentration, and K_m, the Michaelis-Menten constant, defined as $K_m = (k_{-1} + k_2)/k_1$, is the substrate concentration at which the enzymatic velocity is half of V_{max} (**Figure 1.4**).

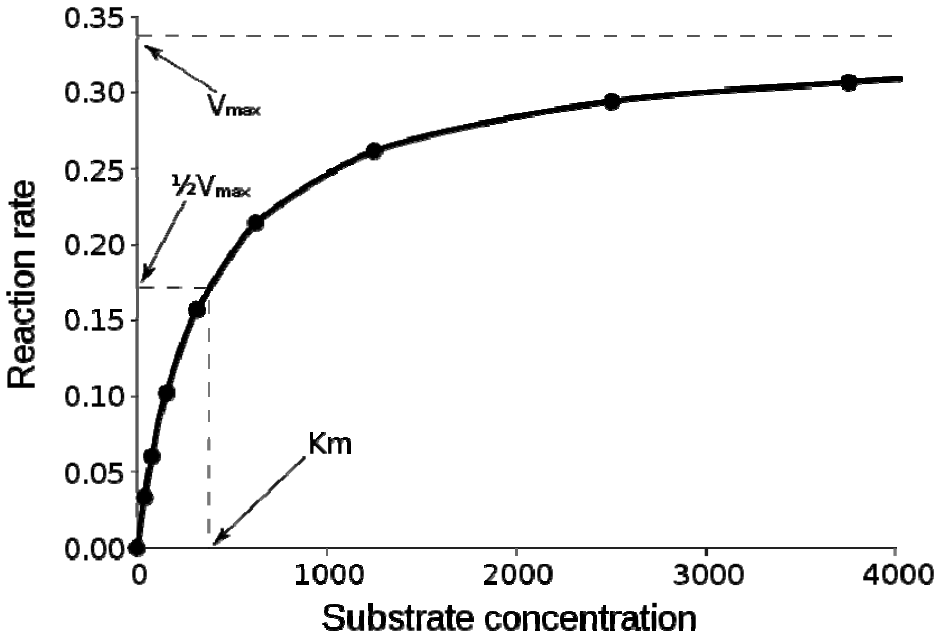

Figure 1.4 Saturation curve for an enzyme showing the relation between the concentration of substrate and rate.

1.4 Lanthanide Luminescence

The intricate optical properties of the trivalent lanthanide ions, hereafter Ln^{III}, are fascinating and originate in the special features of the electronic $[Xe]4f^n$ configurations (n = 0-14). These configurations generate a rich variety of electronic levels, the number of which is given by [14!/n!(14 - n)!], translating into 3003 for Eu(III) and Tb(III)[25]. They are characterized by three quantum numbers, S, L and J, within the frame of Russel-Saunders spin-orbit coupling scheme. The energies of these levels are well-defined due to the shielding of the 4f orbitals by the filled $5s^25p^6$ subshells, and they are a little sensitive to the chemical environments in which the lanthanide ions are inserted. As a corollary, inner-shell 4f-4f transitions which span both the visible and near-infrared (NIR) ranges are sharp and easily recognizable (**Figure 1.5**). In addition, because these transitions are formally parity forbidden, the lifetimes of the excited states are long, which allows the use of time-resolved detection, a definitive asset for bioassays [26-27], and luminescence microscopy [28].

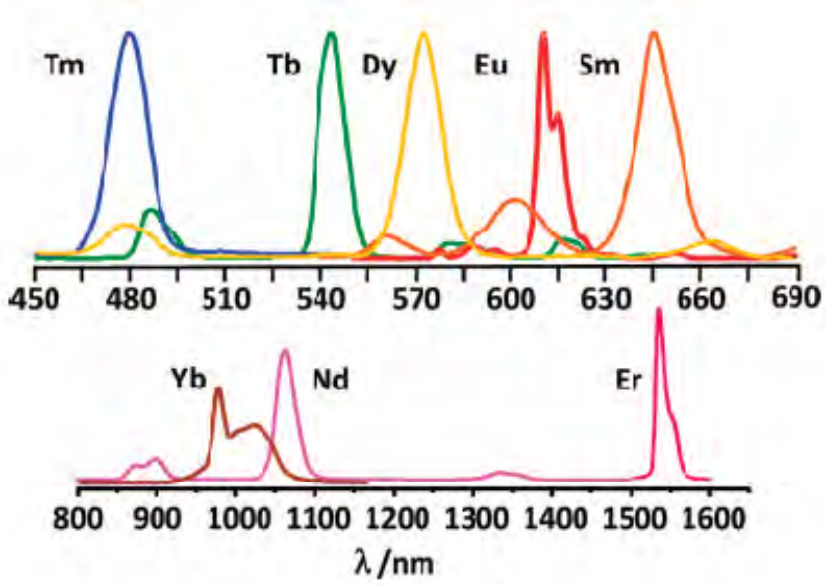

Firgure 1.5 Luminescence spectra of some lanthanide

The only drawback of f-f transitions, their faint oscillator strengths, may in fact be turned into advantages. Indeed, Weissman demonstrated in 1942 that excitation of lanthanide complexes into the ligand states results in metal-centered luminescence [29]. Part of the energy absorbed by the organic receptors is transferred onto Ln^{III} excited states and sharp emission bands originating from the metal ion are detected after rapid internal conversion to the emitting level. The phenomenon is termed sensitization of the metal-centered luminescence (also referred to as antenna effect) and is quite complex. Several energy migration paths may be involved, e.g., exchange or superexchange (Dexter), dipole-dipole, or dipole-multipole (Förster) mechanisms,[30] which entail the participation of several ligand levels, singlet, triplet, and/or intraligand charge transfer (ILCT) states. A commonly observed energy migration path though goes through the long-lived triplet states of the ligand(s) [31]. Alternatively, other states may funnel energy onto the metal ion such as intracomplex ligand-to-metal (LMCT) charge transfer states [32], $4f^5d$ states [33], or metal-to-ligand (^{1}MLCT, ^{3}MLCT) charge transfer states from chromophores containing dtransition metal ions [34] such as Cr^{III} [35], Re^{I} [36], Ru^{II} [37-38], Os^{II} [39-40], Co^{III} [41], Ir^{III} [42], or Pt^{II} [43-45]. These d-ions are essentially used for the sensitization of NIR luminescence [46]. The sensitization process generates two advantages. First, while Ln^{III} ions display a negligible Stokes' shift upon direct excitation, owing to the inner nature of the 4f-orbitals, ligand excitation results in pseudo Stokes' shifts which are often far larger than those of organic fluorophores, henceforth allowing easy spectral discrimination of the emitted light. Second, Ln^{III} ions are usually good quenchers of triplet states so that photobleaching is substantially reduced.

1.5 Enzymatic Biosensors

1.5.1 Definition of biosensors

Unfortunately, the terminology on biosensors is not systematic. Medical doctors tend to refer to “biosensors” as solid-phase-based diagnostic devices such as those for glucose, pregnancy markers, or cardiac markers. They are better referred to as test strips. Others (mainly bioorganic chemists) often refer to molecular bioprobes as biosensors. However, true biosensors are solid state, not certain molecules, give a reading after having been contacted with the sample to be analyzed, and do not require the addition of reagents. It is noted at this early stage of the review that the world still does not have a fully reversible glucose sensor for in vivo use over >1 months, which would be a great relief to the 4-5% of the population suffering from various forms of diabetes and that would enable the construction of an artificial pancreas. Definitions of biosensors have been given but are diverse [47-49]. However, all include the use of a biological component such as an enzyme, an antibody, a polynucleic acid, or even whole cells or tissue slices. In other words, a pH electrode capable of sensing the pH of blood is not a biosensor by all current definitions, as is xenon gas that can be used to probe the structure and dynamics of a protein [50]. Certain authors confuse the terms sensor and probe; we are referring such authors to the homepage of the world’s largest manufacturer of bioprobes, which never would refer to its many bioprobes as “sensors”.

1.5.2 General considerations

Determination of such analytes as glucose, lactate, urea, ethanol, phenols, pesticides, and many others is of high significance in clinical medicine, food and environmental analysis, and bioprocess monitoring. The lack of indicators that give changes in color or luminescence at room temperature without addition of (aggressive) reagents and at nearneutral pH, in reasonably short time and in a fully reversible way, has made researchers look for alternatives. Enzymes catalyze reactions with a high degree of specificity, and the products of these reactions (or of reactants consumed)

are detected directly if colored or luminescent, or by using optical transducers. The steady-state concentration of detectable species is, thus, related to the concentration of the analyte. Some enzymatic reactions require the presence of other specific reactants called coenzymes, e.g., nicotinamide adenine dinucleotide or flavine mononucleotide, which change their optical properties during the reaction.

A cross section of the typical enzymatic biosensor is shown in **Figure 1.6**. An indicator layer (often sensitive to oxygen or pH) is spread over a transparent inert support, usually a polyester film. An indicator dye is either directly dissolved in a polymer matrix or, alternatively, covalently immobilized or physically adsorbed on a surface of microbeads, which then are dispersed in the matrix polymer. The indicator layer is responsible for sensing of either cosubstrates consumed or of products produced during the enzymatic reaction. Enzyme(s) can be chemically immobilized onto the surface of a polymer membrane (e.g., cellulose, nylon, or inorganic porous glass) or physically entrapped into a polymer network, e.g., sol-gels, hydrogels, or Langmuir-Blodgett films. To avoid leaching of the enzyme, it is often cross-linked to bovine serum albumin via glutaraldehyde linkers. Alternatively, preactivated membranes may be used. When the analyte (the substrate) diffuses into the enzyme layer, it is converted into products. The indicator layer registers the formation of reaction products or the consumption of coreactants such as oxygen. In **Figure 1.6**, the sensor “sandwich” is mounted on the tip of an optical fiber that transmits excitation light from a light source to the sensor foil and emitted (reflected) light back to a photodetector. However, the majority of biosensors are not based on fiberoptics.

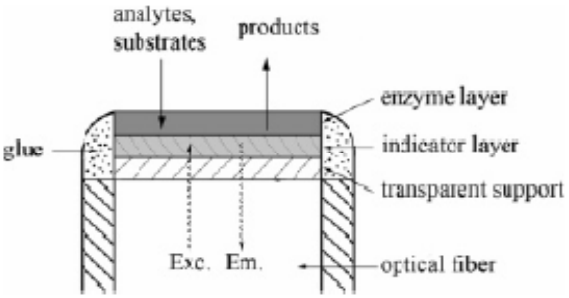

Figure 1.6 Cross section of a fiber-optic enzymatic biosensor. The analyte (substrate) enters the enzyme layer where it is converted into products. The indicator (sensing) layer consists of an indicator dye in a polymer layer and registers the formation of reaction products or the consumption of coreactants such as oxygen. The transparent support is inert and used only to facilitate manufacturing. It may as well be omitted. Exc and Em symbolize the paths of exciting and emitted light, respectively.

Optical sensors that exploit chemi- and bioluminescent reactions are usually simpler because no indicator layer is required. The chemical species generated during an enzymatic process are involved in subsequent reactions that result in the production of light. In this case, other substrates (reagents) are needed along with the sample solution. Most chemi- and bioluminescent reactions are catalyzed by enzymes that have to be co-immobilized in the enzyme layer. Biosensors that make use of the intrinsic optical properties of the enzyme do not require optical transducers and, thus, usually include an enzyme layer placed on a planar support or at the tip of an optical fiber, preferably in a hydrogel.

1.5.3 Enzymatic Glucose Biosensors

Not surprisingly, this is by far the most often investigated type of biosensor. Those based on the use of glucose oxidase (GOx) function on the basis of the following reactions:

$$D-glucose+O_2 \xrightarrow{GOx} D-gluconolatctone+H_2O_2 \quad (1)$$

$$D-gluconolatctone+H_2O_2 \longrightarrow D-gluconate+H^+ \quad (2)$$

The concentration of glucose thus can be related to the amount of oxygen consumed [51-69], the amount of hydrogen peroxide produced [70-85] or the decrease in pH due to the conversion of D-gluconolactone to D-gluconic acid [86-87].

The above equations indicate that the response of such a sensor depends on a number of variables (notwithstanding the effects of temperature and diffusion). The first is pH. If pH transduction is used, the initial pH and the buffer capacity of the sample will govern the shape and the relative signal change. pH also affects enzyme activity. The second is oxygen. Depending on how its concentration is related to that of glucose, different shapes of the response curve and different signal changes will be observed, as can be seen in **Figure 1.7**. If the sample is anaerobic (i.e., does not contain any oxygen), no signal change will be detectable. If oxygen is present in large excess, the concentration of oxygen is low, and diffusional processes are fast, hardly any signal changes will be detectable once the steady-state equilibrium is reached. It also needs to be reminded that the shapes are quite different for standing samples, stirred samples, and flowing samples. Finally, the quantity (more precisely, the activity) of immobilized GOx will strongly affect the signal change and the response time.

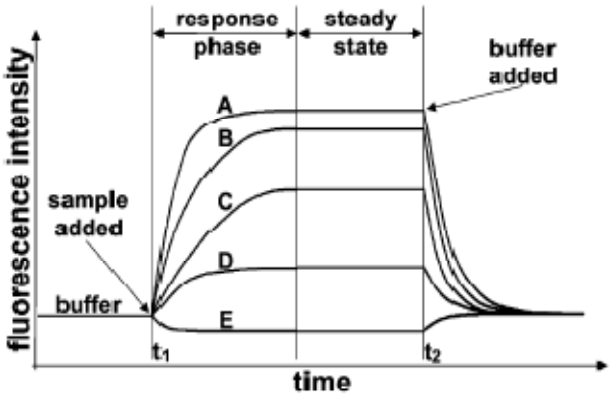

Figure 1.7 Typical signal shapes that can be obtained if a glucose sensor based on immobilized glucose oxidase and using an oxygen sensor as the transducer (in contact with air-saturated buffer) is exposed to flowing samples containing various levels of oxygen and glucose, respectively, and then again to air-saturated buffer. See the text for an explanation of shapes and signal changes.

This is shown in **Figure 1.7** for flowing samples. The sensor is first equilibrated with a buffer solution saturated with air. The flow of buffer is then replaced by a flowing sample at time t_1. At time t_2, the sample is replaced by a flow of buffer again. Various curves (A-E) are obtained depending on the levels of oxygen and glucose in the sample:

(A) No oxygen and no glucose in the sample; the shape of the response is mainly determined by the rate of the diffusion of oxygen out of the sensor membrane into the sample flow. The same signal level is reached (even faster) if the sample contains no oxygen but a relatively large concentration of glucose.

(B) Response to a sample where $[O_2] \ll$ [glucose]; all oxygen in the sensor is quickly consumed as a result of enzymatic oxidation and of diffusion.

(C) Air-saturated sample where $[O_2] >$ [glucose]; the shape is mainly determined by the rate of the enzyme-catalyzed oxidation of glucose.

(D) Sample where $[O_2] \gg$ [glucose]; the steady-state signal is smaller than that in (C).

(E) Sample without glucose where the O_2 is lower than at air saturation.

These are exemplary plots; the shapes and steady-state intensities also depend on the activity of the enzyme, the flow rates, and the thicknesses of the various layers (and, thus, on the oxygen storage capacity). Note that the shapes for flowing samples are quite different from those obtained with standing samples and that even these can differ depending on whether they are stirred or not.

Detection of glucose via the quantity of hydrogen peroxide formed appears to be the most attractive approach since it works at virtually zero background, even though it also is affected by the initial O_2 in the sample. Optical continuous sensors for H_2O_2 are scarce.

1.6 The catalytic enzyme, *β*-glucosidase

The catalytic enzyme, *β*-glucosidase (**Figure 1.8**) is a glucosidase enzyme that acts upon *β*1->4 bonds linking two glucose or glucose-substituted molecules (i.e., the disaccharide cellobiose). It is an exocellulase with specificity for a variety of *β*-glucosidase-D-glycoside substrates. It catalyzes the hydrolysis of terminal non-reducing residues in *β*-D-glucosides with release of glucose [88]. Cellulose is largely composed of polymers of beta-bond linked glucose molecules, and *β*-glucosidases are required by organisms (some fungi, bacteria, termites) that can consume it. These enzymes are a powerful tool for degradation of plant cell walls for pathogens. Lysozyme, an enzyme secreted in tears to prevent bacterial infection of the eye, is also a *β*-glucosidase that cleaves *β*1→4 bonds between N-acetylglucosamine and N-acetylmuramic acid sugars within the peptidoglycan cell walls of gram-negative bacteria.

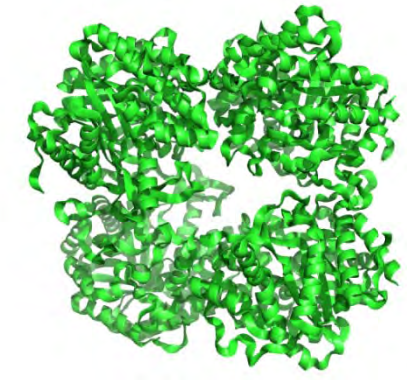

Figure 1.8 The structure of *β*-glucosidase from bacterium *Clostridium cellulovorans*.

CHAPTER II

LITERATURE REVIEWS

2.1 Literature reviews of enzymatic probe system

The development of site-specific reagents necessarily depends on the knowledge of specific biochemical reactions, which should include the chemical structure of catalysts, substrates, modifiers and products of enzymatic processes. A few is known about catalytic sites of most enzymes, therefore comparison of substrates with analogues may be one of the experimental approaches to study this problem. It also follows that the extensive information related to analytical enzymology (catalytic properties of isolated enzymes, enzymatic composition of cells) has to preceed the meaningful application of specific probes in complex systems. On the basis of pharmacokinetics, the complete in vivo targeting agent has not yet been developed. Macromolecular targeting moieties such as monoclonal antibodies are highly specific and can be delivered in high concentrations to the target, but have the undesirable feature of prolonged clearance of unbound molecules, leading to a high background signal. On the other hand, small molecules are rapidly cleared, thus improving the signals over background noise. Therefore, to combine the desirable features of both approaches, an antibody based targeting molecule is employed to achieve highly specific delivery with a signaling molecule that is only activated within the target cancer cells. This approach is contrast with enzymatically activated probes which are activated upon the reaction with target molecule.

Most small molecular probes have been developed for fluorescence spectrophotometry. Currently, the available fluorescent probes can be classified into two groups indicating autofluorescent protein (AFP) based probes and small organic molecule probes. Either probes bind or specifically react to sensors on the cell, leading to the marked changes in the optical properties such as the wavelength or the intensity of emitted light. Several photochemical mechanisms can be employed to achieve these results. One mechanism, fluorescence resonance energy transfer (FRET), is frequently used for AFP-based probes. For example, Miyawaki et al. [89] have demonstrated a

calcium ion sensitive AFP-based probes, comprised of two different AFPs bound by a linker and a calcium-binding moiety. Upon binding to a calcium ion, the orientation or the distance between two AFPs is altered, leading to a change in the efficiency of the resonance energy transfer. This is reflected in the relative ratio of two emission peaks, thus providing a direct readout of the concentration of calcium ion (**Figure 2.1**). This mechanism is quite suitable for AFP based probes, and a wide variety of probes with specific photochemical sensitivities have been developed.

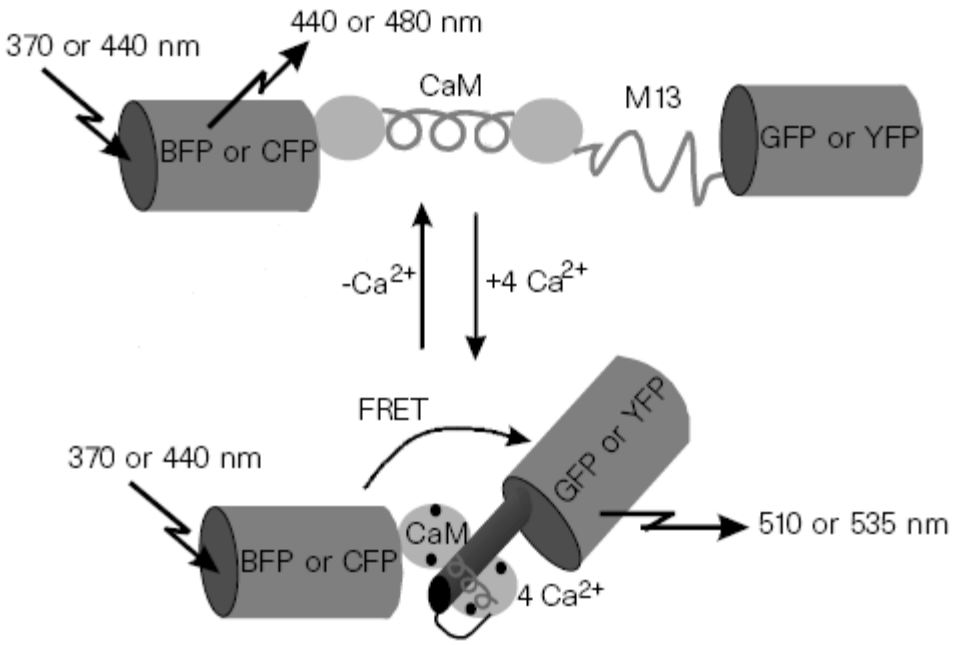

Figure 2.1 Scheme showing how FRET between green fluorescent proteins (GFPs) can measure Ca^{2+}. The GFPs are drawn as simple rigid cylinders, reflecting their crystal structures. Schematic structures of calmodulin (CaM) without Ca^{2+}, disordered unbound M13, and the Ca^{2+}-calmo-dulin-M13complex are derived from crystallography, NMR and modeling, but the relative orientations of the GFPs are unknown

For enzymatically fluorescent probes, the FRET mechanism can also be employed. However, because two fluorophores are necessary for this type of probe, the overall molecular size is relatively large, which sometimes impedes efficient cellular uptake of the probe. Therefore, other mechanisms are frequently used to develop small molecule fluorescent probes. A classic strategy is to develop small optical probes that alter their absorption spectra upon reaction with a target analyte.

Another strategy for developing activatable fluorescent probes is based on xanthenes fluorophores such as fluorescein and rhodamine. Boris et al. [90] have synthesized Diacetylated fluorescein (FDA) that has no color and no fluorescence due to its intramolecularlactone structure. Upon reaction with esterase, two acetyl groups are cleaved to release the fluorescein that has strong fluorescence. Thus, the activity of the target esterase can be monitored by exciting at 490 nm and monitoring for the emission light at 515 nm (**Figure 2.2**). Studies on the fluorochromatic activity of additional fluorescein derivatives gave further insight into the mechanism of the reaction. Increasing the chain length of the aliphatic acid moiety decreased the effectiveness of the ester as substrate in both intact cells and extracts. Almost the same strategy can be applied to the rhodamine based protease probe [91] (**Figure 2.3a**). Dipeptidylrhodamine ((Cbz-Arg-NH_2)-Rhodamine) has no color and no fluorescence, upon cleavage of two amide bonds by the target peptidase and generate highly fluorescent rhodamine (**Figure 2.3b**). However, a pitfall is that the increase in fluorescence is not directly proportional to enzymatic activity because the reactions require two-step cleavages to yield the highly fluorescent product.

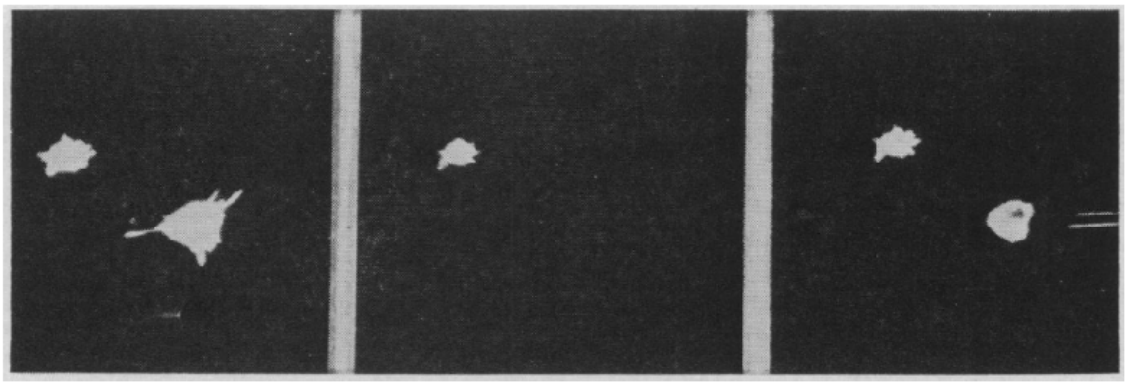

Figure 2.2 Release of intracellular fluorescein by cell damage with a micropipette. The left figure is a photomicrograph of two cells that have been allowed to hydrolyze FDA and thus have accumulated fluorescein. The two other photomicrographs were taken immediately after the cell on the right side was punctured with a micropipette. The difference between the middle and the right pictures is that for the latter the blue filter was removed from the exciting light.

a)

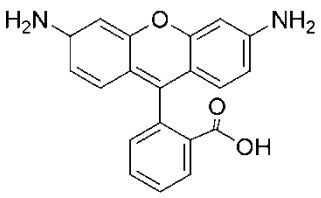

Rhodamine

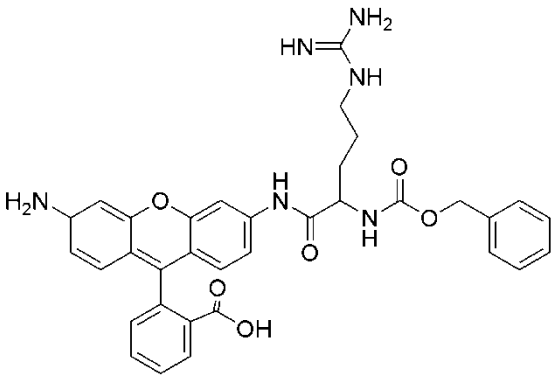

Cbz-Arg-NH-Rhodamine

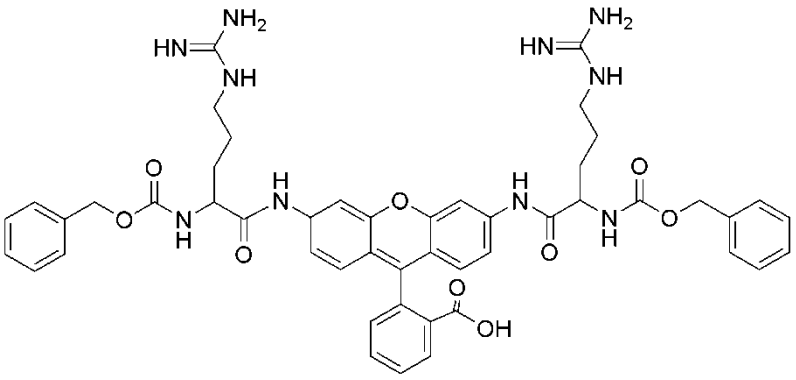

$(Cbz\text{-}Arg\text{-}NH)_2$-Rhodamine

b)

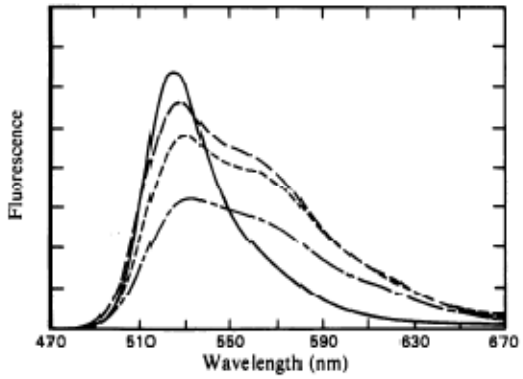

Figure 2.3 a) Fluorogenic substrates for serine proteineses b) Corrected fluorescence emission spectra for Rhodamine (1.36 μM), $(Cbz\text{-}Arg\text{-}NH)_2$-Rhodamine (0.10mM), synthetic Cbz-Arg-NH-Rhodamine(4.78 μM), and trypsin-produced Cbz-Arg-NH-Rhodamine (2.95 μM)

Next, a newly strategy utilizing intramolecular spirocyclization was interest and reported. Kenmoku et al. [92] have developed new tetramethylrhodamine (TMR) derivatives that show different dependences of their behavior upon the environment. X-ray crystallography demonstrates that specific rhodamine derivatives that bear a hydroxymethyl or a mercaptomethyl group instead of the original carboxy group show unique intramolecular spirocyclic structures. By regulating the spirocyclization and modulating the absorbance and fluorescence of the rhodamine derivatives before and after the reaction with target analytes, it was possible to develop a new activation strategy for fluorescent probes (**Figure 2.4a**). For instance, a novel fluorescent probe that specifically detects hypochlorous acid, an acid found in phagosomes, was successfully developed using this strategy. This sensor (**HySOx**) has no color and no fluorescence in aqueous solution at pH 7.4 due to a mercaptomethyl group that results in a spirocyclic structure. **HySOx** reacts with hypochlorous acid to yield a highly fluorescent rhodamine by the oxidation of sulfur. Indeed, the production of hypochlorous acid inside phagosomes of living neutrophils could be successfully monitored in real time using **HySOx** and was tolerant to autoxidation and photobleaching under bioimaging conditions (**Figure 2.4b**).

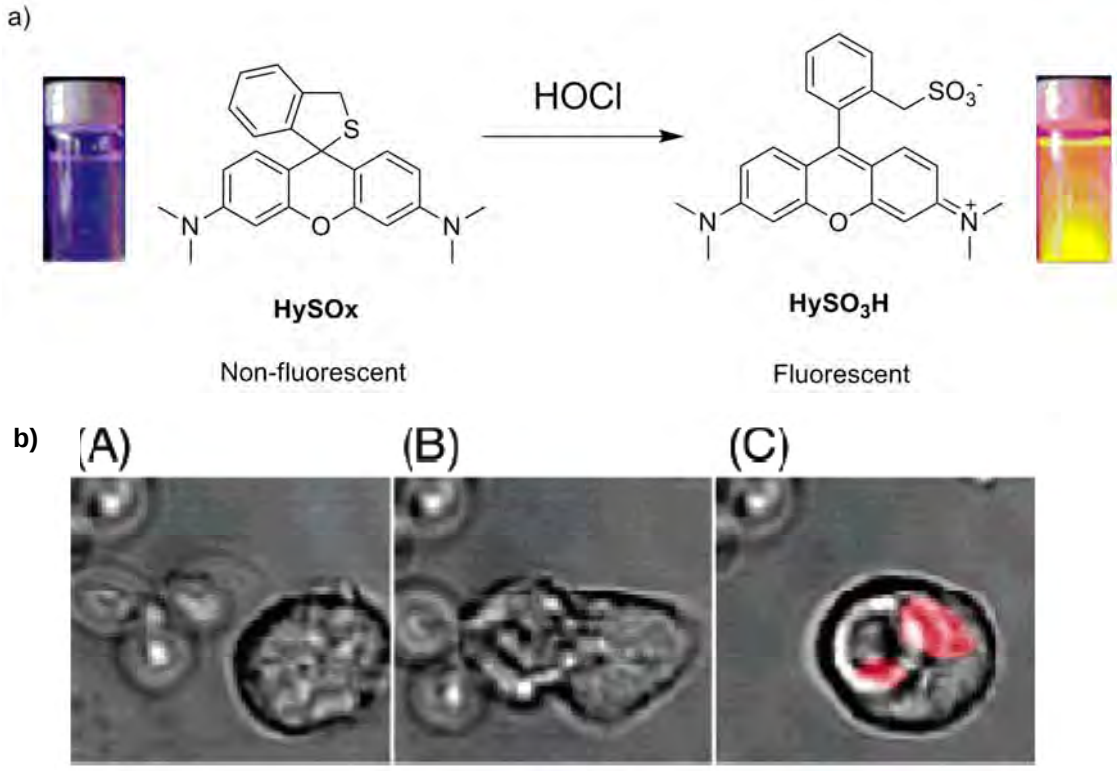

Figure 2.4 a) Scheme of **HySOx** activation reacted with hypochlorous acid. b) Fluorescence microscopy imaging of porcine neutrophil by confocal microscopy (A) Zymosan particles are near the neutrophil. (B) The neutrophil engulfs the zymosan. (C) Phagocytosis is complete.

In addition, more widely applicable mechanism for developing fluorescent probes is photoinduced electron transfer (PeT). PeT is a widely accepted mechanism for fluorescence quenching in which electron transfer from the electron donor moiety to the electron acceptor moiety of the fluorophore. Recently, Miura et al. [93] were reported that fluorescein could be considered to be part of a directly linked between benzoic acid moiety (electron donor) and xanthene moiety (electron acceptor) system. In other words, the intramolecular PeT could precisely control the fluorescence properties of fluorescein derivatives. However, PeT was not thought to be possible in long wavelength fluorophores, and indeed almost all the photochemical reports of PeT utilized UV-excitable fluorophores. They found that when the fluorescein structure was deconstructed into two parts, the benzoic acid moiety as the PeT donor and the xanthene ring as the fluorophore, only small alterations in absorbance were observed

among fluorescein and its derivatives. Moreover, the dihedral angle between the benzoic acid moiety and the xanthene ring is almost 90°, which suggests that there is little ground-state interaction between these two parts. They found that when the HOMO energy of the benzoic acid moiety was higher than a certain threshold, PeT occurred efficiently, resulting in little fluorescence. On the other hand, when the HOMO energy is lower than the threshold as is the case for generic fluorescein, the rate of PeT slows and the molecule becomes highly fluorescent. Further, this strategy has been used not only with fluorescein but also with a wide range of long wavelength excitable families of fluorophores.

Recently, Ueno et al. [94] found that the fluorescein molecule could be understood as a directly linked donor-acceptor system (**Figure 2.5a**). The two parts are conjugatively uncoupled since they are orthogonal to each other, and their fluorescence properties can be modulated by intramolecular photoinduced electron transfer (PeT) from the benzene moiety to the acceptor fluorophore (acceptor-excited PeT; a-PeT). These findings enabled us to design flexibly many kinds of functional fluorescence probes based on the change of the oxidation potential of the benzene moiety upon encountering a target molecule for singlet oxygen. In this way, establishment of a rational design strategy made it possible to develop novel fluorescence probes for target molecules with high efficiency. Moreover, a newlyprincipal for controlling the fluorescence properties of the fluorescein molecule based on electron transfer from the excited fluorophore to the benzene moiety (donor-excited PeT; d-PeT), the opposite direction to a-PeT has been reported (**Figure 2.5b**). In other words, when the LUMO energy of the benzoic acid moiety is lower than a certain threshold, the rate of d-PeT is quite fast, this derivative will be nonfluorescent. This finding also provides a basis for a new and practical strategy for the rational design of novel functional fluorescent probes.

a)

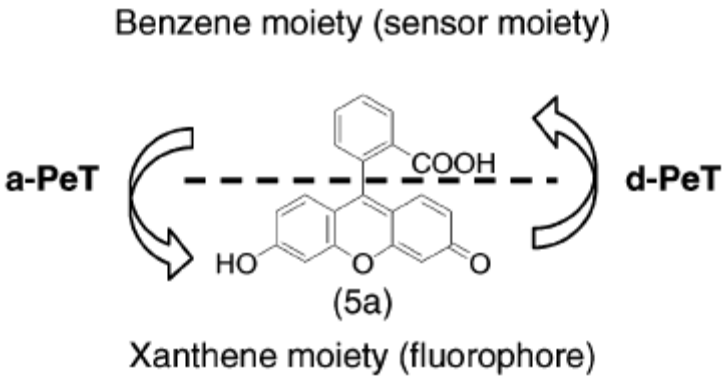

b)

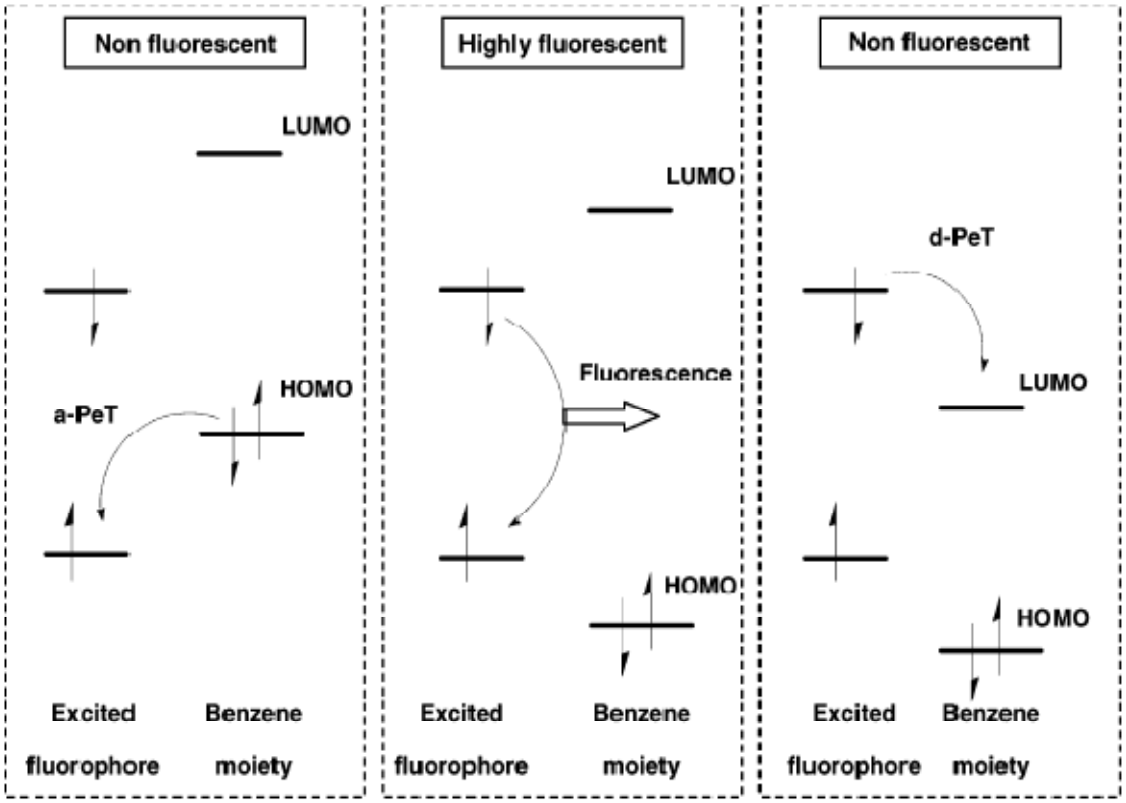

Figure 2.5 a) Fluorescein was divided into two parts, the benzene moiety and xanthene moiety. b) Schematic molecular orbital diagram of the fluorescence off/on switch including the PeT process.

Singlet oxygen ($^1O_2$), an excited state of molecular oxygen, has aroused much interest as a chemical and biological oxidant. The chemical reactivity of $^1O_2$ is well characterized since $^1O_2$ is useful for organic synthesis and has unique reactivity. Singlet oxygen is thought to be an important toxic species in vivo since it can oxidize

various kinds of biological molecules such as DNA, proteins, and lipids. To develop singlet oxygen sensitive fluorescent probes, Naoki [95] and Kumi [96] et al. have reported to design and synthesis fluorescent probes for singlet oxygen. The *endo*-addition of singlet oxygen to anthracene, was utilized which yields the corresponding thermostable *endo*-peroxide product that HOMO energy is much lower than that of the starting anthracene. Thus, the initial fluorescence of **DPAXs** and **DMAXs** was efficiently quenched by PeT that threshold level for the HOMO level of the benzoic acid moiety calculated with the PM3 method is around -8.9 eV, but was recovered by the reaction with singlet oxygen because the rate of PeT is quite slow due to the lowered HOMO energy of thermostable *endo*-peroxides (**Figure 2.6**). Further, the *endo*-addition reaction is specific for singlet oxygen, making these probes quite selective for sensing singlet oxygen in a variety of biological system.

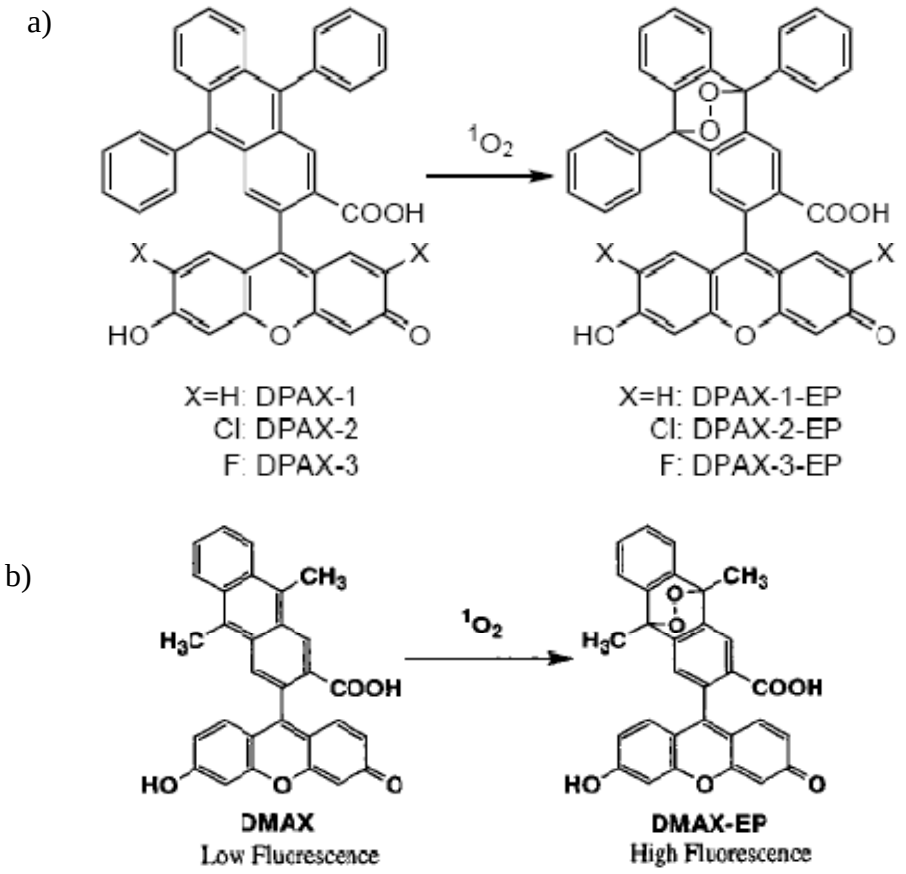

Figure 2.6 Reactions of a) **DPAXs** and b) **DMAX** with Singlet Oxygen

Nitric oxide (NO), which is synthesized through conversion of L-arginine to L-citrulline by NO synthase in vivo, is an important signaling molecule involved in the regulation of a wide range of physiological and pathophysiological mechanisms. Nagano et al. [97-100] have successfully developed nitric oxide sensitive fluorescent probes (**DAFs**, **DAMBOs**, **DARs** and **DACs**) by using the reaction of NO with phenylenediamines fluorophore to yield corresponding benzotriazoles fluorophore (**Figure 2.7**). The HOMO energy of phenylenediamines is extremely high due to the existence of two strong electron donating amino groups, which leads to efficient quench to fluorophores by PeT. The PeT mechanism is applicable to a wide range of fluorophores such as fluoresceins, rhodamines, BODIPYs, cyanines, and etc. On the other hand, because the HOMO energy of benzotriazoles is relatively low, the resulting products of these probes when bound to NO were highly fluorescent. Therefore, these probes work quite well as selective and sensitive fluorescent probes for NO. However, users of these probes must be cautious that these probes are not reactive with NO itself, but rather reactive with NO^+ or its equivalent species. NO is easily oxidized by a O_2 molecule to yield NO^+ or its equivalent species, so these compounds can be used as NO probes under aerobic conditions. However, if these probes are used under anaerobic conditions, no fluorescence increase will be observed whether in the presence of NO or not. Moreover, the nitric oxide sensitive fluorescent probes were applied to pratical bioimaging fluorescent probe of NO produced in cell.

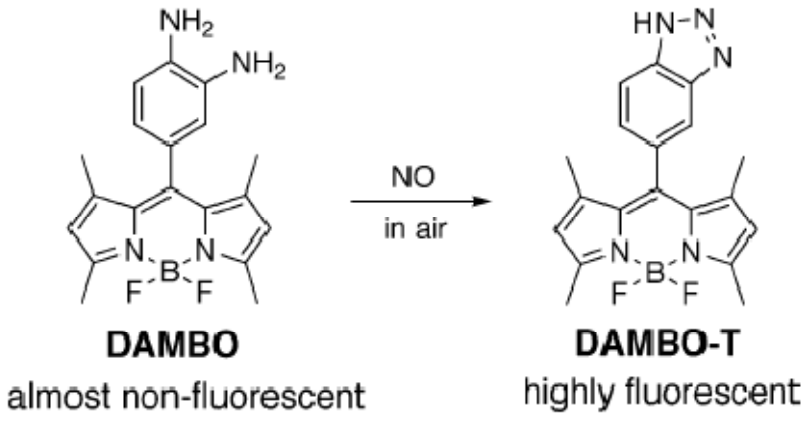

Figure 2.7 Reaction of **DAMBO** with NO

Reactive oxygen species (ROS) are chemically reactive molecules containing oxygen. Examples include oxygen ions and peroxides. Reactive oxygen species are highly reactive due to the presence of unpaired valence shell electrons. ROS form as a natural byproduct of the normal metabolism of oxygen and have important roles in cell signaling. However, during times of environmental stress, ROS levels can increase dramatically. This may result in significant damage to cell structures. This cumulates into a situation known as oxidative stress. ROS are also generated by exogenous sources such as ionizing radiation. Interestingly, the reactivity of each ROS differs substantially. For example, while the hydroxyl radical is quite short lived and strongly reactive, thus promoting oxidation of alkanes and arenes, hydrogen peroxide is relatively inert and stable. Thus, it is of interest to generate in vivo probes that detect highly reactive oxygen species (hROS) such as hydroxyl radical, peroxynitrite, and hypochlorite. For selective monitoring of hROS productionand distinguish specific species in cells, Kenichi et al. [101] have developed **HPF** and **APF** as novel fluorescence probe (**Figure 2.8**). These compounds are based on fluorescein as a fluorophore but utilize the *O*-dearylation reaction of phenols andanilines to create selective reactions catalyzed by hROS. **HPF** and **APF** were almost non-fluorescent due to the intramolecular PeT from the hydroxy or aminophenoxy group attached to the xanthene ring of fluorescein. These electron donor moieties are cleaved off by the reaction with hROS to yield highly fluorescent fluorescein. **HPF** can selectively detect hydroxyl radical and peroxynitrite among various ROS, and **APF** detects hypochlorite also and that are highly resistant to autoxidation. They can be used in enzymatic and cellular systems. They are greatly superior to the existing fluorescent probes for ROS, and are expected to have many chemical andbiological applications.

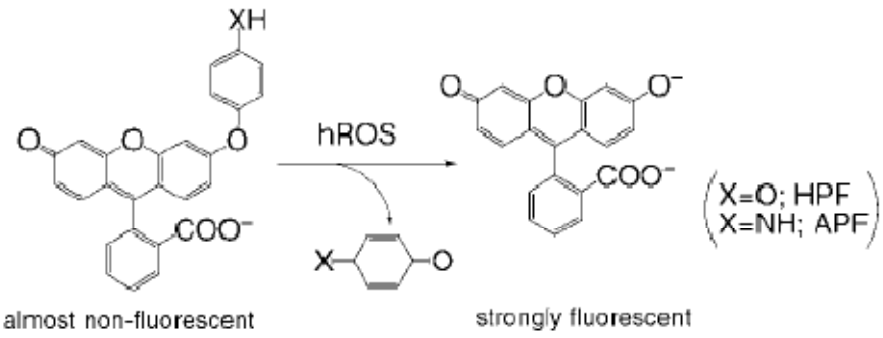

Figure 2.8 Scheme of *O*-dearylation reaction of **HPF** and **APF** with hROS.

Yuchiro et al. [102] have synthesized **MitoHR** and **MitoAR** as another type of hROS selective probe based on tetramethylrhodamine as a fluorescent probe (**Figure 2.9**). The same *O*-dearylation reaction used in **HPF** and **APF** was utilized as the key reaction with hROS, **MitoHR** and **MitoAR** are almost nonfluorescent because of the fast rate of intramolecular PeT from the benzene bound hydroxy or aminophenoxy group attached to tetramethylrhodamine. These probes can selectively detect damage to the mitochondria caused by hROS, because Mitochondria are believed to be the major source of intracellular reactive oxygen species. With these probes, it was possible to successfully observe that as little as 10 μM H_2O_2 can cause hROS damage to mitochondria in HL-60 cells.

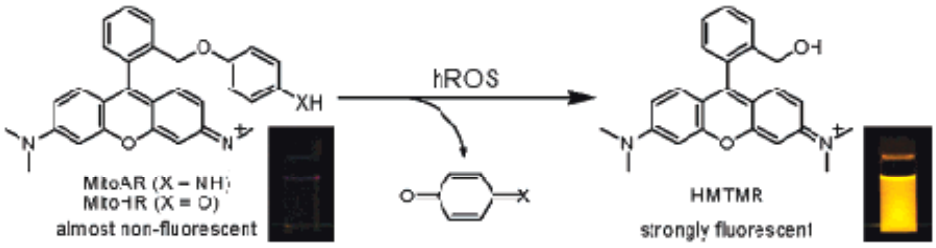

Figure 2.9 The reaction of **MitoAR** and **MitoHR** with hROS.

Peroxynitrite is an oxidant and nitrating agent. Because of its oxidizing properties, peroxynitrite can damage a wide array of molecules in cells, including DNA and proteins. Formation of peroxynitrite in vivo has been ascribed to the reaction of the free radical superoxide with the free radical nitric oxide. Recently, Ueno et al. [103] have developed **NiSPYs** as fluorescent probes (**Figure 2.10**). **NiSPYs** are the firstfluorescent probes, which show a marked fluorescence increase after nitration by peroxynitrite, which are sensitive to peroxynitrite by adjusting the HOMO and LUMO energies of the fluorophore and the reactive moiety for peroxynitrite. **NiSPYs** were almost completely nonfluorescent in the absence of peroxynitrite but became highly fluorescent upon reaction with peroxynitrite.

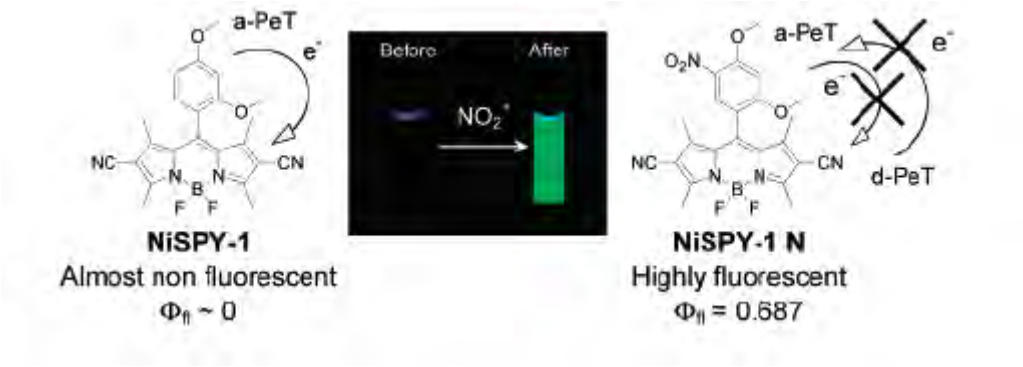

Figure 2.10 Scheme and photo of **NiSPY-1** before and after reaction with NO_2BF_4.

Enzymatically activated fluorescent probes generally diffuse uniformly in the cytoplasmic matrix, which is advantageous for detecting ROS production that was generated in cytoplasmic matrix. However, mostly fluorogenic compounds are well known to leak out from living cells through anion transporters expressed on the cell membrane, which obstruct quantitative detection and sensitive of target analytes due to the decreasing concentration of probes in the cells. Calcein is a very hydrophilic fluorescent dye and is well known not to leak from living cells. Thus, calcein based fluorescent probes could be more sensitive and reliable probes especially for long-term observations. In order to develop fluorescence probes that offer high sensitivity inside living cells, efficient retention of the probes and products within the cells is critical. Recently, Izumi et al. [104] was reported that the fluorescence property of calcein can also be controlled precisely by the PeT mechanism, and calcein derivatives were synthesized highly sensitive fluorescence probes, **APC** and **DCl-DA Cal**, for hROSor RNS, respectively. Acetoxymethyl (AM) ester derivatives of these probes can permeate the cell membrane and become retained in the cytoplasmic matrix after cleavage of the AM ester by ubiquitous esterases found in living cells. In the absence of their respective analyte, **APC** and **DCl-DA Cal** were almost nonfluorescent, but became highly fluorescent upon reaction with nitric oxide and hROS, respectively (**Figure 2.11**). After activation, they were retained in living cells, leading to amplification of the signal. As a result, **DACals** and **APC** were more sensitive to low concentrations of nitric oxide and hROS in living cells. These fluorescence probes and their fluorescent products show good intracellular retention compared with conventional fluorescent probes and are suitable for the visualization of low levels of

physiological molecules and for long-term observation in living cells. This design concept is expected to be applicable to a broad range of fluorescent probes and should be especially valuable for developing superior cellular imaging probes based on fluoresceinand other cytoplasmic matrix diffusible fluorophores.

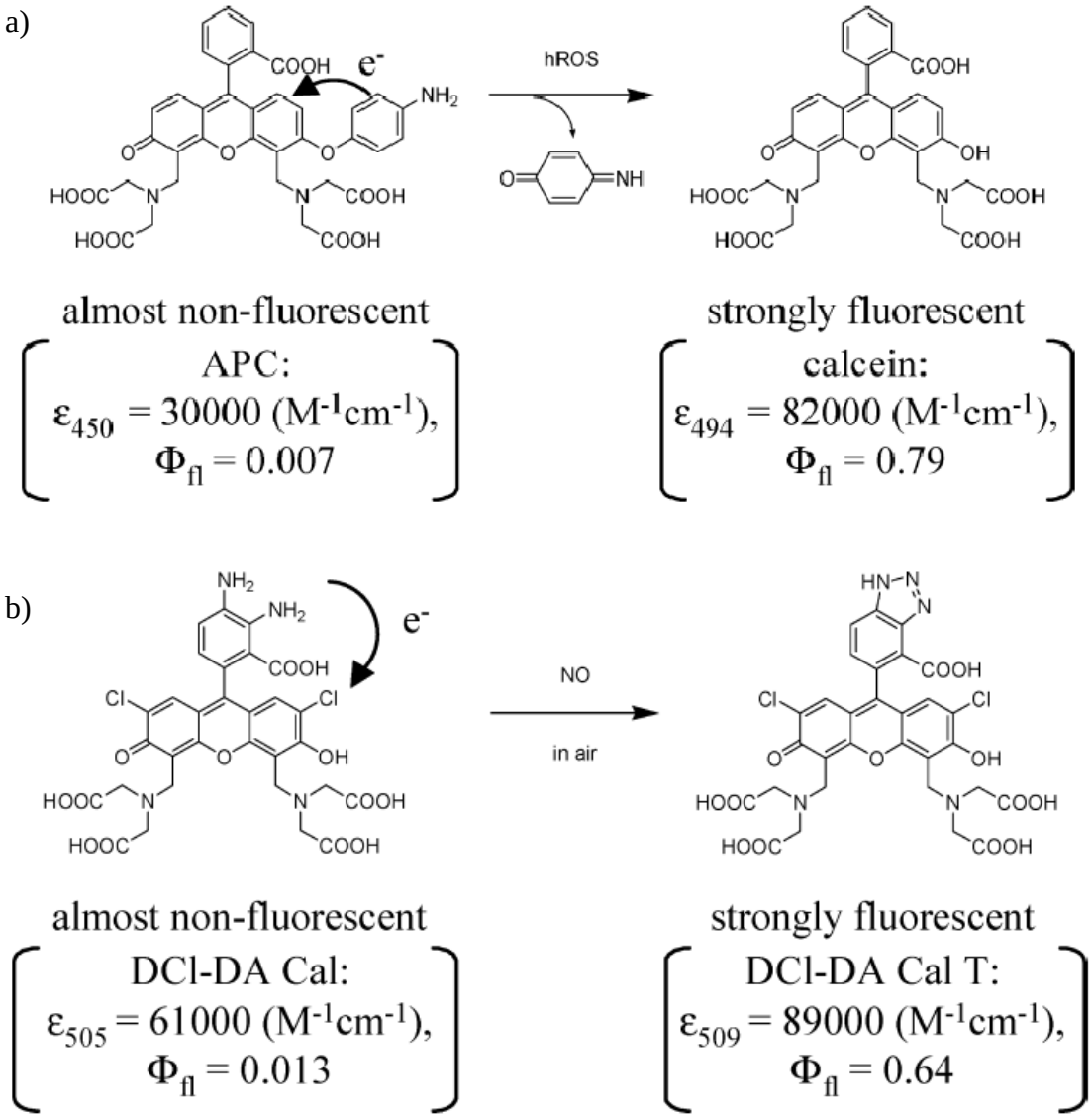

Figure 2.11 Reaction of a) **APC** and b) **DCl-Da Cal** with hROS

The concept of PeT is not restricted to developing fluorescent probes for ROS, but is also applicable for a wide range of enzymes. Glutathione S-transferase (GST) is a family of dimeric enzymes involved in phase II detoxification reactions. They participate in a wide range of processes, including xenobiotic biotransformation, drug metabolism and protection against endogenous ROS-induced toxic products, biosynthesis of prostaglandins and steroid hormones, and degradation of aromatic amino acids. Recently, Fujiwara at el. [105] has reported a novel fluorescent probe for GST activity, **DNAFs**, and a cell membrane-permeable variant (**DNAT-Me**) was successfully developed using 3,4-dinitrobenzanilide (**NNBA**) as a specific substrate and d-PeT as a mechanism for fluorescence quenching (**Figure 2.12**). DNAT-Me is switched "on" after GST-catalyzed glutathionylation. This agent has excellent kinetic parameters for monitoring the enzymatic activity in living cells. These results indicate that DNAT-Me should be useful not only for GST inhibitor screening but also for studies on the mechanisms of drug resistance in cancer cells.

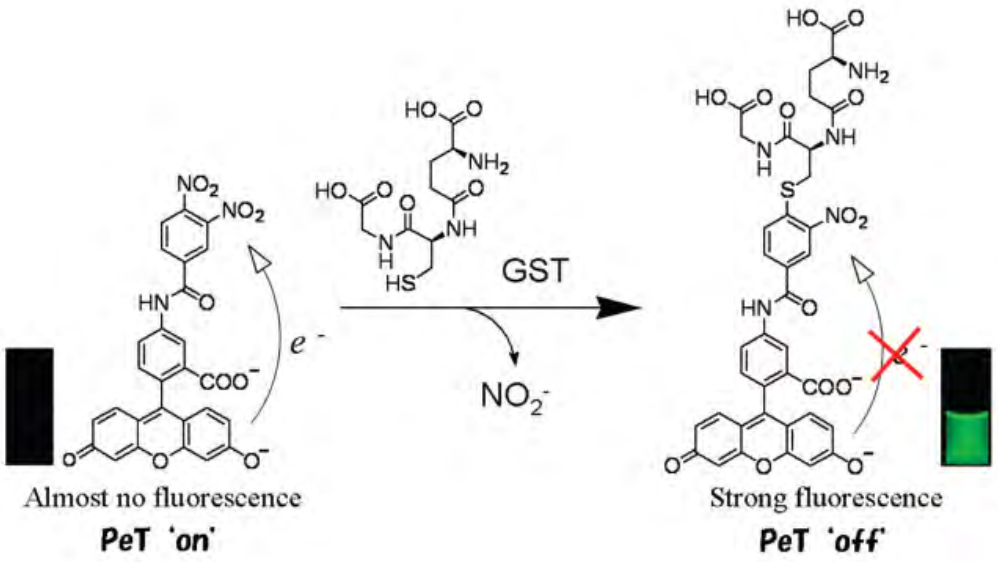

Figure 2.12 GST-Catalyzed Glutathionylation of **DNAF1**

Urano et al. [106] reported a newly fluorescein derivative called Tokyo Green (**TG**) that replaces the carboxylic moiety with a methoxy or methyl group. **TG** dyes are easily synthesized in high yields by the C-C bond coupling reaction. Moreover, by precisely controlling the HOMO energy of the benzene moiety, they were able to construct another rational design strategy for newly fluorescent probes. The value of

this approach is exemplified by a highly sensitive and membrane permeable fluorescent probe for *β*-galactosidase called **TG-*β*Gal** (**Figure 2.13**). Using **TG-*β*Gal**, an application of optical imaging for the detection of small cancer implants with high signal contrast was recently reported, especially in terms of sensitivity and for real-time imaging of living cells.

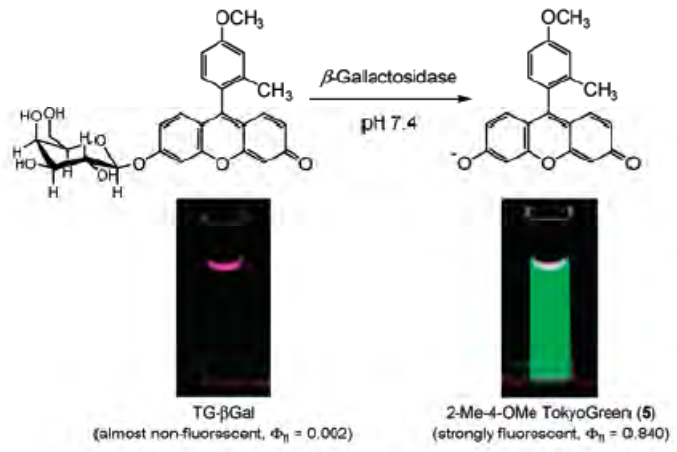

Figure 2.13 Reaction of **TG-*β*Gal** and photos before and after the reaction with *β*-galactosidase.

Moreover, the value of this approach is exemplified by its application to develop a novel, highly sensitive and membrane-permeable fluorescence probe for *β*-galactosidase, which is the most widely used reporter enzyme.Further, on the basis of the same strategy, **TG-phos** [107] (**Figure 2.14**) for alkaline phosphatase, which is also a widely used reporter enzyme, and **TG-NPE** [108] as highly activatable and rapidly caged fluorophores were successfully developed.

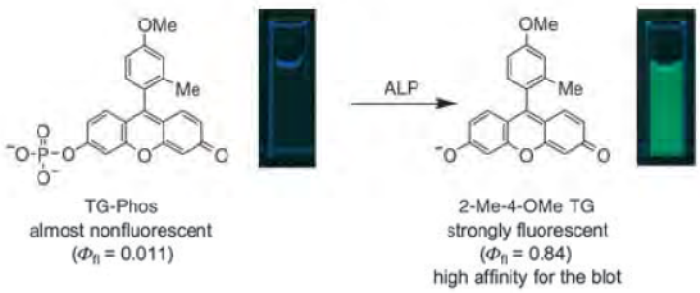

Figure 2.14 Reaction scheme and photo of **TG-Phos** with ALP to yield fluorescent hydrolyzed products.

Recently, Hama et al. [109] found that a lectin targeted optical imaging technique that used a fluorescein and avidin conjugate was effective for the visualization of peritoneal implants in a mouse ovarian cancer model (**Figure 2.15**). Using a combination of lectin targeting and activatable fluorescent probes. These results suggest that targeted molecular imaging with a labeled fluorescent lectin ligand system is a promising technique for the detection of disseminated submillimeter foci of cancer.

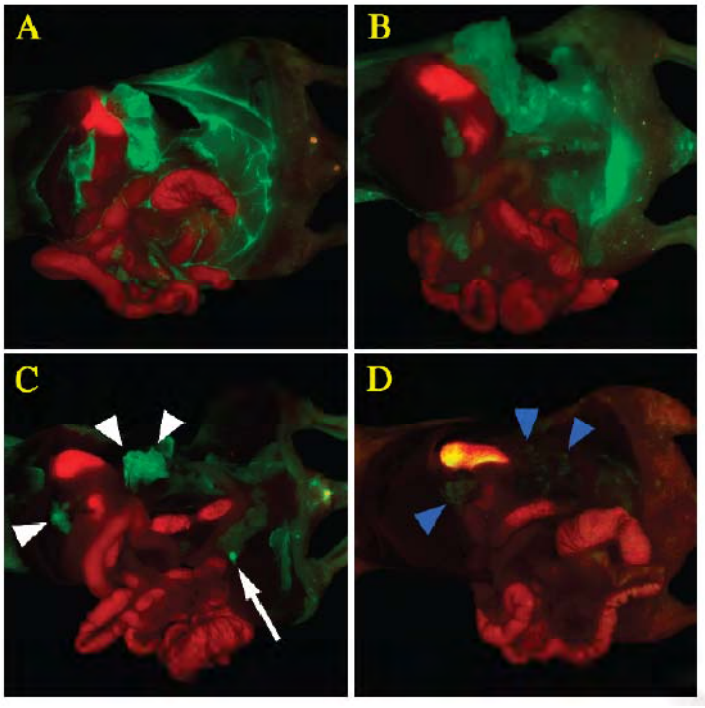

Figure 2.15 In vivo spectral fluorescence images of tumor-bearing mice. Composite images (red: autofluorescence; green: FITC fluorescence) were obtained 1, 2, 4 and 8 hours after injection of 50 µg of Avidin –FITC (A, 1 hour; B, 2 hours; C, 4 hours; D, 8 hours). (A and B) High fluorescence intensity was observed in tumor foci, but the background signal was still high within 2 hours postinjection. (C) Aggregated tumor foci (white arrowheads) and a small tumor nodule (white arrow) measuring < 5 mm are clearly shown 4 hours postinjection. (D) At 8 hours postinjection, the fluorescence from tumor foci (blue arrowheads) became very weak and almost unidentifiable. Imaging is optimized at approximately 4 hours postinjection.

However, Urano et al. [110] demonstrated an even more sensitive and selective imaging method. Using two step procedure in which lectin was first used to localize *β*-galactosidase on cancer cells and then was subsequently targeted by the administration of a highly sensitive fluorescent probe, very small implants with low background signal were achieved. The presence of *β*-galactosidase led to specific targeting fluorescence activation within the tumor. The result was a newly activated fluorescent probe for targeting the tumor (**AM-TG-*β*Gal**) that dramatically increases fluorescence emission when the tumor cells are prelabeled with *β*-galactosidase as an activating enzyme (**Figure 2.16**). Since the tumor-targeted enzyme can catalyze numerous substrate turnovers, a great number of fluorescent molecules could be activated, leading to a high tumor to background ratio. It was possible to see a strong fluorescence signal within prelabeled tumor cells after only 1 h of incubation with **AM-TG-*β*Gal**. Moreover, this procedure provides a tumor-specific, long-lived, and highly activated fluorescence signal. Studies to examine the feasibility of using this approach in video-assisted laparoscopic surgery are in progress. The present results indicate that chemistry based tuning of chemical properties (both fluorescence and cell permeability) could be the key to the development of small molecular in the fields of biology and clinical medicine.

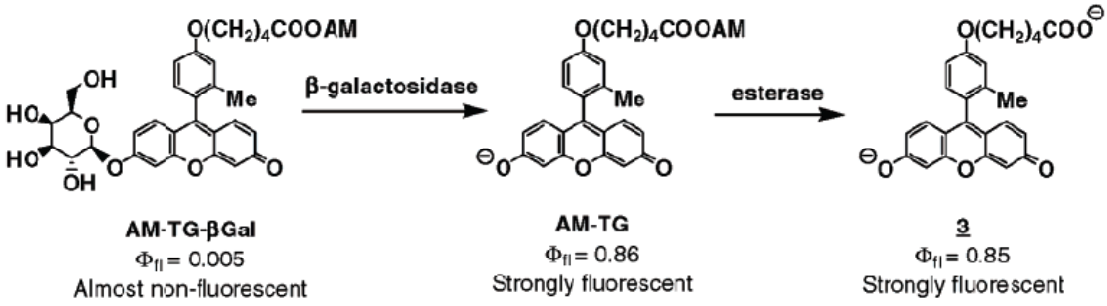

Figure 2.16 The newly developed fluorescence probe, **AM-TG-*β*Gal**, which shows a large fluorescence increase upon reaction with *β*-galactosidase and is further hydrolyzed by intracellular esterase to the free carboxylate, which is well retained in the cells without loss of fluorescence.

2.2 Literature reviews of lanthanide nanopaticles system

Recently, amorphous nanoparticles of supramolecular coordination polymer networks are spontaneously self-assembled from nucleotides and lanthanide ions in water. Nishiyabu et al [111] have demonstrated the spontaneous formation of nanoparticles of adaptive supramolecular networks self-assembled from nucleotides and lanthanide ions (**Figure 2.17**). These supramolecular networks display adaptive inclusion ability toward anionic molecules that dyes were isolated in supramolecular shells without aggregation. It reflects that growing supramolecular networks bind and accommodate anionic dyes by flexibly adapting to the shape of guest molecules. The adaptive inclusion ability of nucleotide/lanthanide nanoparticles is also applicable to nanosized guests such as gold nanoparticles and ferritin were also wrapped by the supramolecular shells. In addition, these nucleotide/lanthanide nanoparticles also serve as scaffolds for immobilizing enzymes. Moreover, they exhibit enhanced intrinsic functions such as nucleobase to lanthanide energy transfer, MR imaging properties. Adsorption of polyelectrolytes on nanoparticles surfaces improves their water solubility, and these nanoparticles show satisfactory biocompatibility. These features provide a simple way to design multifunctional nanomaterials.

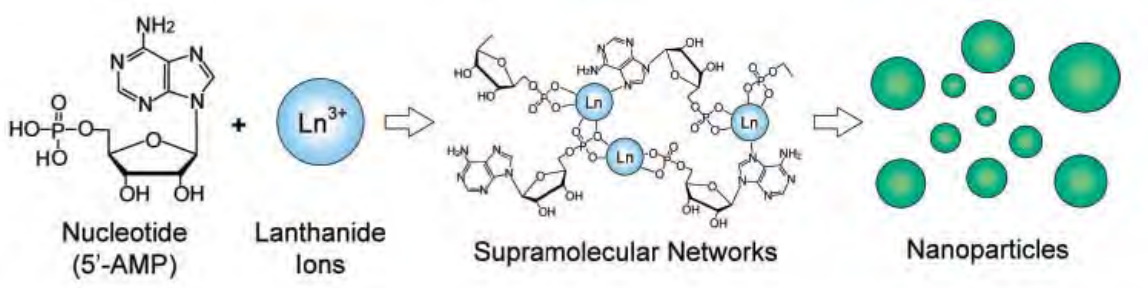

Figure 2.17 A schematic illustration of nanoparticle formation through the self-assembly of 5′-AMP and Ln^{3+} ions.

Despite these interesting phenomena, however, very little is known about the basic properties of coordination networks, including their effect on the properties of confined guest molecules. As the networks are formed from nucleotides and lanthanide ions in aqueous media, it is expected to influence the degree of hydration, thermal mobility, and conformational freedom of water-soluble guest molecules. Kimizuka et al. [112] describe unique interfacial properties of polymeric coordination shells self-assembled from nucleotides and lanthanide ions. The encapsulation of guest molecules in nucleotide– lanthanide nanoparticles was performed as displayed in **Figure 2.18**. The confined environment remarkably enhanced the luminescence intensity of the functional dyes, induced circular dichroism, and showed barrier properties against dissolved molecular oxygen. Thus, the adaptive inclusion by coordination networks provides opportunity to disclose latent functionality of guest molecules in water. These features would have an impact on the research of coordination nanoparticles.

Figure 2.18 A schematic illustration of the adaptive inclusion of guest dye molecules by growing nanoparticles of nucleotides and lanthanide ions in water.

2.3 Objective and the scope of this research

The aim of this research is to develop effective fluorescence sensors for enzymatic probe systems to determine biomolecules. Therefore, this research was separated into two parts for easy understanding and studies. The new anthraquinone consist of active site (boronic and glycoside) based fluorosensor for enzymatic probe have been designed, synthesized, and characterized. In the first part, the probe comprises a spectroscopic unit of anthraquinone imidazole unit and a boronic acid unit reactive part for detection of glucose using indirect method. In this method, the reaction of glucose and glucose oxidase were generated the gluconic acid and hydrogen peroxide which can react with boronic based anthraquinone. The reaction of hydrogen peroxide and boronic acid results expected to determine the glucose via the fluorescence change on a following shown in **Scheme 2.1**. In the second part, the probe contains a spectroscopic unit of anthraquinone imidazole unit and a glycoside (*β*-glucoside) unit as a reactive moiety for *β*-glucosidase (**Scheme 2.1**) using fluorescence spectrophotometry. Additionally, we attempt to apply all fluorescence sensory molecules to incorporate in the nanomaterial with the expectation of improvement of fluorescence response for detection.

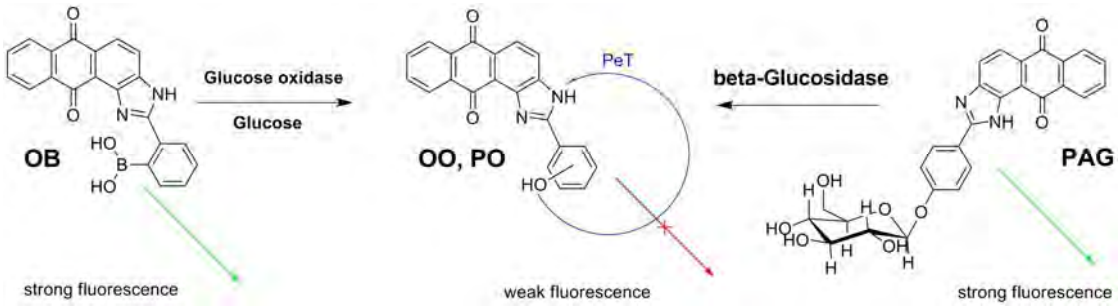

Scheme 2.1 Reaction scheme of **OB** and **PAG** before and after the reaction with glucose oxidase and *β*-glucosidase, respectively.

CHAPTER III

EXPERIMENTAL

3.1 Synthesis of fluorogenic compound receptors

3.1.1 Analytical measurements and materials

All materials and solvents chemicals were purchased from Aldrich, Fluka and Merck as standard analytical grade and were used without further purification. Commercial grade solvents such as dichloromethane, ethyl acetate, hexane and methanol were purified by distillation. Anhydrous solvents such as dichloromethane were dried over CaH_2 and freshly distillation under nitrogen atmosphere. Column chromatography was carried out on silica gel (Kieselgel 60, 0.063-0.200 mm, Merck). Thin layer chromatography (TLC) was performed on silica gel plates (Kieselgel 60, F_{254}, 1 mm). Compounds on TLC plates were detected by the UV-light

Nuclear Magnetic Resonance (NMR) spectra were recorded on a Varian Mercury Plus 400 NMR spectrometer. All chemical shifts were reported in part per million (ppm) using the residual proton or carbon signal in deuterated solvents as internal references. MALDI-TOF mass spectra were carried out on Bruker Daltonics MALDI-TOF using 2-cyano-4-hydroxy cinnamic acid (CCA) as matrix. High resolution mass spectra were determined on Bruker Daltonics DataAnalysis 3.3 with an electrospray ion source using methanol as a solvent

For the absorption or fluorescence measurement, compounds were dissolved in dimethylsulfoxide (DMSO, fluorometricgrade, Dojindo) to obtain 1mM stock solutions. These stock solutions were diluted with buffer as specified in the figure legends to the desired concentration. All absorption spectra were obtained with Hewlett Packard 8452A Diode Array Spectrometer. All fluorescence spectra were obtained with Varian Cary Eclipse Fluorescence Spectrophotometer. Scanning electron microscopy (SEM) was performed on a JEOL JSM-6510A with a high resolution of 3.0 nm at 30 kV. Samples were grounded using aluminuim stub.

Transmission electron microscopy (TEM) was performed on a JEOL JEM 2010 with the field emission gun operated at 200 kV

3.1.2 Experimental procedure

3.1.2.1 Preparation of R-(5,5-dimethyl-1,3,2-dioxaborinan-2-yl)benzaldehyde (R = 2 : 1o, 4 : 1p).

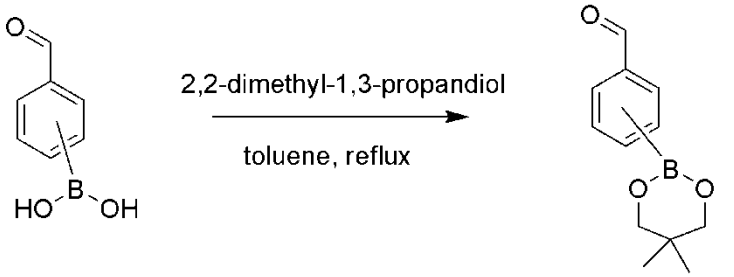

1o : *o*-isomer
1p : *p*-isomer

Into a two-neck round bottom flask equipped with a magnetic bar and a Dean-Stark equipment to remove water, the corresponding formyl phenyl boronic acid (0.150 g, 1 mmol) and 2,2-dimethyl-1,3-propandiol (0.104 g, 1mmol) were heated at reflux in toluene (30 mL) for 12 hours. Subsequently, the solvent was evaporated under reduced pressure to give a crude product as clear oil for ortho isomer (**1o**) and as a white solid for para isomer (**1p**). The crude product was used in the next step without purification.

Characterization data for 1o and 1p

^{1}H NMR (DMSO-d_6, 400 MHz)

Compound 1o : [ortho isomer] δ (ppm) : 10.52 (s, 1H), 7.89 (t, 1H, *J* = 7.6 Hz), 7.79 (d, 1H, *J* = 7.2 Hz), 7.24 (t, 1H, *J* = 7.6 Hz), 7.16 (d, 1H, *J* = 7.2 Hz), 3.81 (s, 2H), 3.48 (s, 2H), 1.07 (s,3H), 0.90 (s, 3H). (**Figure A.1**)

Compound 1p : [para isomer] δ (ppm) : 10.03 (s, 1H), 7.95 (d, 2H, *J* = 8.0 Hz), 7.85 (d, 2H, *J* = 8.0 Hz), 3.79 (s, 4H), 1.03 (s,6H). (**Figure A.2**)

3.1.2.2 Preparation of 2-(R-(5,5-dimethyl-1,3,2-dioxaborinan-2-yl) phenyl)-1H-anthra[1,2-d]imidazole-6,11-dione (R = 2 : 2o, 4 : 2p).

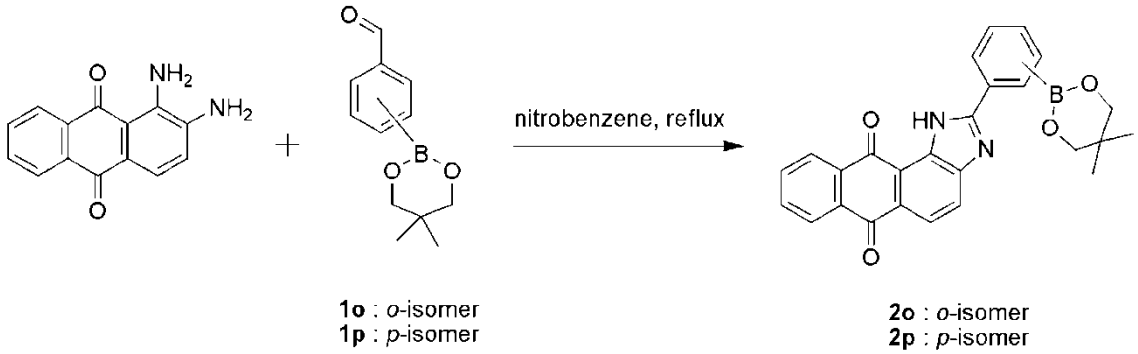

Into a two-neck round bottom flash equipped with a magnetic bar, the corresponding formylphenylboronate ester (0.218 g, 1 mmol) in nitrobenzene (25 mL) was added drop wise to a solution of 1,2-diamino-1,4-anthraquinone (0.238 g, 1 mmol) in nitrobenzene (75 mL).The reaction mixture was slowly heated up to 150 ^{o}C for 1 day under nitrogen atmosphere. The solution was cooled to room temperature and then the precipitate slowly formed. The precipitate was filtered and washed with diethyl ether to give a brown solid the protecting product **2o** (0.196 g, 45 %yield) and a yellow solid of the protecting product **2p** (0.262 g, 60 %yield).

Characterization data for 2o and 2p

^{1}H NMR (DMSO-d_6, 400 MHz)

Compound 2o :[ortho isomer] δ (ppm) : 13.56 (s, 1H), 8.41 (d, 1H, *J* = 6.4 Hz), 8.25-8.13 (m, 4H), 7.94-7.92 (m, 2H), 7.57-7.50 (m, 3H), 3.70 (s, 4H), 1.07 (s, 6H). (**Figure A.3**)

Compound 2p :[para isomer] δ (ppm) : 10.18 (s, 1H), 8.40 (t, 1H, *J* = 8.2 Hz), 8.29-8.21 (m, 4H), 8.13-8.05 (m, 2H), 7.97-7.93 (m, 3H), 3.78 (s, 2H), 3.11 (s, 2H), 0.97 (s, 3H) 0.72 (s, 3H). (**Figure A.4**)

3.1.2.3 Preparation of R-(6,11-dioxo-6,11-dihydro-1H-anthra[1,2-d]imidazol-2-yl)phenylboronic acid (R = 2 : OB, 4 : PB).

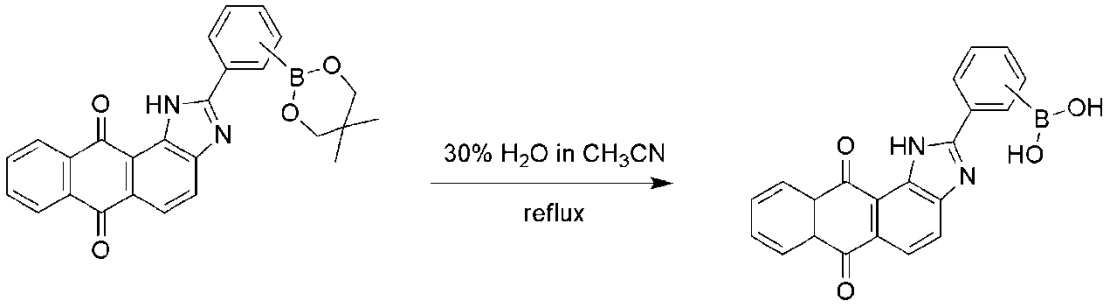

2o : *o*-isomer
2p : *p*-isomer

OB : ortho isomer
PB : para isomer

Protecting groups of 2-(R-(5,5-dimethyl-1,3,2-dioxaborinan-2-yl) phenyl)-1H-anthra[1,2-d]imidazole-6,11-dione (R = 2 : **2o**, 4 : **2p**) (0.436 g, 1 mmol) were removed by refluxing in 30 mL of 30% H_2O:CH_3CN. The yellow solid of product **OB** and brown solid of product **PB** was filtered and washed with diethyl ether to provide a desired product in a quantitative yield.

Characterization data for OB and PB

^{1}H NMR (DMSO-d_6, 400 MHz)

Compound OB : [ortho isomer] δ (ppm) : 13.76 (s, 1H), 8.26-8.21(m, 2H), 8.14 (d, 2H, *J* = 6.8 Hz), 7.99 (d, 2H, *J* = 6.0 Hz), 7.94-7.92 (m, 1H), 7.75 (d, 1H, *J* = 8.4 Hz), 7.68 (d, 2H, *J* = 6.8 Hz). (**Figure A.5**)

Compound PB : [para isomer] δ (ppm) : 10.97 (s, 1H), 9.21 (d, 1H, *J* = 7.6 Hz), 9.11-9.00 (m, 3H), 8.96-8.86 (m, 2H), 8.78-8.74 (m, 3H), 7.73 (d, 1H, *J* = 8.4 Hz). (**Figure A.6**)

^{13}C NMR (DMSO-d_6, 100.6 MHz)

Compound OB : [ortho isomer] δ (ppm) : 182.36, 182.00, 181.50, 159.60, 148.58, 133.60, 132.59, 132.33, 131.91, 129.68, 129.23, 128.49, 128.04, 126.84, 126.66, 126.23, 126.12, 124.74, 121.60, 120.93, 118.58. (**Figure A.13**)

Compound PB : [para isomer] δ (ppm) : 183.02, 182.25, 160.21, 149.19, 137.13, 132.99, 132.88, 130.07, 130.01, 128.00, 127.31, 126.99, 126.69, 126.13, 124.90, 124.12, 120.97, 120.91, 119.67, 118.57, 115.54. (**Figure A.14**)

High Resolution Mass spectrometer (ESI-HRMS)

Compound OB : m/z : for $(M + CH_3OH + H_2O + H^+)$ Anal. Calc. = 419.13
Found. = 419.123 (**Figure A.23**)

Compound PB : m/z : for $(M + CH_3OH + H_2O + H^+)$ Anal. Calc. = 419.13
Found. = 419.097 (**Figure A.24**)

3.1.2.4 Preparation of 2-(R-hydroxyphenyl)-3H-anthra[2,1-d]imidazole-6,11-dione (R = 2 : OO, 4 : PO).

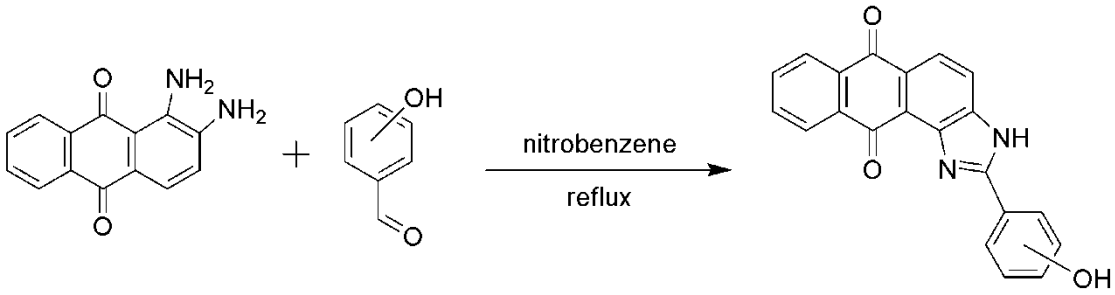

OO : ortho isomer
PO : para isomer

Into a two-neck round bottom flask equipped with a magnetic bar, the corresponding hydroxybenzaldehyde (0.122 g, 1 mmol) in nitrobenzene (10 mL) was added drop wise to a solution of 1,2-diamino-1,4-anthraquinone (0.238 g, 1 mmol) in nitrobenzene (40 mL). The reaction mixture was slowly heated up to 150 ^{o}C for 48 hours under nitrogen atmosphere. The solution was cooled to room temperature and then, the precipitate slowly formed. The precipitate was filtered and washed with diethyl ether (20 ml) to give a dark brown solid of the product **OO** (0.384 g, 64 %yield) and give a brown solid of the product **PO** (0.265 g, 78 %yield).

Characterization data for OO and PO

^{1}H NMR (DMSO-d_6, 400 MHz)

Compound OO δ (ppm) : 12.73 (s, 1H), 12.01 (s, 1H), 8.42 (d, 1H, *J* = 8.0 Hz), 8.16 (s, 2H), 8.07 (m, 1H), 8.71 (d, 1H, *J* = 16 Hz), 7.90 (s, 2H), 7.42 (t, 1H, *J* = 7.6 Hz), 7.09 (d, 1H, *J* = 8.4 Hz), 7.03 (t, 1H, *J* = 7.2 Hz). (**Figure A.7**)

Compound PO δ (ppm) : 12.86 (s, 1H), 10.18 (s, 1H), 8.26 (d, 2H, *J* = 7.6 Hz), 8.17 (s, 2H), 8.00 (s, 2H), 7.89-7.88 (m, 2H), 6.91 (d, 2H, *J* = 8 Hz). (**Figure A.8**)

3.1.2.5 Preparation of (3R,4S,5S,6S)-2-(acetoxymethyl)-6-(X-(6,11-dioxo-6,11-dihydro-3H-anthra[2,1-d]imidazol-2-yl)phenoxy)-5-hydroxytetrahydro-2H-pyran-3,4-diyl diacetate (X = 2 : OAPG, 4 : PAPG).

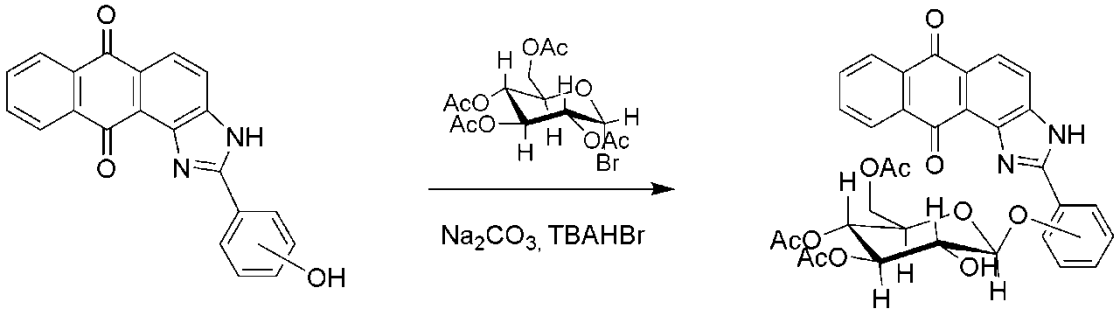

OO : ortho isomer
PO : para isomer

OAPG : ortho isomer
PAPG : para isomer

Into round bottom flask with a magnetic bar, acetobromoglucose (0.205 g, 0.5 mmol), 5 equivalent of **OO** or **PO** (0.850 g, 2.5 mmol) and tetrabutylammonium hydrogen bromide (TBAHBr, 1 equiv.) were vigorously stirred at room temperature in CH_2C1_2 (10 mL) and 1 M Na_2CO_3 (5 mL). After 6 hours, the reaction mixture was worked up by adding dichloromethane (20 mL). The organic phase was washed with distilled water (2 x 20 mL) and sat. NaCI (20 mL). The organic extracts were dried with $NaSO_4$, filtered and evaporated under reduced pressure to give a dark brown solid which was purified on silica gel column chromatography (CH_2Cl_2:MeOH, 100:2) and recrystallised from ethanol. Compounds **OAPG** or **PABG** were obtained as yellow solid with 0.063 g (20 %yield) and 0.110 g (35 %yield), respectively.

Characterization data for OAPG and PAPG

^{1}H NMR (DMSO-d_6, 400 MHz)

Compound OAPG δ (ppm) : 12.33 (s, 1H), 8.47 (d, 1H, *J* = 1.6 Hz), 8.45 (s, 1H), 8.34 (dd, 1H *J* = 6 Hz, 1.2 Hz), 8.26 (d, 1H, *J* = 8.4 Hz), 8.14 (d, 1H, *J* = 8.4 Hz), (q of d, 2H, *J* = 7.2 Hz, 2.4 Hz), 7.56 (t, 1H, *J* = 7.6 Hz), 7.37 (t, 1H, *J* = 7.6 Hz), 7.29 (s, 1H), 5.68 (t, 1H, *J* = 9.6 Hz), 5.58 (t, 1H, *J* = 8.8 Hz), 5.45 (m, 2H), 4.45 (dd, 1H *J* = 6.4 Hz, 6 Hz), 4.18 (dd, 1H *J* = 9.6 Hz, 2.8 Hz) 3.94 (m ,1H), 2.16-1.83 (m, 9H). (**Figure A.9**)

Compound PAPG δ (ppm) : 8.33 (m, 1H), 8.27 (m, 1H), 8.22 (m, 1H), 8.05 (m, 3H), 7.81 (q, 2H, *J* = 3.2 Hz), 7.17 (d, 2H, *J* = 8.8 Hz), 5.35-5.32 (m, 2H), 5.24-5.18 (m, 2H), 4.33-4.29 (m, 1H), 4.21 (d, 1H, *J* = 10 Hz), 3.98-3.94 (m, 1H), 2.11-2.02 (m, 9H). (**Figure A.10**)

Mass spectrometer

Compound OAPG : MADI-TOF : m/z Anal. Calc. = (M + Na^++ H_2O + $2H^+$) 671.17
Anal. Calc. = (M) 628.17
Found.= (M + Na^++ H_2O + $2H^+$) 671.870
Found.= (M) 628.861 (**Figure A.17**)

Compound PAPG : MADI-TOF : m/z Anal. Calc. = (M + Na^++ H_2O + H^+) 670.17
Anal. Calc. = (M + H^+) 629.17
Found. = (M + Na^++ H_2O + H^+) 670.740
Found. = (M + H^+) 629.769 (**Figure A.18**)

3.1.2.6 Preparation of 2-(X-((2S,3S,4R,5S)-3,4,5-trihydroxy-6-(hydroxymethyl)tetrahydro-2H-pyran-2-yloxy)phenyl)-3H-anthra[2,1-d]imidazole-6,11-dione (X = 2 : OAG, 4 : PAG).

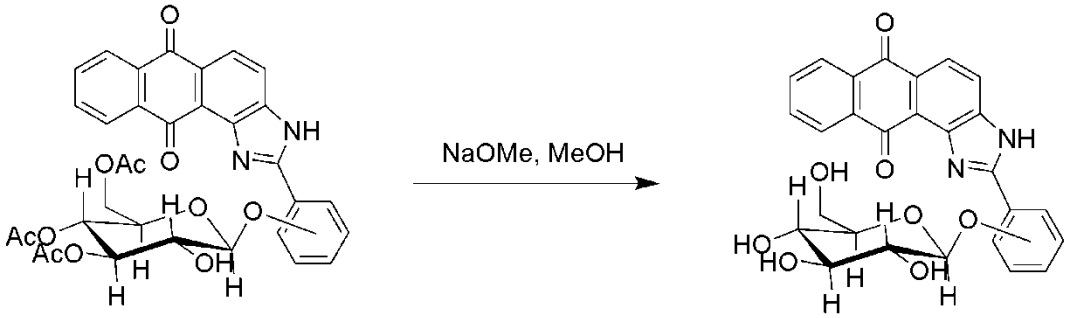

OAPG : ortho isomer
PAPG : para isomer

OAG : ortho isomer
PAG : para isomer

Into a round bottom flask with a magnetic bar, a solution of **OAPG** or **PAPG** (0.0628 g, 0.1 mmol) in methanol (2 mL) and 5 M methanol solution of NaOMe (20 µL, 100 µmol) was added. The mixture was stirred at room temperature for 1 hour and then, neutralized with Amberlite resin IR-120(H^+). The Amberlite IR-120 was filtered off, and the filtrate was evaporated. The residue was purified by column chromatography on silica gel with CH_2Cl_2: MeOH (100:10) as the eluent to give **OAG** or **PAG** as a yellow powder with 0.0447 g (89 %yield) and 0.0457 g (91 %yield), respectively.

Characterization data for OAG and PAG

^{1}H NMR (DMSO-*d*$_6$, 400 MHz)

Compound OAG : [ortho isomer] δ (ppm) : 12.57 (s, 1H), 8.40 (d, 1H, *J* = 8 Hz), 8.25-8.21 (m, 2H), 8.09 (t, 2H, *J* = 15.2 Hz) 7.94-7.92 (m, 2H), 7.59 (t, 1H, *J* = 7.6 Hz) 7.49 (m, 1H), 7.29 (t, 1H, *J* = 7.2 Hz) 5.32 (s, 1H), 5.26 (s, 1H), 5.16 (s, 1H), 4.60 (s, 1H), 3.76 (d, 2H, *J* = 11.2 Hz), 3.57-3.30 (m, 5H). (**Figure A.11**)

Compound PAG : [para isomer] δ (ppm) : 13.13 (s, 1H), 8.37 (d, 2H, *J* = 8.8 Hz), 8.22-8.17 (m, 2H), 8.04 (s, 2H), 7.93-7.90 (m, 2H), 5.40 (s, 1H), 5.14 (s, 1H), 5.08 (s, 1H), 5.03 (d, 1H, *J* = 7.2 Hz), 4.63 (s, 1H), 3.71 (d, 1H, *J* = 11.2 Hz), 3.50-3.16 (m, 5H). (**Figure A.12**)

^{13}C NMR (DMSO-d_6, 100.6 MHz)

Compound OAG : [ortho isomer] δ (ppm) : 183.65, 182.26, 155.74, 154.63, 148.04, 134.62, 134.23, 133.26, 132.91, 130.03, 127.78, 126.91, 126.38, 124.85, 123.20, 120.96, 118.00, 117.00, 102.32, 77.71, 76.56, 73.50, 69.58, 60.74. (**Figure A.15**)

Compound PAG : [para isomer] δ (ppm) : 183.18, 182.33, 159.58, 157.59, 149.41, 134.45, 134.25, 133.12, 132.96, 132.89, 129.77, 127.69, 126.77, 126.20, 124.52, 122.39, 121.03, 118.40, 116.32, 99.96, 77.06, 76.54, 73.22, 69.73, 60.70. (**Figure A.16**)

Mass spectrometer (MADI-TOF**)**

Compound OAG :	m/z for ($M + H^+$)	Anal. Calc.	= 503.14
		Found.	= 503.816 (**Figure A.19**)
Compound PAG :	m/z for = ($M + H^+$)	Anal. Calc.	= 503.14
		Found.	= 503.921 (**Figure A.20**)

High Resolution Mass spectrometer (ESI-HRMS)

Compound OAG : m/z : for ($M + Na^+$)	Anal. Calc. = 525.14	
	Found. = 525.1034 (**Figure A.21**)	
Compound PAG : m/z : for ($M + Na^+$)	Anal. Calc. = 525.14	
	Found. = 525.1045 (**Figure A.22**)	

3.1.2.7 Preparation of difluoroboron curcumin derivatives (CURBF)

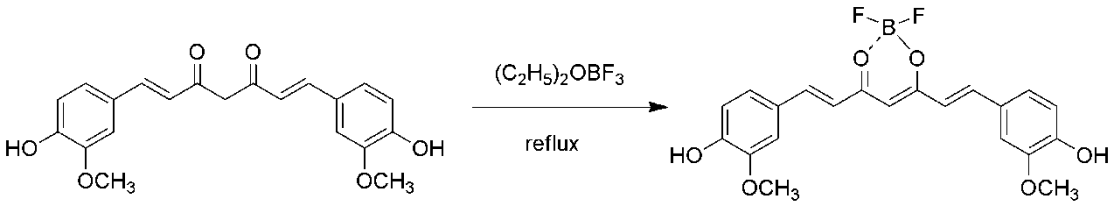

CUR CURBF

Into a 250 mL two-neck round bottom flask, curcumin (2.95 g, 8 mmol) was dissolved in methanol (200 mL) to give a bright yellow solution. Borontrifluoride diethyletherate (1.02 mL, 8 mmol) was added and the solution turned to red suddenly. The reaction was refluxed at 60 ^{o}C for 4 hours under N_2 and then cooled down to room temperature. Solvent was removed under reduced pressure to obtain a red powder. The desired product, **CURBF** 2.72 g (82% yield), was obtained as a red solid after recrystallization in MeOH:EtOAc (1:3).

Characterization data for CURBF

^{1}H NMR (DMSO-*d*$_6$, 400 MHz)

Compound CURBF : δ (ppm) : 10.09 (s, 2H), 7.90 (d, 2H, *J* = 15.6 Hz), 7.45 (s, 2H), 7.32 (d, 2H, *J* = 8.0 Hz), 6.85 (d, 2H, *J* = 8.0 Hz), 6.42 (s, 1H), 3.83 (s, 6H). (**Figure A.25**)

Elemental analysis :

Anal. Calc. for $C_{21}H_{19}BF_2O_6$	C, 60.60; H, 4.60
Found.	C, 60.46; H, 4.71

3.1.3 Fluorogenic compound for nucleotide/lanthanide coordination nanoparticles and surfactant/lanthanide nanoparticles

3.1.3.1 Fluorescien derivative (FLU)

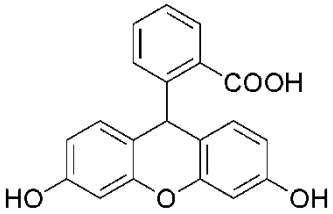

3.1.3.2 Porphyrin derivative (POR)

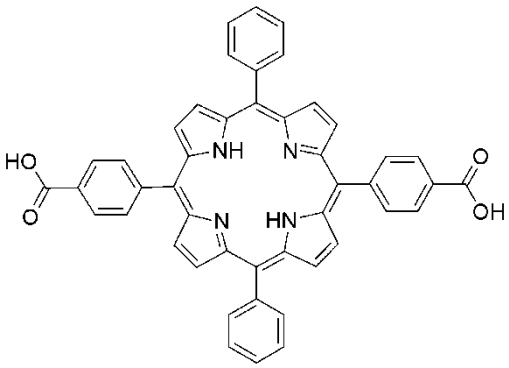

3.1.3.3 1-aminopyrene (APY)

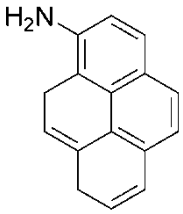

3.1.3.4 Napthalic derivative (NAP)

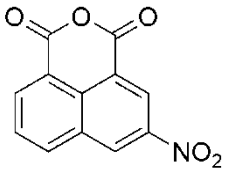

3.2 The enzymatic probe studies of the boronic anthraquinone based sensors

3.2.1 The photochemical studies of boronic anthraquinone based sensors and their derivatives for enzymatic probe system, OB, PB, OO and PO for glucose oxidase

3.2.1.1 UV/Vis spectroscopic screening test of sensors

The sensors were prepared in spectroscopic grade DMSO at concentrations of 2.00 $x10^{-4}$ mol/L as a stock solution. The solution of sensors were mixed with 0.1 M HEPES buffer pH 7.4 to give a final concentration of sensors at 2.00 $x10^{-5}$ mol/L in 10% DMSO aqueous solution. 2.00 mL of sensor solution was placed in a 100.0 mm width quartz cell. UV/Vis spectra were recorded at 25°C after each addition.

3.2.1.2 Fluorescence spectroscopic screening test of sensors

Typically, the sensors were prepared in spectroscopic grade DMSO at concentrations of 2.00 $x10^{-4}$ mol/L as a stock solution. The solution of sensors were mixed with 0.1M HEPES buffer pH 7.4 to give a final concentration of sensors at 2.00 $x10^{-5}$ mol/L, 10% DMSO in aqueous solution. 2.00 mL of sensor solution was placed in a 100.0 mm width quartz cell. Fluorescence spectra were recorded at 25°C after each addition under the following condition:

	OB	**PB**	**OO**	**PO**
Start (nm)	435	416	424	424
End (nm)	800	800	800	800
Excitation (nm)	415	396	404	404
Excitation Slit	10.0	10.0	10.0	10.0
Emission Slit	10.0	10.0	10.0	100
PMT	700	700	800	800
Scan rate	600 nm/min	600 nm/min	600 nm/min	600 nm/min

3.2.1.3 Determination of quantum yield

Quantum yield (Φ_f) was obtained by a relative basis with reference to a standard having known quantum yield. Quantum yield of samples were calculated following equation

$$\Phi_X = \Phi_{STD}\left(\frac{A_{STD}}{A_X}\right)\left(\frac{E_X}{E_{STD}}\right)\left(\frac{\eta_X^2}{\eta_{STD}^2}\right)$$

or

$$\Phi_X = \Phi_{STD}\left(\frac{Grad_X}{Grad_{STD}}\right)\left(\frac{\eta_X^2}{\eta_{STD}^2}\right)$$

Φ_x = quantum yield of the unknown
Φ_{STD} = quantum yield of the standard
A = absorbance of solution
E = integrated fluorescence spectra
η = refractive index of solvent
$Grad_x$ = gradient of unknown
$Grad_{STD}$ = gradient of standard

The integrated fluorescence spectra of a sample were plotted versus absorbance at the excitation wavelength to obtain a gradient of sample. The quininebisulfate in 1*N* H_2SO_4 was used as a reference sample (Φ_f = 0.508 in 1*N* H_2SO_4).

3.2.2 The complexation studies of the boronic anthraquinone based sensors with glucose using fluorescence titration experiments

Typically, the sensors were prepared in spectroscopic grade DMSO at concentrations of 2.00 $x10^{-4}$ mol/L as a stock solution. The stock solutions of glucose were prepared at concentrations of 6.00 $x10^{-3}$ mol/L in 0.1 M HEPES buffer pH 7.4. In a 5.0 mL beaker, 0.30 mL of the stock solution of sensor was mixed with the portions of stock solution of glucose to give final concentration of glucose according to **Table 3.1**. After volume were adjusted to 3.00 mL with 0.1M HEPES buffer pH 7.4 to give a final concentration of sensors at 2.00 $x10^{-5}$ mol/L in 10% DMSO aqueous solution, the mixtures was stirred at room temperature for 10 minutes and placed in a 100.0 mm width quartz cell and then fluorescence spectra were recorded at 25°C under the following condition:

	OB	**PB**
Start (nm)	435	416
End (nm)	800	800
Excitation (nm)	415	396
Excitation Slit	10.0	10.0
Emission Slit	10.0	10.0
PMT	700	800
Scan rate	600 nm/min	600 nm/min

Table 3.1 Volume of the glucose stock solution (6.00×10^{-3}mol/L) and the final concentration of glucose in 3.00 mL

Volume of glucose stock solution (μL)	Final concentration of glucose in 3.00 mL (M)
10	2.00×10^{-5}
20	4.00×10^{-5}
30	6.00×10^{-5}
40	8.00×10^{-5}
50	1.00×10^{-4}
60	1.20×10^{-4}
70	1.40×10^{-4}
80	1.60×10^{-4}
90	1.80×10^{-4}
100	2.00×10^{-4}
200	4.00×10^{-4}
300	6.00×10^{-4}
400	8.00×10^{-4}
500	1.00×10^{-3}
1000	2.00×10^{-3}

3.2.3 The reaction studies of the boronic anthraquinone based sensors with hydrogen peroxide using fluorescence titration experiments

Typically, the sensors were prepared in spectroscopic grade DMSO at concentrations of 2.00 $x10^{-4}$ mol/L as a stock solution. The stock solutions of hydrogen peroxide were prepared at the concentrations of 6.00 $x10^{-3}$ mol/L in 0.1M HEPES buffer pH 7.4. In a 5.0 mL vial, 0.30 mL of the stock solution of sensor was mixed with the portions of stock solution hydrogen peroxide to give final concentration of hydrogen peroxide according to **Table 3.2**. After volume were adjusted to 3.00 mL with 0.1M HEPES buffer pH 7.4 to give a final concentration of sensors at 2.00 $x10^{-5}$ mol/L in 10% DMSO aqueous solution. The mixtures was stirred at room temperature for 60 minutes and placed in a 100.0 mm width quartz cell and then fluorescence spectra were recorded at 25°C under the following condition:

	OB	**PB**
Start (nm)	435	416
End (nm)	800	800
Excitation (nm)	415	396
Excitation Slit	10.0	10.0
Emission Slit	10.0	10.0
PMT	700	800
Scan rate	600 nm/min	600 nm/min

Table 3.2 Volume of the hydrogen peroxide stock solution (6.00×10^{-3}mol/L) and the final concentration of hydrogen peroxide in 3.00 mL

Volume of hydrogen peroxide stock solution (μL)	Final concentration of hydrogen peroxide in 3.00 mL (M)
10	2.00×10^{-5}
20	4.00×10^{-5}
30	6.00×10^{-5}
40	8.00×10^{-5}
50	1.00×10^{-4}
60	1.20×10^{-4}
70	1.40×10^{-4}
80	1.60×10^{-4}
90	1.80×10^{-4}
100	2.00×10^{-4}
200	4.00×10^{-4}
300	6.00×10^{-4}
400	8.00×10^{-4}
500	1.00×10^{-3}
1000	2.00×10^{-3}

3.2.4 Fluorescence measurement for the optimizing condition of the enzymatic probe system

Fluorescence measurements in this section were performed under the following condition:

	OB
Start (nm)	435
End (nm)	800
Excitation (nm)	415
Excitation Slit	10.0
Emission Slit	10.0
PMT	700
Scan rate	600 nm/min

3.2.4.1 The studies on the effect of unit of glucose oxidase

In a 10.0 mL vial, 0.30 mL of 2.00 $x10^{-4}$ mol/L of a sensor in spectroscopic DMSO was mixed with 100 μL of 6.00 $x10^{-2}$ mol/L glucose in 0.1M HEPES buffer pH 7.4 and adjusted to 3.00 mL to give final concentration of sensors at 2.00 $x10^{-5}$ mol/L in 10% DMSO aqueous solution. Then glucose oxidase (GOx) in various portions according to **Table 3.3** was added to the solution mixture of the sensor and the glucose. After stirred for 60 minutes, the mixture sample was placed in a 100.0 mm width quartz cell, and the fluorescence spectra were then recoded at room temperature.

Table 3.3 Volume of the GOx (3 mg/ 1 mL) and the final unit of GOx in 3.00 mL

Volume of the glucose oxidase solution(μL)	Final unit of glucose oxidase in 3.00 mL (unit)
5	1.5
10	3
15	4.5
20	6
30	9

3.2.4.2 The studies on the effect of temperature

In a 10.0 mL vial, 0.30 mL of 2.00 $x10^{-4}$ mol/L of a sensor in spectroscopic DMSO was mixed with 100 μL of 6.00 $x10^{-2}$ mol/L glucose in 0.1M HEPES buffer pH 7.4 and adjusted to 3.00 mL to give final concentration of sensors at 2.00 $x10^{-5}$ mol/L in 10% DMSO aqueous solution. Then, 6 units of glucose oxidase were added to the solution mixture of the sensor and the glucose. One mixture was stirred at room temperature and another was stirred at 37°C for 60 minutes and placed in a 100.0 mm width quartz cell and then, the fluorescence spectra were recorded at room temperature.

3.2.4.3 The studies on the reaction time

In a 100.0 mm width quartz cell, 0.30 mL of 2.00 $x10^{-4}$ mol/L of a sensor in spectroscopic DMSO was mixed with 100 μL of 6.00 $x10^{-2}$ mol/L glucose in 0.1M HEPES buffer pH 7.4 and adjusted to 3.00 mL to give final concentration of sensors at $2x10^{-5}$ mol/L in 10% DMSO aqueous solution. Then 6 units of glucose oxidase were added to the solution mixture of the sensor and the glucose. The mixture was stirred at

room temperature and then, the fluorescence spectra were recorded at room temperature every 5 minutes.

3.2.5 Fluorescence measurement of boronic anthraquinone based sensors (OB) in optimum condition of the enzymatic probe system for glucose detected by glucose oxidase

Typically, the sensors were prepared in spectroscopic grade DMSO at concentrations of 2.00 x 10^{-4} mol/L as a stock solution. The stock solutions of glucose were prepared at concentrations of 6.00 x 10^{-3} mol/L in 0.1M HEPES buffer pH 7.4. In a 10.0 mL vial, 0.30 mL of the stock solution of sensor was mixed with the portions of stock solution of glucose to give final concentration of glucose according to **Table 3.4**. After volume were adjusted to 3.00 mL with 0.1M HEPES buffer pH 7.4 to give a final concentration of sensors at 2.00 x 10^{-5} mol/L in 10% DMSO aqueous solution, then 6 units of glucose oxidase were added to the solution mixture of the sensor and the glucose. The mixtures was stirred at 37°C for 60 minutes and placed in a 100.0 mm width quartz cell and then, the fluorescence spectra were recorded at room temperature under the following condition:

	OB
Start (nm)	435
End (nm)	800
Excitation (nm)	415
Excitation Slit	10.0
Emission Slit	10.0
PMT	700
Scan rate	600 nm/min

Table 3.4 Volume of the glucose stock solution (6.00×10^{-3} mol/L) and the final concentration of glucose in 3.00 mL

Volume of glucose stock solution (μL)	Final concentration of glucose in 3.00 mL (M)
5	1.00×10^{-5}
10	2.00×10^{-5}
20	4.00×10^{-5}
30	6.00×10^{-5}
40	8.00×10^{-5}
50	1.00×10^{-4}
100	2.00×10^{-4}
150	3.00×10^{-4}
200	4.00×10^{-4}
500	1.00×10^{-3}
1000	2.00×10^{-3}

3.2.6 The studies of limit of detection of enzymatic probe for glucose

The sensors were prepared in spectroscopic grade DMSO at concentrations of 2.00 x 10^{-4} mol/L as a stock solution. The solution of sensors were mixed with 0.1M HEPES buffer pH 7.4 to give a final concentration of sensors at 2.00 x 10^{-5} mol/L in 10% DMSO aqueous solution. 2.00 mL of sensor solution was placed in a 100.0 mm width quartz cell. Fluorescence spectra were recorded at room temperature after each addition under the following condition for 10 times:

	OB
Start (nm)	435
End (nm)	800
Excitation (nm)	415
Excitation Slit	10.0
Emission Slit	10.0
PMT	700
Scan rate	600 nm/min

3.2.7 The kinetic studies of the boronic anthraquinone based sensors (OB) of the enzymatic probe system using fluorescence spectrophotometry

Typically, the sensors were prepared in spectroscopic grade DMSO at concentrations of 2.00 x 10^{-4} mol/L as a stock solution. The stock solutions of glucose were prepared at concentrations of 6.00 x 10^{-2} mol/L in 0.1M HEPES buffer pH 7.4. In a 10.0 mL vial, 0.30 mL of the stock solution of sensor was mixed with the portions of stock solution of glucose to give final concentration of glucose according to **Table 3.5**. After volume were adjusted to 3.00 mL with 0.1M HEPES buffer pH 7.4 to give a final concentration of sensors at 2.00 x 10^{-5} mol/L in 10% DMSO aqueous solution, then 6 units of glucose oxidase were added to the solution mixture of the sensor and the glucose. The mixtures was stirred at 37°C for 60 minutes and placed in a 100.0 mm width quartz cell and then, the fluorescence spectra were recorded at room temperature every 5 minutes under the following condition:

	OB
Start (nm)	435
End (nm)	800
Excitation (nm)	415
Excitation Slit	10.0
Emission Slit	10.0
PMT	700
Scan rate	600 nm/min

Table 3.5 Volume of the glucose stock solution (6.00×10^{-2} mol/L) and the final concentration of glucose in 3.00 mL

Volume of glucose stock solution (μL)	Final concentration of glucose in 3.00 mL (M)
10	2.00×10^{-4}
15	3.00×10^{-4}
35	7.00×10^{-4}
50	1.00×10^{-3}
70	1.40×10^{-3}
100	2.00×10^{-3}
150	3.00×10^{-3}

3.2.8 Fluorescence measurement of boronic anthraquinone based sensors (OB) in optimum condition of the enzymatic probe system for glucose detection and other competitive saccaharides by glucose oxidase

In a 10.0 mL vial, 0.30 mL of 2.00×10^{-4} mol/L of a sensor in spectroscopic DMSO was mixed with 100 μL of 6.00×10^{-2} mol/L of stock solution including D-glucose, D-galactose, D-fructose, D-sucrose and D-maltose in 0.1M HEPES buffer pH 7.4 and all solutions was adjusted to 3.00 mL to give final concentration of sensors at 2.00×10^{-5} mol/L in 10% DMSO aqueous solution. Then 6 units of glucose oxidase were added to the solution mixture of the sensor and the sugar. The mixture solution was stirred at 37°C for 60 minutes and placed in a 100.0 mm width quartz cell and then fluorescence spectra were recorded at room temperature. Fluorescence measurements of sensors in this section performed under the following condition:

	OB
Start (nm)	435
End (nm)	800
Excitation (nm)	415
Excitation Slit	10.0
Emission Slit	10.0
PMT	700
Scan rate	600 nm/min

3.2.9 Fluorescence measurement of boronic anthraquinone based sensors in optimum condition of the enzymatic probe system in human serum using standard addition

Typically, the sensors were prepared in spectroscopic grade DMSO at concentrations of 2.00 x 10^{-4} mol/L as a stock solution. The stock solutions of glucose were prepared at concentrations of 6.00 x 10^{-2} mol/L in 0.1M HEPES buffer pH 7.4. In a 10.0 mL vial, 0.75 mL of the stock solution of sensor was directly mixed with 10.00 μL of human serum and the portions of stock solution of glucose to give final concentration of glucose according to **Table 3.6**. After volume were adjusted to 3.00 mL with 0.1M HEPES buffer pH 7.4 to give a final concentration of sensors at 5.00 x 10^{-5} mol/L in 10% DMSO aqueous solution, then 6 units of glucose oxidase were added to the solution mixture of the sensor and the glucose. The mixtures solution was stirred at 37°C for 60 minutes and placed in a 100.0 mm width quartz cell and then, the fluorescence spectra were recorded at room temperature under the following condition:

	OB
Start (nm)	435
End (nm)	800
Excitation (nm)	415
Excitation Slit	10.0
Emission Slit	10.0
PMT	600
Scan rate	600 nm/min

Table 3.6 Volume of the glucose stock solution (6.00×10^{-2} mol/L) and the final concentration of glucose in 3.00 mL

Volume of glucose stock solution (μL)	Final concentration of glucose in 3.00 mL (M)
0	0
10	2.00×10^{-4}
20	4.00×10^{-4}
30	6.00×10^{-4}
40	8.00×10^{-4}

3.3 The enzymatic probe studies of the glycoside anthraquinone based sensors

3.3.1 The photochemical studies of glycoside anthraquinone based sensors and theirs derivatives for enzymatic probe system, OAG, PAG, OO and PO for β-glucosidase

3.3.1.1 UV/Vis spectroscopic screening test of sensors

The sensors were prepared in spectroscopic grade DMSO at concentrations of 2.00 $x10^{-4}$ mol/L as a stock solution. The solution of sensors were mixed with 0.1M HEPES buffer pH 7.4 to give a final concentration of sensors at 2.00 $x10^{-5}$ mol/L in 10% DMSO aqueous solution. 2.00 mL of sensor solution was placed in a 100.0 mm width quartz cell. UV/Vis spectra were recorded at 25°C after each addition.

3.3.1.2 Fluorescence spectroscopic screening test of sensors

Typically, the sensors were prepared in spectroscopic grade DMSO at concentrations of 2.00 $x10^{-4}$ mol/L as a stock solution. The solution of sensors were mixed with 0.1M HEPES buffer pH 7.4 to give a final concentration of sensors at 2.00 $x10^{-5}$ mol/L in 10% DMSO aqueous solution. 2.00 mL of sensor solution was placed in a 100.0 mm width quartz cell. Fluorescence spectra were recorded at 25°C after each addition under the following condition:

	OAG	**PAG**	**OO**	**PO**
Start (nm)	428	435	428	444
End (nm)	800	800	800	800
Excitation (nm)	408	415	408	424
Excitation Slit	10.0	10.0	10.0	10.0
Emission Slit	10.0	10.0	10.0	100
PMT	800	800	800	800
Scan rate	600 nm/min	600 nm/min	600 nm/min	600 nm/min

3.3.2 Fluorescence measurement for the optimizing condition of the enzymatic probe system

Fluorescence measurements in this section were performed under the following condition:

	OAG	**PAG**
Start (nm)	428	435
End (nm)	800	800
Excitation (nm)	408	415
Excitation Slit	10.0	10.0
Emission Slit	10.0	10.0
PMT	800	800
Scan rate	600 nm/min	600 nm/min

3.3.2.1 The studies on the effect of unit of β-glucosidase

In a 100.0 mm width quartz cell, 0.30 mL of 2.00 $x10^{-4}$ mol/L of a sensor in spectroscopic DMSO was mixed with 0.1M HEPES buffer pH 7.4 and adjusted to 3.00 mL to give final concentration of sensors at 2.00 $x10^{-5}$ mol/L in 10% DMSO aqueous solution. Then, β-glucosidase in various portions according to **Table 3.7** was added to the solution of the sensor. After stirred the sample for 5 minutes, the fluorescence spectra were then, recoded at room temperature.

Table 3.7 Volume of the β-glucosidase and the final unit of β-glucosidase in 3.00 mL

Volume of the β-glucosidase solution(μL)	Final unit of β-glucosidase in 3.00 mL (unit)
64.5	3
86	4
107.5	5
129	6

3.3.2.2 The pH dependent experiments

In a 10.0 mL vial, 0.30 mL of 2.00 $x10^{-4}$ mol/L of a sensor in spectroscopic DMSO was mixed with 0.1M various buffer (KH phathalate pH 4 - 5.5 and phosphate pH 6 - 7.5) and all solutions were adjusted to 3.00 mL to give final concentration of sensors at 2.00 $x10^{-5}$ mol/L in 10% DMSO aqueous solution. Then, 6 units of β-glucosidase were added to the solution mixture of the sensor and the glucose. The mixture was stirred at room temperature for 5 minutes and placed in a 100.0 mm width quartz cell and then, the fluorescence spectra were recorded at room temperature.

3.3.2.3 The studies on the effect of temperature

In a 10.0 mL vial, 0.30 mL of 2.00 $x10^{-4}$ mol/L of a sensor in spectroscopic DMSO was mixed with 0.1M HEPES buffer pH 7.4 and adjusted to 3.00 mL to give final concentration of sensors at 2.00 $x10^{-5}$ mol/L in 10% DMSO aqueous solution. Then, 5 units of β-glucosidase were added to the solution of the sensor. The mixture was stirred at room temperature and other mixture was stirred at 37 °C for 5 minutes and placed in a 100.0 mm width quartz cell and then, the fluorescence spectra were recorded at room temperature.

3.3.3 Fluorescence measurement of glycoside anthraquinone based sensors in optimum condition of the enzymatic probe system for β-glucosidase detection

Typically, the sensors were prepared in spectroscopic grade DMSO at concentrations of 2.00 x 10^{-4} mol/L as a stock solution. In a 10.0 mL vial, the portions of stock solution of sensor was mixed with 0.1M HEPES buffer pH 7.4 to give final concentration of sensor according to **Table 3.8**. After volume was adjusted to 3.00 mL with 0.1M HEPES buffer pH 7.4 then, 6 units of β-glucosidase were added to the solution mixture of the sensor. The mixtures was stirred at room temperature for 1 minute and placed in a 100.0 mm width quartz cell and then, the fluorescence spectra were recorded every 2 minutes at room temperature under the following condition:

	PAG
Start (nm)	435
End (nm)	900
Excitation (nm)	415
Excitation Slit	10.0
Emission Slit	10.0
PMT	800
Scan rate	600 nm/min

Table 3.8 Volume of the stock solution of sensor (2.00×10^{-4} mol/L) and the final concentration of sensor in 3.00 mL

Volume of sensor stock solution (mL)	Final concentration of sensor in 3.00 mL (M)
0.15	1.00×10^{-5}
0.30	2.00×10^{-5}
0.60	4.00×10^{-5}

3.3.4 Fluorescence measurements for the optimal condition of the micelle system

Fluorescence measurements in this section were performed under the following condition

	PAG
Start (nm)	435
End (nm)	900
Excitation (nm)	415
Excitation Slit	10.0
Emission Slit	10.0
PMT	600
Scan rate	600 nm/min

3.3.4.1 The studies on the effect of surfactant types

In a 10.0 mL vial, 0.30 mL of 2.00 $x10^{-4}$ mol/L of a sensor in spectroscopic DMSO was mixed with 0.60 mL of 10^{-2} mol/L of a solution of a cetyltrimethylammonium bromide (CTAB), sodium dodecyl sulfate (SDS) or Triton X-100 (TX-100) in 0.1M HEPES buffer pH 7.4. The mixture was stirred for 1 minute and then the volume was adjusted to 3.00 mL with 0.1M HEPES buffer pH 7.4 to give the final concentration of 2.00 $x10^{-5}$ mol/L for the sensor and 2.00 $x10^{-3}$ mol/L for the surfactant. After the sample was stirred for 60 minutes, the mixture was placed in a 100.0 mm width quartz cell and then, the fluorescence spectra were recorded at room temperature.

3.3.4.2 The studies of CTAB concentration effect

In a 10.0 mL vial, 0.30 mL of 2.00 $x10^{-4}$ mol/L of a sensor in spectroscopic DMSO was mixed with a 10^{-2} mol/L cetyltrimethylammonium bromide (CTAB) in various portions according to **Table 3.9** and then, the volume of sample was adjusted to 3.00 mL to give the final concentration of 2.00 $x10^{-5}$ mol/L for the sensor. After the sample was stirred for 60 minutes, the mixture was placed in a 100.0 mm width quartz cell and then, the fluorescence spectra were recorded at room temperature.

Table 3.9 Volume of the stock solution of CTAB (1.00 x 10^{-2} mol/L) and the final concentration of sensor in 3.00 mL

Volume of CTAB stock solution (mL)	Final concentration of CTAB in 3.00 mL (M)
0.00	0
0.30	1.00 x 10^{-3}
0.60	2.00 x 10^{-3}
0.90	3.00 x 10^{-3}

3.3.5 The enzymatically activated fluorescence probe for β-glucosidase in micelle systems using fluorescence spectroscopy

Typically, the sensors were prepared in spectroscopic grade DMSO at concentrations of 2.00 x 10^{-4}mol/L as a stock solution. In a 10.0 mL vial, the portion of stock solution of sensor was mixed with 0.6 mL of 1 x 10^{-2} mol/L cetyltrimethylammonium bromide (CTAB) in 0.1M HEPES buffer pH 7.4. After volume was adjusted to 3.00 mL with 0.1M HEPES buffer pH 7.4 then 6 units of β-glucosidase were added to the solution mixture of the sensor. The mixtures was stirred at room temperature for 1 minute and placed in a 100.0 mm width quartz cell and then, the fluorescence spectra were recorded every 2 minutes at room temperature under the following condition:

	PAG
Start (nm)	435
End (nm)	800
Excitation (nm)	415
Excitation Slit	10.0
Emission Slit	10.0
PMT	600
Scan rate	600 nm/min

3.4 Aqueous coordination nanoparticles by adaptive molecular self-assembly

3.4.1 Preparation of nucleotide/lanthanide coordination nanoparticles

The nucleotides (adenine monophosphate (AMP), cytosine monophosphate (CMP), guanine monophosphate (GMP) and uridine monophosphate (UMP)) were prepared in 0.1M HEPES buffer pH 7.4 at concentration of 1.00 x 10^{-2} mol/L as a stock solution. The stock solutions of lanthanide (terbium, Tb^{3+}) were prepared as stock solution at the concentration of 2.00 x 10^{-2} mol/L in spectroscopic grade DMSO. In a 10.0 mL vial, 0.30 mL of the stock solution of nucleotide was mixed with 0.15 mL of the stock solution of lanthanide to give kind of sample according to **Table 3.10**. Then, 0.15 mL of spectroscopic grade DMSO was added to the solution mixture of the sample. After volume were adjusted to 3.00 mL with 0.1M HEPES buffer pH 7.4 to give a final concentration of sample at 1.00 x 10^{-3} mol/L in 10% DMSO aqueous solution. The mixtures were stirred at room temperature for 60 minutes.

Table 3.10 Show the suspensions of nucleotides (adenine monophosphate (AMP), cytosine monophosphate (CMP), guanine monophosphate (GMP), uridine monophosphate (UMP)) as well as lanthanide (terbium (Tb^{3+}))

	AMP	CMP	GMP	UMP
Tb^{3+}	AMP/ Tb^{3+}	CMP/ Tb^{3+}	GMP/ Tb^{3+}	UMP/ Tb^{3+}

3.4.2 Morphology of nucleotide/lanthanide coordination nanoparticles

The nucleotide/lanthanide coordination nanoparticles were prepared as follows. After keeping the mixtures for 60 minutes, the precipitates formed were ultrasonicated for 1 minute before collected by ultracentrifugation (15000 rpm/15 min). The obtained material was washed with MilliQ water (3.00 mL) around 3 times. Then the resultant aqueous suspensions were redispersed by ultrasonicated and observed by scanning electron microscope measurements (SEM).

3.4.3 Fluorescence and phosphorescence measurement of nucleotide/lanthanide coordination nanoparticles

The nucleotide/lanthanide coordination nanoparticles were prepared as follows. After keeping the mixtures for 60 minutes, the resultant aqueous suspensions were ultrasonicated for 1 minute before fluorescence and phosphorescence measurement. Then, the fluorescence and phosphorescence spectra were recorded at room temperature under the following condition:

	Fluorescence	**Phosphorescence**
Start (nm)	424	400
End (nm)	800	700
Excitation (nm)	404	340
Excitation Slit	10.0	20.0
Emission Slit	10.0	20.0
PMT	600	800
Scan rate	600 nm/min	600 nm/min
Total decay time	-	0.005 s
No. of flashes	-	1
Delay time	-	0.100 ms
Gate time	-	1.0 ms

3.4.4 Fluorescence measurement of dye-doped nucleotide/lanthanide coordination nanoparticles

The adenine monophosphate (AMP) was prepared in 0.1M HEPES buffer pH 7.4 at the concentration of 1.00 x 10^{-2} mol/L as a stock solution. The stock solution of terbium (Tb^{3+}) was prepared at the concentration of 2.00 x 10^{-2} mol/L in spectroscopic grade DMSO. In a 10.0 mL vial, 0.30 mL of the stock solution of nucleotide was mixed with 0.15 mL of the 2.00 x 10^{-4} mol/L of stock solution of dyes (**FLU** and **POR**). Then 0.15 mL of the stock solution of terbium (Tb^{3+}) was added to the solution mixture of the sample. After volume were adjusted to 3.00 mL with 0.1M HEPES buffer pH 7.4 to give a final concentration of lanthanide, nucleotide at 1.00 x 10^{-3} mol/L and dyes at 1.00 x 10^{-5} mol/L in 10% DMSO aqueous solution. The mixtures were stirred at room temperature for 60 minutes. After keeping the mixtures for 60 minutes, the resultant aqueous suspensions were ultrasonicated for 1 minute before fluorescence measurement. Then fluorescence spectra were recorded at room temperature under the following condition:

	FLU	**POR**
Start (nm)	503	462
End (nm)	800	800
Excitation (nm)	493	442
Excitation Slit	5.0	10.0
Emission Slit	5.0	10.0
PMT	400	600
Scan rate	600 nm/min	600 nm/min

3.4.5 Fluorescence measurements of boronic anthraquinone based sensors-doped nucleotide/lanthanide coordination nanoparticles for enzymatic probe

The adenine monophosphate (AMP) was prepared in 0.1M HEPES buffer pH 7.4 at the concentration of 1.00 x 10^{-2} mol/L as a stock solution. The stock solution of terbium (Tb^{3+}) was prepared at the concentration of 2.00 x 10^{-2} mol/L in spectroscopic grade DMSO. In a 10.0 mL vial, 0.30 mL of the stock solution of nucleotide was mixed with 0.15 mL of the 2.00 x 10^{-4} mol/L of stock solution of sensor (**OB**). Then 0.15 mL of the stock solution of gadolinium (Gd^{3+}) and 50 μL of the stock solutions of glucose (6.00 x 10^{-3} mol/L) was added to the solution mixture of the sample. After volume were adjusted to 3.00 mL with 0.1M HEPES buffer pH 7.4 to give a final concentration of lanthanide, nucleotide at 1.00 x 10^{-3} mol/L and sensor at 1.00 x 10^{-5} mol/L in 10% DMSO aqueous solution. The mixtures were stirred at room temperature for 60 minutes. Then, 6 units of glucose oxidase were added to the resultant aqueous suspensions solution of the sensor. The mixtures was stirred at room temperature for 1 minute and ultrasonicated for 1 minute before placed in a 100.0 mm width quartz cell and then, the fluorescence spectra were recorded every 5 minutes at room temperature under the following condition:

	OB
Start	435
End	800
Excitation	415
Excitation Slit	10.0
Emission Slit	10.0
PMT	600
Scan rate	600 nm/min

3.4.6 Fluorescence measurements of glycoside anthraquinone based sensors-doped nucleotide/lanthanide coordination nanoparticles for enzymatic probe

The adenine monophosphate (AMP) was prepared in 0.1M HEPES buffer pH 7.4 at the concentration of 1.00 x 10^{-2} mol/L as a stock solution. The stock solution of terbium (Tb^{3+}) was prepared at the concentration of 2.00 x 10^{-2} mol/L in spectroscopic grade DMSO. In a 10.0 mL vial, 0.30 mL of the stock solution of nucleotide was mixed with 0.15 mL of the 2.00 x 10^{-4} mol/L of stock solution of sensor (**PAG**). Then 0.15 mL of the stock solution of gadolinium (Gd^{3+}) was added to the solution mixture of the sample. After volume were adjusted to 3.00 mL with 0.1M HEPES buffer pH 7.4 to give a final concentration of lanthanide, nucleotide at 1.00 x 10^{-3} mol/L and sensor at 1.00 x 10^{-5} mol/L in 10% DMSO aqueous solution. The mixtures were stirred at room temperature for 60 minutes. Then, 6 units of β-glucosidase were added to the resultant aqueous suspensions solution of the sensor. The mixtures was stirred at room temperature for 1 minute and ultrasonicated for 1 minute before placed in a 100.0 mm width quartz cell and then, the fluorescence spectra were recorded every 2 minutes at room temperature under the following condition:

	PAG
Start	435
End	800
Excitation	415
Excitation Slit	10.0
Emission Slit	10.0
PMT	600
Scan rate	600 nm/min

3.5 Aqueous lanthanide nanoparticles by adaptive molecular self-assembly

3.5.1 Preparation of surfactant/lanthanide nanoparticles

Sodium dodecyl sulfate (SDS) was prepared in 0.1 M HEPES buffer pH 7.4 at the concentration of 1.00 x 10^{-2} mol/L as a stock solution. The stock solutions of lanthanide (terbium (Tb^{3+}), gadolinium (Gd^{3+}), Europium (Eu^{3+}) and Lanthanum (La^{3+})) were prepared at concentrations of 2.00 x 10^{-2} mol/L in spectroscopic grade DMSO. In a 10.0 mL vial, 0.30 mL of the stock solution of surfactant was mixed with 0.15 mL of the stock solution of lanthanide to give the kind of sample according to **Table 3.10**. Then, 0.15 mL of spectroscopic grade DMSO was added to the solution mixture of the sample. After volume were adjusted to 3.00 mL with 0.1M HEPES buffer pH 7.4 to give a final concentration of surfactant and lanthanide at 1.00 x 10^{-3} mol/L in 10% DMSO aqueous solution. The mixtures were stirred at room temperature for 180 minutes.

Table 3.10 Show the suspensions of micelle (sodium dodecyl sulfate (SDS)) and lanthanide (terbium (Tb^{3+}), gadolinium (Gd^{3+}), Europium (Eu^{3+}) or Lanthanum (La^{3+}))

	Tb^{3+}	Gd^{3+}	Eu^{3+}	La^{3+}
SDS	SDS/Tb^{3+}	SDS/Gd^{3+}	SDS/Eu^{3+}	SDS/La^{3+}

3.5.2 Morphology of surfactant/lanthanide nanoparticles

The surfactant/lanthanide nanoparticles were prepared as follows. After keeping the mixtures for 180 minutes, the precipitates formed were ultrasonicated for 1 minute before collected by ultracentrifugation (15000 rpm/15 min). The obtained material was washed with MilliQ water (3.00 mL) around 3 times. Then the resultant aqueous suspensions were redispersed in by ultrasonicated and observed by scanning electron microscope measurements (SEM). The transmission electron microscope (TEM) specimen of surfactant/lanthanide nanoparticles was prepared as follows. The surfactant/lanthanide nanoparticles collected by centrifugation was redispersed in MilliQ water (3.00 mL) by ultrasonicated for 1 minute. A drop of the obtained dispersion was placed on carbon-coated copper grid. After 1 minute, the droplet was removed by adsorbing to a piece of filter paper. The specimen was dried in vacuum and monitored by TEM measurements.

3.5.3 Fluorescence and phosphorescence measurement of surfactant/lanthanide nanoparticles

The surfactant/lanthanide nanoparticles were prepared as follows. After keeping the mixtures for 180 minutes, the resultant aqueous suspensions were ultrasonicated for 1 minute before fluorescence measurement. Then, the fluorescence spectra were recorded at room temperature under the following condition:

	Fluorescence
Start (nm)	424
End (nm)	800
Excitation (nm)	404
Excitation Slit	10.0
Emission Slit	10.0
PMT	600
Scan rate	600 nm/min

3.5.4 The encapsulation studies of dye-doped surfactant/lanthanide nanoparticles using UV/Vis spectrophotometry

Sodium dodecyl sulfate (SDS) was prepared in 0.1M HEPES buffer pH 7.4 at the concentration of 1.00 x 10^{-2} mol/L as a stock solution. The stock solution of gadolinium (Gd^{3+}) was prepared at the concentration of 2.00 x 10^{-2} mol/L in spectroscopic grade DMSO. In a 10.0 mL vial, 0.30 mL of the stock solution of surfactant was mixed with 0.15 mL of the 2.00 x 10^{-4} mol/L stock solution of dyes (**FLU**, **APY**, **NAP**, **CUR** and **CURBF**). Then 0.15 mL of the stock solution of gadolinium (Gd^{3+}) was added to the solution mixture of the sample. After volume was adjusted to 3.00 mL with 0.1M HEPES buffer pH 7.4 to give a final concentration of surfactant, lanthanide at 1.00 x 10^{-3} mol/L and dyes at 1.00 x 10^{-5} mol/L in 10% DMSO aqueous solution. The mixtures were stirred at room temperature for 180 minutes. Then, the resultant aqueous suspensions were ultrasonicated for 1 minute before collected by ultracentrifugation (15000 rpm/15 min). Then the resultant aqueous supernatants were placed in a 100.0 mm width quartz cell. UV/Vis spectra were recorded at 25°C after each addition.

3.5.5 Fluorescence measurement of dye-doped surfactant/lanthanide nanoparticles

Sodium dodecyl sulfate (SDS) was prepared in 0.1M HEPES buffer pH 7.4 at the concentration of 1.00 x 10^{-2} mol/L as a stock solution. The stock solution of gadolinium (Gd^{3+}) was prepared at the concentration of 2.00 x 10^{-2} mol/L in spectroscopic grade DMSO. In a 10.0 mL vial, 0.30 mL of the stock solution of surfactant was mixed with 0.15 mL of the 2.00 x 10^{-4} mol/L stock solution of dyes (**FLU**, **APY**, **NAP**, **CUR** and **CURBF**). Then, 0.15 mL of the stock solution of gadolinium (Gd^{3+}) was added to the solution mixture of the sample. After volume were adjusted to 3.00 mL with 0.1M HEPES buffer pH 7.4 to give a final concentration of surfactant, lanthanide at 1.00 x 10^{-3} mol/L and dyes at 1.00 x 10^{-5} mol/L in 10% DMSO aqueous solution. The mixtures were stirred at room temperature for 180 minutes. Then, the resultant aqueous suspensions were ultrasonicated for 1 minute before fluorescence measurements. Then, the fluorescence spectra were recorded at room temperature under the following condition:

	FLU	**APY**	**NAP**	**CUR**	**CURBF**
Start (nm)	504	265	285	440	537
End (nm)	800	800	800	800	800
Excitation (nm)	494	245	265	420	517
Excitation Slit	5.0	10.0	10.0	10.0	10.0
Emission Slit	5.0	10.0	10.0	10.0	100
PMT	400	400	600	600	600
Scan rate	600 nm/min	600 nm/min	600 nm/min	600 nm/min	600 nm/min

	FLU/ MLNPs	**APY/ MLNPS**	**NAP/ MLNPs**	**CUR/ MLNPs**	**CURBF/ MLNPs**
Start (nm)	504	265	285	440	547
End (nm)	800	800	800	800	800
Excitation (nm)	494	245	265	420	527
Excitation Slit	5.0	10.0	10.0	10.0	10.0
Emission Slit	5.0	10.0	10.0	10.0	100
PMT	400	400	600	600	600
Scan rate	600 nm/min	600 nm/min	600 nm/min	600 nm/min	600 nm/min

3.5.6 The studies on the effect of surfactant types towards PAG using fluorescence spectrophotometry

Cetyltrimethylammonium bromide (CTAB), sodium dodecyl sulfate (SDS) and Triton X-100 (TX-100) were prepared in 0.1M HEPES buffer pH 7.4 at the concentration of 1.00 x 10^{-2} mol/L as a stock solution. The stock solution of gadolinium (Gd^{3+}) was prepared as stock solution at concentrations of 2.00 x 10^{-2} mol/L in spectroscopic grade DMSO. In a 10.0 mL vial, 0.30 mL of the stock solution of surfactant was mixed with 0.15 mL of the 2.00 x 10^{-4} mol/L stock solution of dye (**CURBF**). Then 0.15 mL of the stock solution of gadolinium (Gd^{3+}) was added to the solution mixture of the sample. After volume were adjusted to 3.00 mL with 0.1 M HEPES buffer pH 7.4 to give a final concentration of surfactant, lanthanide at 1.00 x 10^{-3} mol/L and dyes at 1.00 x 10^{-5} mol/L in 10% DMSO aqueous solution. The mixtures were stirred at room temperature for 180 minutes. Then, the resultant aqueous suspensions were ultrasonicated for 1 minute before fluorescence measurement. Then, the fluorescence spectra were recorded at room temperature under the following condition:

	CURBF/MLNPs
Start (nm)	547
End (nm)	800
Excitation (nm)	527
Excitation Slit	10.0
Emission Slit	100
PMT	600
Scan rate	600 nm/min

3.5.7 Fluorescence measurement of glycoside anthraquinone based sensors-doped surfactant/lanthanide coordination nanoparticles for enzymatic probe

Sodium dodecyl sulfate (SDS) was prepared in 0.1M HEPES buffer pH 7.4 at the concentration of 1.00 x 10^{-2} mol/L as a stock solution. The stock solution of gadolinium (Gd^{3+}) was prepared at the concentration of 2.00 x 10^{-2} mol/L in spectroscopic grade DMSO. In a 10.0 mL vial, 0.30 mL of the stock solution of surfactant was mixed with 0.15 mL of the 2.00 x 10^{-4} mol/L stock solution of sensor (**PAG**). Then, 0.15 mL of the stock solution of gadolinium (Gd^{3+}) was added to the solution mixture of the sample. After volume were adjusted to 3.00 mL with 0.1 M HEPES buffer pH 7.4 to give a final concentration of surfactant, lanthanide at 1.00 x 10^{-3} mol/L and sensor at 1.00 x 10^{-5} mol/L in 10% DMSO aqueous solution. The mixtures were stirred at room temperature for 180 minutes. Then, 6 units of β-glucosidase were added to the resultant aqueous suspensions solution of the sensor. The mixtures was stirred at room temperature for 1 minute and ultrasonicated for 1 minute before placed in a 100.0 mm width quartz cell and then, the fluorescence spectra were recorded every 2 minutes at room temperature following condition:

	PAG/MLNPs
Start (nm)	424
End (nm)	800
Excitation (nm)	404
Excitation Slit	10.0
Emission Slit	10.0
PMT	800
Scan rate	600 nm/min

CHAPTER IV

RESULTS AND DISCUSSIONS

4.1 Design concept of enzymatically activated sensors for glucose oxidase

Our research has focused on the design and synthesis of the molecule which can be enzymatic probes for biomolecule such as sugar, protein, etc in vivo. These make use of biocomponents capable of recognizing bio- or chemical species and transforming them into a product through a chemical reaction. This type of biosensor is represented mostly by enzymatic biosensors, which make use of specific enzymes or their combinations. Typically, the fluorogenic sensors consist of receptor units that can react with target biomolecule and signaling units connecting with the spacer. In the field of supramolecule chemistry, recognition events occur via non-covalent interactions including hydrogen bonding, electrostatic interactions, ion-dipole interactions, cation-π interactions and π-π stacking interactions. It is well known that those interactions played an important role in biological systems due to the selectivity and sensitivity. In natural system, an effective non-covalent recognition of host and guest are derived from complicated molecules or systems that are able to expel or strip the solvated water molecules from the binding site of the host guest molecule resulting in perfect recognitions. However, the vivo system has aqueous everywhere then many synthetic receptors based on non-recognition are still incapable function in aqueous system because guest molecules are solvated by water. Consequently, the synthetic receptors used in water are less effective. Moreover, the vivo system has many molecules that able interfere the interaction between the synthetic receptors and the target molecules. In order to overcome the solvation problem and interference from other molecules, the enzymatically activated system was introduced to case in form of sensory molecule. In our research, the boronic acid was candidate for enzymatically activated system by glucose oxidase for glucose detection. Typically, the glucose oxidase produces the gluconic acid and the generated hydrogen peroxide. The previous works reported [113] that boronic acid can be oxidized to be hydroxyl group

by hydrogen peroxide. This approach motivates to design the boronic based receptor to detect glucose by enzymatic probe using fluorescence spectroscopy.

There are two main types of optical biosensors: The first exploits any changes that can occur in the intrinsic optical property of the biomolecule as a result of its interaction with the target analyte. Such changes can occur in absorbance, emission, polarization, or luminescence decay time of a receptor. Such sensors are not numerous because their sensitivity is usually low, and because many effects occur in the deep UV where spectroscopy has academic merits but is difficult to implement when it comes to analyzing complex (such as environmental or clinical) samples. An additional challenge when using intrinsic biosensors consists of the separation of the shortwave signal from background fluorescence (or absorbance). Enzymes using FAD as a coenzyme are examples of more longwave absorbing receptors that undergo intrinsic spectral changes on binding a ligand (during catalytic conversion), as are some cytochromes and hemoglobin. The second type of biosensor is making use of optical labels and probes of various kinds. This requires the biomolecule to be covalently labeled (an extra step) but enables the analytical wavelength(s) to be shifted to almost any desired value. Moreover, luminescence decay times and anisotropy can be adjusted to the desired values, and effects such as dynamic or static quenching can be exploited in a more systematic manner. Not surprisingly, luminescent labels are widely used for this purpose. In recent years, the use of luminescent nanoparticles has strongly increased. Regarding to signaling system, optical output such as color, absorption spectra and especially fluorescence spectra was usually due to sensitivity and uncomplicated instrumental readout. Hypothetically, the conjugation of an electron acceptor such a quinine derivative with electron donor such an imidazole as a main acceptor-donor segment (main A-D system) performs intramolecular charge transfer signaling system which is sensitive to a small perturbation. Conjugative connecting of reactive recognition site as a boronic acid to main A-D site was expected to afford the large response to the recognition events. Designed receptors based on boronic anthraquinone and derivatives were depicted in **Scheme 4.1**

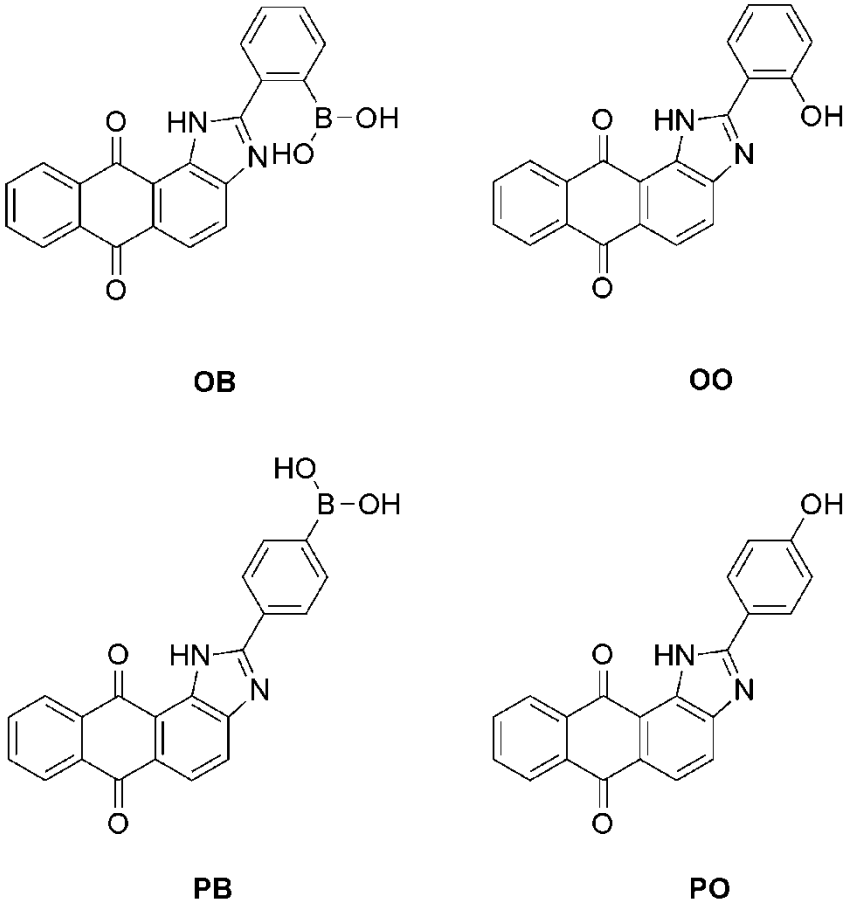

Scheme 4.1 Structures of designed receptors based on anthraquinone, imidazole and boronic acid

From these mentioned above, anthraquinone was chosen to fabricate a main electron acceptor segment of the synthesized receptors and to study the enzymatic probe for glucose by glucose oxidase catalytic enzyme measured by fluorescent measurements. The synthetic pathway is shown in **Scheme 4.2**.

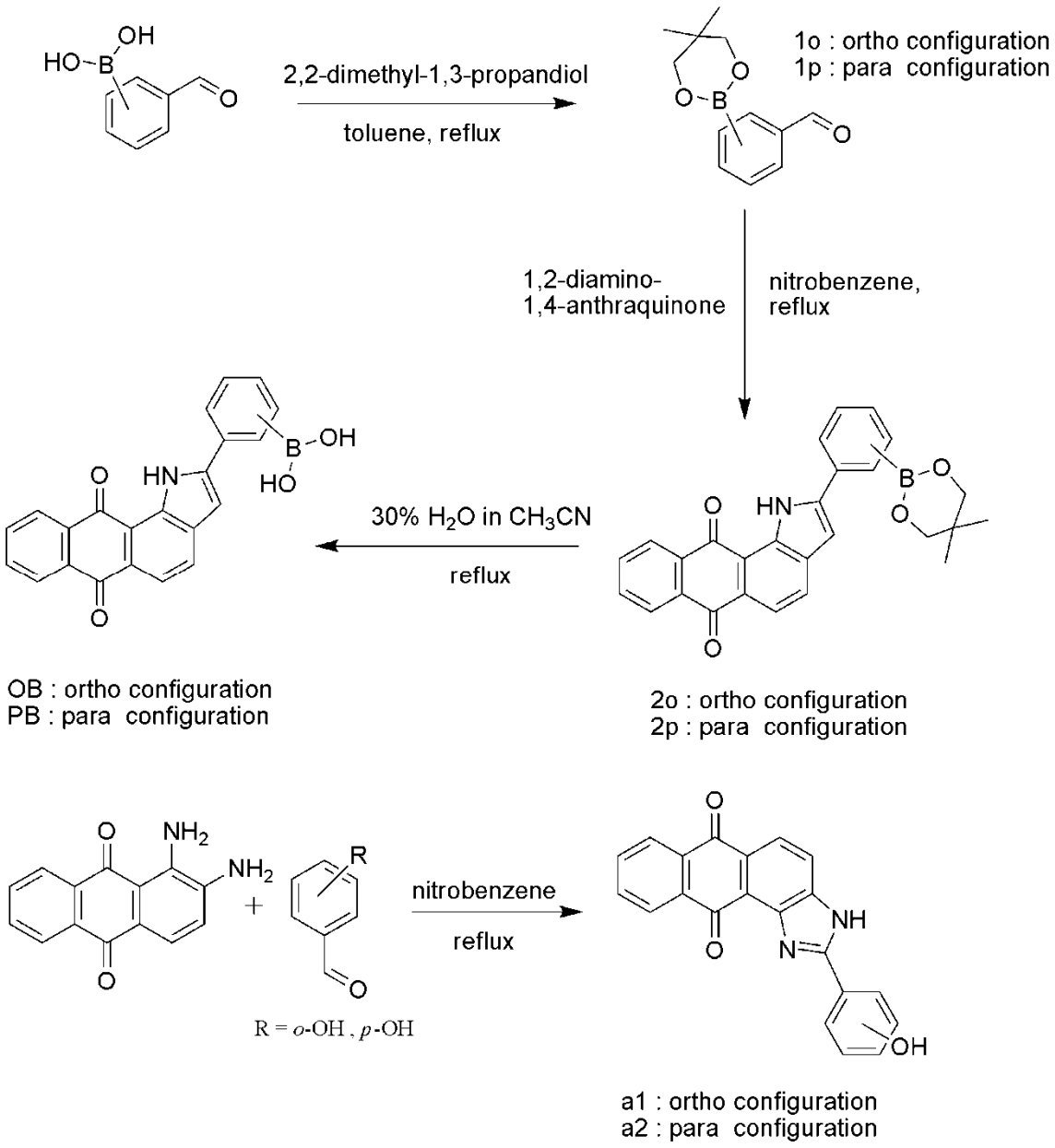

Scheme 4.2 Synthesis pathway of boronic anthraquinone (**OB** and **PB**) and their derivatives (**OO** and **PO**)

4.2 Synthesis and characterization of boronic anthraquinone based sensors and their derivatives

In order to avoid the side reaction due to weak Lewis acid properties of boronic acid, the synthetic pathway was started by protecting the boronic group of appropriated formyl phenyl boronic acids using 2,2-dimethyl-1,3-propandiol in refluxing toluene. Dean-stark apparatus was equipped with the reaction flask in order to remove water from the condensation reaction. After refluxing overnight and removing of toluene, the clear oil of the protected formyl phenyl boronate products were obtained. The crude product was used in the next step without the purification and confirmed by ^{1}H-NMR spectroscopy by the appearance of ethylene chain as a singlet peak at 3.81 and 3.48 ppm for ortho isomer (**1o**) and 3.79 ppm for para isomer (**1p**).

The key step of the synthesis is the oxidative condensation of diamine and aldehyde to yield the desired heterocyclic imidazole. Protecting of compounds **OB** and **PB** (**2o** and **2p**) were prepared by condensation of 1,2-diamino-1,4-anthraquinone with the corresponding formyl phenyl boronate ester in refluxing nitrobenzene and the reaction was kept at 150 ^{o}C for 1 day. Compounds **2o** and **2p** were separated from the reaction mixture by precipitation to obtain a brown solid of the protecting product **2o** (45 %yield) and a yellow solid of the protecting product **2p** (60 %yield). Structure of the heterocyclic products **2o** and **2p** were assured by ^{1}H-NMR spectroscopy (**Figure 4.1**). Interestingly, NH imidazole protons were found at 13.56 and 10.18 ppm for **2o** and **2p**, respectively. This is indicative of a very high acidic proton due to the intramolecular hydrogen bonding between NH-imidazole and oxygen of anthraquinone.

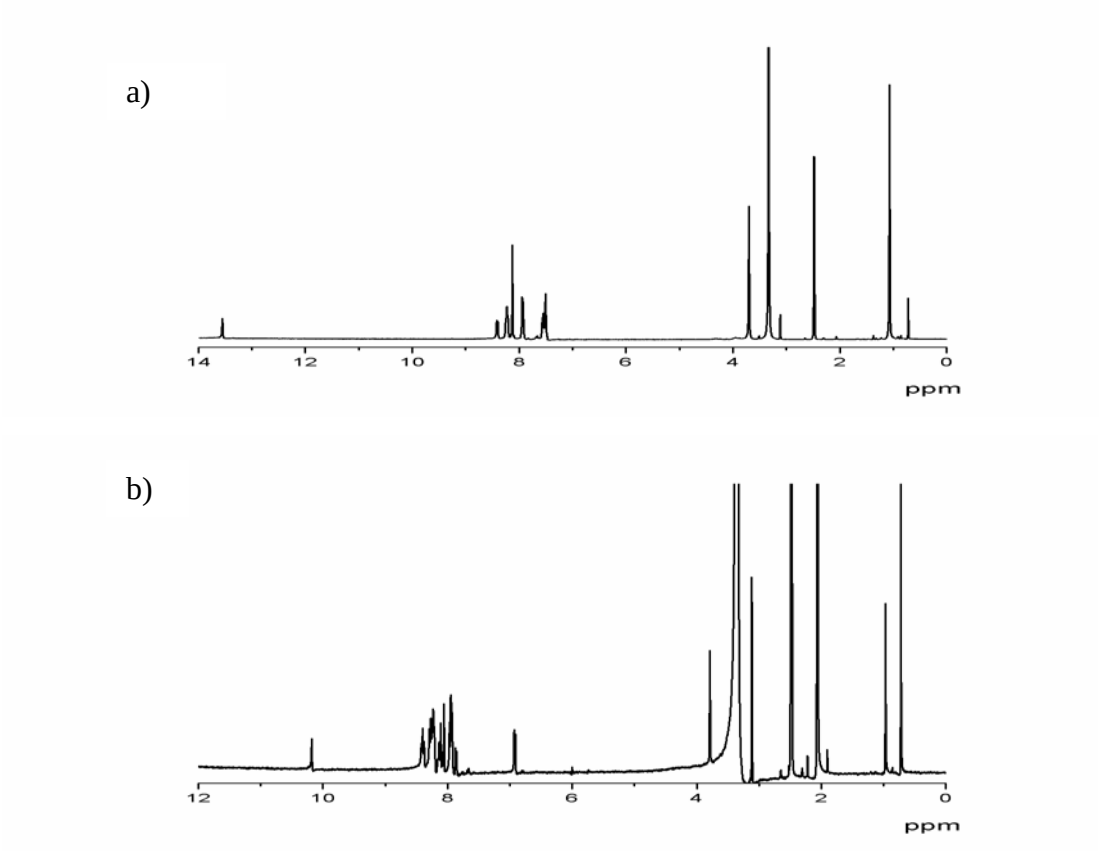

Figure 4.1 ^{1}H-NMR spectra (400 MHz, DMSO-d_6) for a) **2o** and b) **2p**

In order to remove the protecting boronate group, compounds **2o** and **2p** were refluxed in 30%H_2O in CH_3CN to give the protonated sensors **OB** as yellow solids and brown solids of product **PB**. Compounds **OB** and **PB** were characterized by ^{1}H-NMR, MADI-TOF and High resolution mass spectroscopy. As displayed in **Figure 4.2**, ^{1}H-NMR spectra showed that the protecting groups were completely removed by the appearance of hydroxyl signals of the boronic acid moiety and the vanishing of proton signals of the ethoxy chains. Considering each isomer, the ^{1}H-NMR spectrum of **OB** clearly showed the feature of the desired compound by the appearance of signal of acidic protons of imidazole signal at 13.76 ppm.

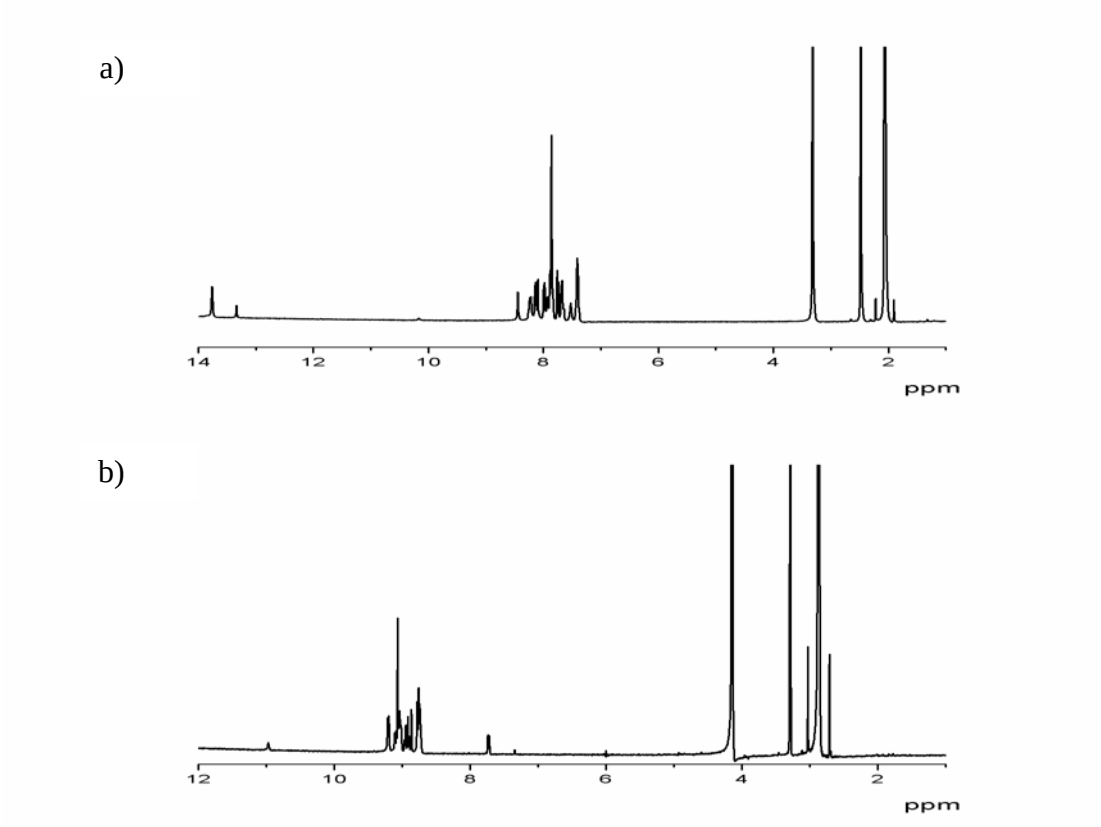

Figure 4.2 ^{1}H-NMR spectra (400 MHz, DMSO-d_6) for a) **OB** and b) **PB**

4.3 The enzymatic probe studies of the boronic anthraquinone based sensors

4.3.1 The photochemical studies of boronic anthraquinone based sensors and their derivatives for enzymatic probe system of OB, PB, OO and PO for glucose oxidase

The absorption properties of boronic anthraquinone (**OB** and **PB**) based sensors and their derivatives (**OO** and **PO**) showed a light yellow color solution and the visible absorption bands at 415, 398, 408 and 424 nm for **OB**, **PB**, **OO** and **PO**, respectively (shown in **Table 4.1** and **Figure 4.3**). From these results, the light yellow color and the visible absorption bands obtained the effect from the migration of electron density from electron donating group of amino on imidazole ring to electron acceptor group of anthraquinone. Compared to the parent compound, 1,2-diamino-1,4-anthraquinone (λ_{max} = 495 nm, $E_g \approx 2.50$ eV, **Figure A.26**), boronic anthraquinone based sensors provided a large energy gap ($E_g \approx 2.98$-3.12 eV) due to the attachment of electron deficient group (boronic acid) to the structure.

Table 4.1 Photophysical properties of the boronic anthraquinone (**OB** and **PB**) based sensors and their derivatives (**OO** and **PO**) in 10% DMSO with 0.1M HEPES buffer at pH 7.4.

Receptors	λ_{abs} (nm)	λ_{em} (nm)	Φ_f[a]
OB	415	609	0.844
PB	398	589	0.377
OO	408	n.d.[b]	0.015
PO	424	n.d.[b]	0.031

[a] Quantum yields were determined using quinine sulfate as the standard (ΦSTD) 0.508 in 1N H_2SO_4.

[b] Values cannot be determined.

As expected, the boronic anthraquinone based sensors exhibit emission properties as listed in **Table 4.1**. Their quantum yield in 10% DMSO with 0.1M HEPES buffer at pH 7.4, in aqueous solution was quite low in the attribution of the characteristic of low lying n-π^* excited state in anthraquinone compound resulting in dominating of intersystem crossing relaxation pathway [121].

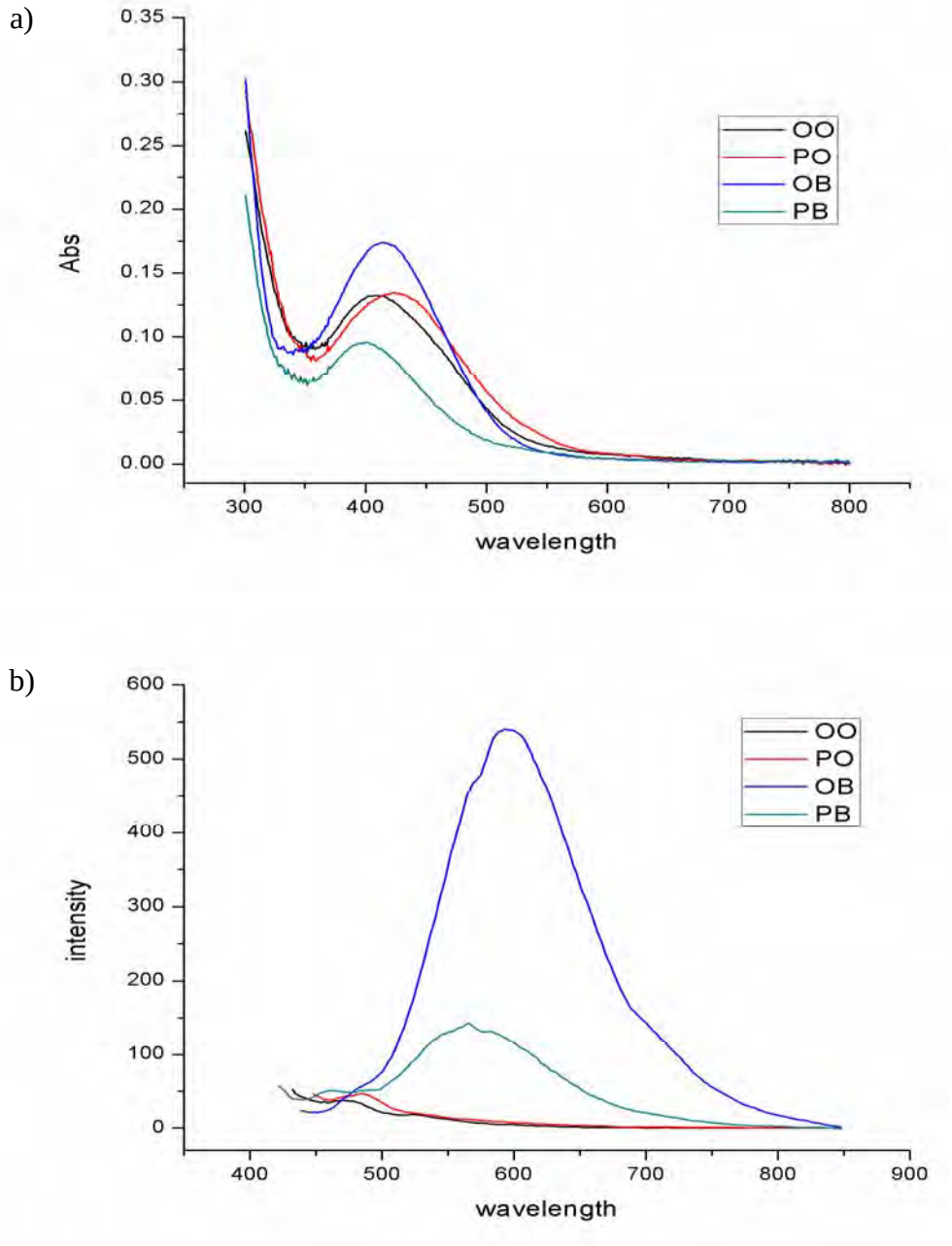

Figure 4.3 a) Absorption spectra and **b)** emission spectra of **OO**, **PO**, **OB** and **PB** in 10% DMSO with 0.1M HEPES buffer at pH 7.4.

4.3.2 The complexation studies of the boronic anthraquinone based sensors with glucose using fluorescence titration experiments

The aim of this work focused on the evaluation of the boronic anthraquinone based sensors used for detection of glucose on enzymatically activated system. A glucose oxidase is an enzyme that can oxidize the glucose to produce hydrogen peroxide and gluconic acid. To apply **OB** and **PB** in complicated systems, they were expected to detect the hydrogen peroxide that was generated from the oxidation of glucose by glucose oxidase which is selective enzyme for only glucose. Our hypothesis is that the amount of the generated hydrogen peroxide was proportional to the amount of glucose. Since **OB** and **PB** curtain boronic group which can actually bind with saccharides. The complexation abilities of sensors (**OB** and **PB**) with various concentration of glucose were investigated by the fluorometric titration in 10% DMSO with 0.1M HEPES buffer at pH 7.4. The fluorescence response of **OB** showed the insignificant changes upon adding glucose (shown in **Figure 4.4**) while the fluorescence response of **PB** showed the large spectral change upon adding glucose (shown in **Figure 4.5**). At high equivalent of glucose, the solution of **PB** became less emissive with a 2-fold fluorescence compared to the absence of glucose. Considering the titration curve (**Figure 4.6**) of **OB** and **PB** with glucose and without glucose oxidase in system, the results showed that **PB** can interact directly with glucose while no effect of glucose towards **OB** was observed. This can be described that boronic acid on para isomer has no steric hindrance for glucose.

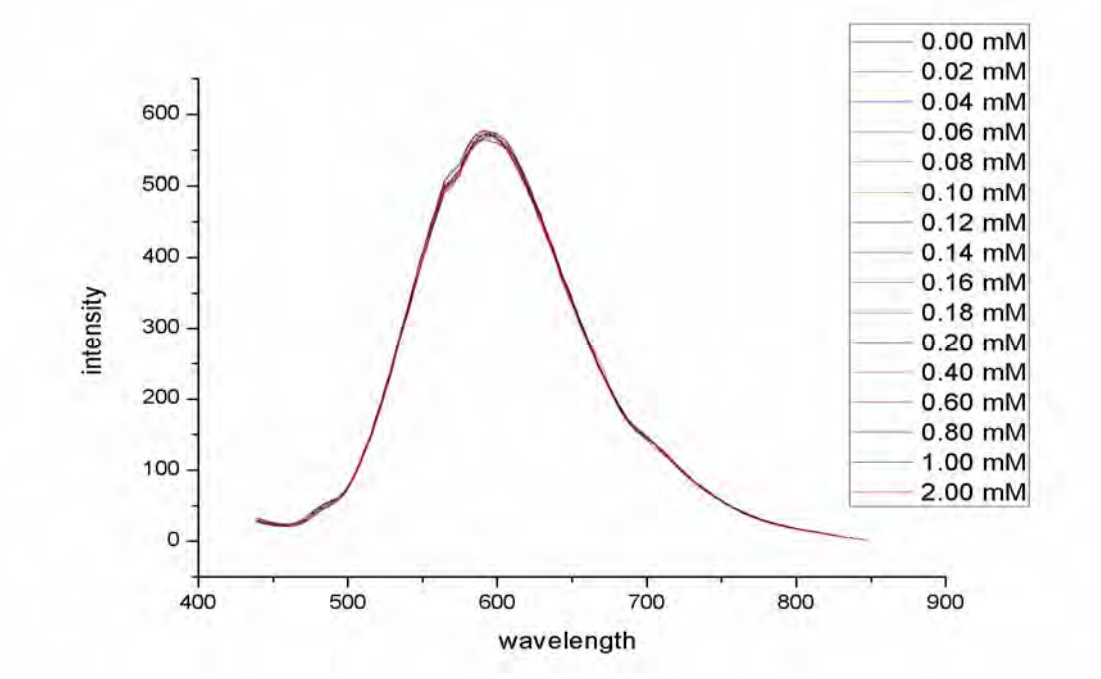

Figure 4.4 Emission spectra of 20 µM **OB** titrated with glucose in 10% DMSO with 0.1M HEPES buffer at pH 7.4.

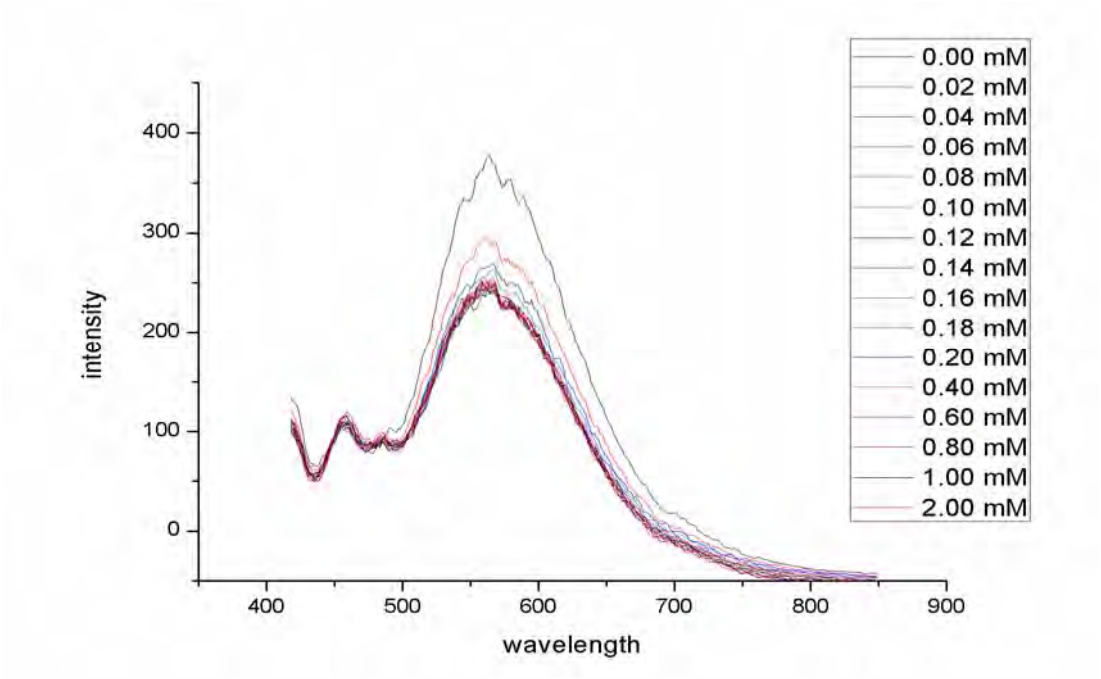

Figure 4.5 Emission spectra of 20 µM **PB** titrated with glucose in10% DMSO with 0.1M HEPES buffer at pH 7.4.

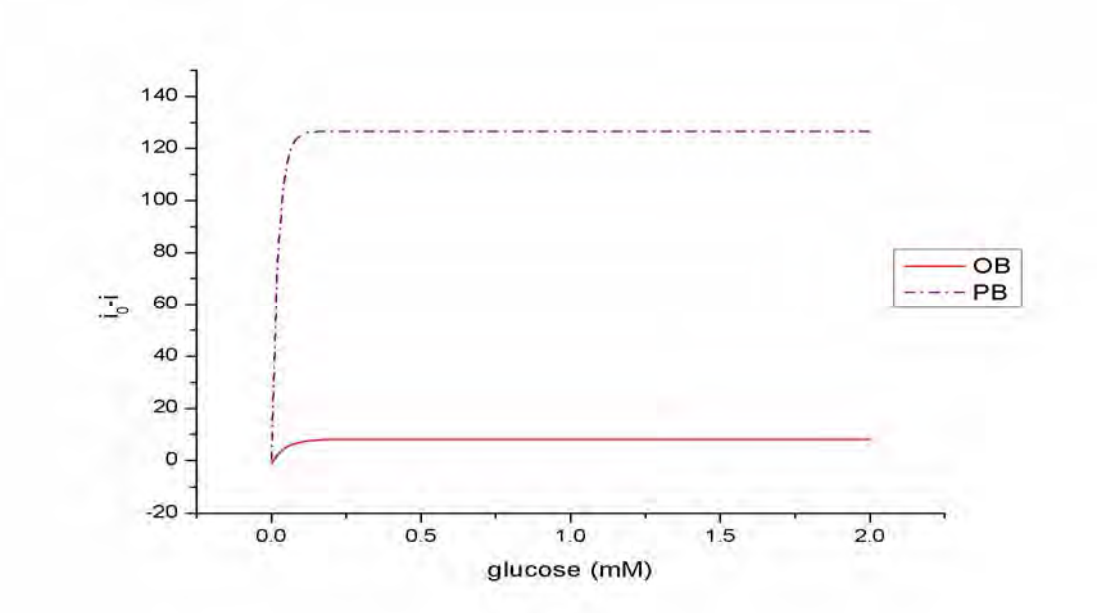

Figure 4.6 Emission intensity at 609 and 589 nm of 20 µM **OB** and **PB**, respectively and titrated with glucose in 10% DMSO with 0.1M HEPES buffer at pH 7.4. $\mathbf{i_0}$ is the intensity in the absence of glucose. **i** is a variation of the emission intensity in the presence of glucose.

4.3.3 The reaction studies of the boronic anthraquinone based sensors with hydrogen peroxide using fluorescence titration experiments

Next, we would like to check the direct reaction of boronic acid and hydrogen peroxide by fluorescence titration in 10% DMSO with 0.1M HEPES buffer at pH 7.4. From the fluorescence spectra and titration curve of **OB** and hydrogen peroxide (**Figure 4.7** and **Figure 4.9**), they exhibited the fluorescence quenching at 609 nm as a function of the concentration of hydrogen peroxide added and the fluorescence response is constant at the high concentration of H_2O_2. In the case of **PB** and H_2O_2 the fluorescence spectra and titration curve (**Figure 4.8** and **Figure 4.9**) at 589 nm increased after adding a small amount of H_2O_2 and then were quenched and gradually constant upon the addition of more amount of H_2O_2. These results suggested that **OB** should be a suitable sensory molecule for detection of H_2O_2 and future applied to the glucose sensing in 10% DMSO with 0.1M HEPES buffer at pH 7.4.

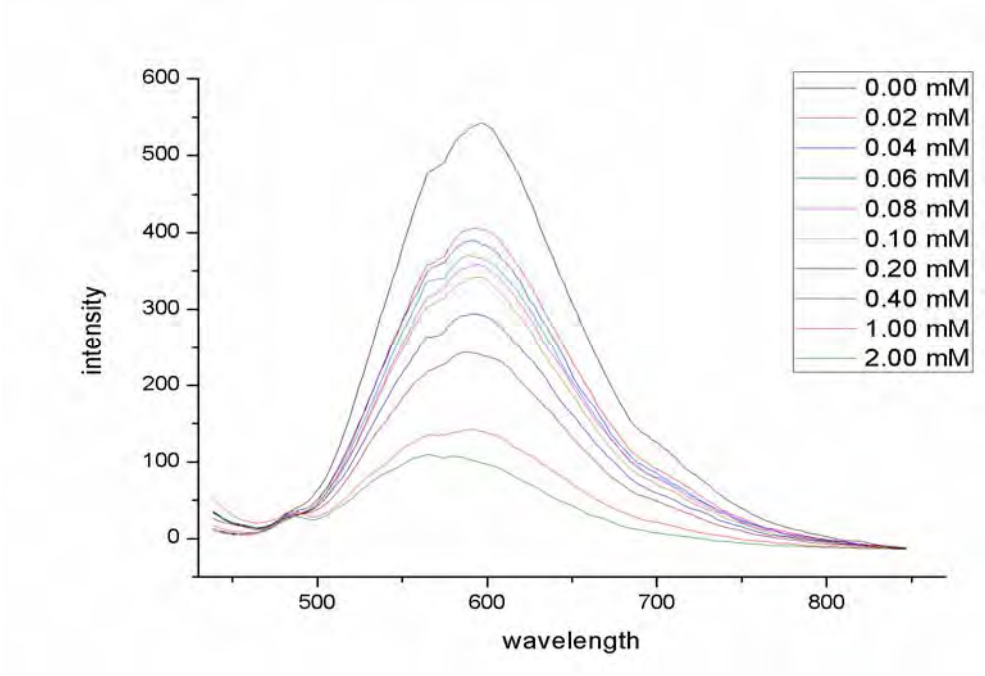

Figure 4.7 Emission spectra of 20 µM **OB** titrated with hydrogen peroxide in 10% DMSO with 0.1M HEPES buffer at pH 7.4.

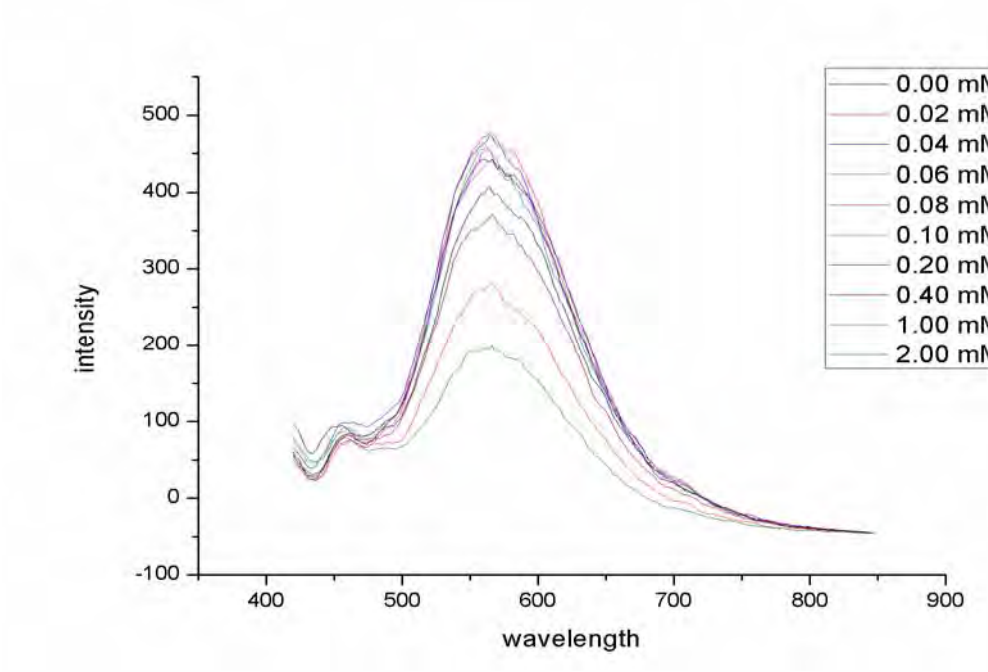

Figure 4.8 Emission spectra of 20 µM **PB** titrated with hydrogen peroxide in 10% DMSO with 0.1M HEPES buffer at pH 7.4.

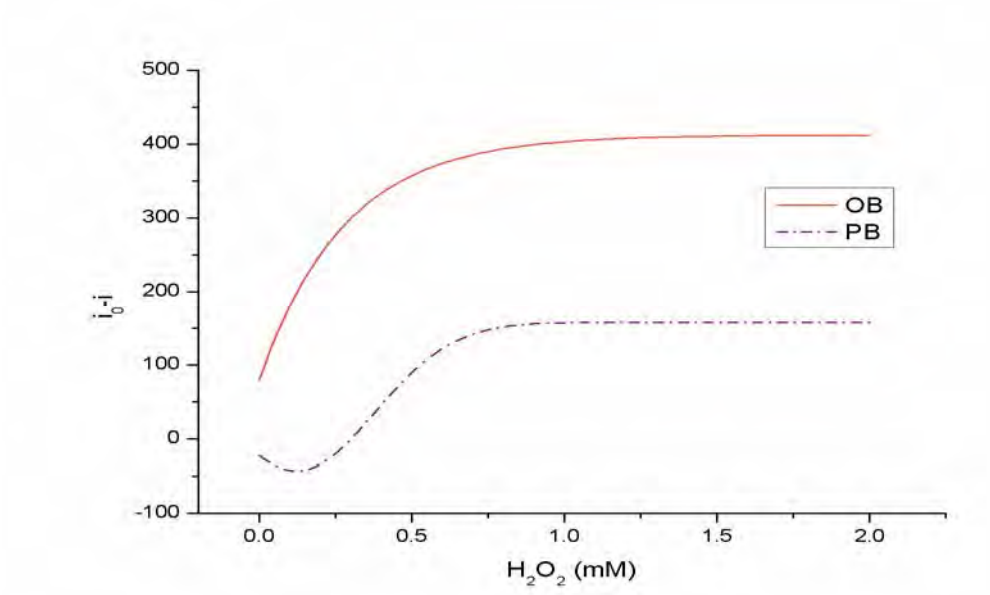

Figure 4.9 Emission intensity at 609 and 589 nm of 20 µM **OB** and **PB**, respectively and titrated with hydrogen peroxide in 10% DMSO with 0.1M HEPES buffer at pH 7.4. $\mathbf{i_0}$ is the intensity in the absence of hydrogen peroxide. **i** is a variation of the emission intensity in the presence of hydrogen peroxide.

4.3.4 Fluorescence measurement for the optimizing condition of the enzymatic probe system

As described above, **OB** is a good candidate for fluorogenic sensor to detect glucose by enzymatic probe with glucose oxidase. The assumed mechanism for detection of glucose was illustrated in **Scheme 4.3** which described that the characteristic **OB** exhibited a strong fluorescence. After adding glucose in the solution of **OB** and glucose oxidase, the boronic based sensor was converted to be hydroxyl group by H_2O_2 which were generated from the reaction of glucose and glucose oxidase. Consequently, the hydroxyl based sensor **OO** showed weak fluorescence intensity. Therefore, we must optimize the condition for enzymatic probe system.

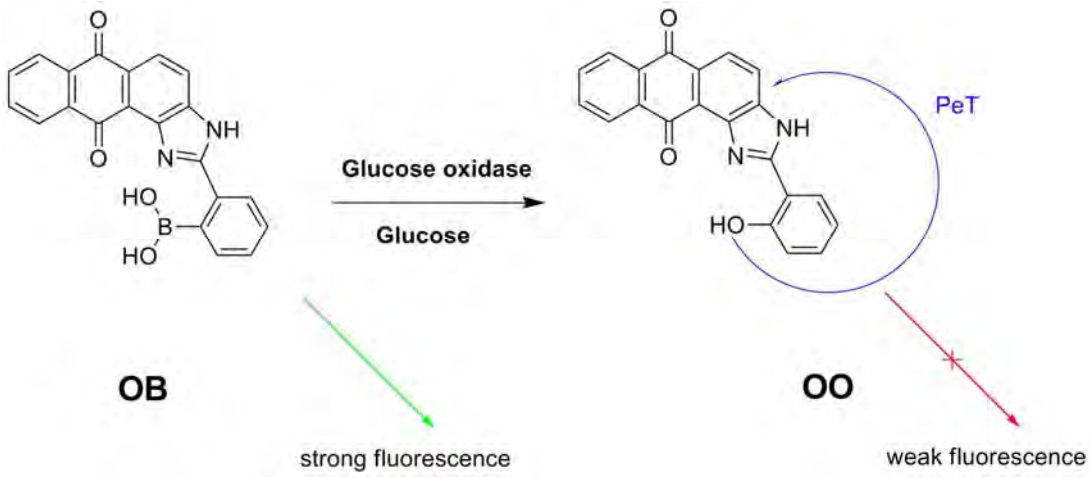

Scheme 4.3 Reaction scheme of **OB** before and after the reaction with glucose oxidase

4.3.4.1 The studies on the effect of amount of glucose oxidase

To optimize the appropriate amount of glucose oxidase for the high efficiency of enzymatic probe system by fluorescence measurements. The amount of unit of glucose oxidase used in this enzymatic probe for **OB** was carried out from 0 to 9 units of glucose oxidase. As the results shown in **Figure 4.10**, the fluorescence responses of **OB** at 6 and 9 units of glucose oxidase displayed a large fluorescence quenching of **OB**. It indicated that this amount of glucose oxidase could generate enough H_2O_2 to interact with boronic acid based sensor (**OB**). To reduce the fluorescence response of glucose oxidase, we have utilized 6 units of glucose oxidase in optimal condition for enzymatic probe system.

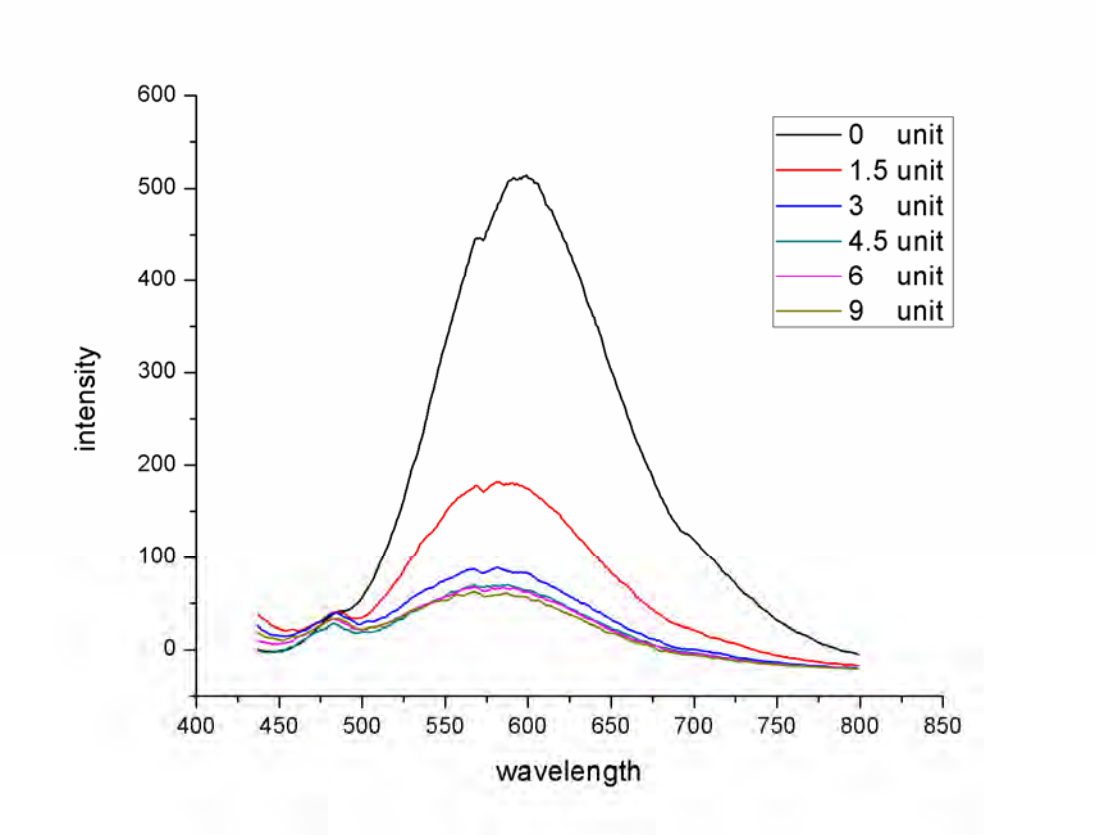

Figure 4.10 Emission intensity of 20 µM **OB** and 2mM of glucose at 609 nm with various unit of glucose oxidase in enzymatic probe system in 10% DMSO with 0.1M HEPES buffer at pH 7.4.

4.3.4.2 The studies on the effect of temperature

Moreover, the optimum enzymatic probe systems with different temperature were also explored. **Figure 4.11** showed the effect of the temperature toward the enzymatic probe system. As expected, a high temperature was able to change emission response better than the room temperature. Therefore, all manipulations of the enzymatic probe system were carried out at 37 ^{o}C temperature.

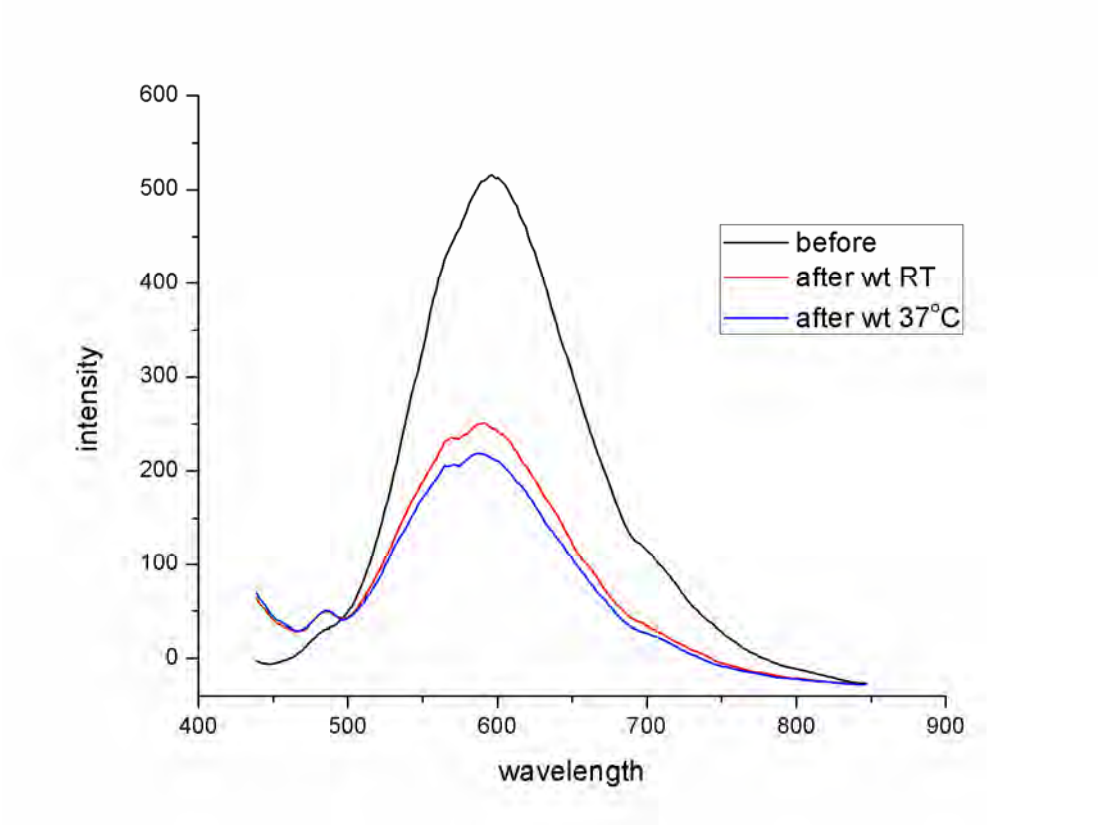

Figure 4.11 Emission intensity of 20 µM **OB** and 2 mM of glucose at 609 nm with room temperature and 37°C in enzymatic probe system in 10% DMSO with 0.1M HEPES buffer at pH 7.4.

4.3.4.3 The studies on the reaction time

To optimize the reaction time, the fluorescence measurement of the solution of sensor (**OB**), glucose and glucose oxidase was monitored every 5 minutes until 120 minutes. (shown in **Figure 4.12**) The emission band at 609 nm of **OB** was gradually decreased upon increase of time. However, we chose the reaction time of 60 minutes which is not too long time and the fluorescence quenching is significant change, in optimizing condition of the enzymatic probe system.

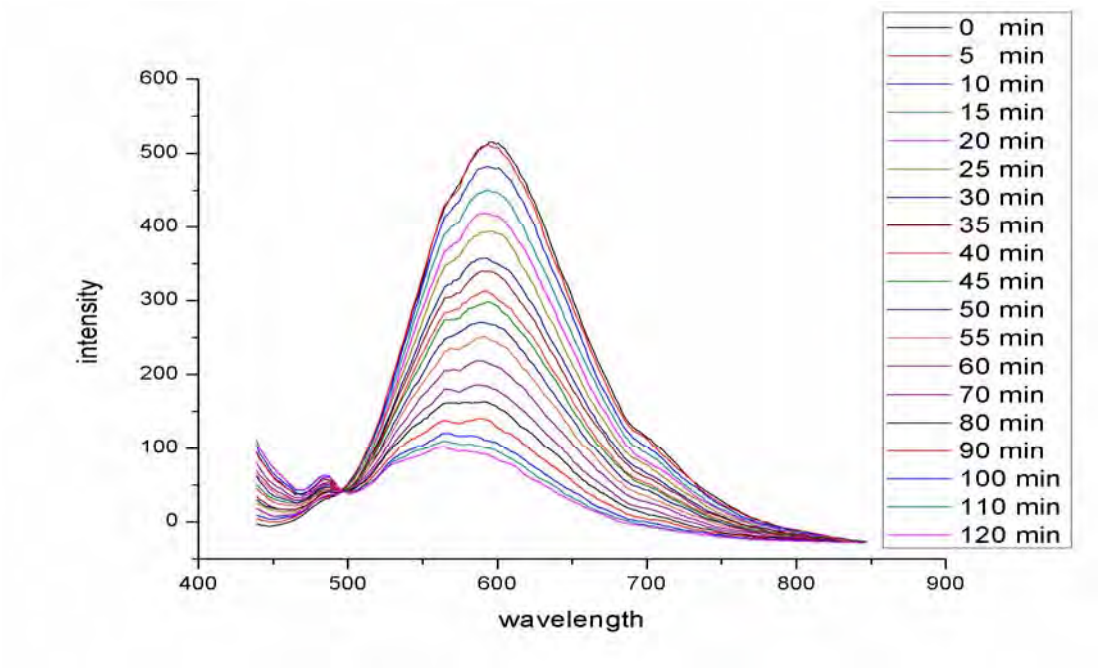

Figure 4.12 Emission intensity of 20 µM **OB** and 2mM of glucose at 609 nm in enzymatic probe system in 10% DMSO with 0.1M HEPES buffer at pH 7.4.

4.3.5 Fluorescence measurement of boronic anthraquinone based sensors (OB) for detection of glucose by glucose oxidase in the optimum condition of the enzymatic probe system

To verify the sensing properties of the boronic anthraquinone based sensors (**OB**), the fluorescence titration between **OB** and glucose in the presence of glucose oxidase was investigated in the optimum condition of enzymatic probe system. As depicted in **Figure 4.13**, the emission band at 609 nm of **OB** was gradually decreased upon the increment of glucose and was approximately constant at high concentration of glucose. To normalize the fluorescence titration of enzymatic probe system of **OB**, the calibration curve was plotted between i_0-i and the glucose concentration (shown in **Figure 4.14**). The fluorescence response was linear in the range of 0.08 to 0.42 mM with the acceptable correlation coefficient (R^2) of 0.99082 (**Figure 4.15**). Therefore, the range of concentration for glucose sensing by the enzymatic probe system is 0.08 -

0.42 mM. The limit of detection (LOD) of **OB** for glucose detection is approximately 0.0114 mM or 11 µM.

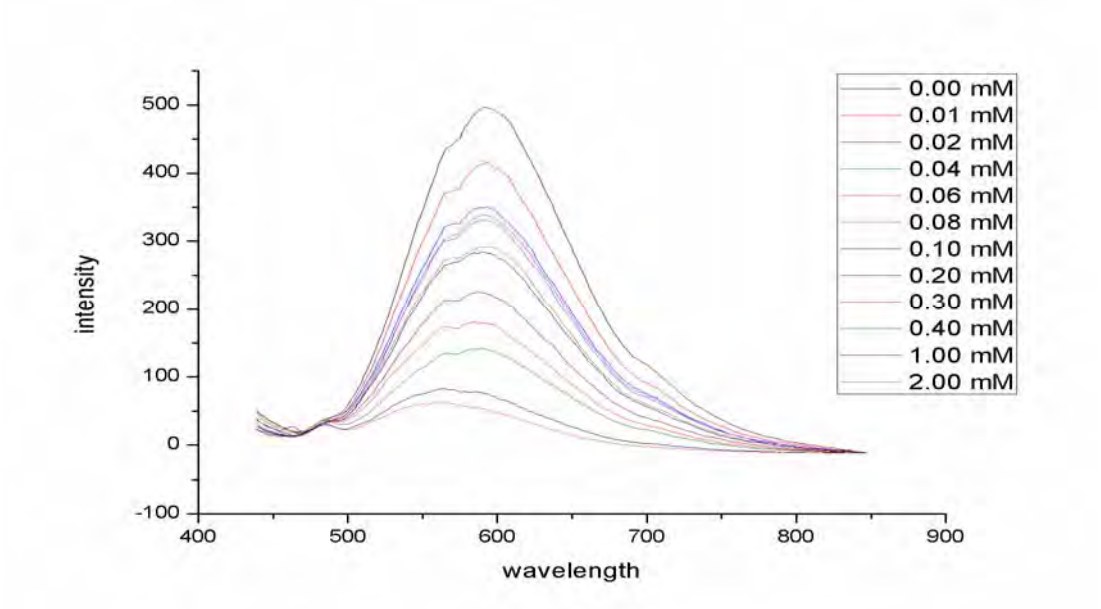

Figure 4.13 Emission intensity of 20 µM **OB** at 609 nm in enzymatic probe system in 10% DMSO with 0.1M HEPES buffer at pH 7.4.

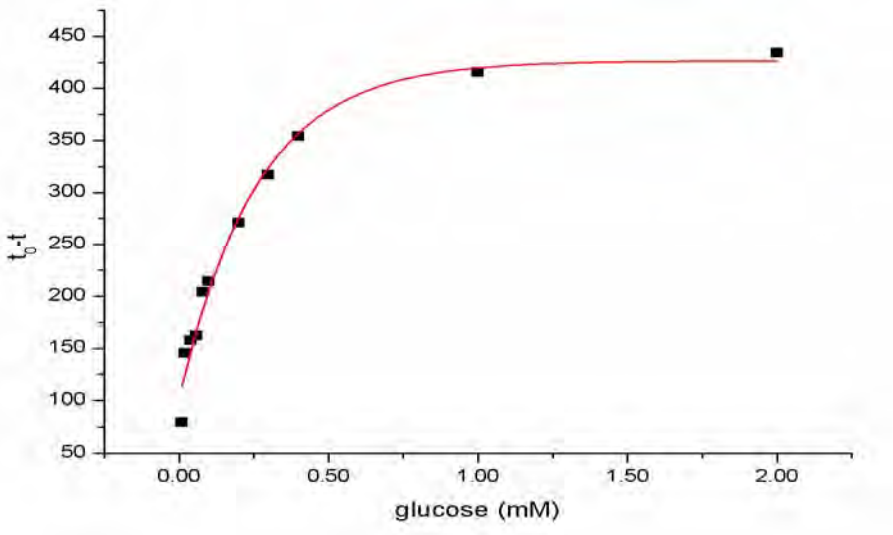

Figure 4.14 Fluorescence titration curve of 20 µM **OB** and 6 units of glucose oxidase titrated with glucose in 10% DMSO with 0.1M HEPES buffer at pH 7.4. The excitation wavelength was 415 nm. The reaction was performed at 37°C and 1 hour. $\mathbf{i_0}$ is the intensity in the absence of glucose. **i** is a variation of the emission intensity in the presence of glucose.

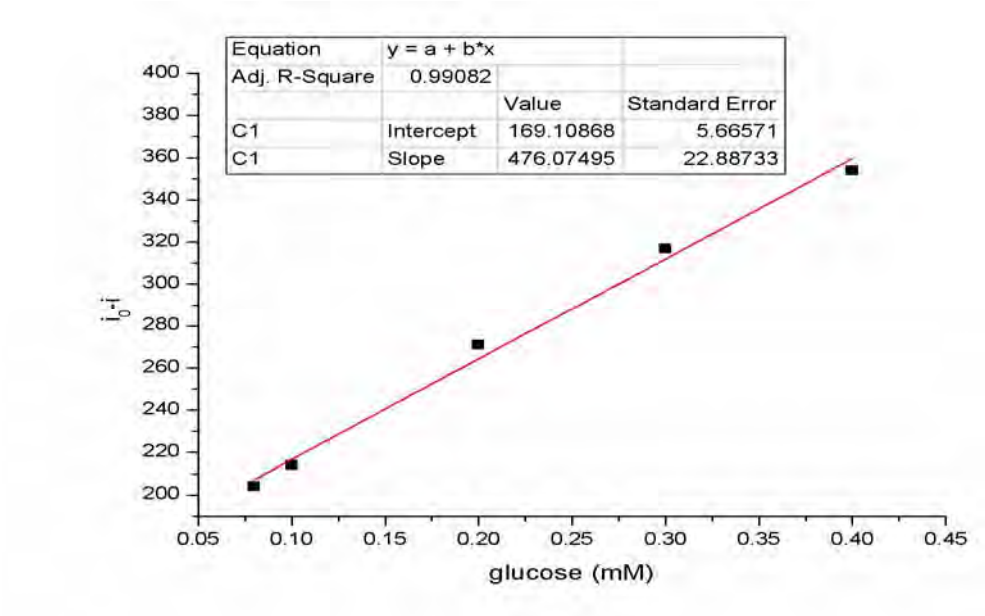

Figure 4.15 Liner calibration curve of 20 µM **OB** and 6 units of glucose oxidase titrate with glucose (0.08-0.42 mM) in 10% DMSO with 0.1M HEPES buffer at pH 7.4. The excitation wavelength was 415 nm. The reaction was performed at 37^{o}C and 1 hour. $\mathbf{i_0}$ is the intensity in the absence of glucose. **i** is a variation of the emission intensity in the presence of glucose.

4.3.6 The kinetic studies of the boronic anthraquinone based sensor (OB) of the enzymatic probe system using fluorescence spectrophotometry

Kinetic parameter such as the Michaelis-Menten constant (K_m) is generally used to evaluate the enzyme biological activity, which can be determined by direct fitting of the initial velocity versus substrate concentration data to the Michaelis-Menten equation. Therefore, the K_m was obtained from graph that was plotted between initial velocity (V_i) and the concentration of glucose (**Table 4.2** and **Figure 4.16**). As shown in **Figure A.27 – A.40**, V_i was calculated from slope of the graph that was plotted between i_0-i (i_0 is the intensity in the absence of glucose and i is a variation of the emission intensity in the presence of glucose) and time. As shown in **Figure 4.16**, V_{max} is calculated to be 5.63 minutes. Interestingly, the K_m calculated is

0.18 mM, which is lower than the previous report [114]. This is implied that the boronic anthraquinone based sensor (**OB**) exhibits a high affinity of glucose sensing.

Table 4.2 Data of slope, standard error and correlation coefficient (R^2) for kinetic measurement using **OB** in enzymatic probe system by glucose oxidase

Glucose (mM)	slope	standard error	R^2
0.20	2.80392	0.06468	0.99365
0.30	3.37564	0.07396	0.99474
0.70	4.84820	0.08782	0.9967
1.00	4.97450	0.10267	0.99533
1.40	5.09527	0.21845	0.98724
2.00	5.04667	0.18071	0.98858
3.00	5.00599	0.03998	0.99943

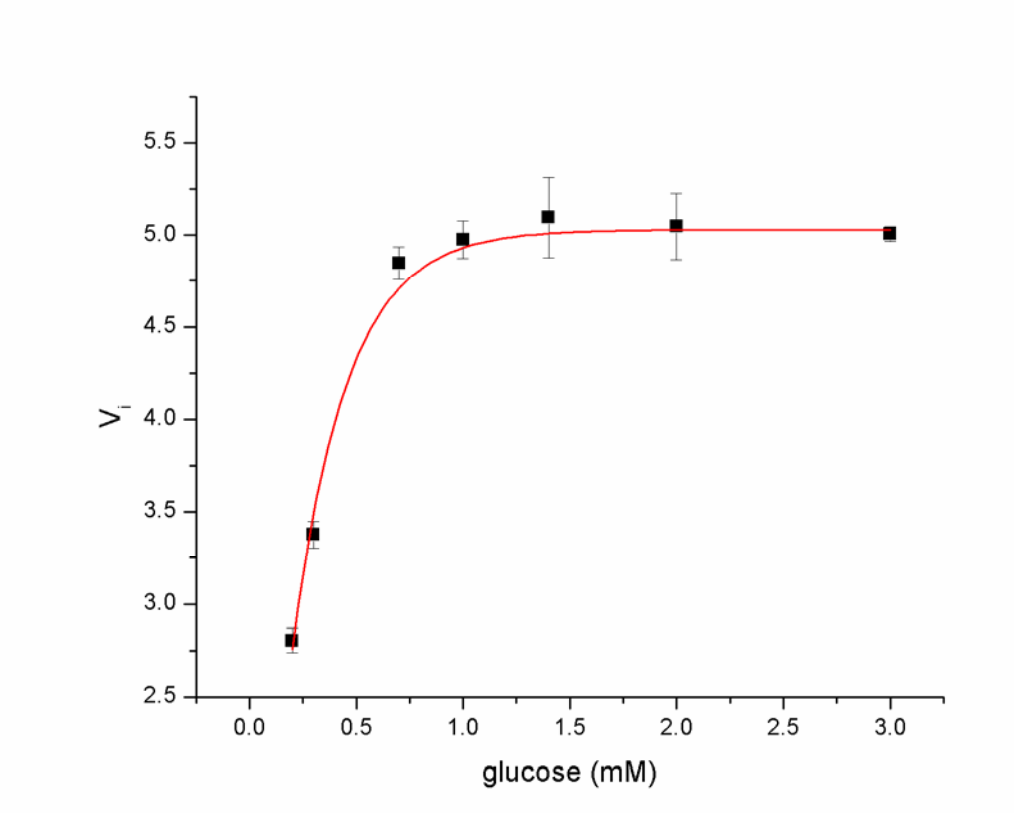

Figure 4.16 Kinetic curve of **OB** in enzymatic probe system by glucose oxidase

4.3.7 Fluorescence measurement of boronic anthraquinone based sensors (OB) in optimum condition of the enzymatic probe system for detection of glucose and other competitive saccaharides by glucose oxidase

An important feature of **OB** is to investigate its high selectivity toward glucose over the other competitive saccaharides. The effect of other sacharides including D-galactose, D-fructose, D-sucrose and D-maltose were also studied in optimum condition of the enzymatic probe system. As shown in **Figure 4.17**, the competitive saccarides did not lead to any significant fluorescence changes. Interestingly, the emission spectrum of **OB** was gradually intensified by the addition of fructose. Moreover, for enzymatic probe system in the presence of miscellaneous competitive saccarides and glucose, the fluorescence responses showed the similar change in the case of glucose with **OB** in the enzymatic probe system. Thus, **OB** is indicative of the great selectivity for glucose in this enzymatic probe system.

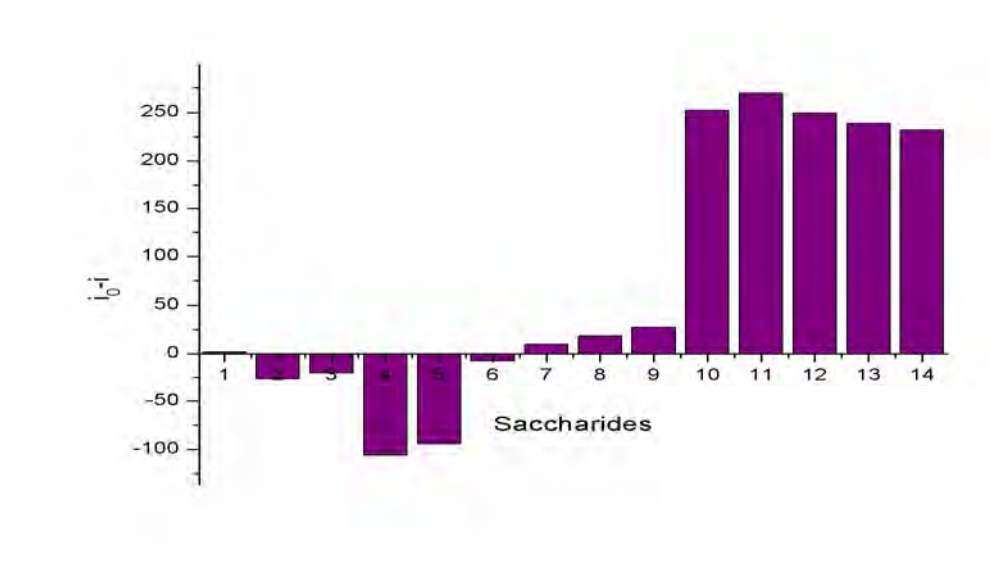

Figure 4.17 Fluorescence responses of **OB** (20 μM) to 0.2 mM glucose [1] or to competitive saccharides (2 mM) [2: galactose, 3: galactose + GOx, 4: fructose, 5: fructose + GOx, 6: sucrose, 7: sucrose + GOx, 8: maltose, 9: maltose + GOx] in the presence of another saccharide interference (0.2 mM glucose, 2 mM compettitive saccaharides) [10: glu + GOx, 11: glu + galactose + GOx 12: glu + fructose + GOx, 13: glu + sucrose + GOx, 14: glu + maltose + GOx].

4.3.8 Fluorescence measurement of boronic anthraquinone based sensors in optimum condition of the enzymatic probe system in human serum using standard addition

To examine the feasibility of applying **OB** for clinical diagnosis, we conducted experiments using human serum. From Figure 4.18, the standard addition of OB in enzymatic probe system is not consistant with the theoretical standard addition. Thus OB could not be acceptable for determination of glucose in human serum.

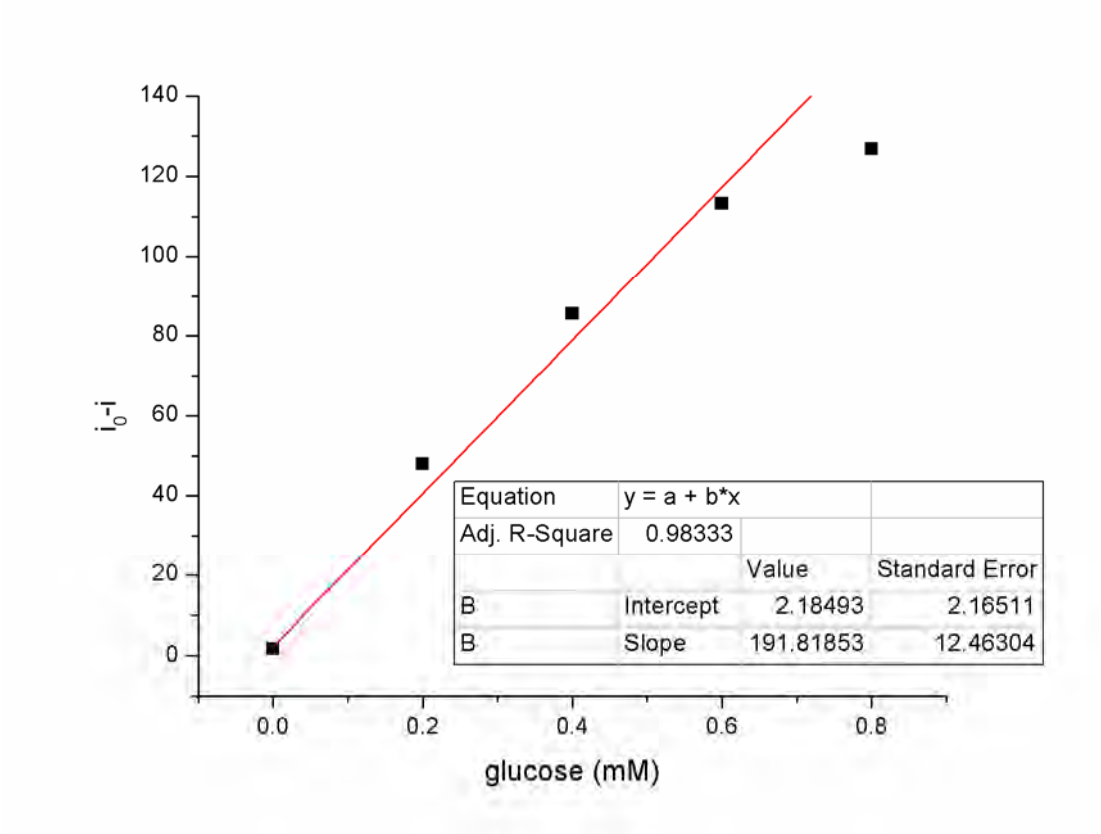

Figure 4.18 Standard addition of **OB** in enzymatic probe system by glucose oxidase for determining glucose in human serum

4.4 Design concept of enzymatically activated sensors for β-glucosidase

In recent years, glycosidases are important reporter for the gene markers in technique Enzyme-linked immunosorbent assay (ELISA) [115-117], also known as an enzyme immunoassay (EIA). Performing an ELISA involves at least one antibody with specificity for a particular antigen. The sample with an unknown amount of antigen is immobilized on a solid support. After the antigen is immobilized, the detected antibody is added with a result of forming a complex with the antigen. The detected antibody can be covalently linked to an enzyme, or can itself be detected by a secondary antibody that is linked to an enzyme through bioconjugation. Between each step, the plate is typically washed with a mild detergent solution to remove any proteins or antibodies that are not specifically bound. After the finally washed step, the plate is developed by adding an enzymatic substrate to produce a visible signal, which can monitor the quantity of antigen in the sample. In this thesis we have focused on synthesis and development of enzymatic substrate as fluorogenic sensors that are specific to target enzyme. In the nature, there are many *O*-aryl glycosides having anthraquinones as their structural subunit without fluorescent properties [118]. Our effort is to synthesize the fluorogenic compounds bearing the *O*-aryl glycosides on anthraquinone for the purpose of β-glucosidase probe by fluorescence spectroscopy (**Scheme 4.4**). Anthraquinone was modified by oxidation condensation of diamine and aldehyde yielding the desired heterocyclic imidazole. Hypothetically, the conjugation of an electron acceptor such as quinone derivative with electron donor such as imidazole as a main acceptor-donor segment (main A-D system) performs intramolecular charge transfer of the sensory system which is sensitive to a small perturbation. Conjugative connecting of sensory moiety to main A-D site was expected to afford a large response to the enzymatic reaction with sensory moiety.

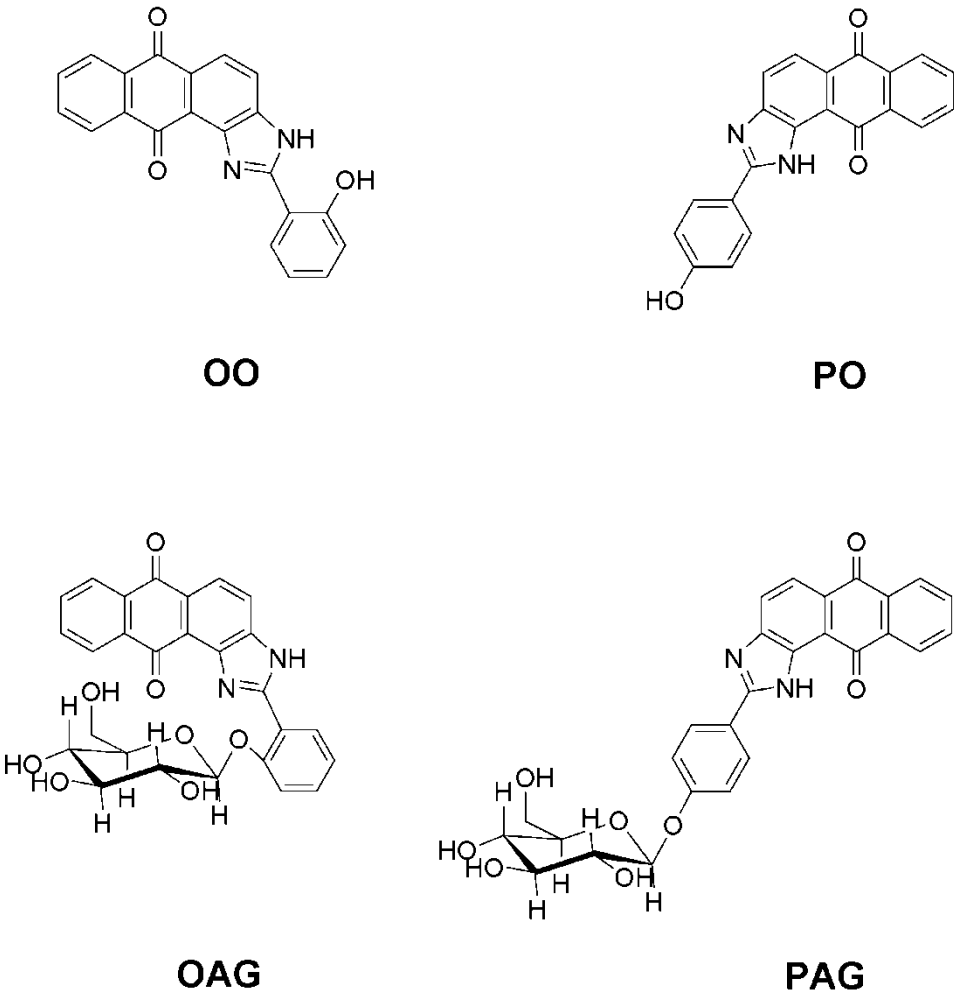

Scheme 4.4 Structures of designed receptors based on anthraquinone, imidazole and *O*-aryl glycosides

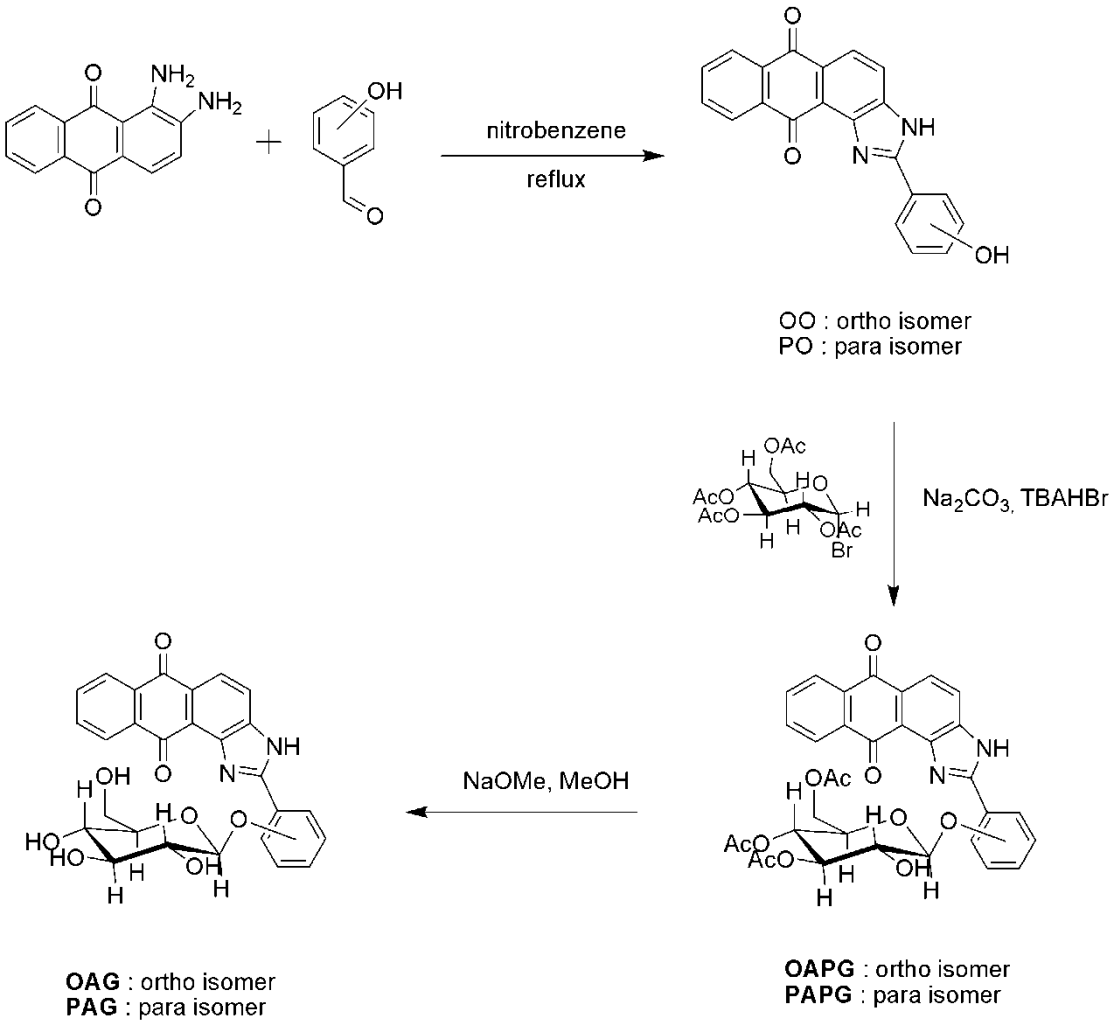

Scheme 4.5 Synthesis pathway of glycoside anthraquinone (**OAG** and **PAG**) and their derivatives (**OO** and **PO**)

4.5 Synthesis and characterization of glycoside anthraquinone based sensors and their derivatives

As a fluorophore, anthraquinone was selected to formulate an electron acceptor segment of the synthesized sensors. The schematic illustration of the synthetic pathway of sensors, **OAG** and **PAG** was shown in **Scheme 4.5**. The first step of the synthesis is the oxidative condensation of diamine and aldehyde to yield the desired heterocyclic imidazole. Compounds **OO** and **PO** were prepared by the condensation of 1,2-diamino-1,4-anthraquinone with ortho- or para-hydroxybenzaldehyde in refluxing nitrobenzene and the reaction was kept stirring at 150 ^{o}C. Compounds **OO** and **PO** were precipitated in the reaction. The dark brown solid of **OO** and the brown solid of **PO** were obtained in 64% and 78% yields, respectively. The ^{1}H-NMR spectra of **OO** and **PO** displayed the characteristic peaks of imidazole proton (NH) at 12.73 ppm and the appearance of hydroxy proton of **OO** and **PO** at 12.01 ppm and 10.21 ppm, respectively (**Figure 4.19**).

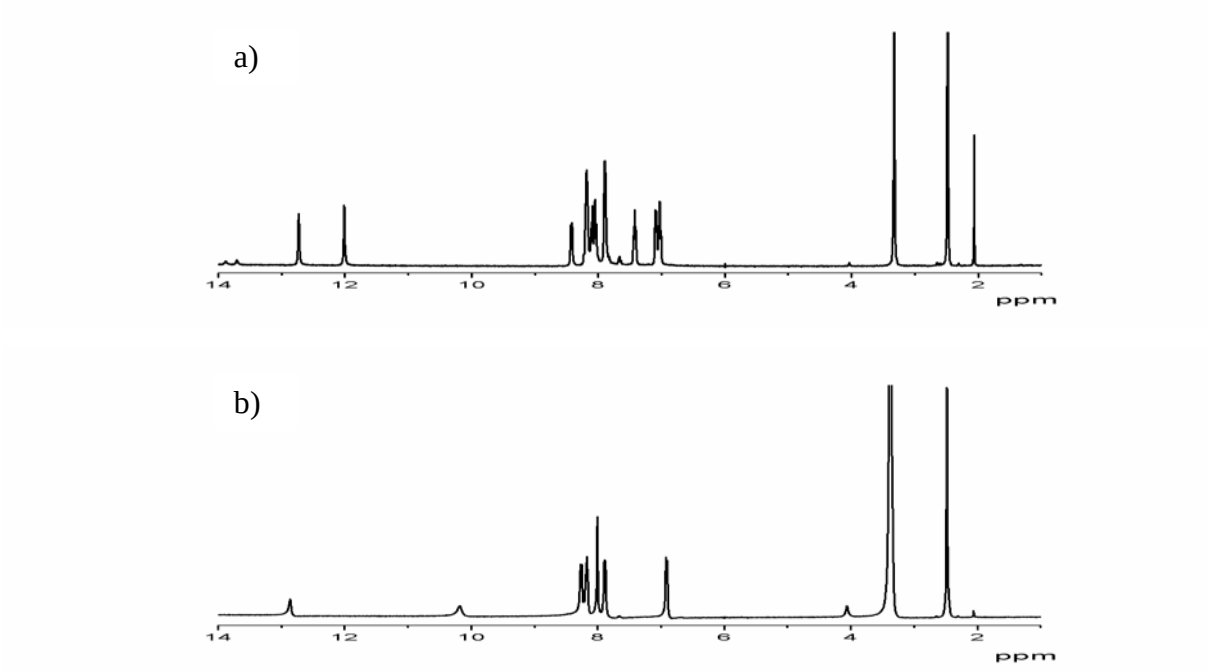

Figure 4.19 ^{1}H-NMR spectra (400 MHz, DMSO-d_6) for a) **OO** and b) **PO**

The key step of the synthesis is glycosylation of anthraquinone derivatives, **OO** and **PO**, under phase transfer catalysts (PTC) condition. This method has been used successfully with masses of nucleophiles applying bromo sugars as glycosyl donors. Glycosylation of **OAPG** and **PAPG** were prepared by the reaction between the glucosyl bromide and **OO** or **PO** in dichloromethane as the organic phase and Na_2CO_3 as an aqueous phase in the presence of tetrabutylammonium hydrogen bromide (TBAHBr) as catalyst. After the reaction was stirred for 6 hours at room temperature, the 2-*O*-deactylated glucosyl imidazole anthraquinone with the complete *β*-selective form was obtained in 20% yield for OAPG and 35%yields for PAPG. The ^{1}H-NMR spectra of **OAPG** and **PAPG** showed the characteristic peaks of glucose pyranose protons (CH) at 5.45-5.68 ppm, methylene protons on glucose pyranose (CH_2) at 4.18 and 3.94 ppm and methyl protons (CH_3) of acetyl group at 2.16-1.83 ppm (**Figure 4.20**). The MALDI-TOF mass spectra showed the intense peak at 629.769 m/z corresponding to **OAPG** and **PAPG**.

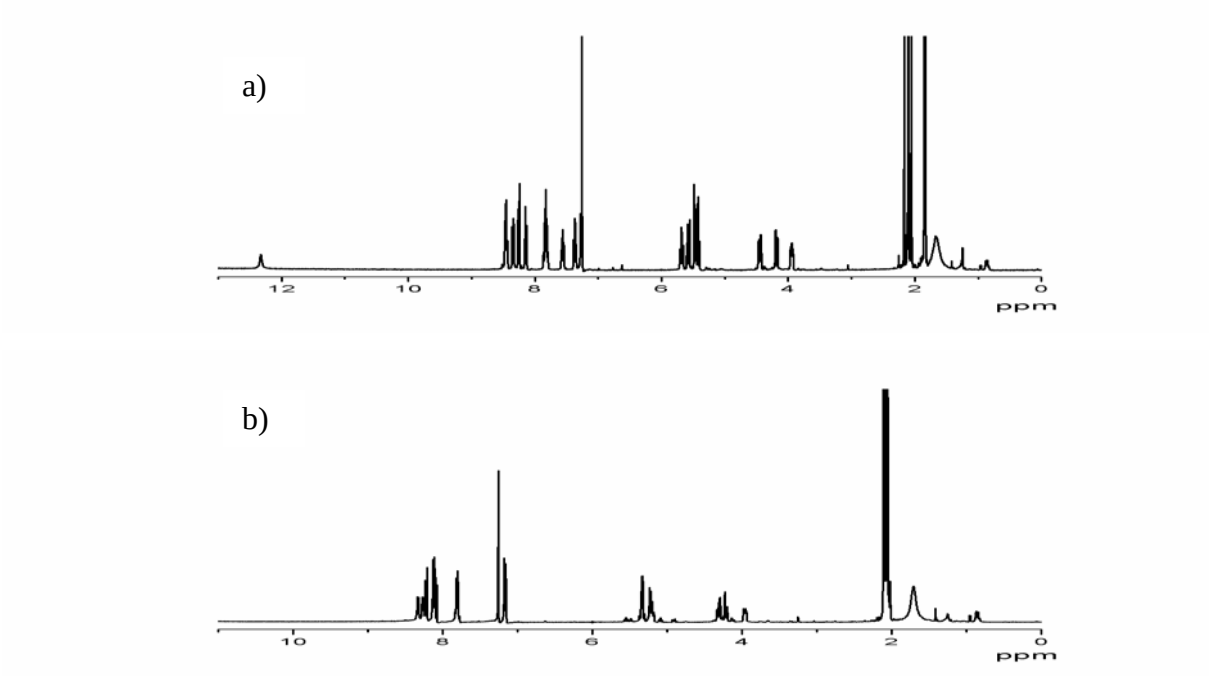

Figure 4.20 ^{1}H-NMR spectra (400 MHz, DMSO-d_6) for a) **OAPG** and b) **PAPG**

In order to remove the protecting group, compounds **OAPG** and **PAPG** were stirred in NaOMe for 60 minutes at room temperature. The reaction mixture was neutralized with Amberlite resin IR-120 to give the *O*-glucosyl imidazole anthraquinone, **OAG** and **PAG** in 89% and 91% yields, respectively. The ^{1}H-NMR spectra of **OAG** and **PAG** showed the hydroxy protons of glucose pyranose (OH) at 5.40, 5.14, 5.08 and 4.63 ppm. The observation of the doublet resonance at 5.03 ppm with J coupling of 7.2 Hz was assigned as the anomeric proton (CH) of glucose revealing the characteristic beta-formed glucoside (**Figure 4.21**). The intense peak at 503.921 m/z of MALDI-TOF MS confirmed the structures of **OAG** and **PAG**.

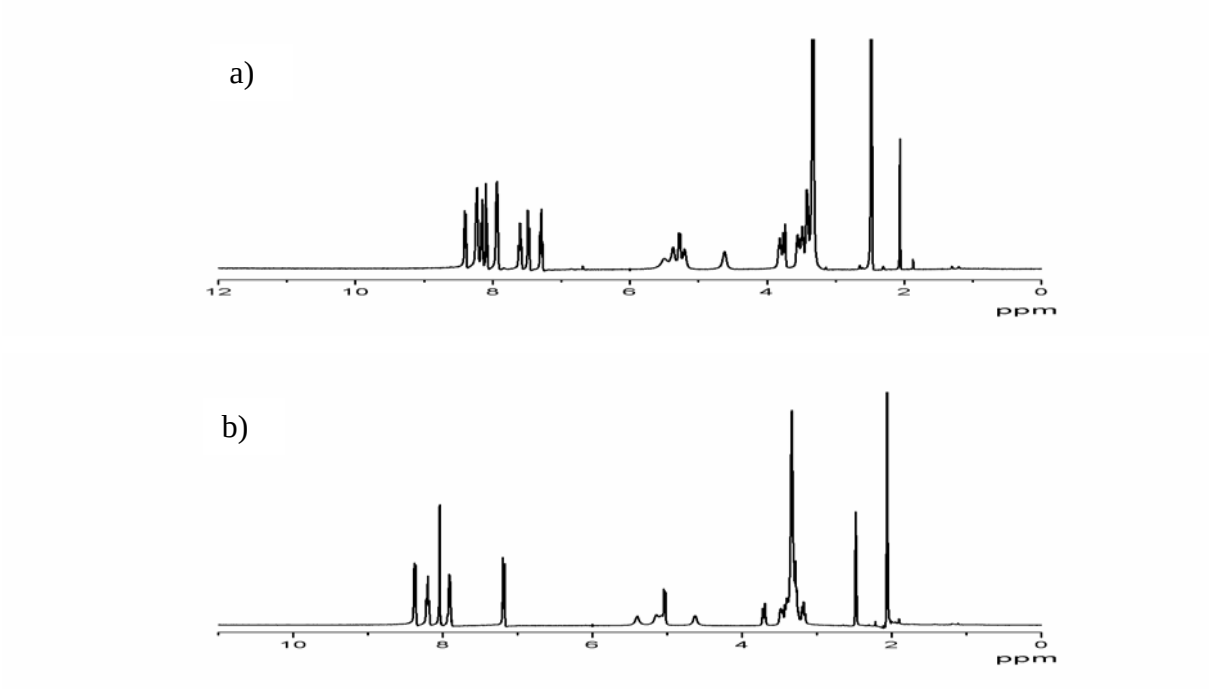

Figure 4.21 ^{1}H-NMR spectra (400 MHz, DMSO-d_6) for a) **OAG** and b) **PAG**

4.6 The enzymatic probe studies of the glycoside anthraquinone based sensors

4.6.1 The photochemical studies of glycoside anthraquinone based sensors and their derivatives for enzymatic probe system, OAG, PAG, OO and PO for *β*-glucosidase

The absorption properties of glycoside anthraquinone (**OAG** and **PAG**) based sensors and their derivatives (**OO** and **PO**) showed a light yellow color solution and visible absorption bands at 408, 415, 408 and 424 nm for **OAG**, **PAG**, **OO** and **PO**, respectively (shown in **Table 4.3** and **Figure 4.22a**). From these results, the light yellow color and the visible absorption bands affected from the migration of electron density from electron donating group of amino on imidazole ring to electron acceptor group of anthraquinone. Compared to the parent compound, 1,2-diamino-1,4-anthraquinone (λ_{max} = 495 nm, $E_g \approx$ 2.50 eV, **Figure A.26**) and glycoside anthraquinone based sensors provided a large energy gap ($E_g \approx$ 2.98-3.12 eV) due to the attachment of electron deficient group (*O*-glucosyl) to the structure.

Table 4.3 Absorption and fluorescence properties of the newly developed *β*-glucosidase substrates (**OAG** and **PAG**) and their *β*-glucosidase-catalyzed hydrolysis Products (**OO** and **PO**)

Receptors	λ_{abs} (nm)	λ_{em} (nm)	Φ_f[a]
OAG	408	589	0.288
PAG	415	610	0.214
OO	408	n.d.[b]	0.015
PO	424	n.d.[b]	0.031

[a] Quantum yields were determined using quinine sulfate as the standard (ΦSTD) 0.508 in 1N H_2SO_4.

[b] Values cannot be determined.

As shown in **Table 4.3** and **Figure 4.22b**, the anthraquinone glycoside based sensors (**OAG** and **PAG**) in 10% DMSO with 0.1M HEPES buffer at pH 7.4 exhibited the emission band at 589 and 609 nm, respectively. Interestingly, the control

compounds (**OO** and **PO**) showed very low quantum yields. It can be explained that the hydroxyl group behaves as PeT process toward fluorophore. In consistent with our hypothesis, after adding the *β*-glucosidase into the solution of **OAG** or **PAG**, the *O*-aryl glucose attached in **OAG** or **PAG** was cleaved to provide the **OO** or **PO** which displayed the fluorescence quenching.

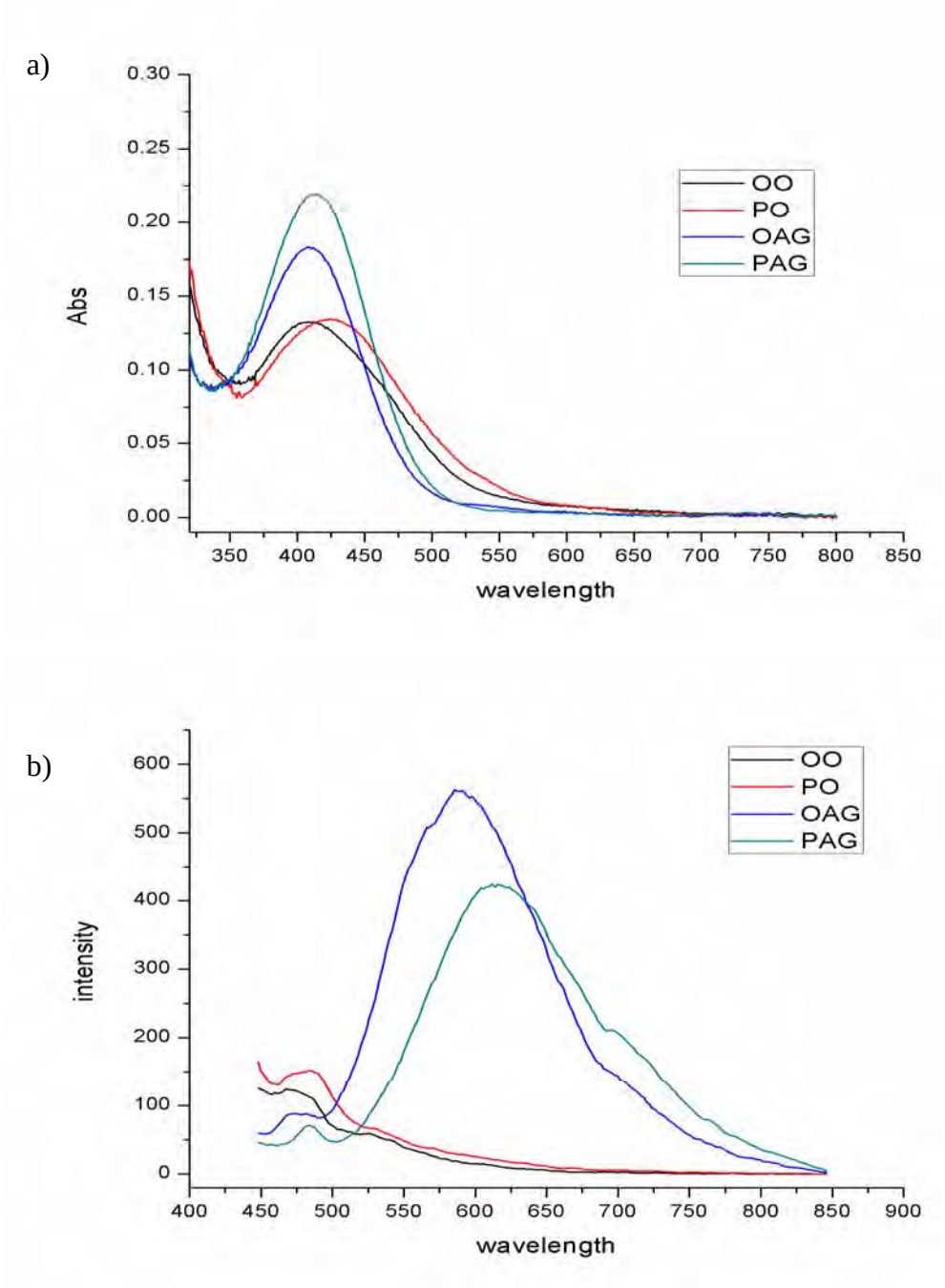

Figure 4.22 a) Absorption and **b)** emission spectra of **OAG**, **PAG**, **OO** and **PO** in 100 mM HEPES buffer pH 7.4, 10% DMSO in aqueous solution.

4.6.2 Fluorescence measurement for the optimizing condition of the enzymatic probe system

Based on the above findings, we attended to develop an enzymatic probe based on PeT. A *β*-glucosidase is a glucosidase enzyme that acts upon *β*1-4 bonds linking two glucose or glucose-substituted molecules. It is an exocellulase with specificity for a variety of *β*-D-glycoside substrates. It catalyzes the hydrolysis of terminal non-reducing residues in *β*-D-glucosides with release of glucose. The design of the probe is shown in **Scheme 4.6**. The glucose was attached through an *O*-glycoside bond to the hydroxy group of the fluorescence off/on switch moiety of **OO** and **PO**. The synthesized compounds (**OAG** and **PAG**) were displayed a strong fluorescence. After the cleavage of the glycoside by *β*-glucosidase, **OAG** and **PAG** would be converted to **OO** and **PO**, whose fluorescence would be quenched by PeT process. Like all catalysts, enzyme activity is also affected by pH, temperature and the concentration of substrate. Therefore, we should optimize the condition for enzymatic probe system.

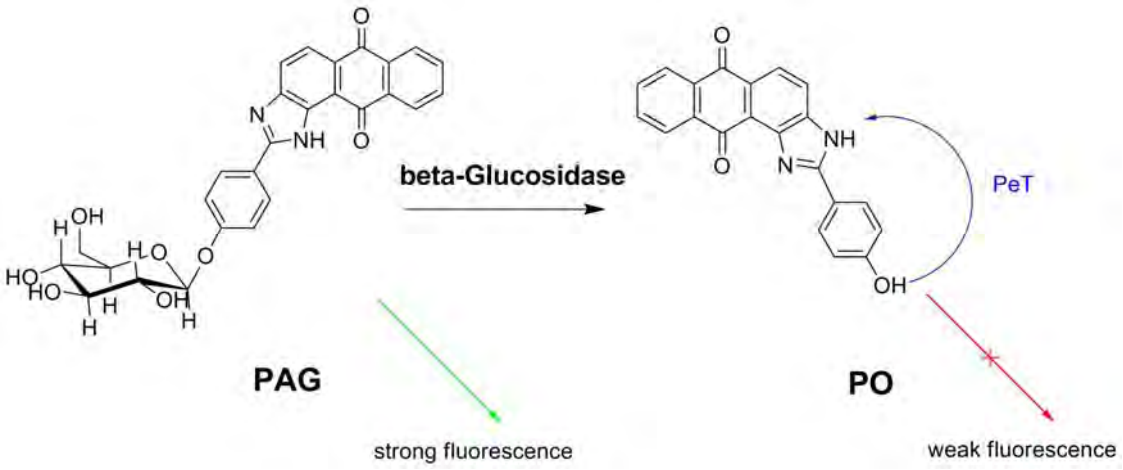

Scheme 4.6 Reaction scheme of **OAG** and **PAG** before and after the reaction with *β*-glucosidase

4.6.2.1 The studies on the effect of sensor concentrations

The various concentrations of sensors (**PAG** and **OAG**) were also examined in the presence of 6 units of β-glucosidase in enzymatic system. The fluorescence response **PAG** was displayed in **Figure A.41** and **Figure 4.23**. The enzymatic system showed the highest response fluorescence with the concentration of **PAG** at 0.04 mM. After adding 6 units of β-glucosidase into the **PAG** solution at 0.04 mM, the fluorescence intensity was remarkably quenched. However, the fluorescence intensity of **PAG** in the presence of β-glucosidase was significantly quenched when the concentration of **PAG** at 0.02 mM. Therefore, we chose the optimal concentration of **PAG** at 0.02 mM for all manipulations in this enzymatic probe system. On the other hand, the fluorescence responses **OAG** was not consistent with our hypothesis (**Figure A.42** and **Figure 4.24**). Then, **OAG** could not be applied in this enzymatic probe.

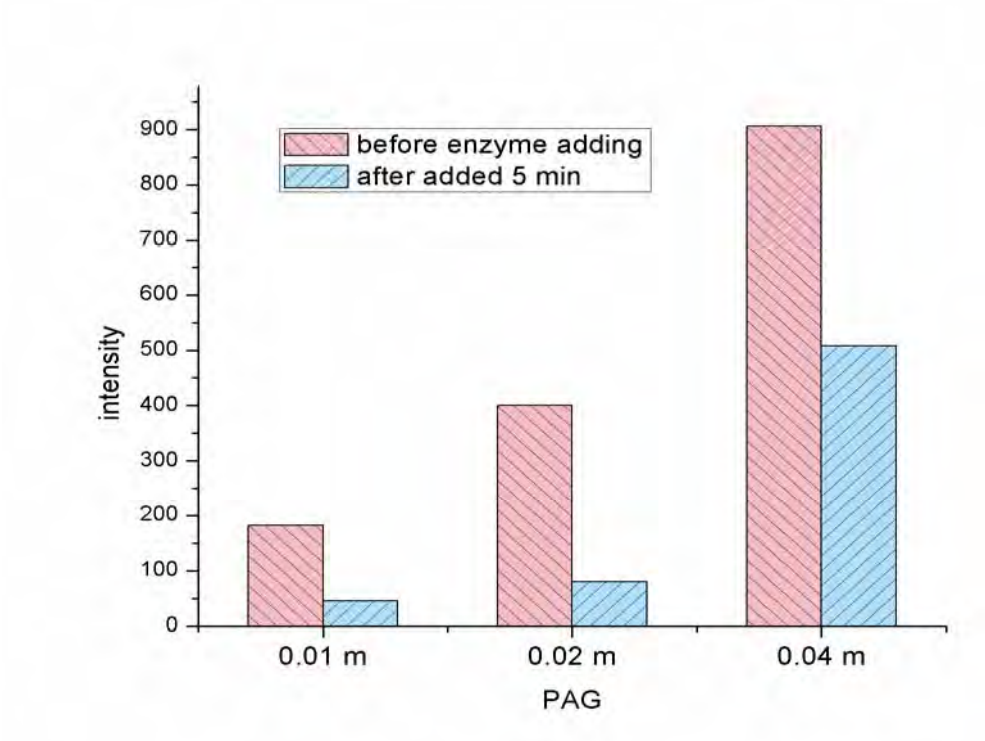

Figure 4.23 Fluorescence responses of **PAG** at 610 nm in enzymatic probe system in 0.1 M phosphate buffer pH 6, 10% DMSO in aqueous solution.

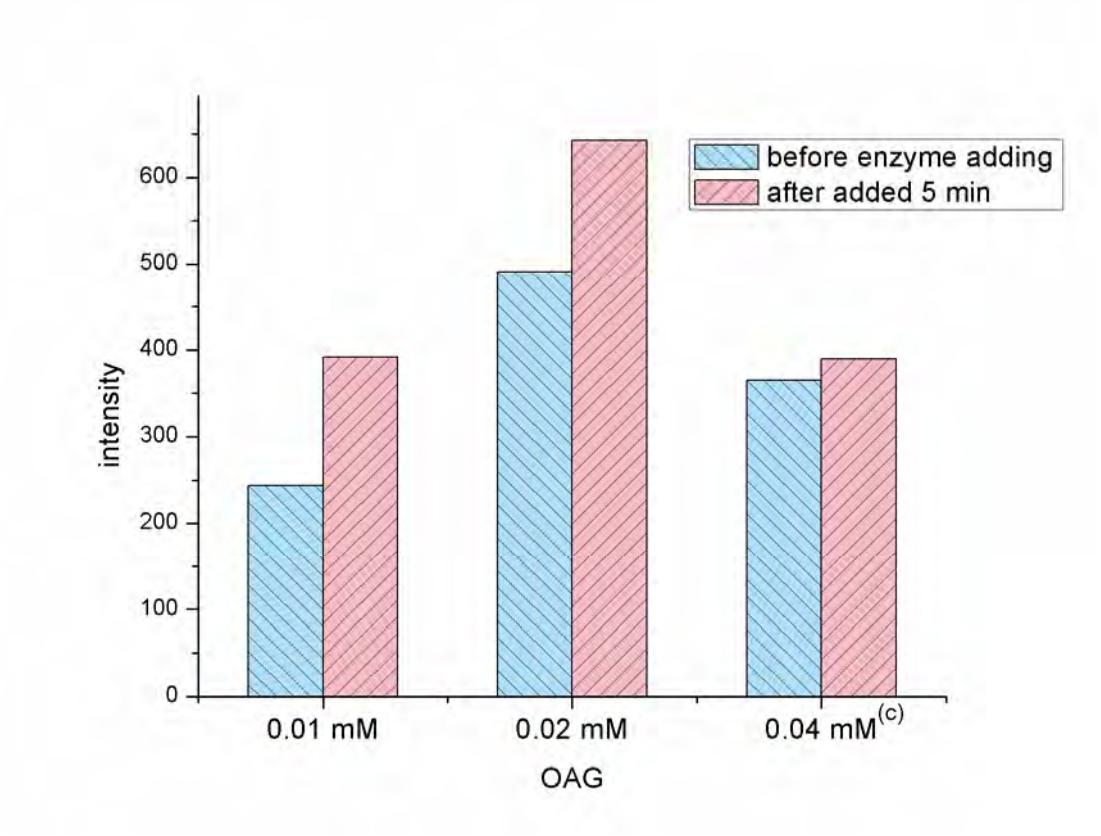

Figure 4.24 Fluorescence responses of **OAG** at 585 nm in enzymatic probe system in 0.1 M phosphate buffer pH 6, 10% DMSO in aqueous solution. (c) Fluorescence measurement at PMT 700.

4.6.2.2 The pH-dependent experiments

To verify the sensitivity and activity of enzymatic probe for detection of β-glucosidase, the sensor **PAG** was studied in various pH solution. As illustrated in **Figure A.43** and **Figure 4.25**, the enhancements of fluorescence intensity at 610 nm were observed upon the pH value less than pH 6.0. Although, **PAG** exhibited high fluorescence intensity and a large fluorescence change upon the addition of enzyme in the range of pH 4.0-5.5, the activity of enzymatic system found in biological system actually works in the pH of 6.0 - 7.4. Therefore, all experiments will be carried out at the pH 6 in 0.1 M phosphate buffer with the optimized condition of the enzymatic probe system.

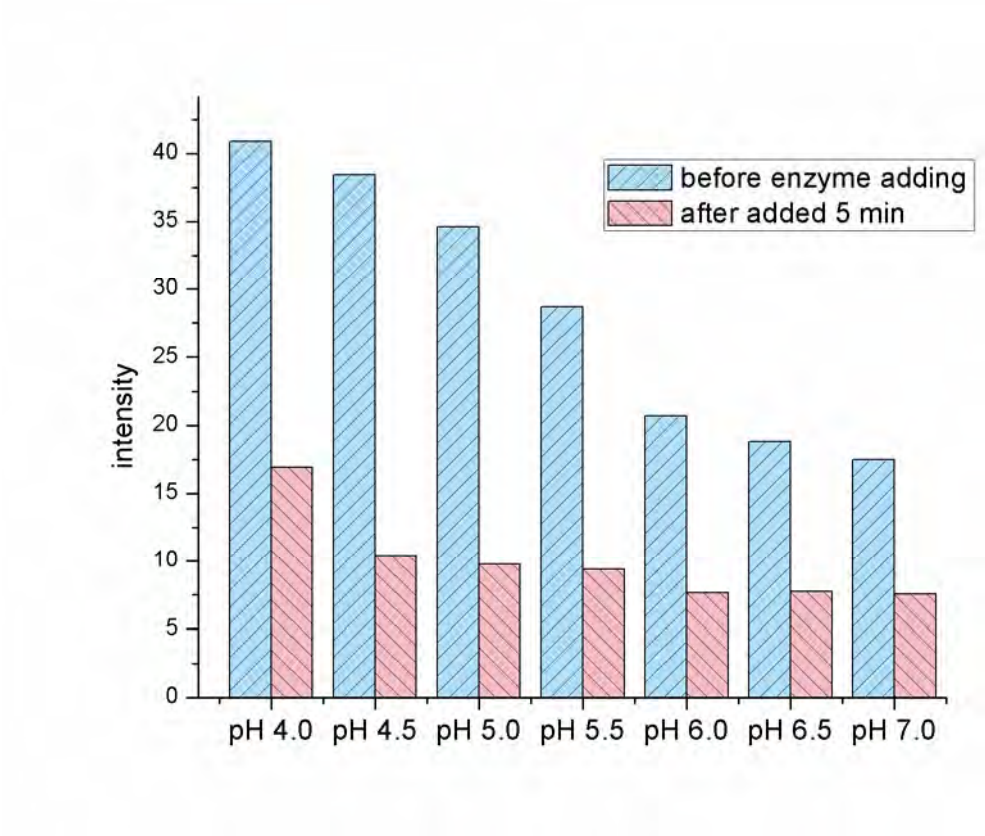

Figure 4.25 Fluorescence responses of 0.02 mM **PAG** at 610 nm with various pH in enzymatic probe system, 10% DMSO in aqueous solution.

4.6.2.3 The studies on the effect of temperature

Next, the optimum enzymatic probe systems with different temperature were also explored. **Figure A.44** and **Figure 4.26** showed the effect of the temperature towards the enzymatic probe system at 37 ^{o}C and at room temperature. As expected, **PAG** in the enzymatic system studied at high temperature has performed a larger emission change than that studied at room temperature. This is a reason that **PAG** for β-glucosidase sensing was carried out at 37 ^{o}C in the optimized condition of the enzymatic probe system.

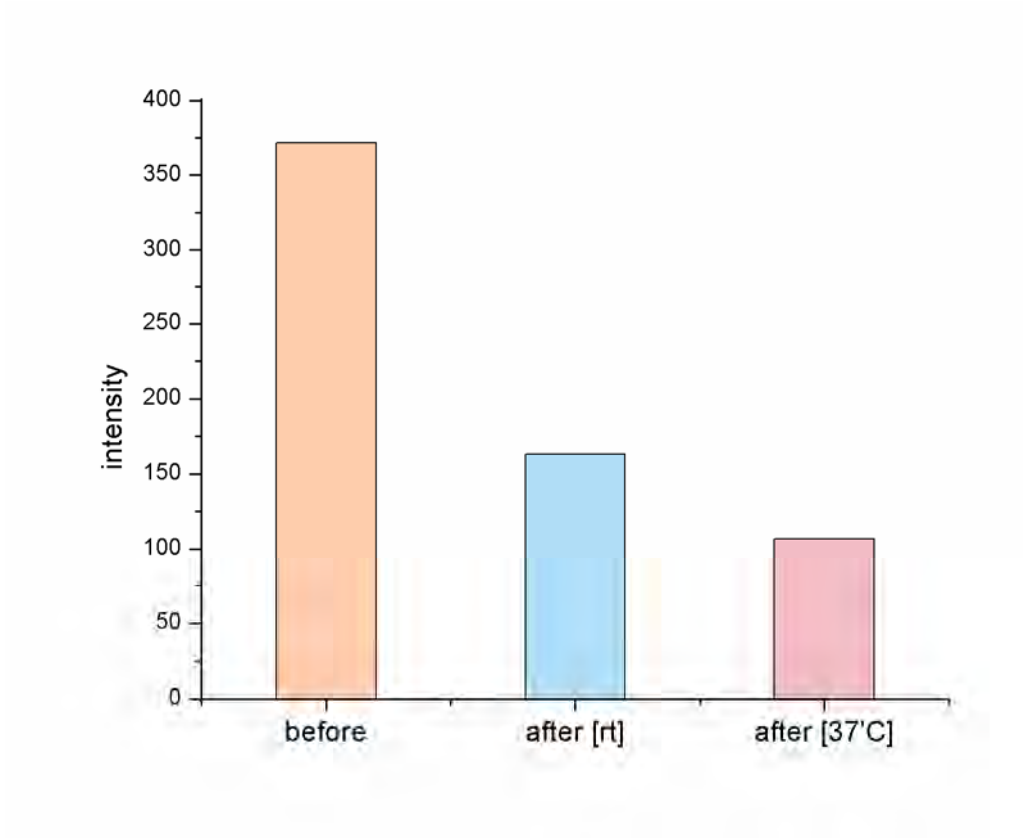

Figure 4.26 Emission intensity of 0.02 mM **PAG** at 610 nm with room temperature and 37^{o}C in enzymatic probe system in 0.1 M phosphate buffer pH 6, 10% DMSO in aqueous solution.

4.6.2.4 The studies on the effect of unit of *β*-glucosidase

To optimize the appropriate condition to obtain the highest efficiency of enzymatic probe system for fluorescence measurements, the amount of unit of *β*-glucosidase was examined for the fluorescence responses of sensor (**PAG**). According to and **Figure 4.27**, the emission response of **PAG** was remarkably changed upon the addition of a high amount of unit of *β*-glucosidase. Unfortunately, with very high amount of *β*-glucosidase in the enzymatic system, the characteristic fluorescence of *β*-glucosidase was intensed approximately 495 nm which can disturb the emission band of **PAG** (as shown in **Figure A.45**). Therefore, we chose 6 units of *β*-glucosidase in optimizing condition of the enzymatic probe system of **PAG**.

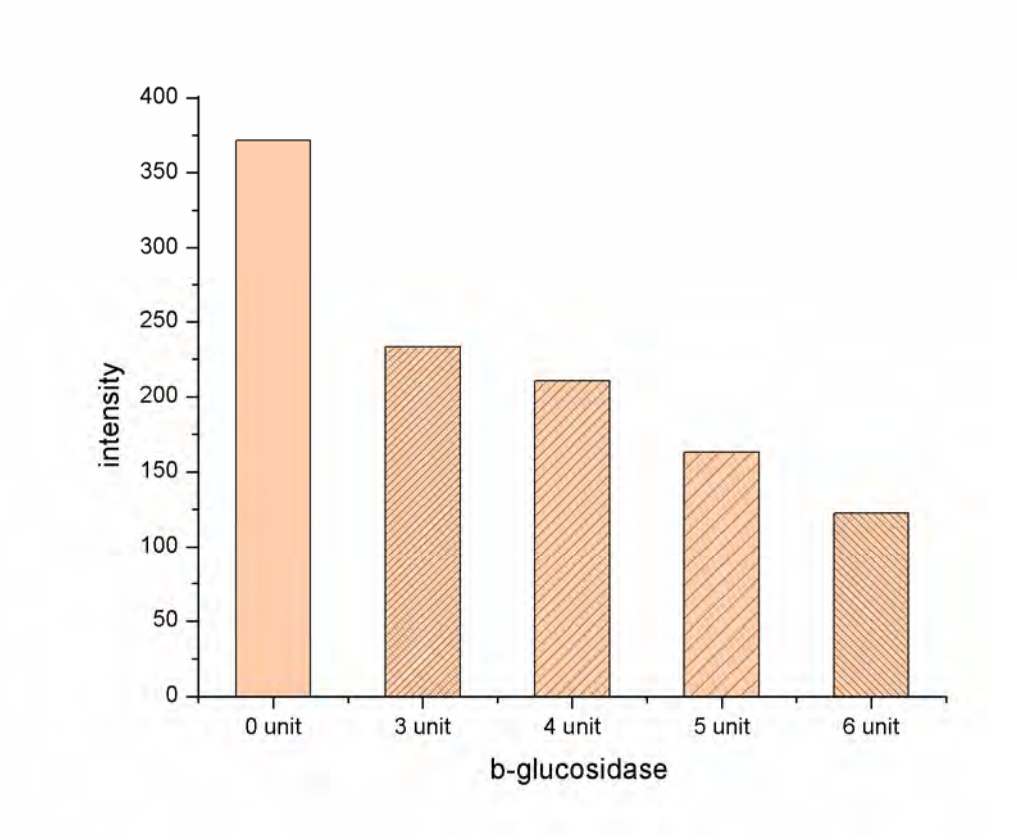

Figure 4.27 Emission intensity of 0.02 mM **PAG** at 610 nm with various unit of *β*-glucosidase in enzymatic probe system in 0.1 M phosphate buffer pH 6, 10% DMSO in aqueous solution.

4.6.3 Fluorescence measurement of glycoside anthraquinone base sensors in optimum condition of the enzymatic probe system for *β*-glucosidase detected

As described previously, the glycoside anthraquinone based sensors (**PAG**) was used in optimum condition of the enzymatic probe system for determining *β*-glucosidase. As illustrated in **Figure 4.28a**, the emission band at 610 nm of **PAG** which clearly performed quenching after *β*-glucosidase was added for 5 minutes. Moreover, the change of emission spectra of **PAG** was slowly decreased in a time dependent manner until complete quenching was achieved (**Figure 4.28b**). Although these results suggest that **PAG** was able to detect the enzyme in enzymatic reaction but fluorescence assay in a system has a high background signal level. Consequently, we intended to develop the glycoside anthraquinone based sensors (**PAG**) for determining the *β*-glucosidase in micelle systems.

a)

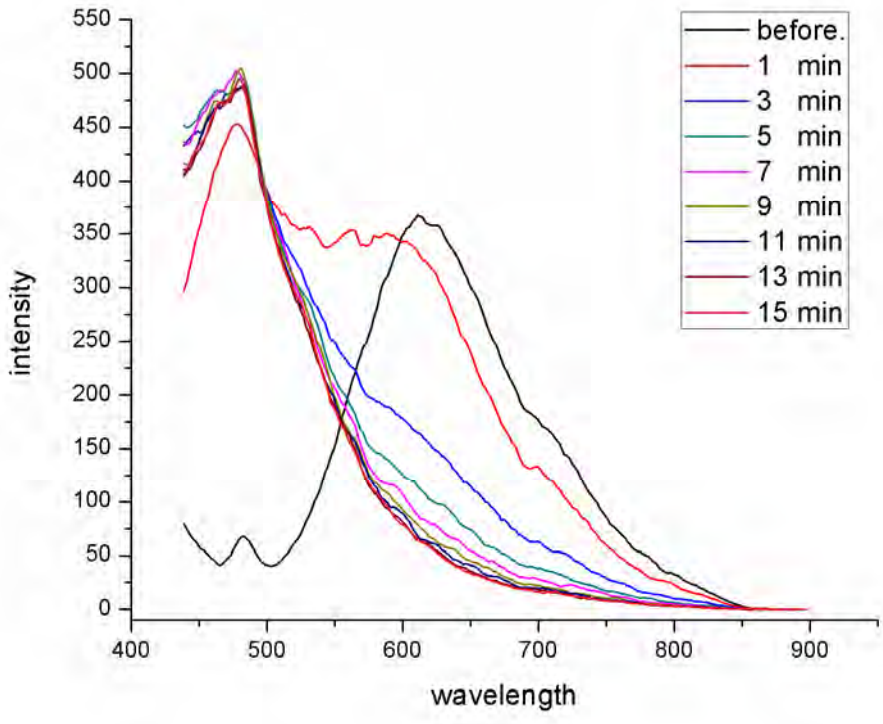

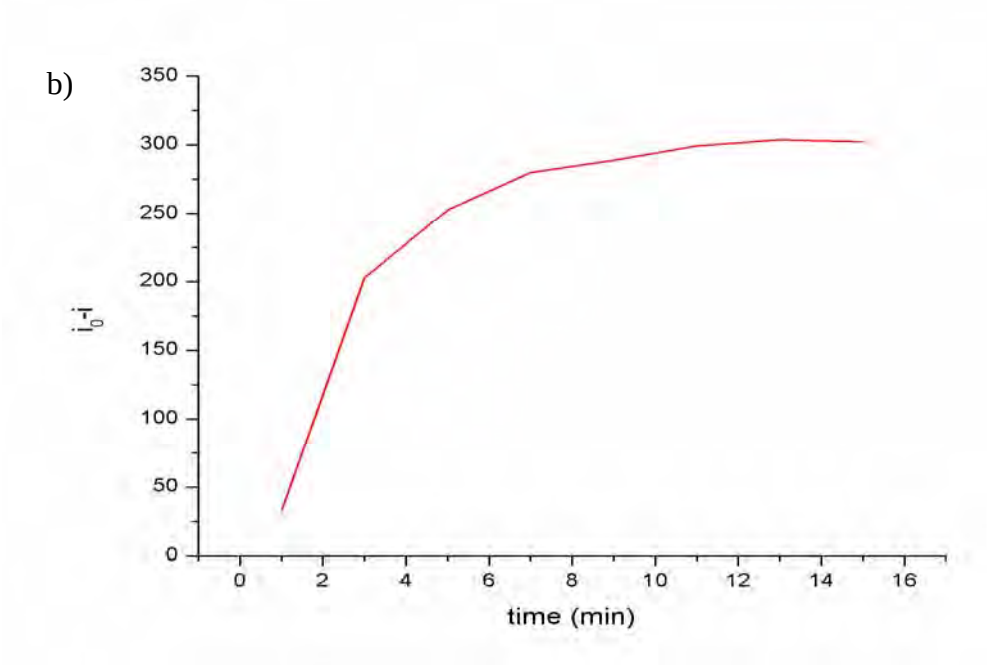

Figure 4.28 Reaction of **PAG** with *β*-glucosidase. **a)** Emission spectra of 0.02 mM **PAG** at 0, 1, 3, 5, 7, 9, 11, 13 and 15 minutes after the addition of *β*-glucosidase (6 units). **b)** Flurescence responses of **PAG** in enzymatic reaction at 610 nm. The reaction was performed in 0.1 M phosphate buffer pH 6, 10% DMSO in aqueous solution at 37 °C. $\mathbf{i_0}$ is the intensity of **PAG** in the presence of *β*-glucosidase at 0 min. **i** is **PAG** in the presence of *β*-glucosidase at various times

4.7 The enzymatic probe studies of the glycoside anthraquinone based sensors in micelle system

4.7.1 Fluorescence measurements for the optimized condition of the micelle system

To overcome the background fluorescence of *β*-glucosidase, we have developed to improve signaling of **PAG** in the enzymatic probe system for a task of *β*-glucosidase sensing. In our approach, the incorporation of sensor into micelle system would increase the solubility of sensor and enhance the fluorescence intensity of sensor. Therefore, the finding of the appropriate condition for micelle system in this task would be extremely realized.

4.7.1.1 The studies on the effect of surfactant types

To optimize the appropriate condition to obtain the highest efficiency of enzymatic probe system of **PAG**. Three types of surfactants including neutral (Triton X-100), anionic (SDS) and cationic (CTAB) surfactants were examined for the fluorescence responses in the presence of 6 units of *β*-glucosidase. As expected, all cationic, anionic and neutral surfactants offered the improvement of the solubility of **PAG** in water by hydrophobic insertion of the sensor into micelles. As illustrated in **Figure A.46**, the emission spectra of **PAG** at 584 nm were remarkably enhanced in CTAB system. In the case of TX-100 system, the sensor showed a moderate fluorescence response. For SDS anionic surfactant system, the fluorescence response was slightly changed. Interestingly, the fluorescence spectrum of **PAG** and *β*-glucosidase in CTAB micelle system displayed a 350-fold fluorescence quenching at 584 nm (**Figure 4.29**).

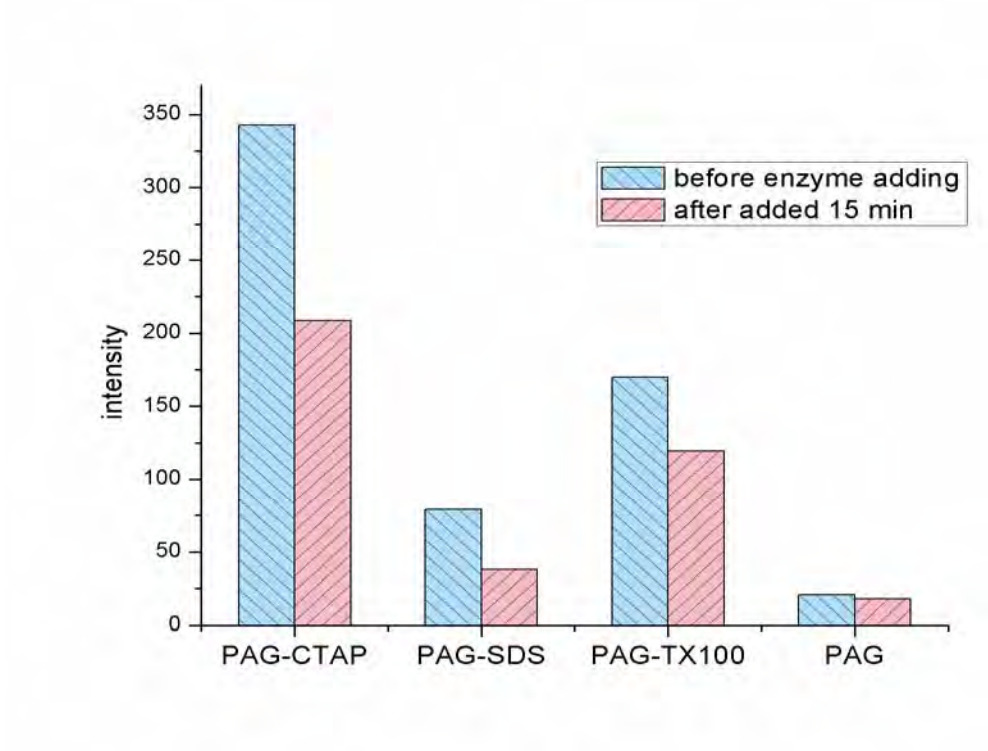

Figure 4.29 Fluorescence responses at 584 nm of 0.02 mM **PAG** with various types of 1 mM surfactants in enzymatic probe system. The reaction was performed in 0.1 M phosphate buffer saline pH 7.4, 10% DMSO in aqueous solution at 37 °C.

4.7.1.2 The studies of CTAB concentration effect

Moreover, the effect of CTAB concentrations was also studied as shown in **Figure A.47** and **Figure 4.30**. The concentration of CTAB at 2 and 3 mM in micellar system provided a large change of fluorescence response of **PAG**. Therefore, we have chosen 2 mM of CTAB (100 equivalents compared to the sensor) in the optimum condition of **PAG** for β-glucosidase sensing in micelle system.

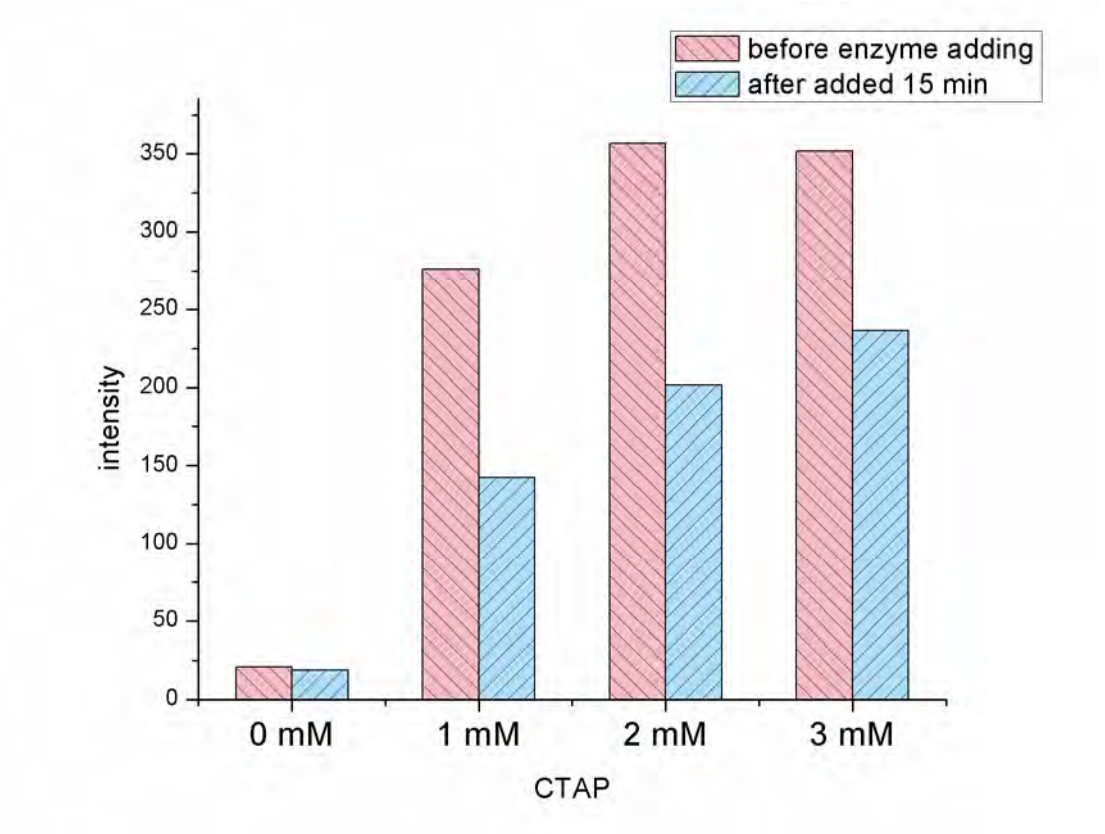

Figure 4.30 Fluorescence responses at 584 nm of 0.02 mM **PAG** in various concentration of CTAB in enzymatic probe system with 0.1 M phosphate buffer saline pH 7.4, 10% DMSO in aqueous solution.

4.7.2 The enzymatically activated fluorescence probe for *β*-glucosidase in micelle systems using fluorescence spectroscopy

From the results of the incorporation of sensor **(PAG)** in the CTAB micelle, this system can improve the enzymatic probe of **PAG** for determining the *β*-glucosidase. According to **Figure 4.31a**, the observation of the emission band at 584 nm without the emission band at 495 nm indicated that **PAG** in the presence of *β*-glucosidase in CTAB micelle can get rid of the interference of emission response from *β*-glucosidase. Therefore, **PAG** in CTAB micelle can improve the sensitivity of this enzymatic probe. For sensing studied as shown in **Figure 4.31b**, the emission band at 584 nm of **PAG** in CTAB micelle clearly performed quenching after *β*-glucosidase was added. However, the changing of emission spectrum of **PAG** and *β*-glucosidase in CTAB micelle was slowly decreased upon the time-dependent manner.

a)

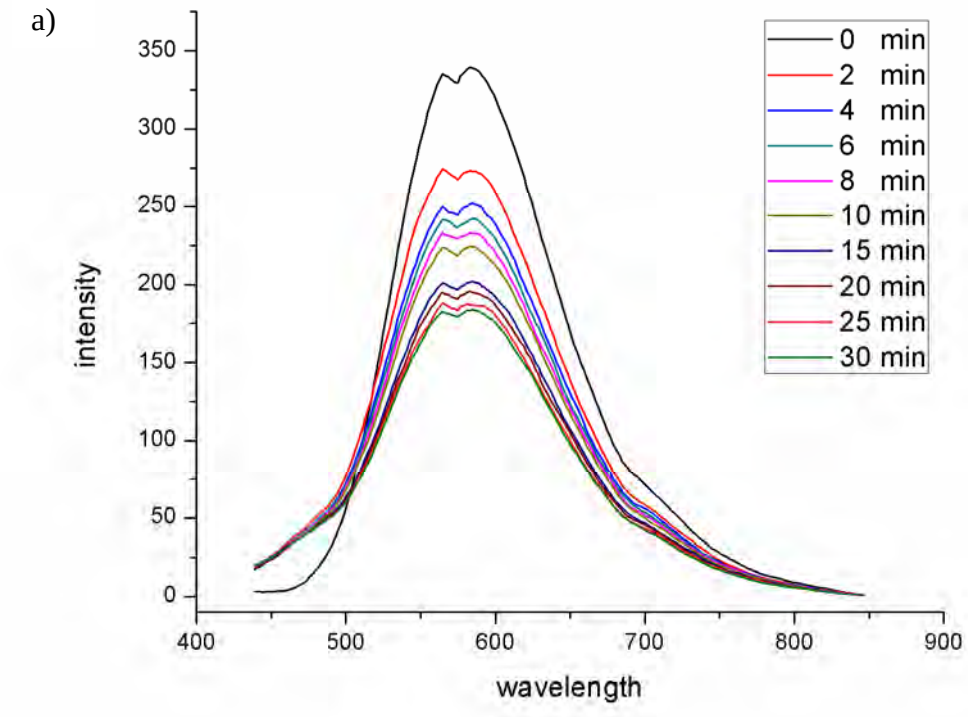

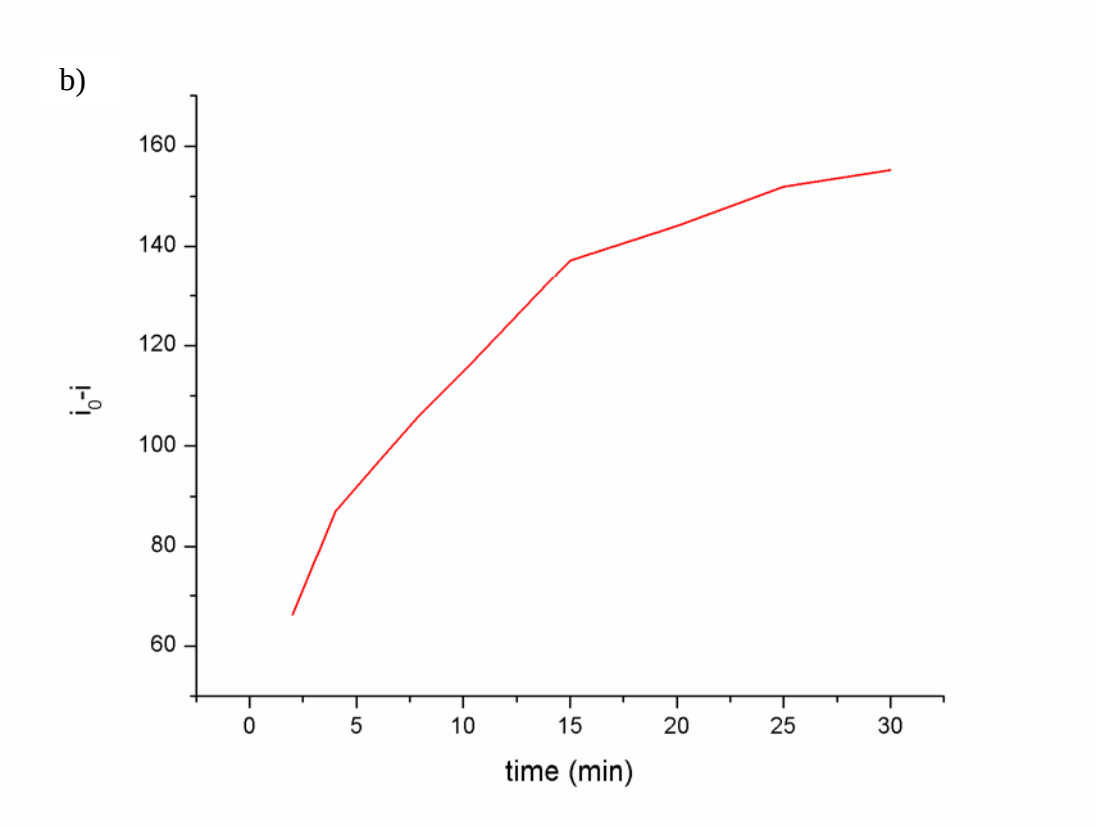

Figure 4.31 Reaction of **PAG** with *β*-glucosidase in CTAB micelle (a) Emission spectra of 0.02 mM **PAG** in 2mM CTAB at 0, 2, 4, 6, 8, 10, 15, 20, 25 and 30 minutes after the addition of *β*-glucosidase (6 units). (b) Flurescence responses at 584 nm of **PAG** and *β*-glucosidase in CTAB micelle upon varying time of reaction. All experiments were performed in 0.1 M phosphate buffer saline pH 7.4, 10% DMSO in aqueous solution at 37 °C. The excitation wavelength was 415 nm. $\mathbf{i_0}$ is the emission intensity if **PAG** in the absence of *β*-glucosidase. **i** is the emission intensity of **PAG** in the presence of *β*-glucosidase at various time.

4.8 Aqueous coordination nanoparticles by adaptive molecular self-assembly

4.8.1 Preparation and morphology of nucleotide/lanthanide coordination nanoparticles

Spontaneous self assembly of nucleotides and lanthanide ions without the guest material was investigated. In the case of preparation of nucleotide/lanthanide nanoparticles, the mixing of nucleotides and lanthanide ions in water spontaneously gives nanoparticles in aqueous suspensions. As described in the experimental sections, mixing of the solution of Tb^{3+} with nucleotides (adenine monophosphate (AMP), cytosine monophosphate (CMP), guanine monophosphate (GMP) and uridine monophosphate (UMP)) in HEPES buffer (pH 7.4) resulted in white precipitates. These precipitates were washed with milliQ water several times and collected by ultracentrifugation. These coordination nanoparticles are redispersed in milliQ water by ultrasonication. Then, the morphology of the corresponding nanoparticles was investigated by scanning electron microscopy (SEM, **Figure 4.32**). The results showed small particles and unity of the prepared nanoparticles.

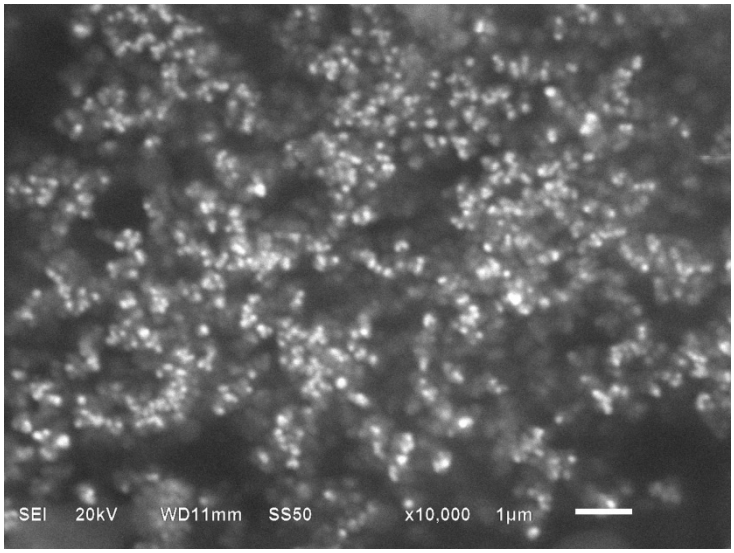

Figure 4.32 SEM micrographs of AMP/ Tb^{3+} CONPs collected by ultracentrifugation.

4.8.2 Fluorescence and phosphorescence measurement of nucleotide/lanthanide coordination nanoparticles

To obtain information on the coordination environment in AMP/Tb^{3+}, CMP/Tb^{3+}, GMP/Tb^{3+} and UMP/Tb^{3+} nanoparticles, luminescence properties were investigated. It is known that emission intensity of Tb^{3+} ions is sensitized by energy transfer from an excited state of a donor to the emissive $^5D_4$ state of Tb^{3+} ions. Because nucleic acids exhibit strong π-π^* absorption in the 250-280 nm range, the coordination of nucleobases to Tb^{3+} ions allows UV light absorbed by the nucleobases to be converted to the luminescence of Tb^{3+} ions. As illustrated in **Figure 4.33b**, the comparison of luminescence spectra obtained for various aqueous nucleotide/lanthanide coordination nanoparticles indicated that the case of GMP/Tb^{3+} nanoparticles showed strong emission bands in the visible region at 489 ($^5D_4 \rightarrow {}^7F_6$), 544 ($^5D_4 \rightarrow {}^7F_5$), 586 ($^5D_4 \rightarrow {}^7F_4$) and 621 nm ($^5D_4 \rightarrow {}^7F_3$), which is promoted by coordination of O6 and N7 moieties to Tb^{3+} ions [119]. On the other hand, the weak luminescence observed form AMP/Tb^{3+}, CMP/Tb^{3+} and UMP/Tb^{3+} nanoparticles could also be ascribed by the presence of water molecules existing the coordination sphere. Luminescence of lanthanide ions are often quenched in water, due to deactivation of the excited states through O-H vibrational modes of the coordinated water molecules [120]. These results indicated that GMP can form tighly nanoparticle network with Tb^{3+}. Consequently, nanoparticles network can prevent water not to bind with Tb^{3+} resulting in the observation of high emission band. Therefore, the observed intense emission band of Tb^{3+} ions would reflect the hydrophobic environment of the nanoparticle interior.

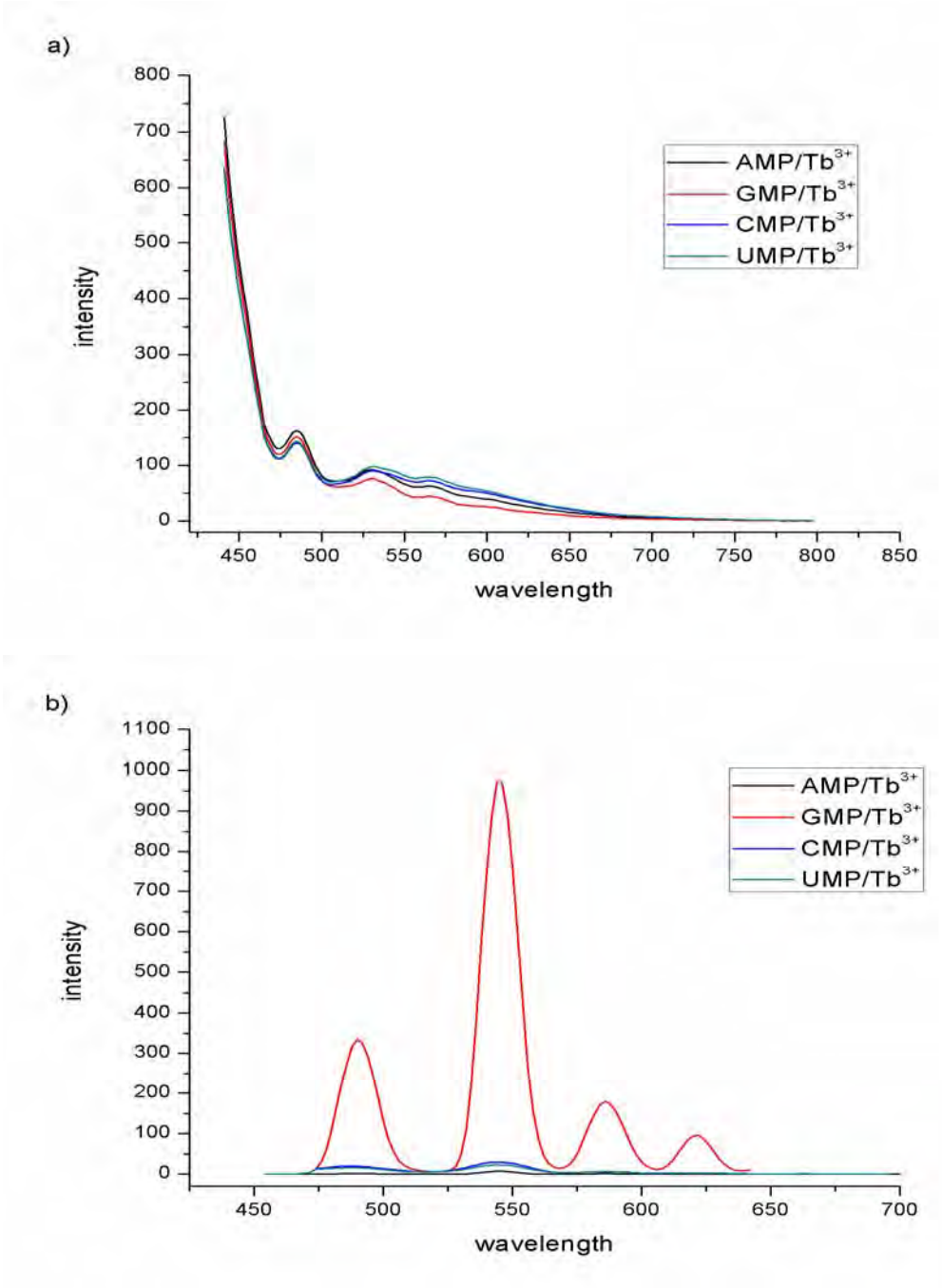

Figure 4.33 Luminescence spectra, a) Fluorescence and b) phosphorescence of aqueous dispersions of AMP/Tb^{3+}, CMP/Tb^{3+}, GMP/Tb^{3+} and UMP/Tb^{3+} nanoparticles in 100 mM HEPES buffer pH 7.4, 10% DMSO in aqueous solution. The excitation wavelength was 404 and 340 nm for fluorescence and phosphorescence measurement, respectively.

4.8.3 Fluorescence measurements of dye-doped nucleotide/lanthanide coordination nanoparticles

To verify the fluorescence response of nucleotide incorporated in nanoparticles, the fluorescence responses of all nucleotide (AMP, CMP, GMP and UMP) show similarly the fluorescence spectra in the range of 450-800 nm (**Figure 4.33a**) which is consistant with fluorescence region of dyes. However, AMP give a poor luminescence response, AMP is thus, a sutable nucleotide for study on dye-doped coordination nanoparticles. The encapsulation of guest molecules in nucleotide/lanthanide nanoparticles was performed by mixing aqueous lanthanide and aqueous solutions containing nucleotides and dye molecules. Typically, terbium (Tb^{3+}) was added to an aqueous mixture of adenosine monophosphate (AMP) disodium salt and dyes. Water soluble dyes (**FLU** and **POR**) were employed as guest molecules to evaluate the inclusion properties of nucleotide/lanthanide networks. As shown in **Figure 4.34**, Very strong fluorescence was observed for **FLU** at 517 nm and **POR** at 662 nm in aqueous solutions without AMP and Tb^{3+}. In contrast, the quenching of emission intensity was observed when **FLU** and **POR** was incorporated in AMP/Tb^{3+} coordination nanoparticles indicating the hydrophobic environment inside coordination nanoparticles. Since both dyes (**FLU** and **POR**) preferred to show high fluorescence intensity in aqueous solution, they perform poor fluorescence responses in the hydrophobic environment.

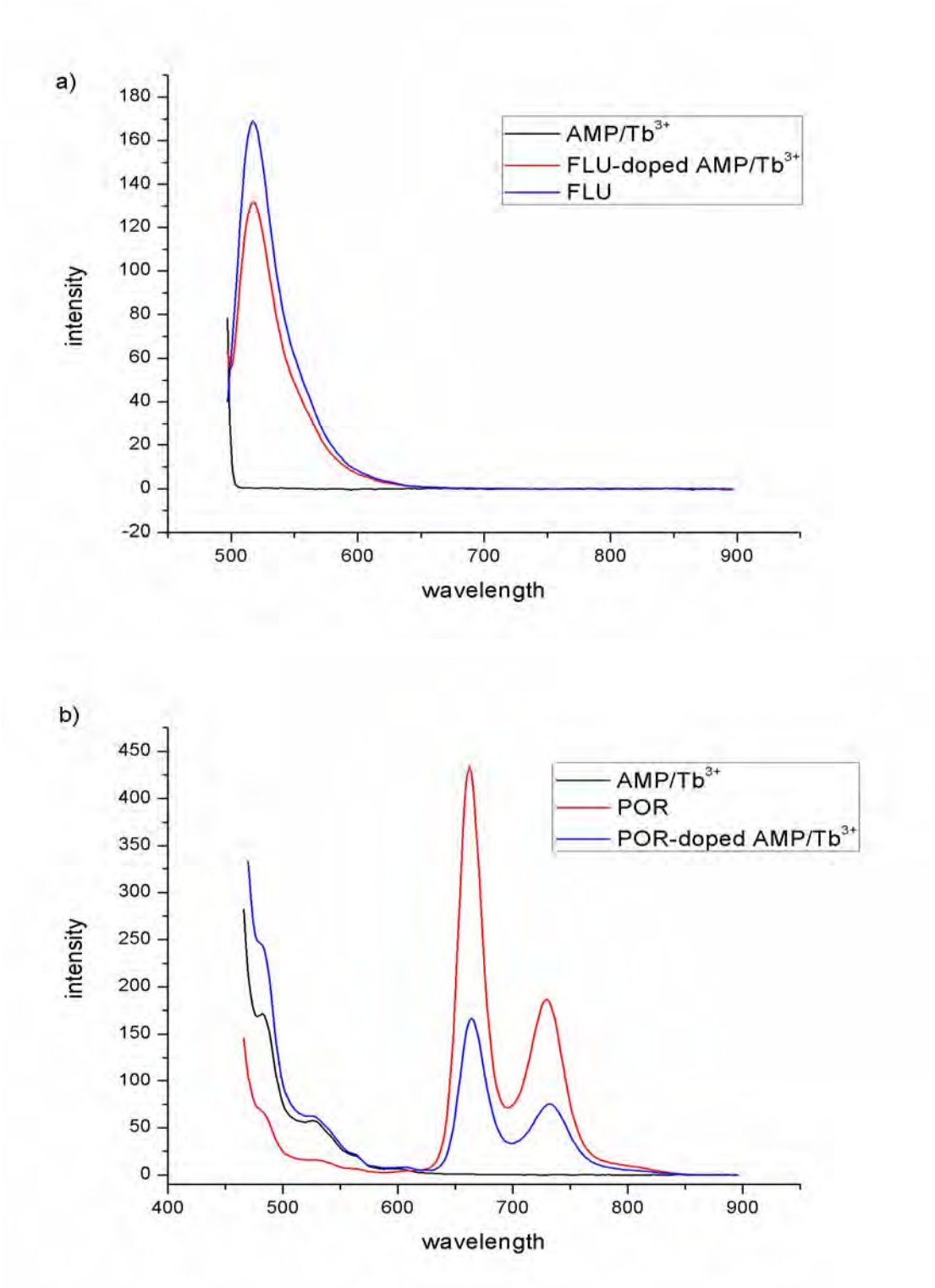

Figure 4.34 Fluorescence of aqueous dispersions of a) **FLU** and b) **POR** doped in AMP/ Tb^{3+} nanoparticles in 100 mM HEPES buffer pH 7.4, 10% DMSO in aqueous solution. The excitation wavelength was 493 and 442 nm for **FLU** and **POR** measurement, respectively.

4.8.4 Fluorescence measurements of boronic anthraquinone based sensors-doped nucleotide/lanthanide coordination nanoparticles for enzymatic probe

The literature review [112] and the successful encapsulation of dyes (**FLU** and **POR**) in nucleotide/lanthanide coordination nanoparticles alerted we to develop the enzymatic probe for determination of glucose by glucose oxidase in coordination nanoparticles system. Coordination nanoparticles were prepared by adding the solution of Tb^{3+} to mixtures of AMP and boronic anthraquinone based sensors (**OB** and **OO**) dissolved in HEPES buffer. In **figure 4.35**, the fluorescence spectra of the encapsulation of **OB** and **OO** in coordination nanoparticles remained unchange in the presence of glucose and glucose oxidase suggesting that **OB** was unable to be use in enzymatic probe under coordination nanoparticles system.

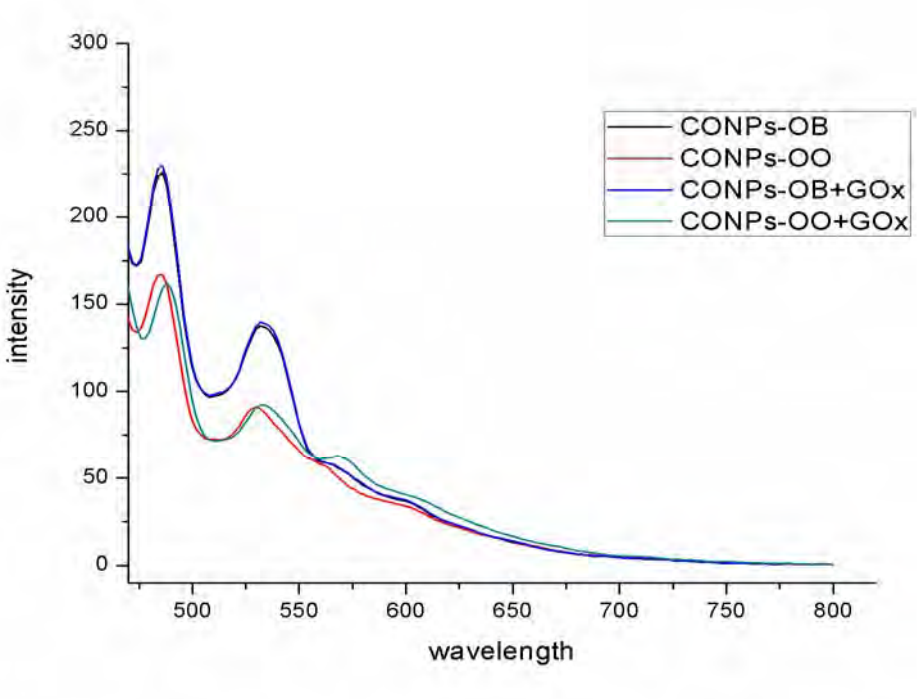

Figure 4.35 Fluorescence spectra of aqueous suspension of **OB**-doped AMP/Tb^{3+}, **OO**-doped AMP/Tb^{3+}, **OB**-doped AMP/Tb^{3+}+GOx and **OO**-doped AMP/Tb^{3+}+GOx in 100 mM HEPES buffer pH 7.4, 10% DMSO in aqueous solution. The excitation wavelength was 415 nm.

4.8.5 Fluorescence measurements of glycoside anthraquinone based sensors-doped nucleotide/lanthanide coordination nanoparticles for enzymatic probe

The adaptive inclusion ability of nucleotide/lanthanide coordination nanoparticles is also applied to incorporate **PAG** or **PO** in nanoparticles. Coordination nanoparticles were prepared by adding the solution of Tb^{3+} to mixtures of AMP and glycoside anthraquinone based sensors (**PAG** and **PO**) dissolved in HEPES buffer. In **figure 4.36** related the encapsulation of **PAG** and **PO** in coordination nanoparticles, the fluorescence spectra of sensor remained unchanged in the presence of *β*-glucosidase. Therefore, **PAG** did not suitably serve as a enzymatic probe incorporated in the coordination nanoparticles system. In contrast, fluorescence spectra of **PAG** in HEPES buffer pH 7.4 were changed significantly upon the addition of *β*-glucosidase in the solution. This signified that these coordination nanoparticles could not promote the *β*-glucosidase sensing of **PAG**.

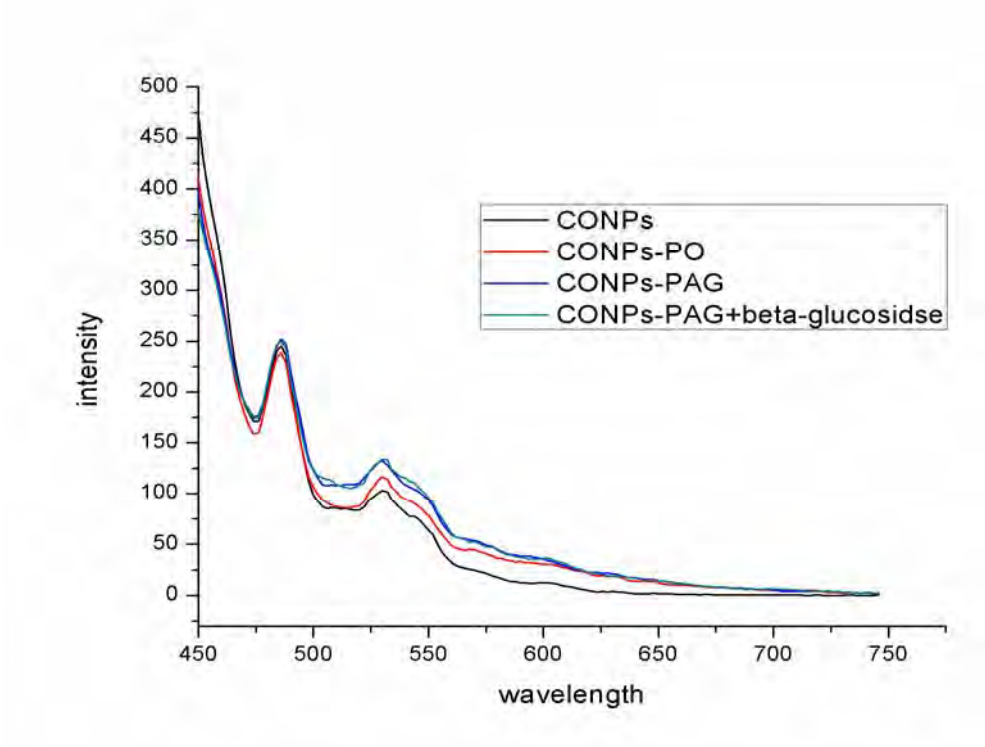

Figure 4.36 Fluorescence spectra of aqueous suspension of **PAG**-doped AMP/Tb^{3+}, **PO**-doped AMP/Tb^{3+}, **PAG**-doped AMP/Tb^{3+}+ *β*-glucosidase and **PO**-doped AMP/Tb^{3+}+ *β*-glucosidase in 100 mM HEPES buffer pH 7.4, 10% DMSO in aqueous solution. The excitation wavelength was 415 nm.

4.9 Aqueous lanthanide nanoparticles by adaptive molecular self-assembly

4.9.1 Preparation and morphology of surfactant/lanthanide nanoparticles

Since, these surfactant/lanthanide nanoparticles are novel formation of coordination nanoparticles, we have investigated the influence on the formation of coordination nanoparticles by varying lanthanides. Firstly, we have focused on the preparation of surfactant/lanthanide nanoparticles using the anion surfactant (dodecyl sulfate (SDS)) incorporated in lanthanide (terbium (Tb^{3+}), gadolinium (Gd^{3+}), Europium (Eu^{3+}) and Lanthanum (La^{3+})) to yield surfactant/lanthanide nanoparticles systems. As described in the experimental sections, mixing of the lanthanide with equivalent of surfactant in HEPES buffer (pH 7.4) resulted in white precipitates. These precipitates were washed with milliQ water several times and collected by ultracentrifugation and redispersed in milliQ water by ultrasonication. Particle morphology was determined by scanning electron microscope measurements (SEM, **Figure 4.37a**) showing the circle of particles. The transmission electron microscope (TEM) (**Figure 4.37b**) display the particle size after purification for the complete series of sample prepared at room temperature, as determined by TEM measurements. Perhaps the most interesting observation is that the type of lanthanide ion has a rather large effect on the particle size. The TEM image of samples SDS/Tb^{3+}, SDS/Gd^{3+} and SDS/La^{3+} reveal that the case of SDS/Tb^{3+} and SDS/Gd^{3+} nanoparticles showed estimately the formation of particles with diameters of 50 nm (in **Figure A.48-A.49**) and also are unity and compact. From the close-up TEM image, the texture of the focused particles of SDS/Tb^{3+} and SDS/Gd^{3+} (inset in **Figure 4.37b**) showed clearly the organic cover on the nanoparticles and the organic network observing from the gray shadow around the black circle (spot) of nanoparticles. On the other hand, the formaytion of SDS/La^{3+} nanoparticles showed approximate diameters of 35 nm (in **Figure A.50**) and the unclear observation of the black spot and the gray shadow around spot indicated a poor nanoparticles formed. Since the agglomerated particles were protected by the surfactant during their growth, this agglomeration is also the reason for the regular shape of the particles, which can observed in the inset in **Figure 4.37(1b)** and **Figure 4.37(2b)**. Conversely, the SDS/La^{3+} sample were not exhibited a

certain degree of agglomeration, where the particles seem to be reversibly fused together in shown in the inset in **Figure 4.37(3b)**.

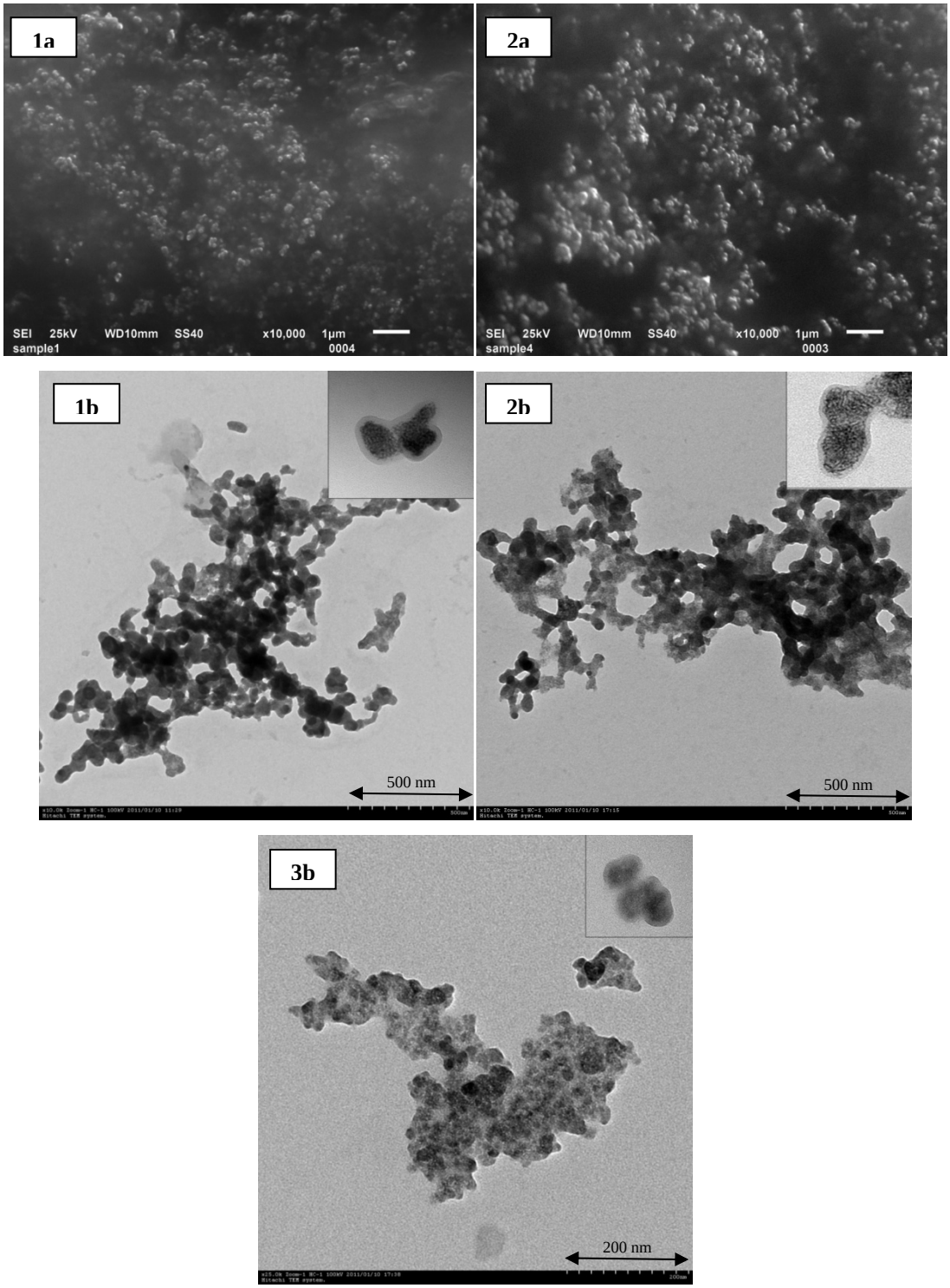

Figure 4.37 a) SEM micrographs of sample 1a) SDS/Tb^{3+} and 2a) SDS/Gd^{3+} **b)** TEM micrograph of sample 1b) SDS/Tb^{3+}, 2b) SDS/Gd^{3+} and 3b) SDS/La^{3+}; inset are a close-up showing the texture of one of the particles.

4.9.2 Fluorescence and phosphorescence measurement of surfactant/lanthanide nanoparticles

To obtain the information on the coordination environment in SDS/Tb^{3+} and SDS/ Gd^{3+} nanoparticles, luminescence properties were investigated. It is known that emission intensity of Tb^{3+} ions is sensitized by energy transfer from an excited state of a donor to the emissive $^5D_4$ state of Tb^{3+} ions. As illustrated in **Figure 4.38b**, the observed enhancement of phosphorescence response for SDS/Tb^{3+} can ascribe to the confinement in SDS environments. To verify the fluorescence response of type of lanthanide incorporated in nanoparticles, the fluorescence responses of Gd^{3+} and Tb^{3+} show similarly the fluorescence spectra in the range of 300-800 nm (**Figure 4.38a**) which is consistant with fluorescence region of dyes to a poor fluorescence response, Both Gd^{3+} and Tb^{3+} is a sutable lanthanides for study with dye-doped nanoparticles.

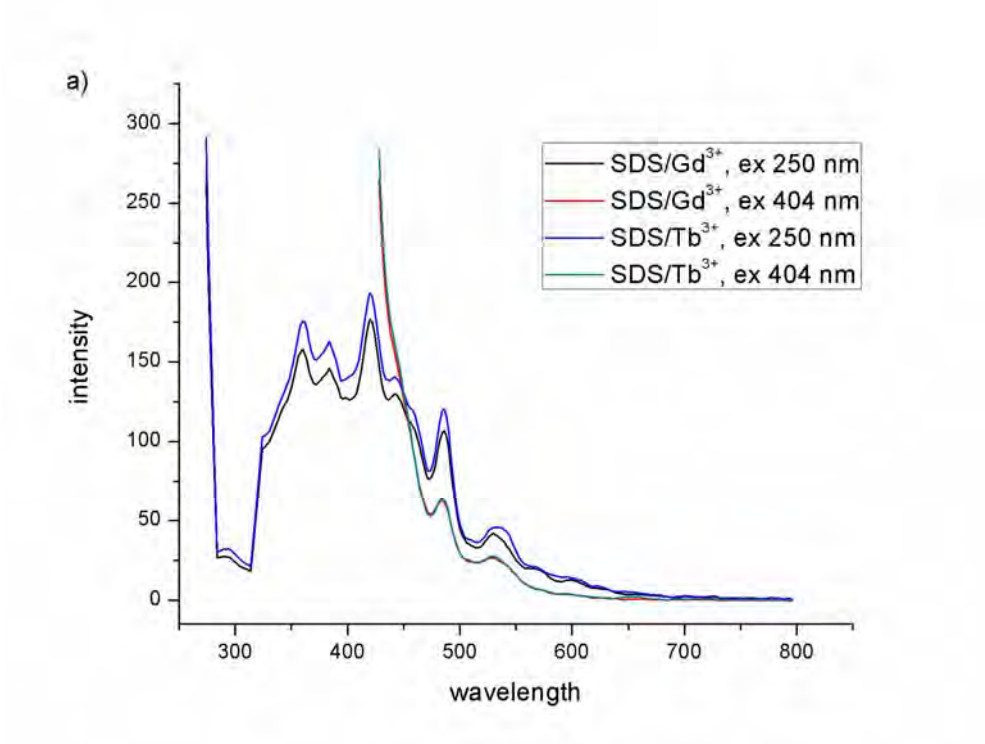

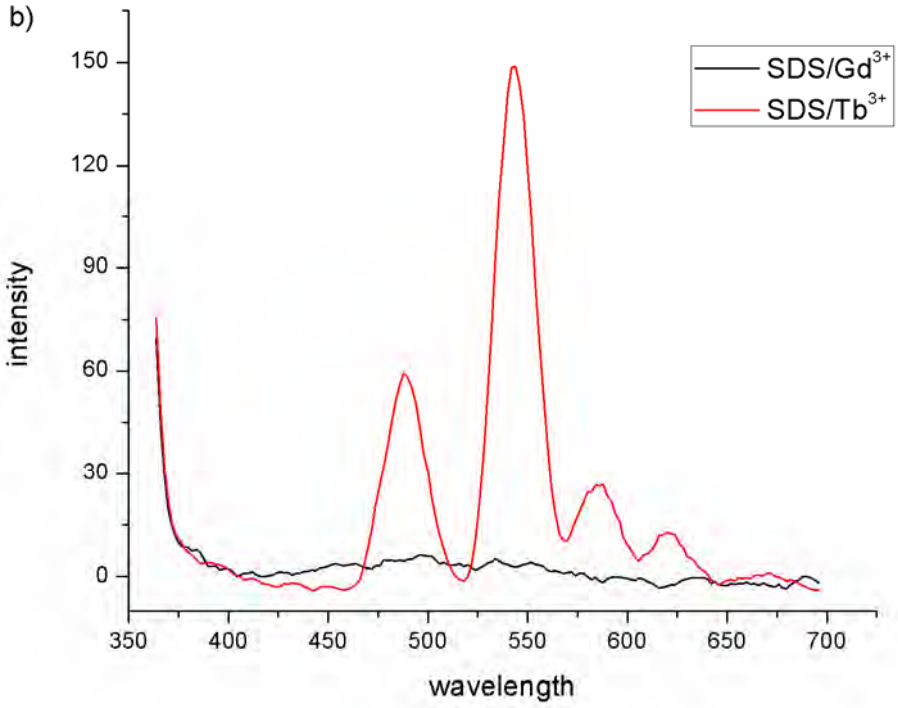

Figure 4.38 Luminescence spectra, **a)** Fluorescence and **b)** phosphorescence of aqueous dispersions of SDS/Tb^{3+} and SDS/Gd^{3+} nanoparticles in 100 mM HEPES buffer pH 7.4, 10% DMSO in aqueous solution. The excitation wavelength was 250 and 404 for fluorescence and 340 nm for phosphorescence measurement.

4.9.3 The encapsulation studies of dye-doped surfactant/lanthanide nanoparticles using UV/Vis spectrophotometry

To encapsulate dyes (**FLU**, **APY**, **NAP**, **CUR** and **CURBF**) in surfactant/lanthanide nanoparticles, aqueous mixture of dodecyl sulfate (SDS) and dye was prepared prior to the addition of gadolinium (Gd^{3+}). After keeping the mixture for 180 minutes, the suspensions were ultrasonicated for 1 minute before the UV/Vis measurements. The amount of dyes unbound to nanoparticles was determined by measuring the absorption intensities of the supernatants after centrifugation of the aqueous mixture. It was found that dyes **APY**, **NAP**, **CUR** and **CURBF** were encapsulated in SDS/Gd^{3+} nanoparticles with the binding ratio of 51.42, 70.56, 99.52 and 99.84 %, respectively (**Figure 4.39**).

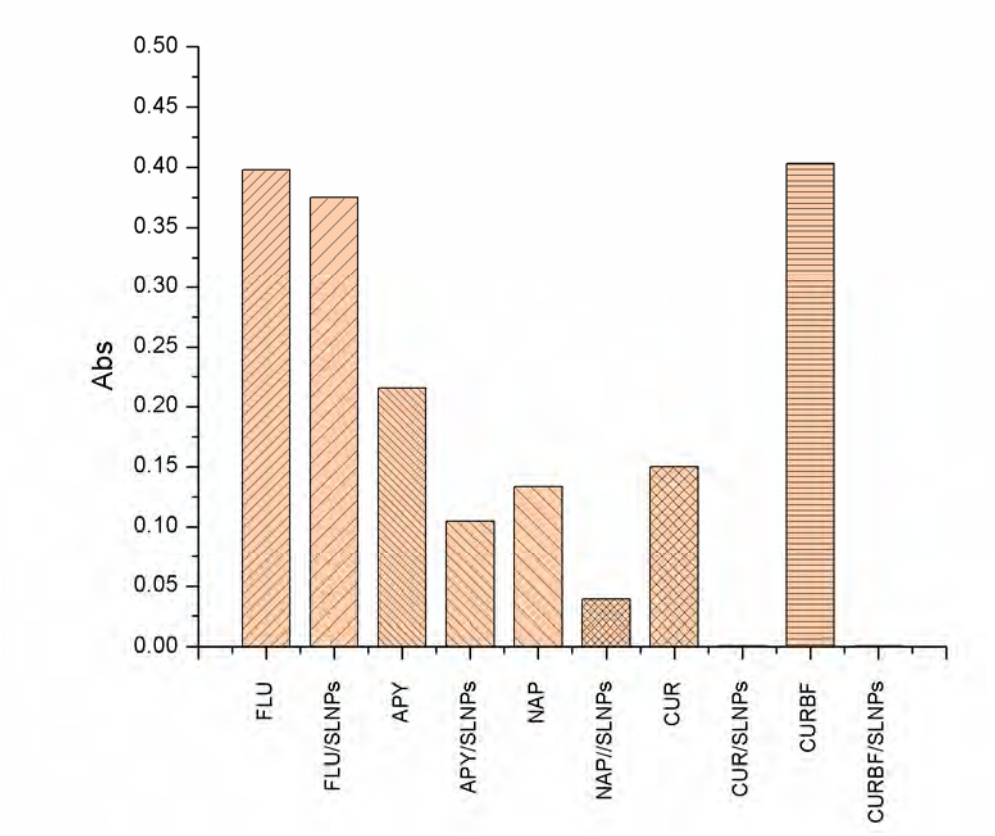

Figure 4.39 UV/Vis absorption spectra of **FLU**, **APY**, **NAP**, **CUR** and **CURBF** and the supernatants of dyes-doped SDS/Gd^{3+} nanoparticles in aqueous system.

4.9.4 Fluorescence measurement of dye-doped surfactant/lanthanide nanoparticles

The encapsulation of guest molecules in surfactant/lanthanide nanoparticles was performed by mixing aqueous lanthanide and aqueous solutions of surfactant and dye molecules. Gadolinium (Gd^{3+}) was added to an aqueous mixture of sodium dodecyl sulfate (SDS) and dyes. Water soluble dyes (**FLU**, **APY**, **NAP**, **CUR** and **CURBF**) were employed as guest molecules to evaluate inclusion properties of surfactant/lanthanide networks. As displayed in **Figure 4.40a** and **Figure 4.40b**, Very strong fluorescence was observed for **FLU** and **APY** in aqueous solution. About, the quenching of emission intensity was observed when **FLU** and **APY** was incorporated in SDS/Gd^{3+} nanoparticles indicating the hydrophobic environment inside coordination nanoparticles. These results are possibly caused by a low amount of dyes incorporated in SDS/Gd^{3+} nanoparticles. In the case of the encapsulation of **NAP** and **CUR** in SDS/Gd^{3+} nanoparticles, the fluorescence spectra showed insignificant changes compared to the SDS/Gd^{3+} nanoparticles without dyes (**figure 4.40c** and **Figure 4.40d**).

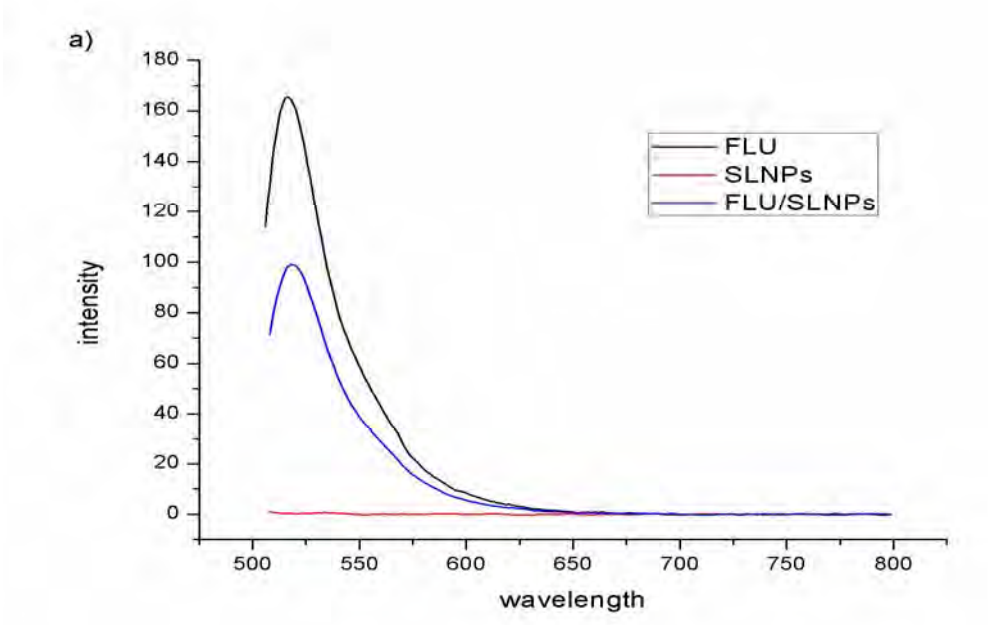

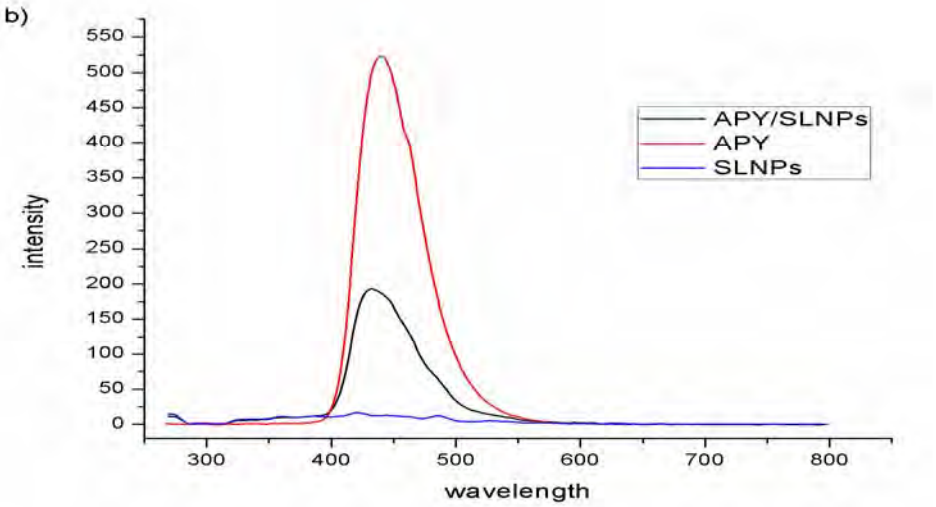
b)
intensity
wavelength
APY/SLNPs
APY
SLNPs

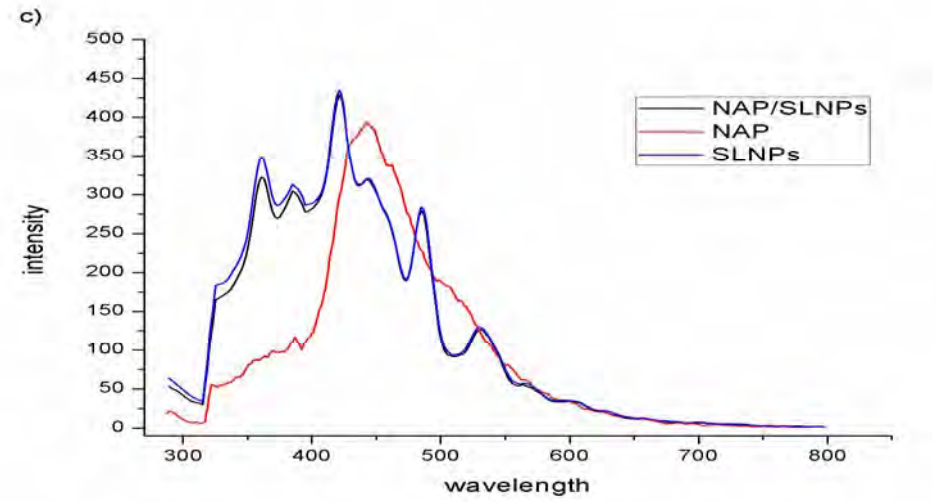
c)
intensity
wavelength
NAP/SLNPs
NAP
SLNPs

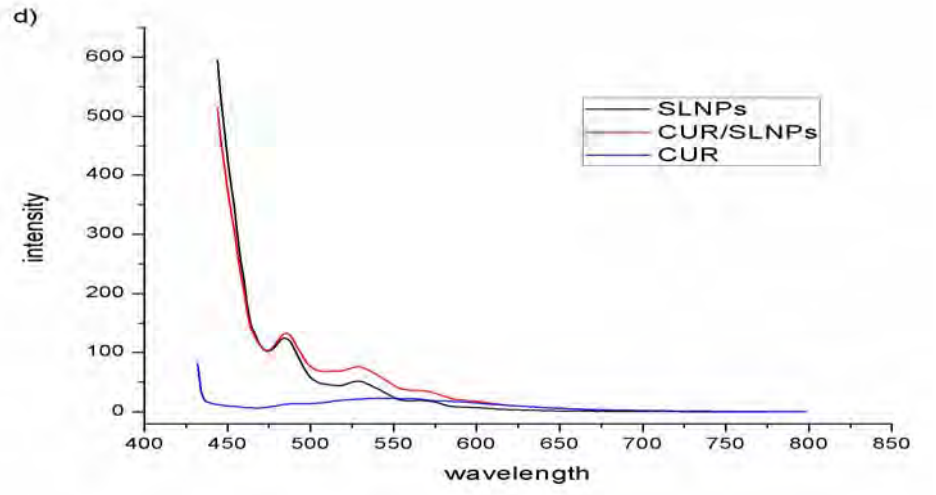
d)
intensity
wavelength
SLNPs
CUR/SLNPs
CUR

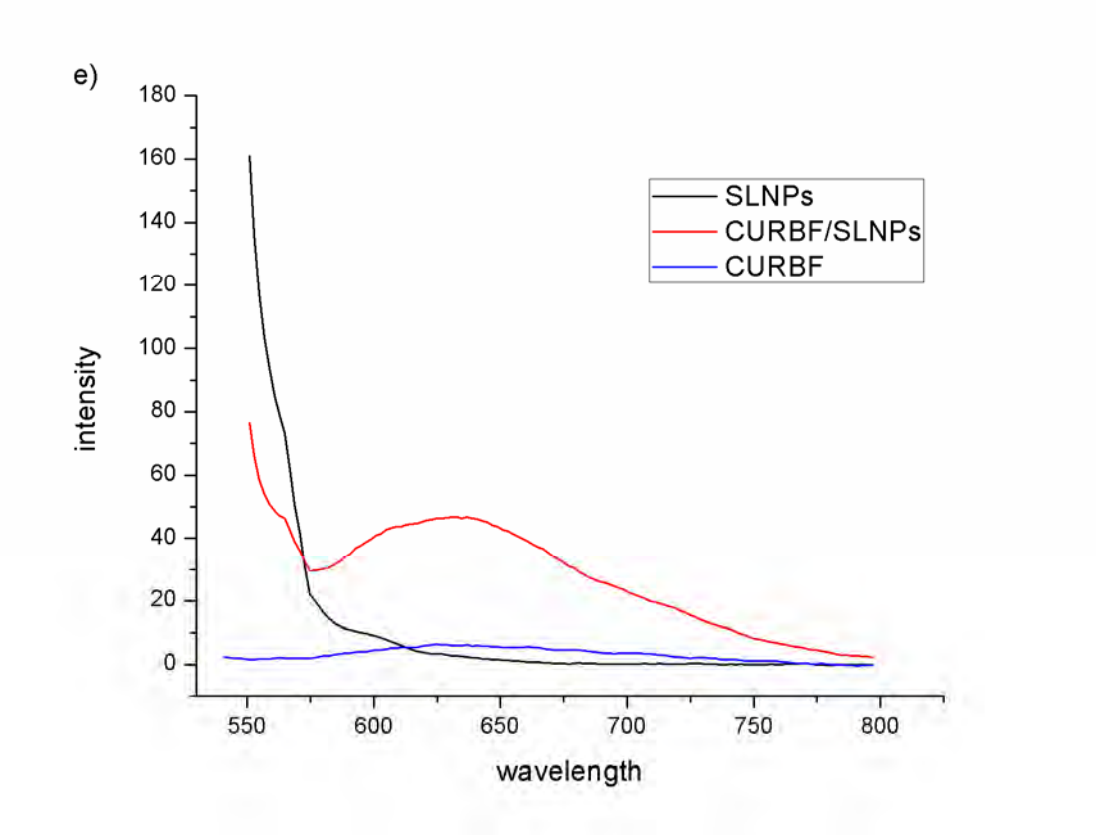

Figure 4.40 Fluorescence spectra of aqueous dispersion of a) **FLU**, b) **APY**, c) **NAP**, d) **CUR** and e) **CURBF** doped surfactant/lanthanide nanoparticles in aqueous system.

Interestingly, the **CURBF**-doped SDS/MLNPs in HEPES buffer pH 7.4 exhibited higher fluorescence response than **CURBF** in HEPES buffer solution (shown in **Figure 4.40e**). This result indicated the coordination networks of SDS and Gd^{3+} ion exert barrier property against aqueous environment. Since the characteristic of the emission band for **CURBF** displayed in high region of wavelength, the emission band corresponding to SDS/Gd^{3+} nanoparticles did not disturb to the emission band of **CURBF**.

4.9.5 The studies on the effect of surfactant types using fluorescence spectrophotometry

The successful encapsulation of dyes (**CURBF**) in surfactant/lanthanide nanoparticles alerted us to develop the enzymatic probe for determine *β*-glucosidase in nanoparticles system. We have focus on studying the various type of surfactant (SDS, CTAB and TX-100), for the preparation of surfactant/lanthanide nanoparticles. Mixing of the lanthanide with equivalent of surfactant in HEPES buffer pH 7.4 resulted in white and yellow precipitates for nanoparticles and dye-dope nanoparticles, respectively. As illustrated in **Figure 4.41**, **PAG** in all types of surfactant formed as nanoparticles system showed a high fluorescence enhanctment in particular of **PAG** incorporated in CTAB/Gd^{3+} system. However, no different emission spectra of **PAG** incorporated in CTAB or TX-100 with and without Gd^{3+} were observed. Interestingly, **PAG** incorporated in SDS/Gd^{3+} nanoparticles which exhibited approximately 60-fold fluorescence enchantment at 610 nm compared to **PAG** incorporated SDS. Since our aim is to utilize the lanthanide to improve the fluorescence response of sensory molecule, thus, selected the coordination of SDS/Gd^{3+} nanoparticles to apply for the enzymatic probe system of **PAG** in *β*-glucosidase sensing

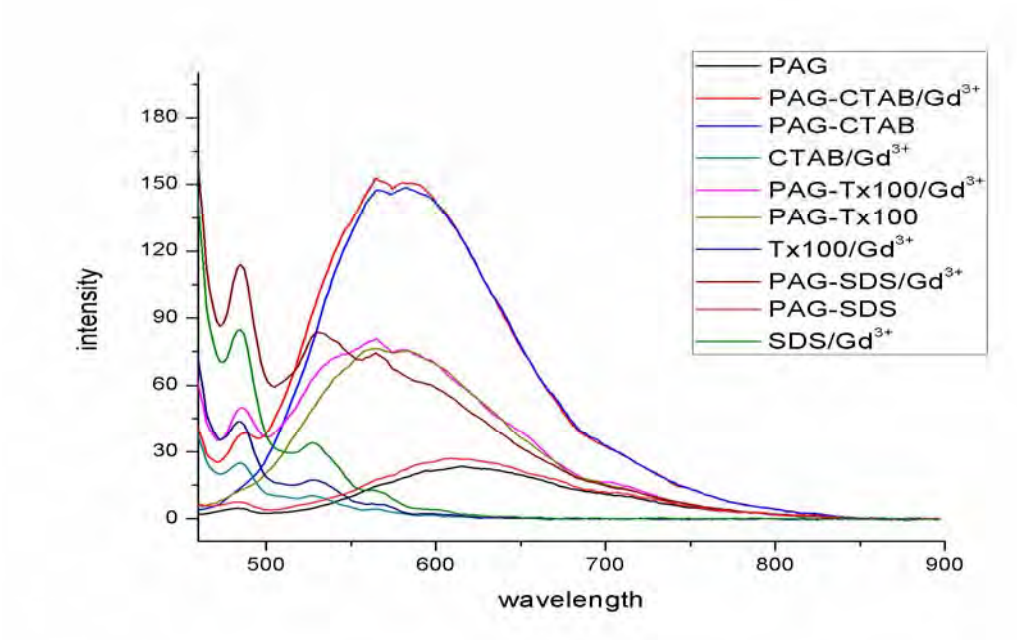

Figure 4.41 Fluorescence spectra of **PAG**-doped surfactant/lanthanide nanoparticles in various surfactant types and **PAG** in various micelle systems.

4.9.6 Fluorescence measurement of glycoside anthraquinone based sensors-doped surfactant/lanthanide nanoparticles for enzymatic probe

From the successful encapsulation of dyes (**PAG**) in SDS/Gd^{3+} nanoparticles described above, we took an effort to develop the enzymatic probe for determining β-glucosidase in nanoparticles system. This nanoparticles studied consist of Gd^{3+}, SDS and HEPES. Nanoparticles were prepared by adding the solution of Gd^{3+} to the mixtures of SDS and glycoside anthraquinone based sensors (**PAG**) dissolved in HEPES buffer. As shown in **Figure 4.43**, the emission band of **PAG** at 610 nm was intensed in the nanoparticles system. After adding β-glucosidase, the emission band at 610 nm was gradually quenched as a function of time with the concomitant of the fluorescence enhancement in range of 450-550 nm corresponding to the characteristic fluorescence of β-glucosidase.

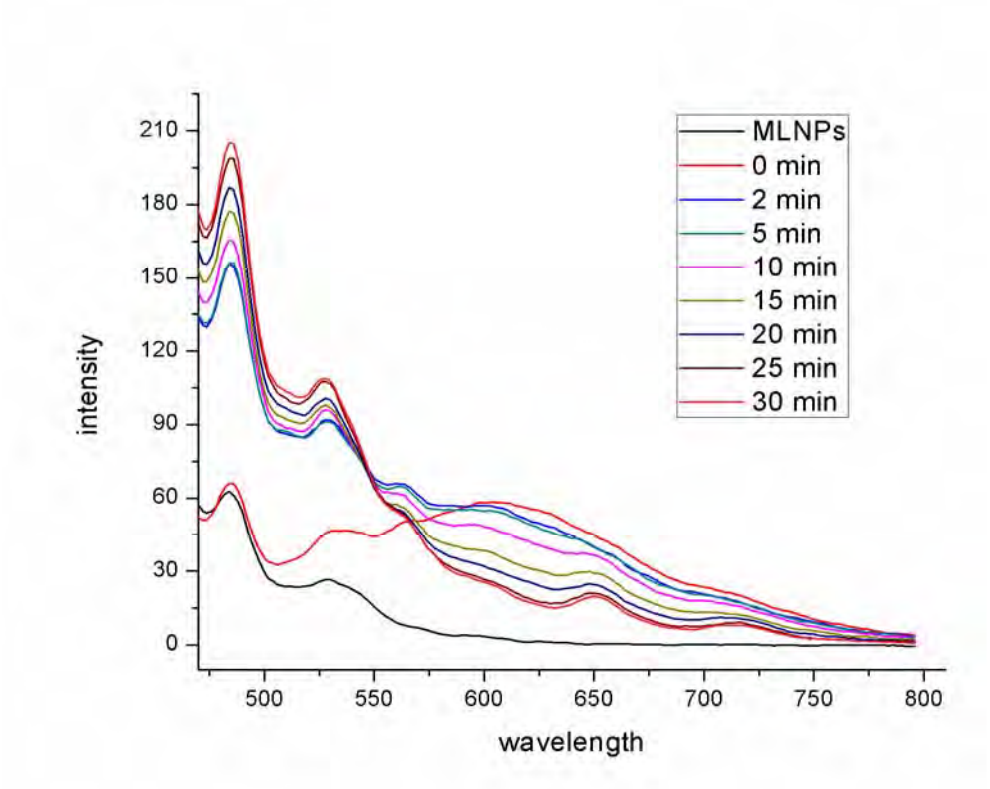

Figure 4.42 Emission spectra of 0.01 mM **PAG** incorporated SDS/Gd^{3+} nanoparticles at 0, 2, 5, 10, 25 and 30 minutes after the addition of β-glucosidase (6 units). The reaction was performed in 0.1 M HEPES buffer pH 7.4, 10% DMSO in aqueous solution at 37 °C. The excitation wavelength was 415 nm

CHAPTER V

CONCUSION

We have successfully synthesized the fluorogenic compounds based on boronic anthraquinone (**OB** and **PB**) and glycoside anthraquinone (**OAG** and **PAG**). Firstly, we developed boronic anthraquinone based sensors (**OB** and **PB**) for determining glucose by enzymatic probe system with glucose oxidase using fluorescence spectrophotometry. This method was described that the reaction of glucose oxidase with glucose in the presence of oxygen produced the gluconic acid and hydrogen peroxide which can convert the boronic acid based boronic anthraquinone (**OB**) to be hydroxyl group in 10% DMSO with 100 mM HEPES buffer at pH7.4. The fluorescence response of **OB** was dramatically quenched after adding glucose oxidase in the solution of **OB** and glucose. For **PB**, it was found that it can bind with glucose directly. Thus, it could not be used for glucose sensing via the enzymatic system of glucose oxidase. **OB** is a good candidate for fluorogenic sensor to detect glucose in enzymatic probe system by glucose oxidase. The optimum condition used for enzymatic probe system of **OB** was amount of glucose oxidase at 6 units and the temperature at 37 ^{o}C and the reaction time of 60 minutes. The working concentration of glucose in enzymatic probe system of **OB** by glucose oxidase is 0.08 to 0.42 mM. The K_m value for the Michaelis-Menten constant is 0.18 mM under V_{max} value of 5.63 minutes.

Additionally, we have focused on developing the glycoside anthraquinone based sensors (**OAG** and **PAG**) for detection of β-glucosidase using fluorescence spectrophotometry. The optimum condition used in this study was the concentration of **PAG** at 0.02 mM, anount of β-glucosidase at 6 units, the temperature at 37^{o}C in 10% DMSO with 0.1M phosphate buffer at pH 6. From the fluorescence results, **PAG** is a good candidate for detection of β-glucosidase under fluorescence quenching. To improve the fluorescence response of **PAG** in β-glucosidase sensing, we have taken an effort to apply **PAG** incorporated in three materials including a micellar system, adaptive self-assembled nucleotide/lanthanide nanoparticles and surfactant/lanthanide nanoparticles. In the case of the micellar system, the fluorescence response of **PAG**

was found to be intensed in CTAB micelles better than in SDS and TX-100 micelles. The CTAB micelle provided a significant improvement in sensitivity and selectivity with a 150-fold fluorescence enhancement of **PAG**. Interestingly, the disappearance of fluorescence responses of β-glucosidase in CTAB micellar system suggested that no fluorescence of β-glucosidase disturbed the signal of **PAG** in detection of β-glucosidase. Upon the addition of β-glucosidase into the solution of **PAG** incorporated in CTAB micelle at PBS buffer pH 7.4, the fluorescence responses were significantly decreased. Concerning the encapsulated **PAG** in the adaptive self-assembled nucleotide/lanthanide nanoparticles, it was found that the fluorescence response of **PAG** in this system remained unchanged upon adding the β-glucosidase. Thus, these nucleotide/lanthanide nanoparticles could not improve the β-glucosidase sensing of **PAG**. Finally, we have developed the enzymatic probe for determination of β-glucosidase by luminescence enhancement of surfactant/lanthanide nanoparticles. These prepared nanoparticles consist of Gd^{3+}, SDS and HEPES. **PAG** incorporated in SDS/Gd^{3+} nanoparticles exhibited approximately 60-fold fluorescence enchantment at 610 nm. After adding β-glucosidase, the emission band at 610 nm was gradually quenched upon increasing of time. The SDS/Gd^{3+} nanoparticles can also enhance the fluorescence response of β-glucosidase in the range of 450-550 nm. However, **PAG** incorporated in CTAB micelle can serve as the most powerful tool for the task of β-glucosidase sensing because this methodology can suppress the fluorescence response of β-glucosidase.

REFERENCES

[1] Lakowicz, J. R. *Principles of Fluorescence Spectroscopy, 3rd edition*. Springer: New York, 2006.

[2] Valeur, B. *Molecular Fluorescence, Principles and Applications*; Wiley-VCH Verlag GmbH: Weinheim, Germany, 2002.

[3] Turro, N. J. *Modern Molecular Photochemistry of Organic Molecules*; University Science Books: New York, 2009.

[4] Lakowicz, J. R., Ed. *Principles of Fluorescence Spectroscopy*; Plenum Publishers Corp.: New York, 1999.

[5] de Silva, A. P., et al. *Chem. ReV*. 97 (1997): 1515.

[6] Aoki, I., Sakaki, T., and Shinkai, S. *J. Chem. Soc., Chem. Commun*. (1992): 730.

[7] Ji, H.-F., Dabestani, R., Brown, G. M., and Sachleben, R. A. *Chem. Commun*. (2000): 833.

[8] Ji, H.-F., Brown, G. M., and Dabestani, R. *Chem. Commun*. (1999): 609.

[9] Martínez-Máñez, and R., Sancenón, F. *Chem. ReV*. 103 (2003): 4419.

[10] Valeur, B., and Leray, I. *Coord. Chem. ReV*. 205 (2000): 3.

[11] Valeur, B., Bourson, J., Pouget, J., and Czarnik, A. W. *Fluorescent Chemosensors for Ion and Molecule Recognition*; ACS Symposium Series 538; American Chemical Society: Washington, DC, 1993; p25.

[12] Rettig, W., and Lapouyade, R. *In Probe design and chemical sensing*; Lakowicz, J. R., Ed.; Topics in Fluorescence Spectroscopy; Plenum: New York, 4 (1994): 109.

[13] Löhr, H.-G., and Vögtle, F. *Acc. Chem. Res*. 18 (1985): 65.

[14] Akkaya, E. U., Huston, M. E., and Czarnik, A. W. *J. Am. Chem. Soc*. 112 (1990): 3590.

[15] Michaelis, L., and Menten, M. L. *Biochem. Z*. 49 (1913): 333.

[16] Lu, H. P., Xun, and L., Xie, X. S. *Science* 282 (1998): 1877.

[17] Schenter, G. K., Lu, H. P., and Xie, X. S. *J. Phys. Chem. A* 103 (1999): 10477.

[18] Xie, S. *Single Mol*. 4 (2001): 229.

[19] Kou, S. C., Cherayil, B. J., Min, W., English, B. P., and Xie, X. S *J. Phys. Chem. B* 109 (2005): 19068.

[20] Günter, W. *Chem ReV*. 102 (2002): 1.

[21] Shimada, T., Nakanishi, K., and Morihara, K. *Bull. Chem. Soc. Jpn*. 65 (1992): 954.

[22] Ohya, Y., Miyaoka, J., and Ouchi, T. *Macromol. Rapid Commun*. 17 (1996): 871.

[23] Voet, D., Voet, J. G., and Pratt, C. W. *Fundamentals of Biochemistry*; J. Wiley: New York, (1999).

[24] Segel, I. H. *Enzyme Kinetics: Behavior and Analysis of Rapid Equilibrium and Steady-State Enzyme Systems*; Wiley: New York, (1993).

[25] Bünzli, J.-C. G., and Eliseeva, S. V. *In Springer Series on Fluorescence, Lanthanide Spectroscopy, Materials, and Bio-applications*; Springer Verlag: Berlin, 2010; Chapter 2, in press.

[26] Nishioka et al In *Handbook on the Physics and Chemistry of Rare Earths*; Elsevier Science BV: Amsterdam, 37 (2007): 171.

[27] Yuan, J., and Wang, G. *Trends Anal. Chem*. 25 (2006): 490.

[28] Connally, R. E., and Piper, J. A. *Ann. N. Y. Acad. Sci.* 1130 (2008): 106.

[29] Weissman, S. I. *J. Chem. Phys*. 10 (1942): 214.

[30] de Sá, et al. *Coord. Chem. ReV*. 196 (2000): 165.

[31] Eliseeva, S. V., and Bünzli, J.-C. G. *Chem. Soc. ReV*. 39 (2010): 189.

[32] Blasse, G. *Struct. Bonding (Berlin)* 26 (1976): 45.

[33] Zolin, V. F. et al. *J. Alloys Compd*. 380 (2004): 279.

[34] Faulkner, S., Natrajan, L. S., Perry, W. S., and Sykes, D. *Dalton Trans*. (2009): 3890.

[35] Imbert, D., Cantuel, M., Bünzli, J.-C. G., Bernardinelli, G., and Piguet, C. *J. Am. Chem. Soc*. 125 (2003): 15698.

[36] Pope, S. J. A., Coe, B. J., Faulkner, S., Bichenkova, E. V., Yu, X., and Douglas, K. T. *J. Am. Chem. Soc*. 126 (2004): 9490.

[37] Lazarides, T., Sykes, D., Faulkner, S., Barbieri, A., and Ward, M. D. *Chem.sEur. J*. 14 (2008): 9389.

[38] Torelli, S., Delahaye, S., Hauser, A., Bernardinelli, G., and Piguet, C. *Chem.sEur. J*. 10 (2004): 3503.

[39] Lazarides, T., Tart, N. M., Sykes, D., Faulkner, S., Barbieri, A., and Ward, M. D. *Dalton Trans*. (2009): 3971.

[40] Riis-Johannessen, T., Dupont, N., Canard, G., Bernardinelli, G., Hauser, A., and Piguet, C. *Dalton Trans*. (2008): 3661.

[41] Lazarides, T., Davies, G. M., Adams, H., Sabatini, C., Barigelletti, F., Barbieri, A., Pope, S. J. A., Faulkner, S., and Ward, M. D. *Photochem. Photobiol. Sci*. 6 (2007): 1152.

[42] Mehlstäubl, M., Kottas, G. S., Colella, S., and De Cola, L. *Dalton Trans*. (2008): 2385.

[43] Xu, H. B., Zhang, L. Y., Chen, X. M., Li, X. L., and Chen, Z. N. *Cryst. Growth. Des*. 9 (2009): 569.

[44] Ziessel, R., Diring, S., Kadjane, P., Charbonnière, L. J., Retailleau, P., and Philouze, C. *Chem. Asian J*. 2 (2007): 975.

[45] Shavaleev, N. M., Moorcraft, L. P., Pope, S. J. A., Bell, Z. R., Faulkner, S., and Ward, M. D. *Chem. Commun*. (2003): 1134.

[46] Comby, S., and Bünzli, J.-C. G. In *Handbook on the Physics and Chemistry of Rare Earths*; Gschneidner, K. A., Jr., Bünzli, J.-C. G., Pecharsky, V. K., Eds.; Elsevier Science BV: Amsterdam, 37 (2007): 217.

[47] Göpel, W., Hesse, J., and Zemel, J. N., Eds. Sensors: *A Comprehensive Survey*; VCH Publishers: Weinheim, Germany, 2 (1991): 1.

[48] Hulanicki, A., Geab, S., and Ingman, F. *Pure Appl. Chem*. 63 (1991): 1247.

[49] Thevenot, D. R., Toth, K., Durst, R. A., and Wilson, G. S. *Biosens. Bioelectron*. 61 (2001): 121.

[50] Hilty, C., Lowery, T. J., Wemmer, D. E., and Pines, A. *Angew. Chem., Int.* Ed. 45 (2005): 70.

[51] Xu, H., Aylott, J. W., and Kopelman, R. *Analyst* 127 (2002): 1471.

[52] Papkovsky, D. B. *Sens. Actuators, B* 11 (1993): 293.

[53] Papkovsky, D. B., Olah, J., and Kurochkin, I. N. *Sens. Actuators, B* 11 (1993): 525.

[54] Trettnak, W., Leiner, M. J., and Wolfbeis, O. S. *Analyst* 113 (1988):1519.

[55] Dremel, B. A., Schaffar, B. P., and Schmid, R. D. *Anal. Chim. Acta* 225 (1989): 293.

[56] Schaffar, B. P., and Wolfbeis, O. S. *Biosens. Bioelectron*. 5 (1990):137.

[57] Moreno-Bondi, M. C., Wolfbeis, O. S., Leiner, M. J., and Schaffar, B. P. *Anal. Chem*. 62 (1990): 2377.

[58] Dremel, B. A., Li, S. Y., and Schmid, R. D. *Biosens. Bioelectron*. 7 (1992): 133.

[59] Andres, K. D., Wehnert, G., Thordsen, O., and Scheper, T. *Sens. Actuators, B*. 11 (1993): 395.

[60] Valencia-Gonzalez, M. J., Liu, Y. M., Diaz-Garcia, M. E., and Sanz-Medel, A. *Anal. Chim. Acta* 283 (1993): 439.

[61] Li, L., and Walt, D. R. *Anal. Chem*. 67 (1995): 3746.

[62] Neubauer, A., Pum, D., Sleytr, U. B., Klimant, I., and Wolfbeis, O. S. *Biosens. Bioelectron*. 11 (1996): 317.

[63] Rosenzweig, Z., and Kopelman, R. *Anal. Chem*. 68 (1996): 1408.

[64] Rosenzweig, Z., and Kopelman, R. *Sens. Actuators, B* 35-36 (1996): 475.

[65] Wu, X., Choi, M. M. F., and Xiao, D. *Analyst* 125 (2000): 157.

[66] Wolfbeis, O. S., Oehme, I., Papkovskaya, N., and Klimant, I. *Biosens. Bioelectron*. 15 (2000): 69.

[67] Choi, M. M. F., and Wilfred, S. *Analyst* 126 (2001): 1558.

[68] Wu, X. J., and Choi, M. M. F. *Anal. Chim. Acta* 514 (2004): 219.

[69] Zhou, Z., Qiao, L., Zhang, P., Xiao, D., and Choi, M. M. F. *Anal. Bioanal. Chem*. 383 (2005): 673.

[70] Tsai, H. C., and Doong, R. A. *Anal. Biochem*. 334 (2004): 183.

[71] Schaeferling, M., Wu, M., and Wolfbeis, O. S. *J. Fluoresc*. 14 (2004): 561.

[72] Matsubara, C., Kudo, K., Kawashita, T., and Takamura, K. *Anal. Chem.* 57 (1985): 1107.

[73] Abdel-Latif, M. S., and Guilbault, G. G. *Anal. Chim. Acta* 221 (1989): 11.

[74] Blum, L. J. *Enzyme Microb. Technol*. 15 (1993): 407.

[75] Kremeskoetter, J., Wilson, R., Schiffrin, D. J., Luff, B. J., and Wilkinson, J. S. *Meas. Sci. Technol*. 6 (1995): 1325.

[76] Zhou, X., and Arnold, M. A. *Anal. Chim. Acta* 304 (1995): 147.

[77] Marquette, C. A., and Blum, L. J. *Anal. Chim. Acta* 381 (1999): 1.

[78] Harms, D., Meyer, J., Westerheide, L., Krebs, B., and Karst, U. *Anal. Chim. Acta* 401 (1999): 83.

[79] Marquette, C. A., Leca, B. D., and Blum, L. J. *Luminescence* 16 (2001): 159.

[80] Koncki, R., Lenarczuk, T., Radomska, A., and Glab, S. *Analyst* 126 (2001): 1080.

[81] Lenarczuk, T., Wencel, D., Glab, S., and Koncki, R. *Anal. Chim. Acta* 447 (2001): 23.

[82] Zhu, L., Li, Y., and Zhu, G. *Sens. Actuators, B.* 86 (2002): 209.

[83] Zhu, L., Li, Y., Tian, F., Xu, B., and Zhu, G. *Sens. Actuators, B.* 84(2002): 265.

[84] Wolfbeis, O. S., Schaeferling, M., and Duerkop, A. *Microchim. Acta*. 143 (2003): 221.

[85] Heo, J., and Crooks, R. M. *Anal. Chem*. 77 (2005): 6843.

[86] Trettnak, W., Leiner, M. J., and Wolfbeis, O. S. *Biosens.* 4 (1988): 15.

[87] Piletsky, S. A., Panasyuk, T. L., Piletskaya, E. V., Sergeeva, T. A., Elskaya, A. V., Pringsheim, E., and Wolfbeis, O. S. *Fresenius J. Anal. Chem.* 266 (2000): 807.

[88] Cox, M., Lehninger, A. L., and Nelson, D. R. *Lehninger principles of biochemistry*. New York: Worth Publishers, 2000: 306–308.

[89] Miyawaki, A., Llopis, J., Heim, R., McCaffery, J. M., Adams, J. A., Ikura, M., and Tsien, R. Y. *Nature* 388 (1997): 882.

[90] Rotman, B., and Papermaster, B. W. *Proc. Natl. Acad. Sci. U.S.A.* 55 (1966): 134.

[91] Leytus, S. P., Melhado, L. L., and Mangel, W. F. *Biochem. J*. 209 (1983): 299.

[92] Kenmoku, S., Urano, Y., Kojima, H., and Nagano, T. *J. Am. Chem. Soc*. 129 (2007): 7313.

[93] Miura, T., Urano, Y., Tanaka, K., Nagano, T., Ohkubo, K., and Fukuzumi, S. *J. Am. Chem. Soc*. 125 (2003): 8666.

[94] Ueno, T. et al *J. Am. Chem. Soc*. 126 (2004): 14079.

[95] Umezawa, N., Tanaka, K., Urano, Y., Kikuchi, K., Higuchi, T., and Nagano, T. *Angew. Chem., Int. Ed*. 38 (1999): 2899.

[96] Tanaka, K., Miura, T., Umezawa, N., Urano, Y., Kikuchi, K., Higuchi, T., and Nagano, T. *J. Am. Chem. Soc*. 123 (2001): 2530.

[97] Kojima, H., Urano, Y., Kikuchi, K., Higuchi, T., Hirata, Y., and Nagano, T. *Angew. Chem., Int. Ed*. 38 (1999): 3209.

[98] Gabe, Y., Urano, Y., Kikuchi, K., Kojima, H., and Nagano, T. *J. Am. Chem. Soc.* 126 (2004): 3357.

[99] Kojima, H., Hirotani, M., Nakatsubo, N., Kikuchi, K., Urano, Y., Higuchi, T., Hirata, Y., and Nagano, T. *Anal. Chem*. 73 (2001): 1967.

[100] Sasaki, E., Kojima, H., Nishimatsu, H., Urano, Y., Kikuchi, K., Hirata, Y., and Nagano, T. *J. Am. Chem. Soc*. 127 (2005): 3684.

[101] Setsukinai, K., Urano, Y., Kakinuma, K., Majima, H. J., and Nagano, T. *J. Biol. Chem*. 278 (2003): 3170.

[102] Koide, Y., Urano, Y., Kenmoku, S., Kojima, H., and Nagano, T. *J. Am. Chem. Soc.* 129 (2007): 10324.

[103] Ueno, T., Urano, Y., Kojima, H., and Nagano, T. *J. Am. Chem. Soc*. 128 (2006): 10640.

[104] Izumi, S., Urano, Y., Hanaoka, K., Terai, T., and Nagano, T. *J. Am. Chem. Soc*. 131 (2009): 10189.

[105] Fujikawa, Y. et al. *J. Am. Chem. Soc*. 130 (2008): 14533.

[106] Urano, Y., Kamiya, M., Kanda, K., Ueno, T., Hirose, K., and Nagano, T. *J. Am. Chem. Soc*. 127 (2005): 4888.

[107] Kamiya, M., Urano, Y., Ebata, N., Yamamoto, M., Kosuge, J., and Nagano, T. *Angew. Chem., Int. Ed*. 44 (2005): 5439.

[108] Kobayashi, T., Urano, Y., Kamiya, M., Ueno, T., Kojima, H., and Nagano, T. *J. Am. Chem. Soc*. 129 (2007): 6696.

[109] Hama, Y.et al. *Neoplasia* 8 (2006): 607.

[110] Kamiya, M. et al. *J. Am. Chem. Soc*. 129 (2007): 3918.

[111] Ryuhei, N., et al. *J. Am. Chem. Soc*. 131 (2009): 2151.

[112] Ryuhei, N., Carole, A., Ryosuke, G., Takao, N., and Nobuo, K. *Angew. Chem. Int. Ed*. 48 (2009): 9465.

[113] Aaron, E. A., Voytek, S. O., and Christopher, J. C. *J. Am. Chem. Soc*. 128 (2006): 9640.

[114] Kun, Y. et al. *J. Phys. Chem*. *C* 113 (2009): 20169.

[115] Konijn, A. M., Levy, R., Link, G., Hershko, C. J. *Immunol. Methods* 54 (1982): 297.

[116] Armenta, R., Tarnowski, T., Gibbons, I., Ullman, E. F. *Anal. Biochem*. 146 (1985): 211.

[117] Baruch, D., Glickstein, H., Cabantchik, Z. I. *Exp. Parasitol*. 73 (1991): 440.

[118] Tang, L. Y., Wang, Z. J., Fu, M. H., He, Y., Wu, H. W., Huang, L. Q. *Chinese Chemical Letters* 19 (2008): 1083.

[119] Fu, P. K.-L., Turro, C. *J. Am. Chem. Soc.* 121 (1998): 1.

[120] Bünzli, J.-C. G., Piguet, C. *Chem. Soc. Rev*. 34 (2005): 1048.

[121] Value, B. *Molecular fluorescence principle and application*. New York: Wiley-VCH, (2001).

APPENDIX

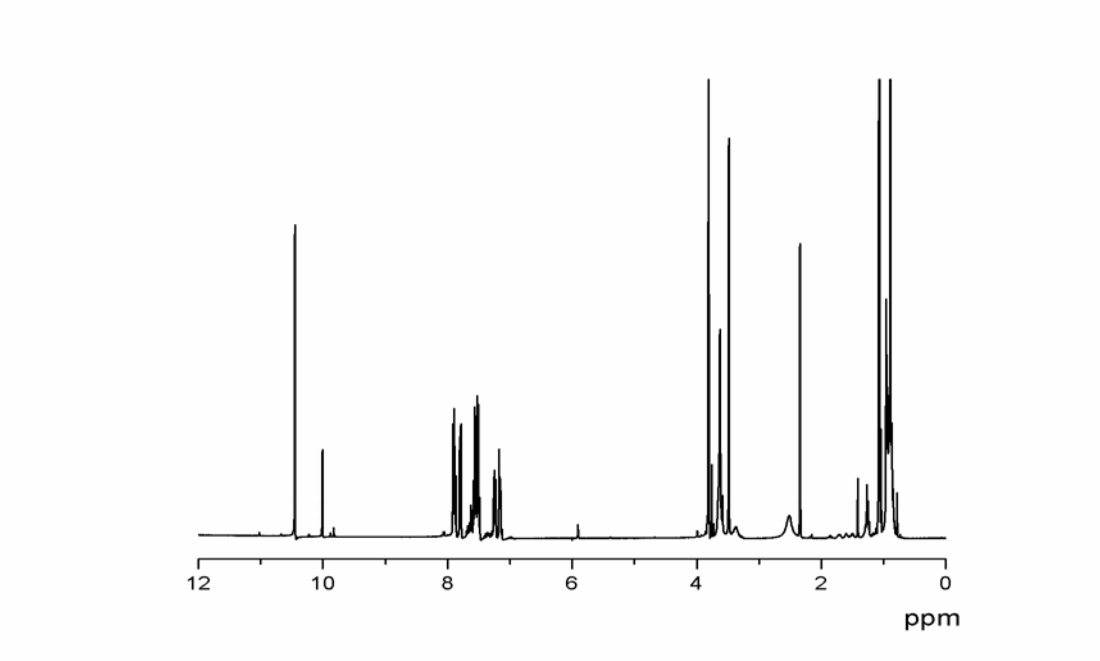

Figure A.1 The ^{1}H-NMR spectrum (400 MHz) of 2-(5,5-dimethyl-1,3,2-dioxaborinan-2-yl)benzaldehyde (**1o**) in DMSO

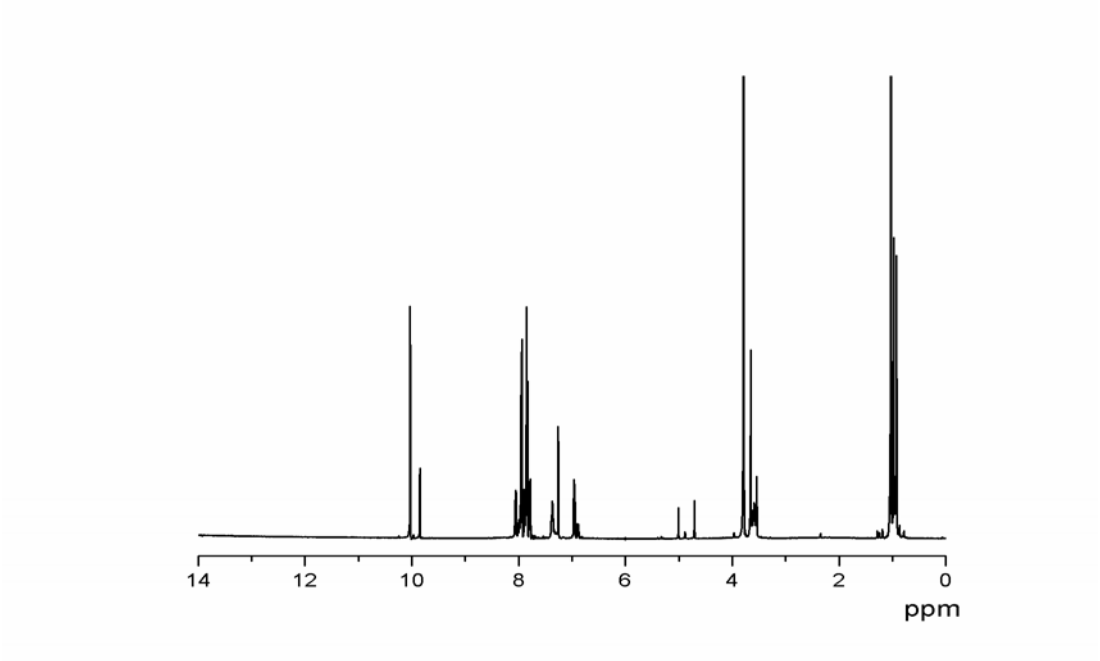

Figure A.2 The ^{1}H-NMR spectrum (400 MHz) of 4-(5,5-dimethyl-1,3,2-dioxaborinan-2-yl)benzaldehyde (**1p**) in DMSO

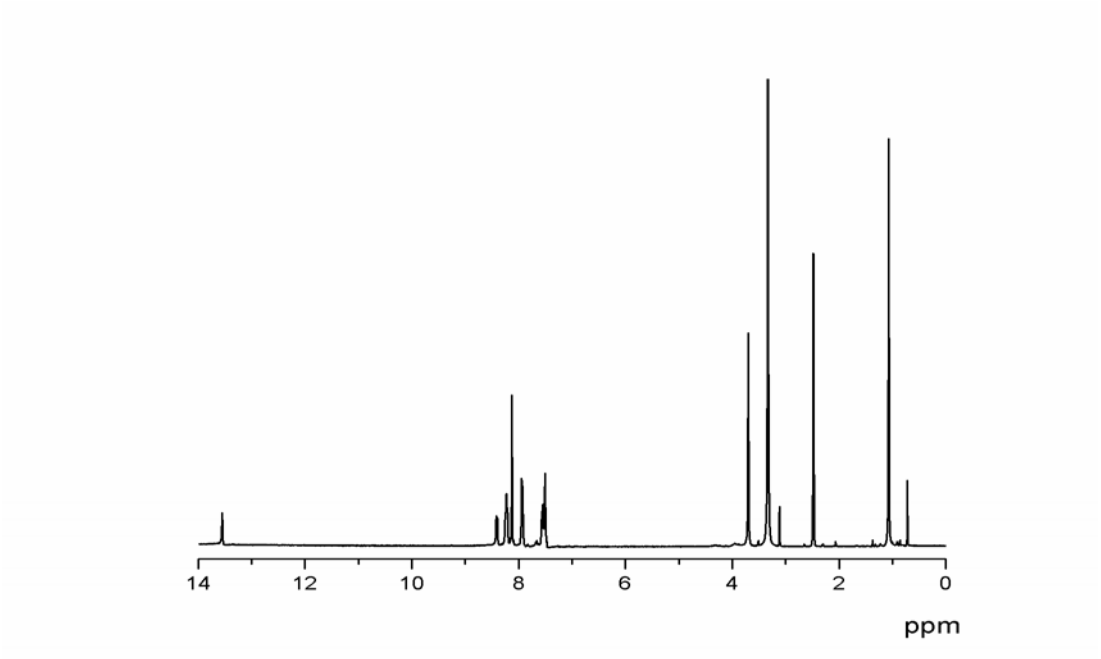

Figure A.3 The ^{1}H-NMR spectrum (400 MHz) of 2-(2-(5,5-dimethyl-1,3,2-dioxaborinan-2-yl) phenyl)-1H-anthra[1,2-d]imidazole-6,11-dione (**2o**) in DMSO

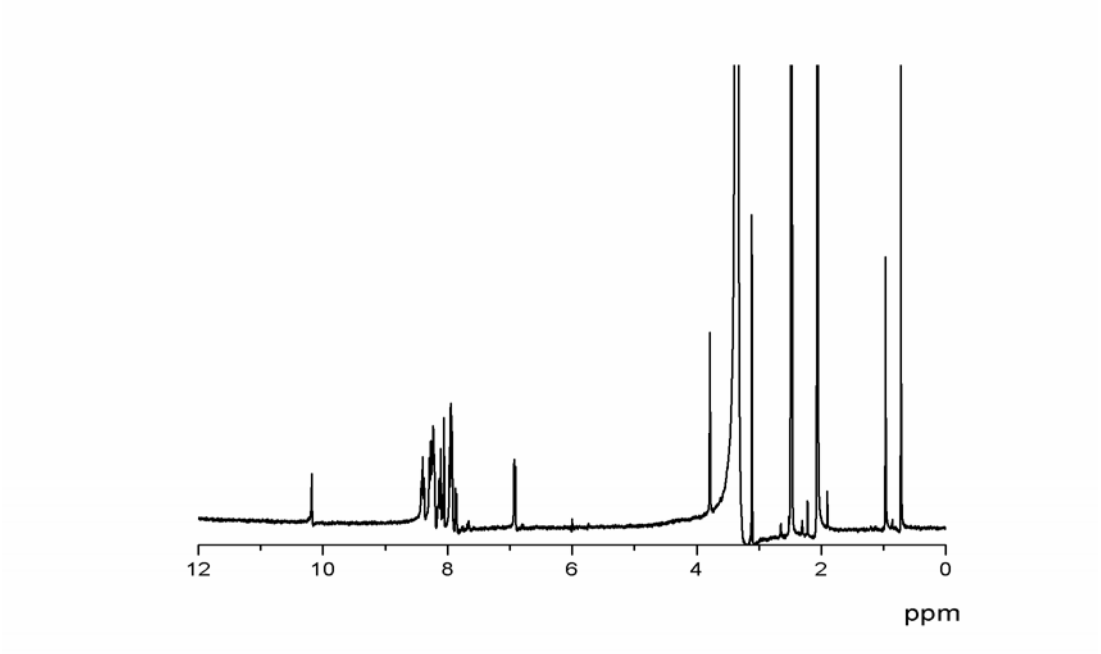

Figure A.4 The ^{1}H-NMR spectrum (400 MHz) of 2-(4-(5,5-dimethyl-1,3,2-dioxaborinan-2-yl) phenyl)-1H-anthra[1,2-d]imidazole-6,11-dione (**2p**) in DMSO

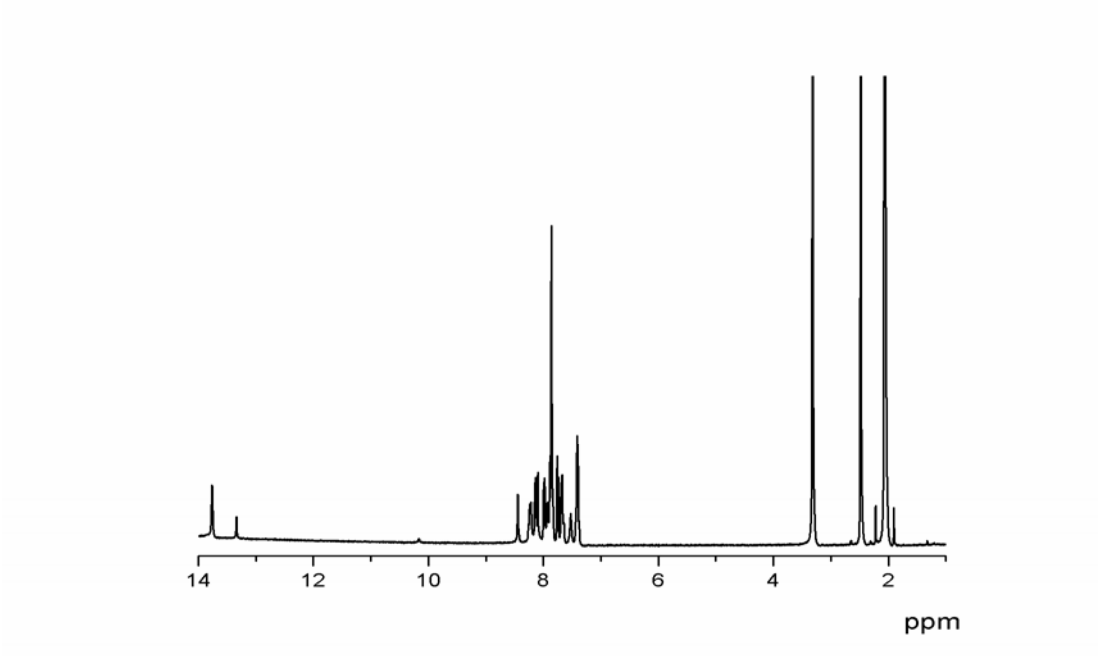

Figure A.5 The ^{1}H-NMR spectrum (400 MHz) of 2-(6,11-dioxo-6,11-dihydro-1H-anthra[1,2-d]imidazol-2-yl)phenylboronic acid (**OB**) in DMSO

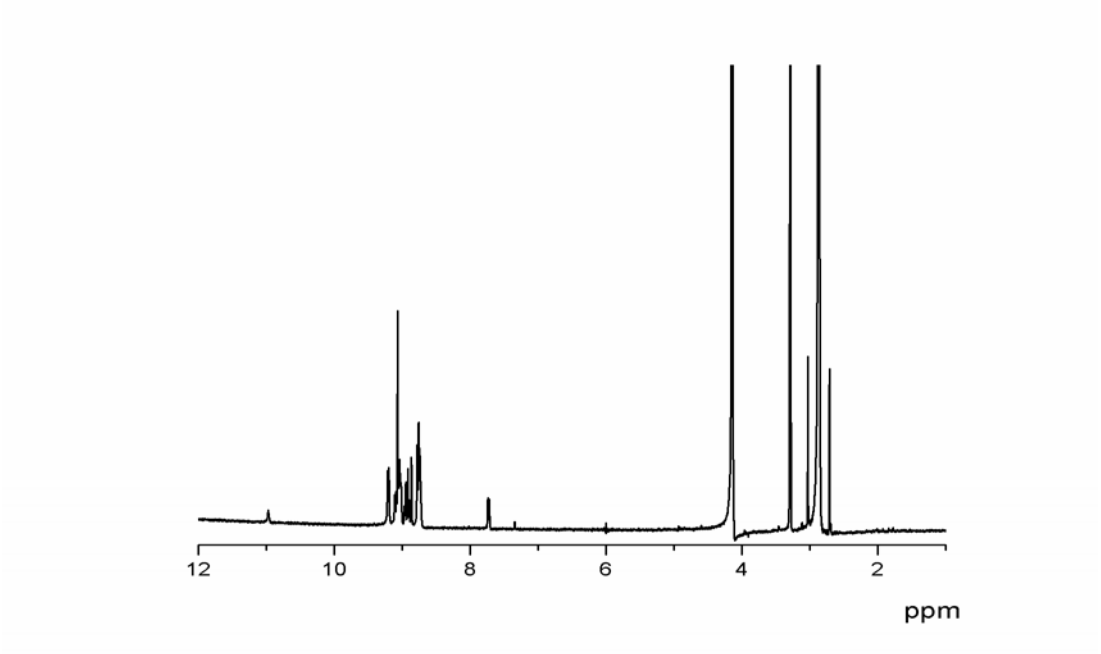

Figure A.6 The ^{1}H-NMR spectrum (400 MHz) of 4-(6,11-dioxo-6,11-dihydro-1H-anthra[1,2-d]imidazol-2-yl)phenylboronic acid (**PB**) in DMSO

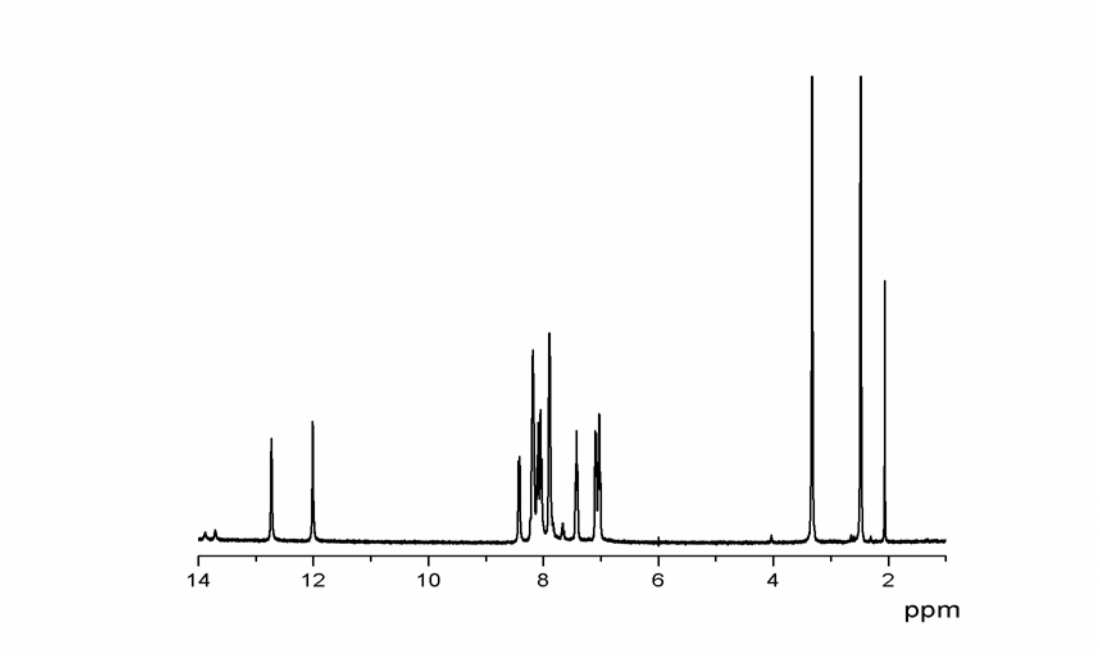

Figure A.7 The ^{1}H-NMR spectrum (400 MHz) of 2-(2-hydroxyphenyl)-3H-anthra[2,1-d]imidazole-6,11-dione (**OO**) in DMSO

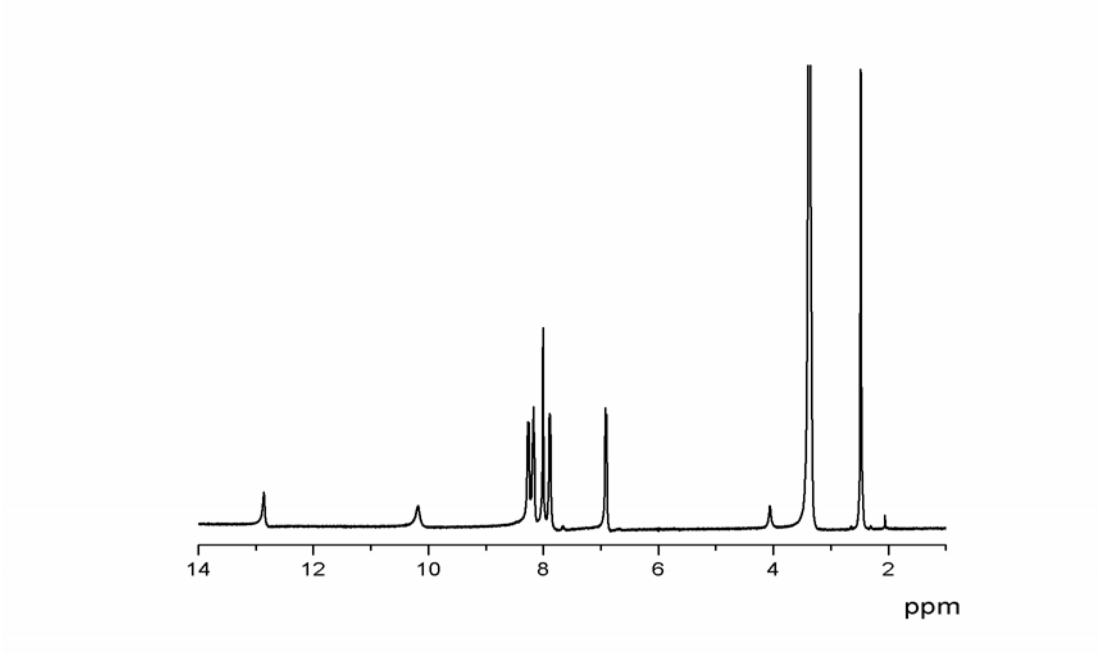

Figure A.8 The ^{1}H-NMR spectrum (400 MHz) of 2-(4-hydroxyphenyl)-3H-anthra[2,1-d]imidazole-6,11-dione (**PO**) in DMSO

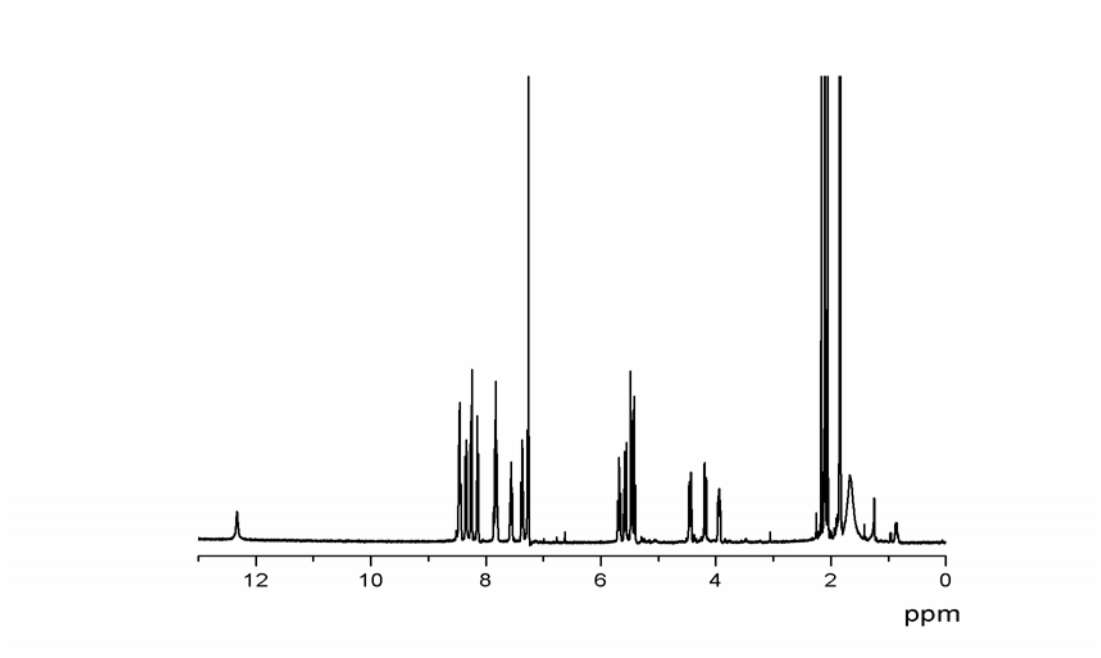

Figure A.9 The ^{1}H-NMR spectrum (400 MHz) of (3R,4S,5S,6S)-2-(acetoxymethyl)-6-(2-(6,11-dioxo-6,11-dihydro-3H-anthra[2,1-d]imidazol-2-yl)phenoxy)-5-hydroxytetrahydro-2H-pyran-3,4-diyl diacetate (**OAPG**) in DMSO

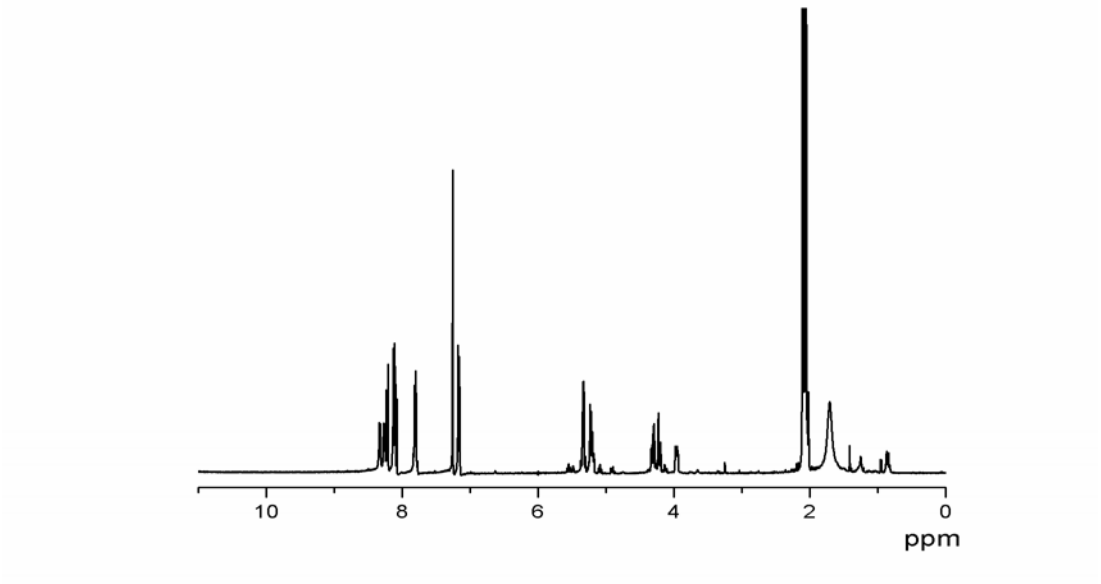

Figure A.10 The ^{1}H-NMR spectrum (400 MHz) of (3R,4S,5S,6S)-2-(acetoxymethyl)-6-(4-(6,11-dioxo-6,11-dihydro-3H-anthra[2,1-d]imidazol-2-yl)phenoxy)-5-hydroxytetrahydro-2H-pyran-3,4-diyl diacetate (**PAPG**) in DMSO

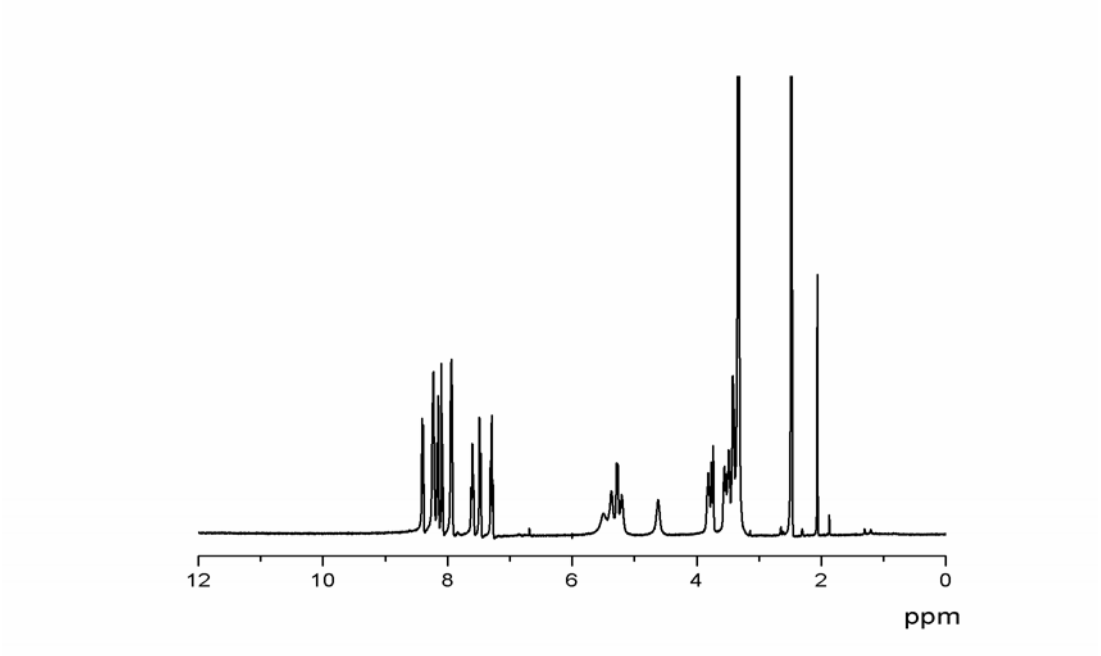

Figure A.11 The ^{1}H-NMR spectrum (400 MHz) of 2-(2-((2S,3S,4R,5S)-3,4,5-trihydroxy-6-(hydroxymethyl)tetrahydro-2H-pyran-2-yloxy)phenyl)-3H-anthra[2,1-d]imidazole-6,11-dione (**OAG**) in DMSO

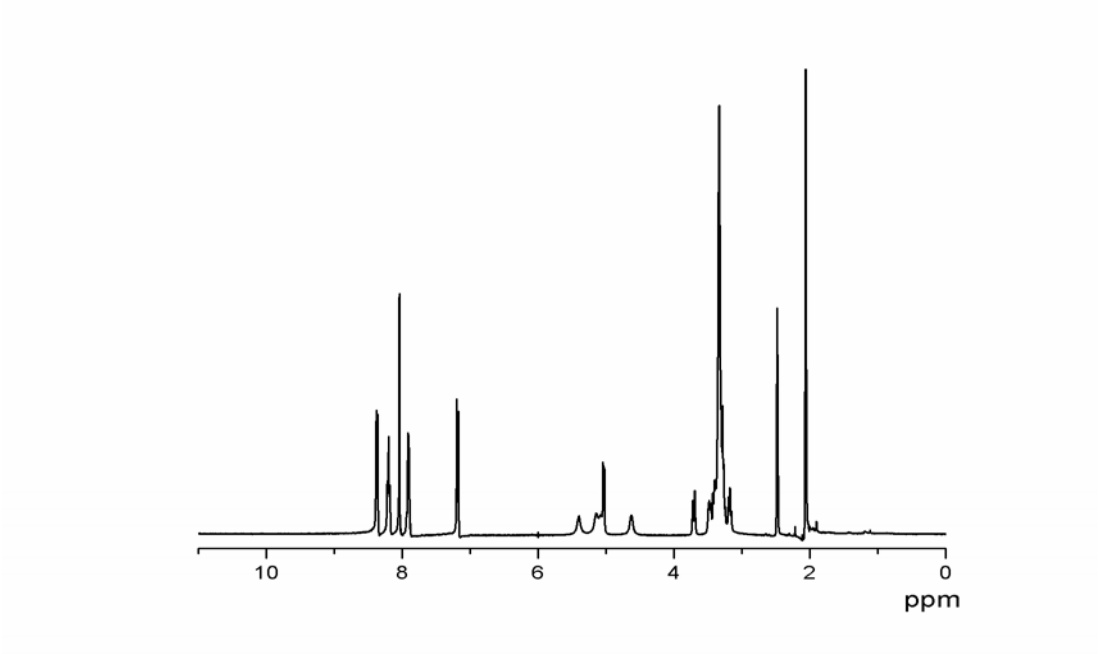

Figure A.12 The ^{1}H-NMR spectrum (400 MHz) of 2-(4-((2S,3S,4R,5S)-3,4,5-trihydroxy-6-(hydroxymethyl)tetrahydro-2H-pyran-2-yloxy)phenyl)-3H-anthra[2,1-d]imidazole-6,11-dione (**PAG**) in DMSO

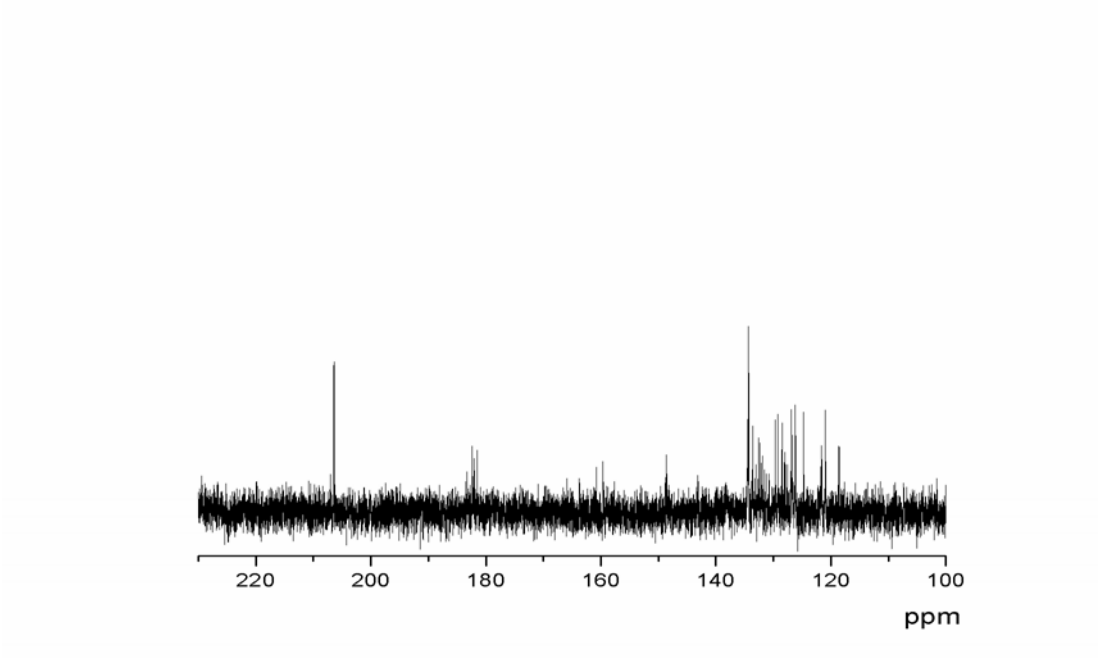

Figure A.13 The ^{13}C-NMR spectrum (106 MHz) of 2-(6,11-dioxo-6,11-dihydro-1H-anthra[1,2-d]imidazol-2-yl)phenylboronic acid (**OB**) in DMSO

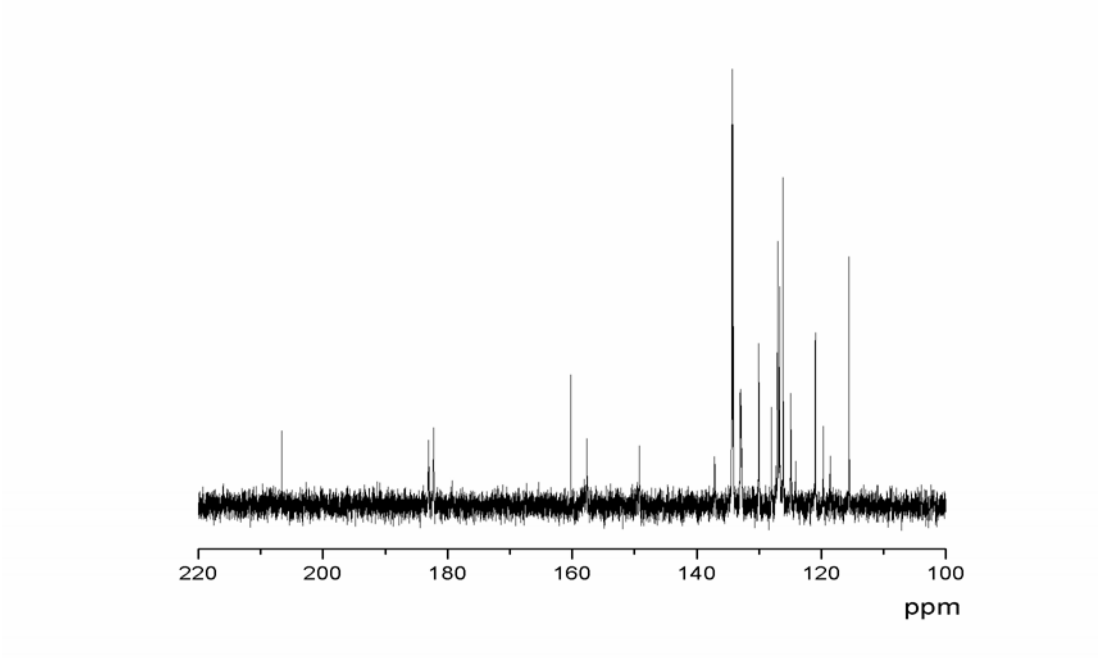

Figure A.14 The ^{13}C-NMR spectrum (106 MHz) of 4-(6,11-dioxo-6,11-dihydro-1H-anthra[1,2-d]imidazol-2-yl)phenylboronic acid (**PB**) in DMSO

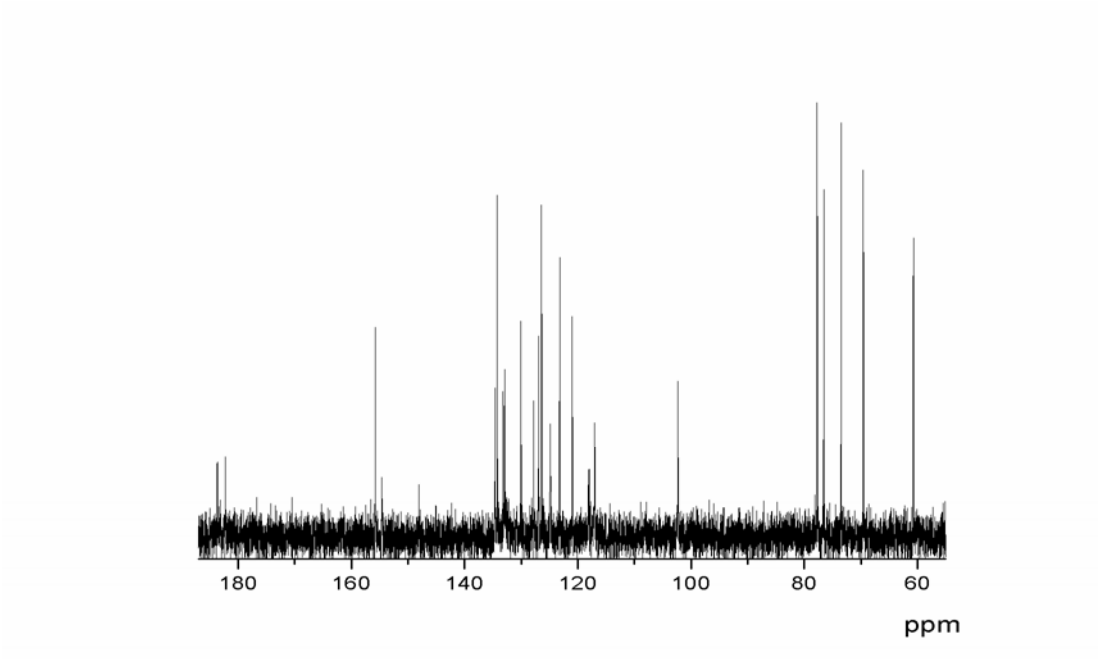

Figure A.15 The ^{13}C-NMR spectrum (106 MHz) of 2-(2-((2S,3S,4R,5S)-3,4,5-trihydroxy-6-(hydroxymethyl)tetrahydro-2H-pyran-2-yloxy)phenyl)-3H-anthra[2,1-d]imidazole-6,11-dione (**OAG**) in DMSO

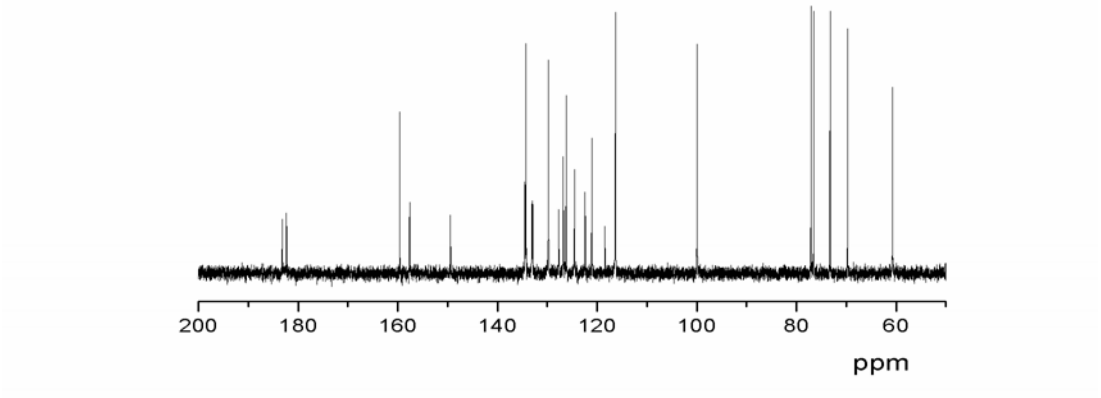

Figure A.16 The ^{13}C-NMR spectrum (106 MHz) of 2-(4-((2S,3S,4R,5S)-3,4,5-trihydroxy-6-(hydroxymethyl)tetrahydro-2H-pyran-2-yloxy)phenyl)-3H-anthra[2,1-d]imidazole-6,11-dione (**PAG**) in DMSO

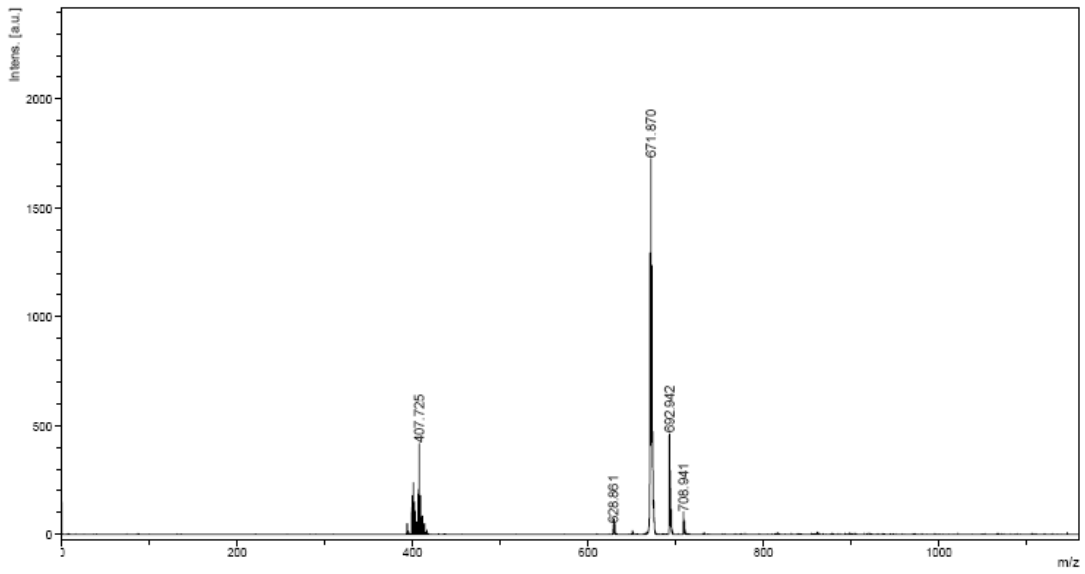

Figure A.17 The mass spectrum (MADI-TOF) of (3R,4S,5S,6S)-2-(acetoxymethyl)-6-(2-(6,11-dioxo-6,11-dihydro-3H-anthra[2,1-d]imidazol-2-yl)phenoxy)-5-hydroxytetrahydro-2H-pyran-3,4-diyl diacetate (**OAPG**)

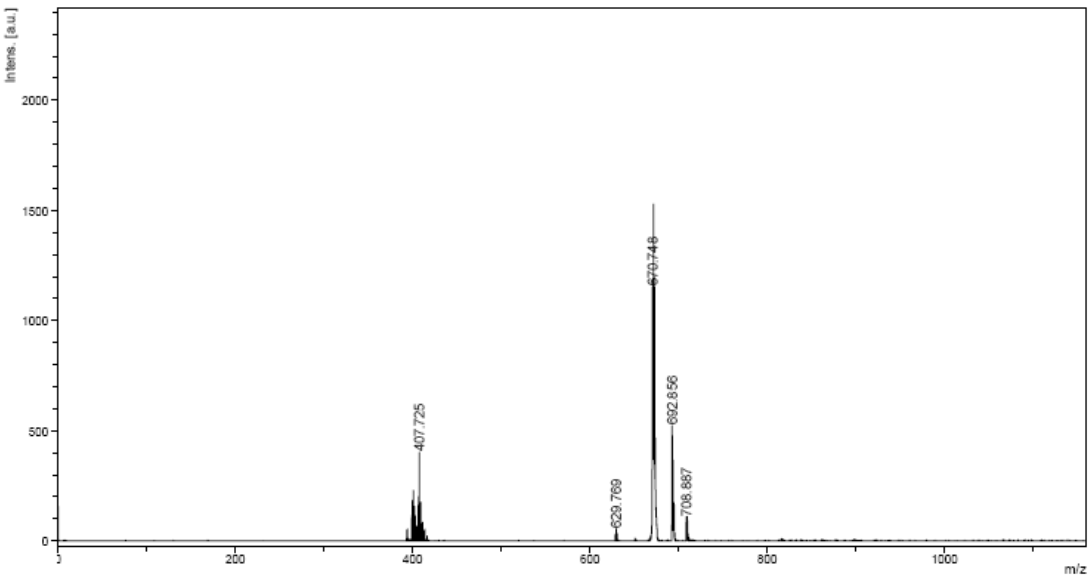

Figure A.18 The mass spectrum (MADI-TOF) of (3R,4S,5S,6S)-2-(acetoxymethyl)-6-(4-(6,11-dioxo-6,11-dihydro-3H-anthra[2,1-d]imidazol-2-yl)phenoxy)-5-hydroxytetrahydro-2H-pyran-3,4-diyl diacetate (**PAPG**)

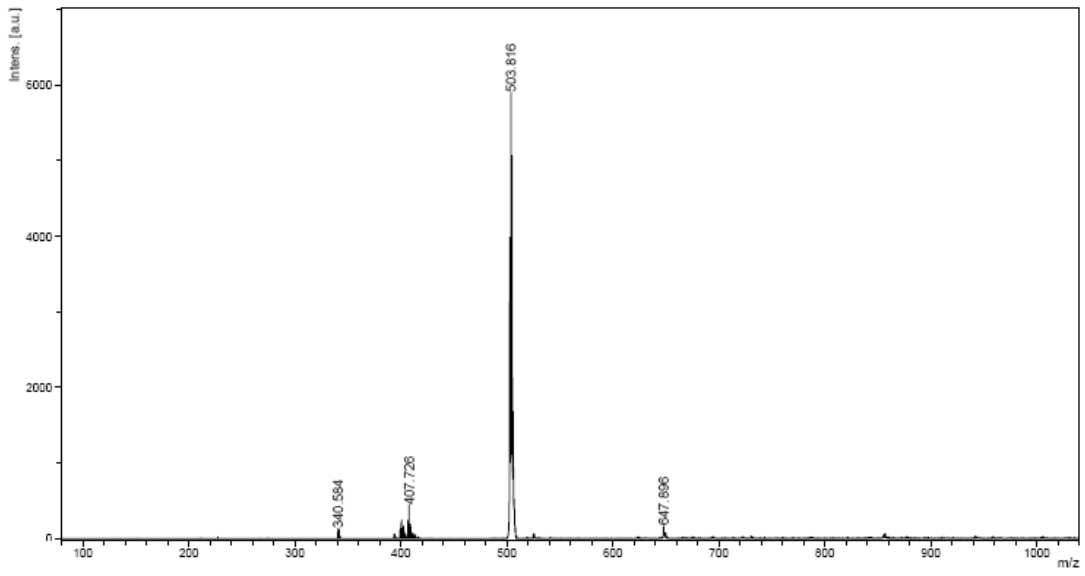

Figure A.19 The mass spectrum (MADI-TOF) of 2-(2-((2S,3S,4R,5S)-3,4,5-trihydroxy-6-(hydroxymethyl)tetrahydro-2H-pyran-2-yloxy)phenyl)-3H-anthra[2,1-d]imidazole-6,11-dione (**OAG**)

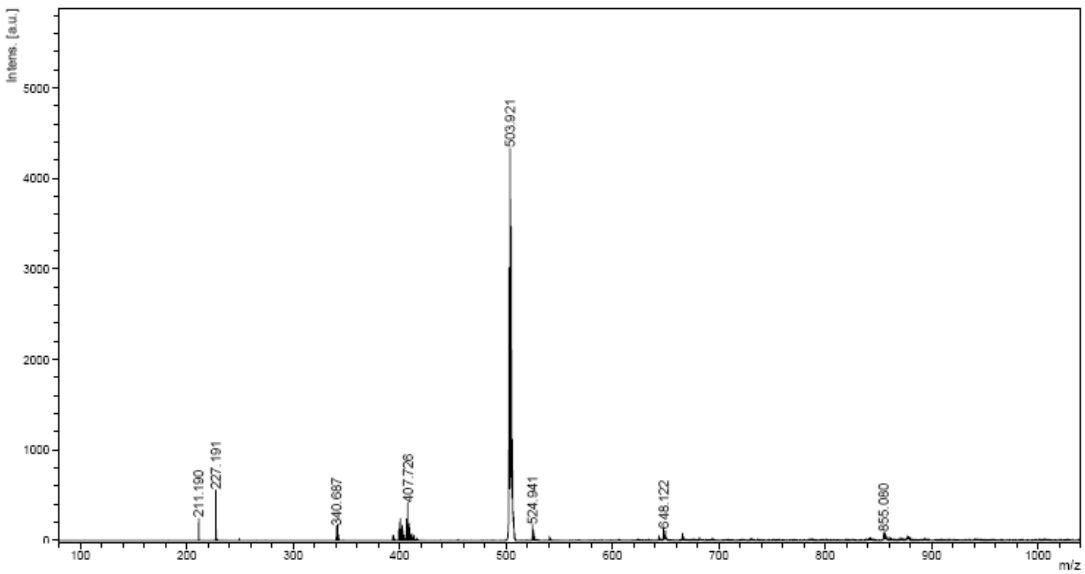

Figure A.20 The mass spectrum (MADI-TOF) of 2-(4-((2S,3S,4R,5S)-3,4,5-trihydroxy-6-(hydroxymethyl)tetrahydro-2H-pyran-2-yloxy)phenyl)-3H-anthra[2,1-d]imidazole-6,11-dione (**PAG**)

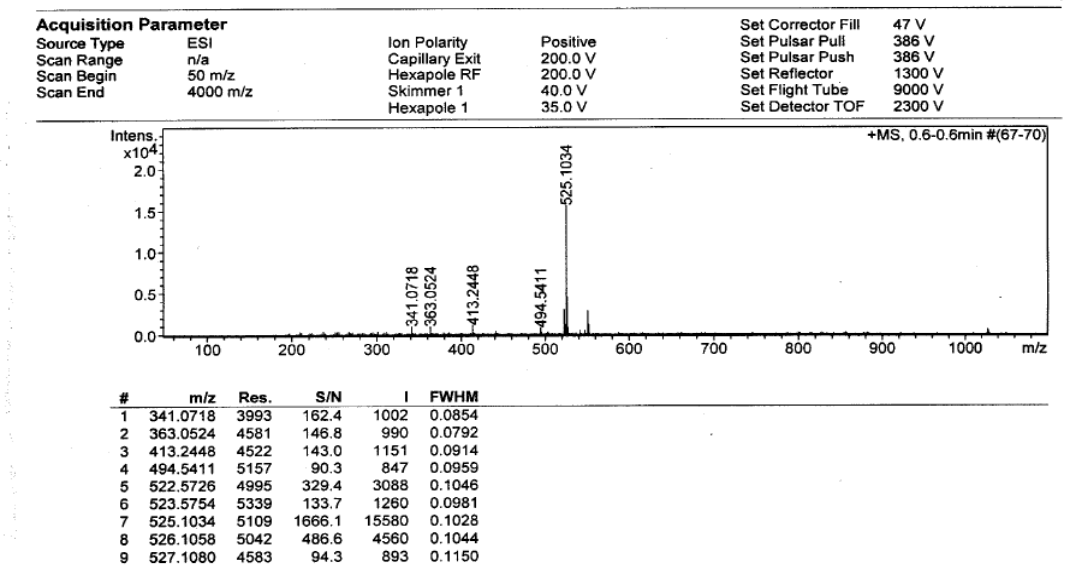

#	m/z	Res.	S/N	I	FWHM
1	341.0718	3993	162.4	1002	0.0854
2	363.0524	4581	146.8	990	0.0792
3	413.2448	4522	143.0	1151	0.0914
4	494.5411	5157	90.3	847	0.0959
5	522.5726	4995	329.4	3088	0.1046
6	523.5754	5339	133.7	1260	0.0981
7	525.1034	5109	1666.1	15580	0.1028
8	526.1058	5042	486.6	4560	0.1044
9	527.1080	4583	94.3	893	0.1150

Figure A.21 The high mass spectrum (ESI) of 2-(2-((2S,3S,4R,5S)-3,4,5-trihydroxy-6-(hydroxymethyl)tetrahydro-2H-pyran-2-yloxy)phenyl)-3H-anthra[2,1-d]imidazole-6,11-dione (**OAG**)

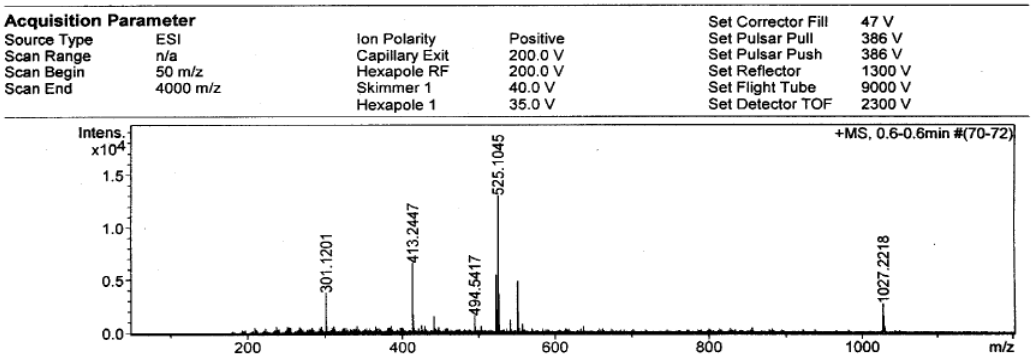

#	m/z	Res.	S/N	I	FWHM
1	301.1201	4928	484.6	3778	0.0611
2	413.2447	4831	529.9	6598	0.0855
3	414.2483	5203	136.9	1718	0.0796
4	494.5417	5116	112.3	1627	0.0967
5	522.5738	4974	380.4	5469	0.1051
6	523.5758	5095	147.8	2137	0.1028
7	525.1045	5131	908.5	13037	0.1023
8	526.1073	4943	255.1	3674	0.1064
9	1027.2218	4546	250.1	2727	0.2259
10	1028.2167	4561	145.5	1597	0.2254

Figure A.22 The high mass spectrum (ESI) of 2-(4-((2S,3S,4R,5S)-3,4,5-trihydroxy-6-(hydroxymethyl)tetrahydro-2H-pyran-2-yloxy)phenyl)-3H-anthra[2,1-d]imidazole-6,11-dione (**PAG**)

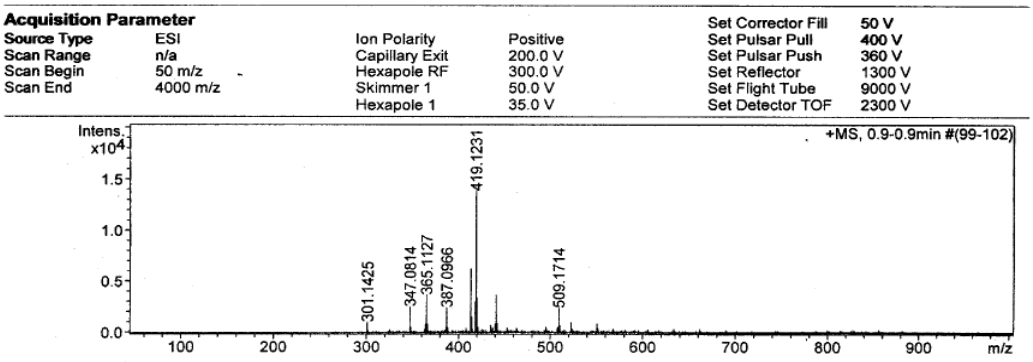

#	m/z	Res.	S/N	I	FWHM
1	301.1425	4505	196.8	1014	0.0669
2	347.0814	4681	372.9	2505	0.0741
3	364.1114	4094	115.4	845	0.0889
4	365.1127	4451	503.9	3694	0.0820
5	366.1180	4409	111.3	823	0.0830
6	387.0966	4508	299.3	2421	0.0859
7	413.2713	4727	695.1	6238	0.0874
8	414.2750	4704	169.8	1535	0.0881
9	418.1262	4558	329.2	3013	0.0917
10	419.1231	4650	1511.7	13862	0.0901
11	420.1262	4677	366.1	3374	0.0898
12	509.1714	4477	244.4	2382	0.1137

Figure A.23 The high mass spectrum (ESI) of 2-(6,11-dioxo-6,11-dihydro-1H-anthra[1,2-d]imidazol-2-yl)phenylboronic acid (**OB**)

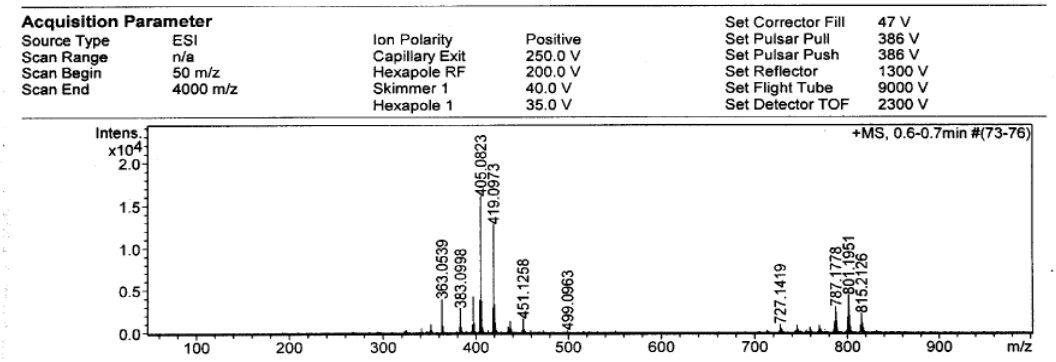

#	m/z	Res.	S/N	I	FWHM
1	351.0729	4648	202.7	1047	0.0755
2	363.0539	4805	732.0	3972	0.0756
3	364.0599	4453	152.7	834	0.0818
4	383.0998	4899	492.2	2892	0.0782
5	396.1185	4626	165.7	1024	0.0856
6	397.1163	4684	689.4	4266	0.0848
7	398.1206	4968	182.9	1138	0.0801
8	404.0867	4785	609.1	3864	0.0845
9	405.0823	4696	2535.6	16131	0.0863
10	406.0852	4696	588.5	3760	0.0865
11	418.1009	5023	447.1	2977	0.0832
12	419.0973	4807	1919.2	12810	0.0872
13	420.1006	4719	499.4	3347	0.0890
14	421.0863	3316	173.4	1168	0.1270

Figure A.24 The high mass spectrum (ESI) of 4-(6,11-dioxo-6,11-dihydro-1H-anthra[1,2-d]imidazol-2-yl)phenylboronic acid (**PB**)

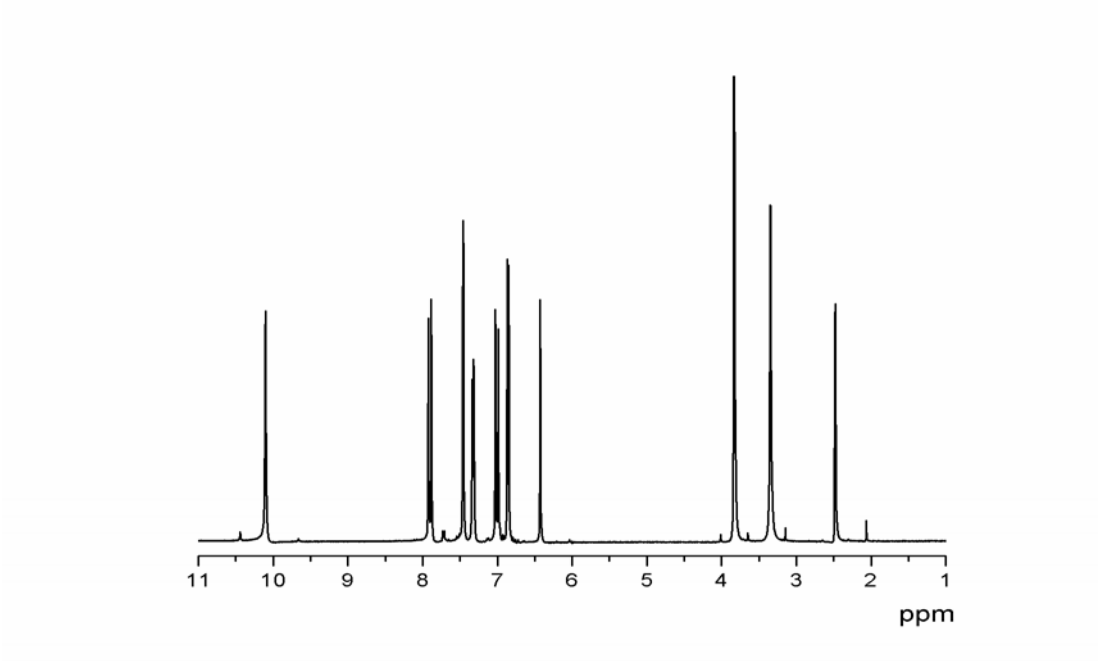

Figure A.25 The ^{1}H-NMR spectrum (400 MHz) of difluoroboron curcumin derivatives (**CURBF**) in DMSO

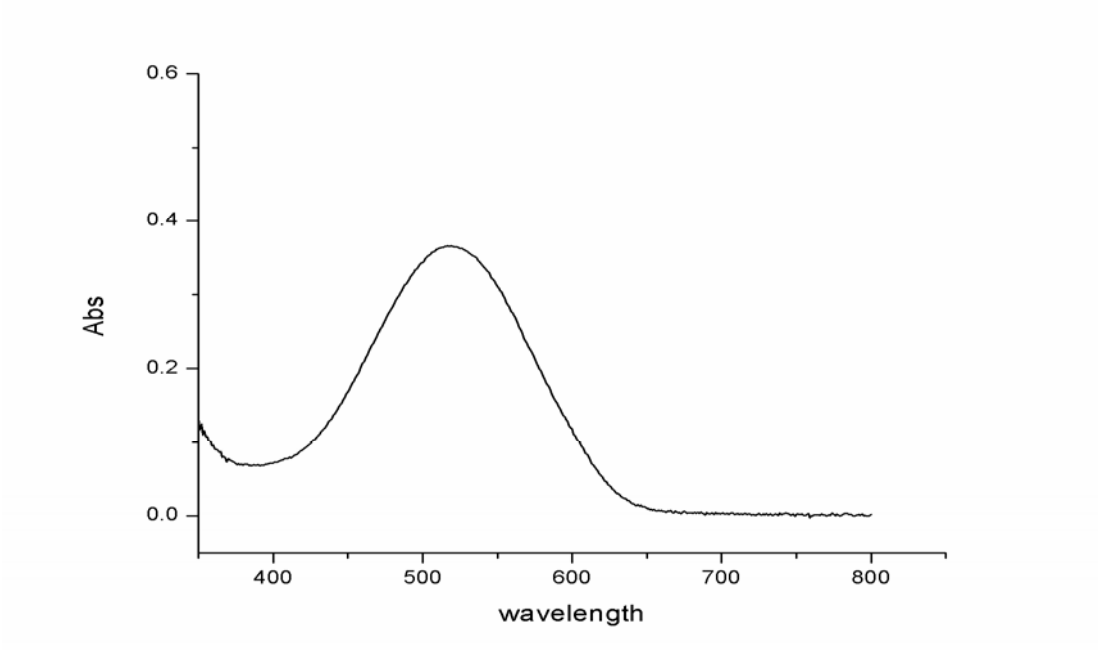

Figure A.26 The UV/Vis spectrum of 1,2-diamino-1,4-anthraquinone $1x10^{-5}$ M in 0.1M HEPES buffer pH 7.4, 10% DMSO in aqueous solution.

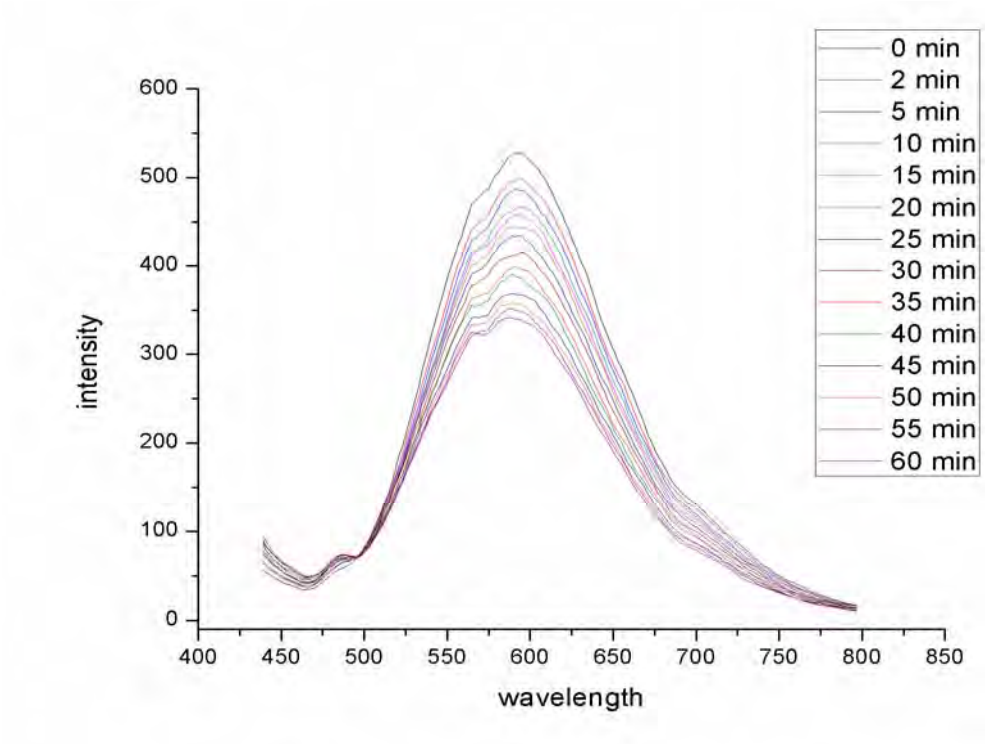

Figure A.27 The fluorescence spectra of kinetic studies of **OB** at 0.2 mM glucose in enzymatic probe system.

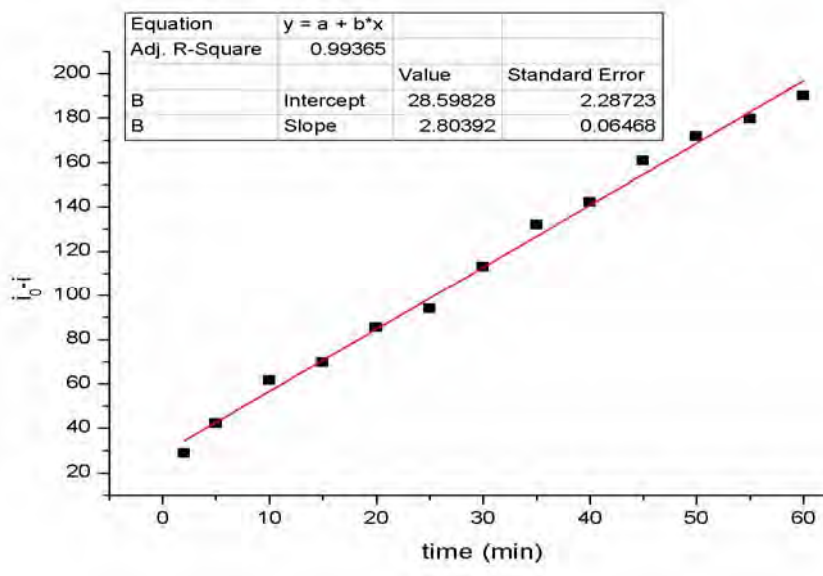

Figure A.28 The emission response against time of kinetic studies of **OB** at 0.2 mM glucose at 593 nm in enzymatic probe system.

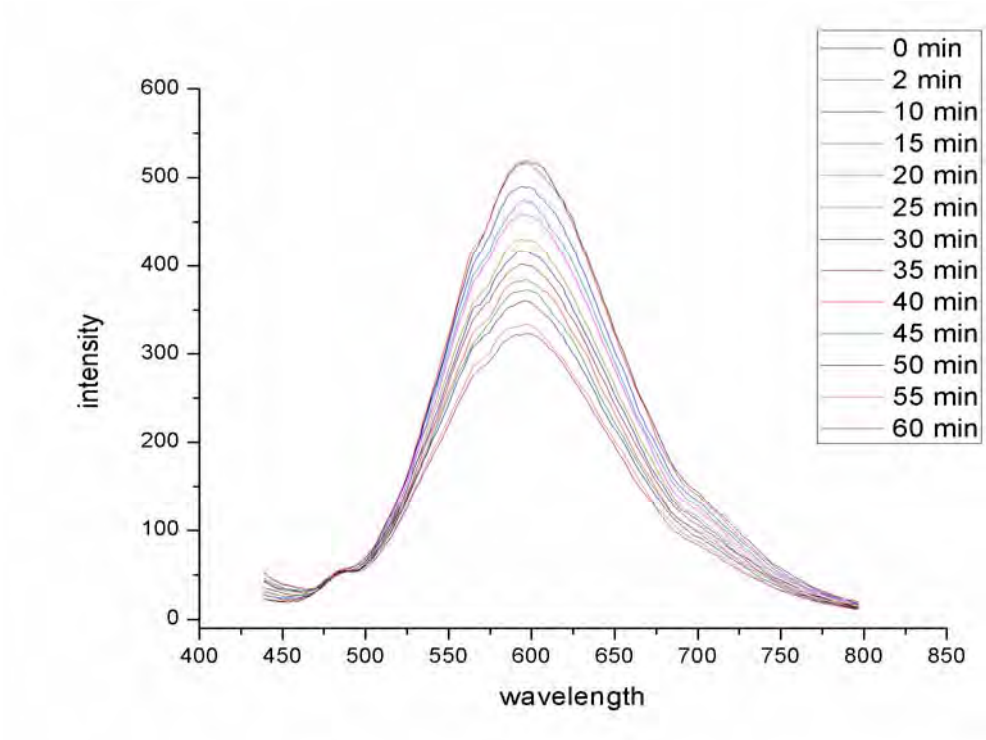

Figure A.29 The fluorescence spectra of kinetic studies of **OB** at 0.3 mM glucose in enzymatic probe system.

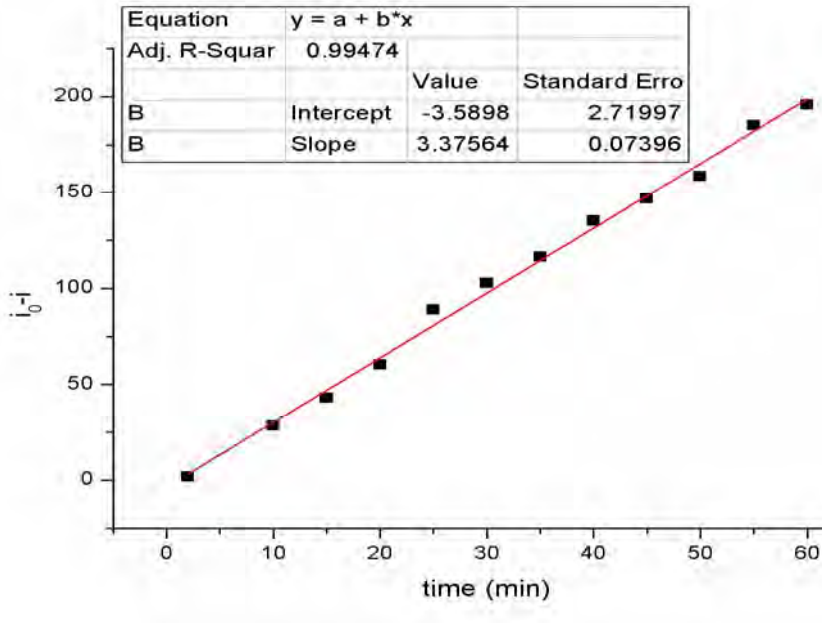

Figure A.30 The emission response against time of kinetic studies of **OB** at 0.3 mM glucose at 593 nm in enzymatic probe system.

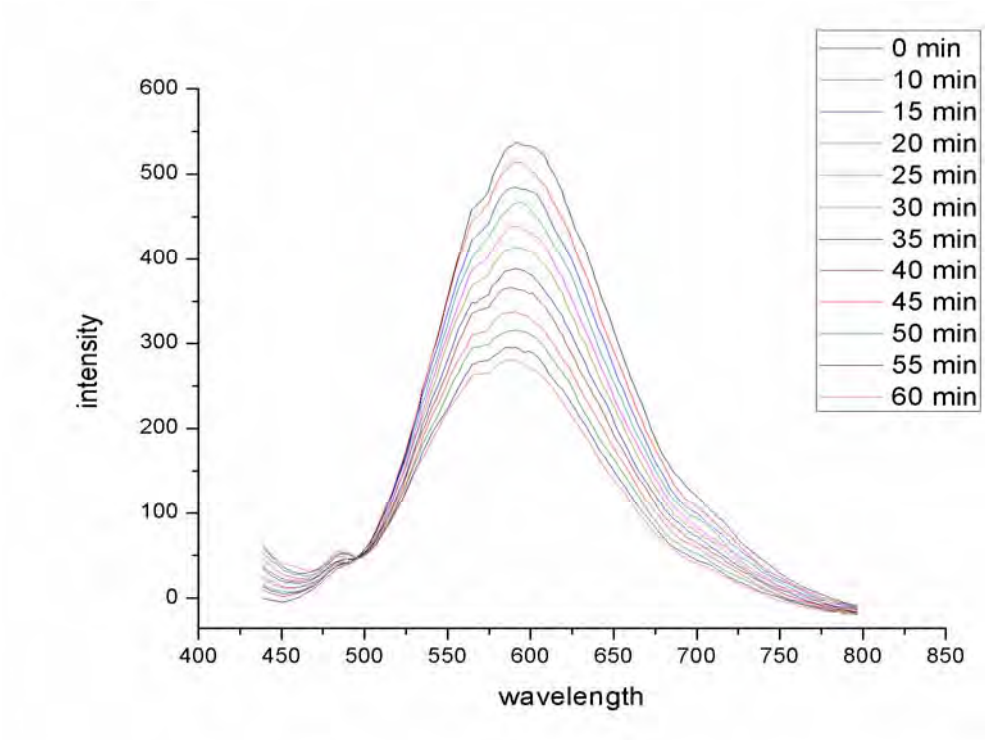

Figure A.31 The fluorescence spectra of kinetic studies of **OB** at 0.7 mM glucose in enzymatic probe system.

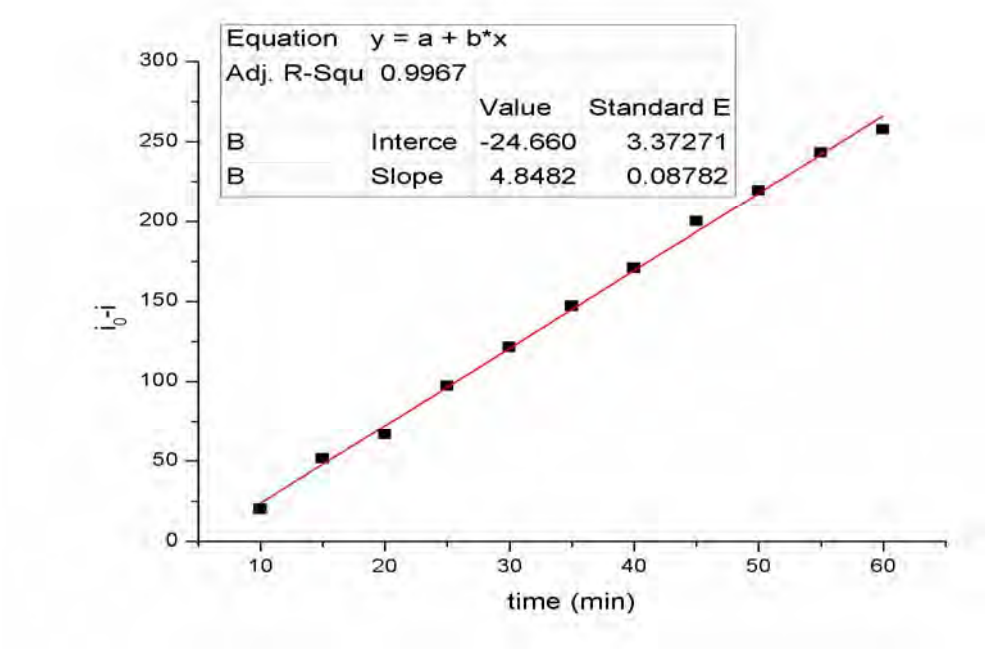

Figure A.32 The emission response against time of kinetic studies of **OB** at 0.7 mM glucose at 593 nm in enzymatic probe system.

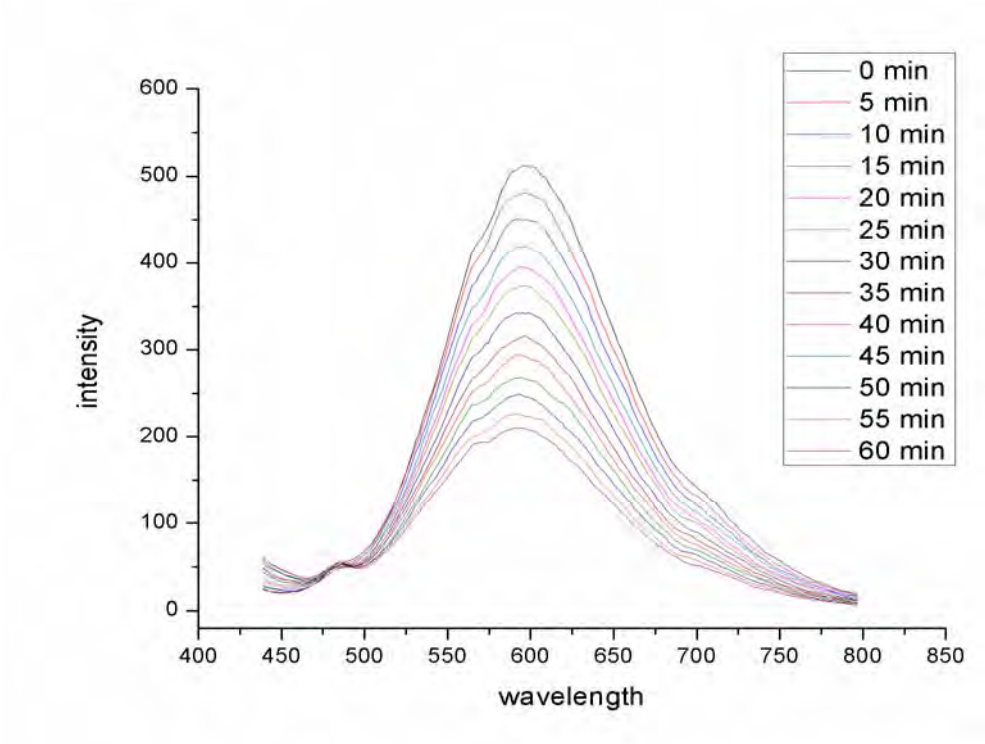

Figure A.33 The fluorescence spectra of kinetic studies of **OB** at 1.0 mM glucose in enzymatic probe system.

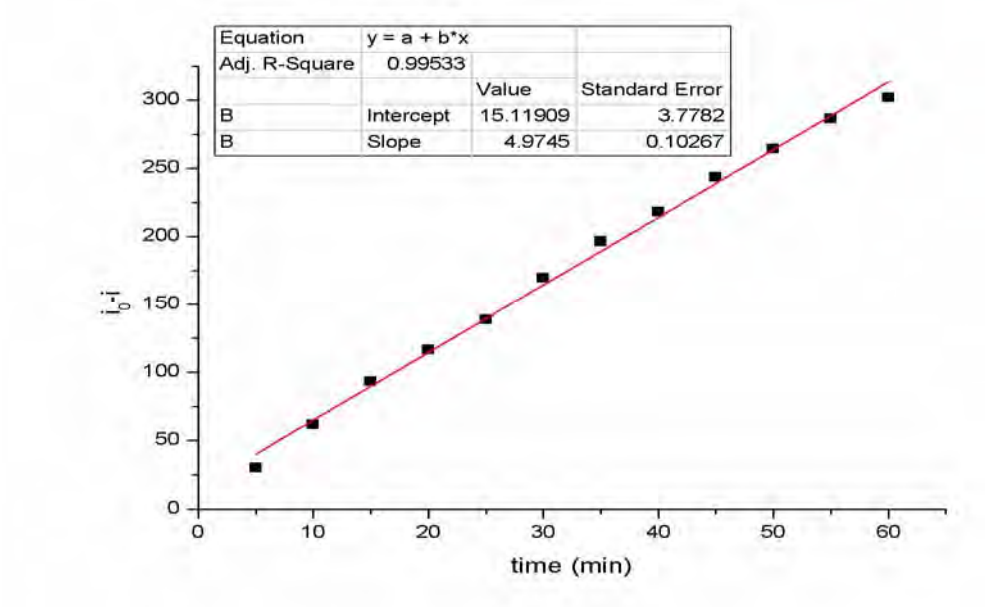

Figure A.34 The emission response against time of kinetic studies of **OB** at 1.0 mM glucose at 593 nm in enzymatic probe system.

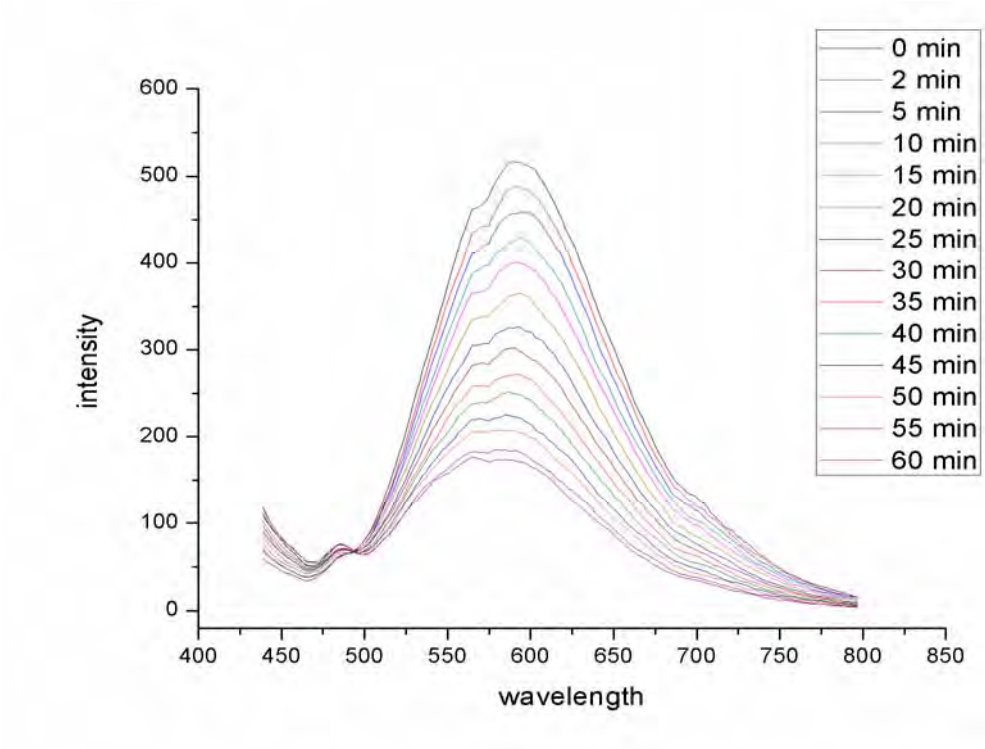

Figure A.35 The fluorescence spectra of kinetic studies of **OB** at 1.4 mM glucose in enzymatic probe system.

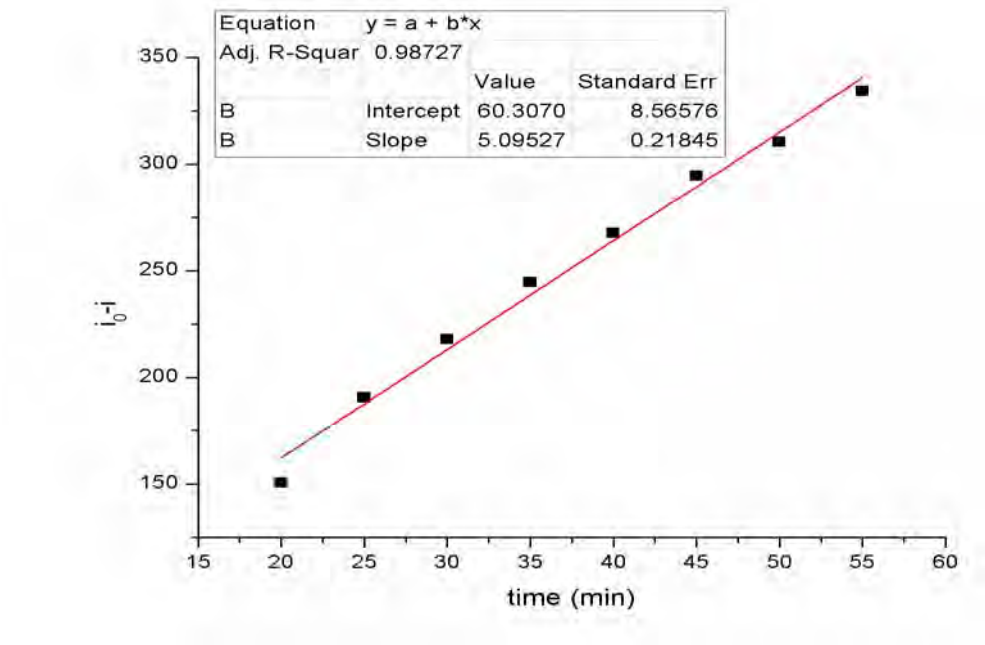

Figure A.36 The emission response against time of kinetic studies of **OB** at 1.4 mM glucose at 593 nm in enzymatic probe system.

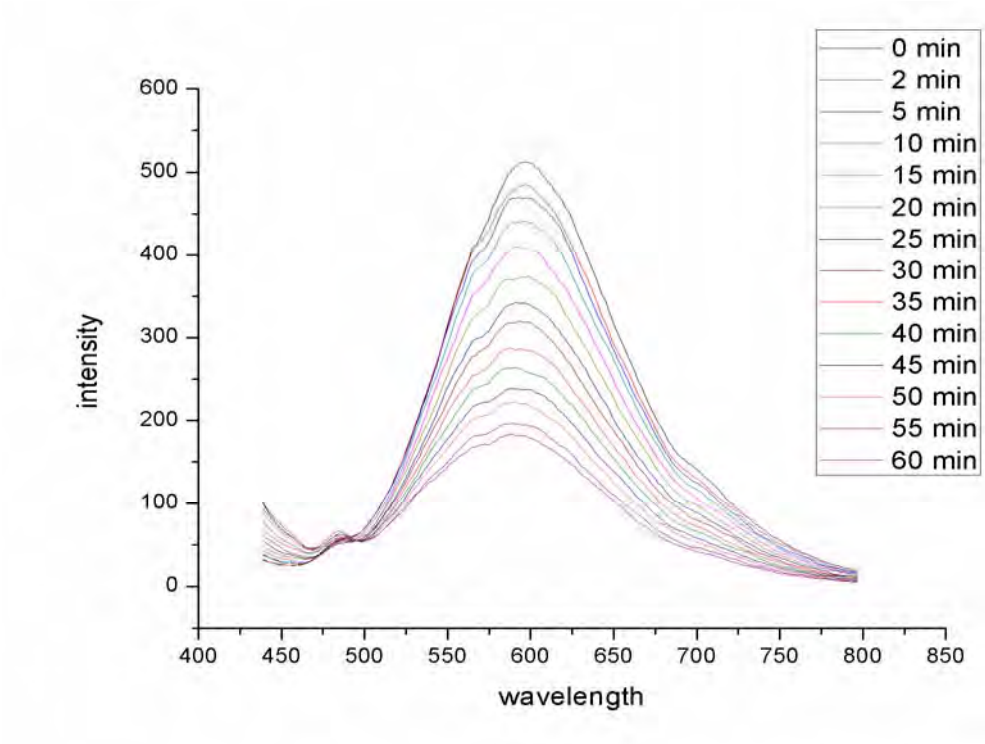

Figure A.37 The fluorescence spectra of kinetic studies of **OB** at 2.0 mM glucose in enzymatic probe system.

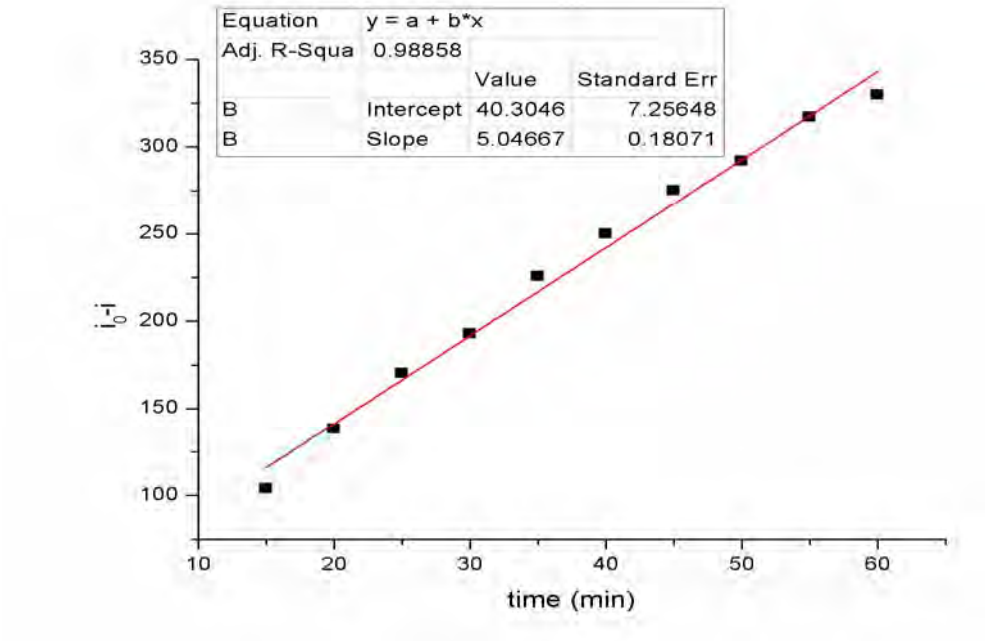

Figure A.38 The emission response against time of kinetic studies of **OB** at 2.0 mM glucose at 593 nm in enzymatic probe system.

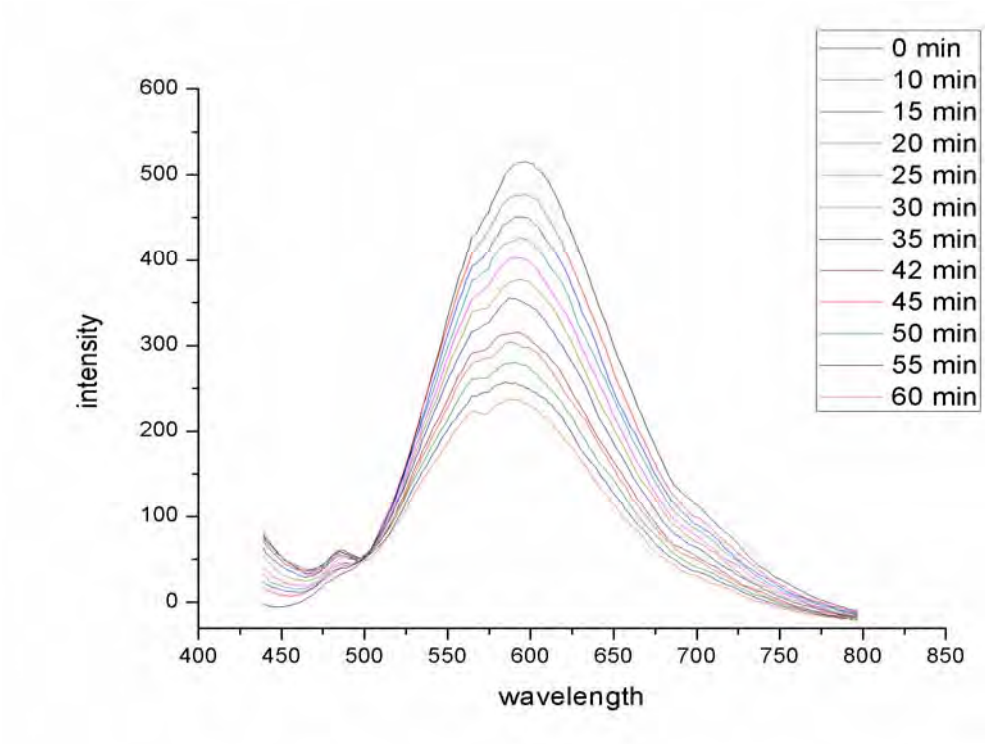

Figure A.39 The fluorescence spectra of kinetic studies of **OB** at 3.0 mM glucose in enzymatic probe system.

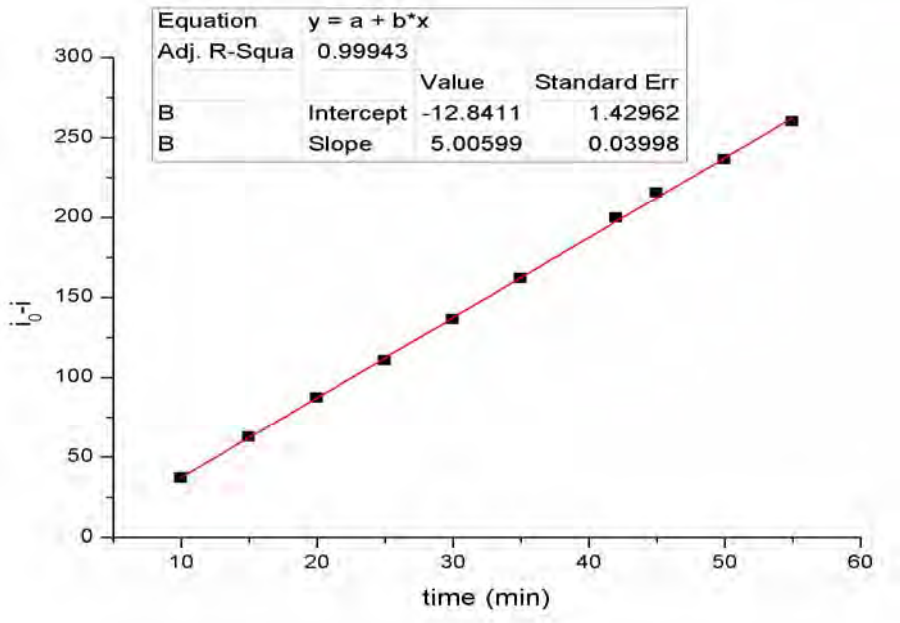

Figure A.40 The emission response against time of kinetic studies of **OB** at 3.0 mM glucose at 593 nm in enzymatic probe system.

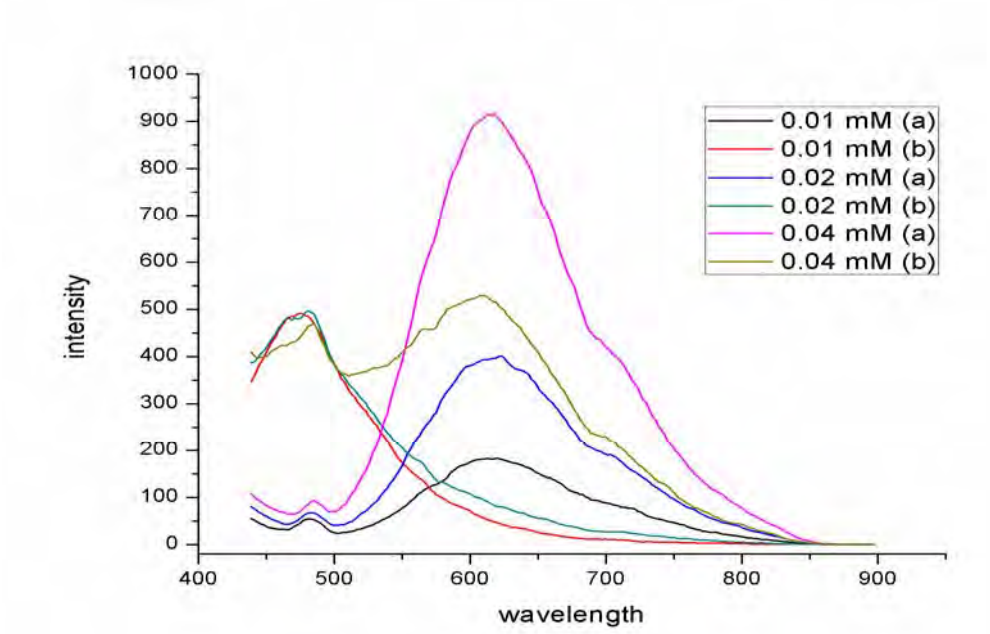

Figure A.41 The fluorescence spectra of various concentrations **PAG** in enzymatic probe system (a) before enzyme adding (b) after added 5 minutes

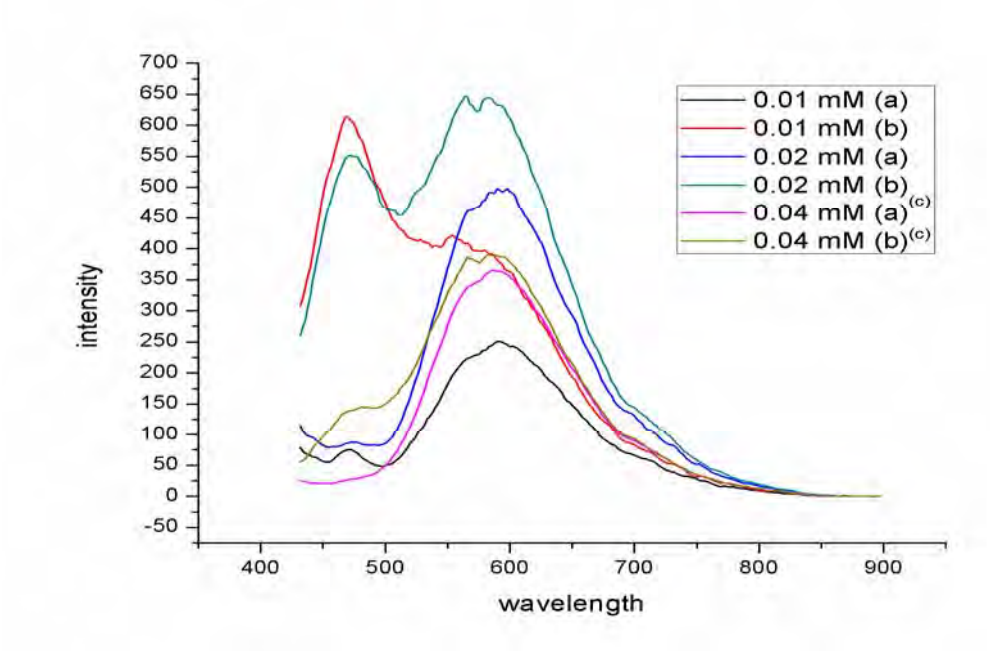

Figure A.42 The fluorescence spectra of various concentrations **OAG** in enzymatic probe system (a) before enzyme adding (b) after added 5 minutes (c) fluorescent measurement at PMT 700

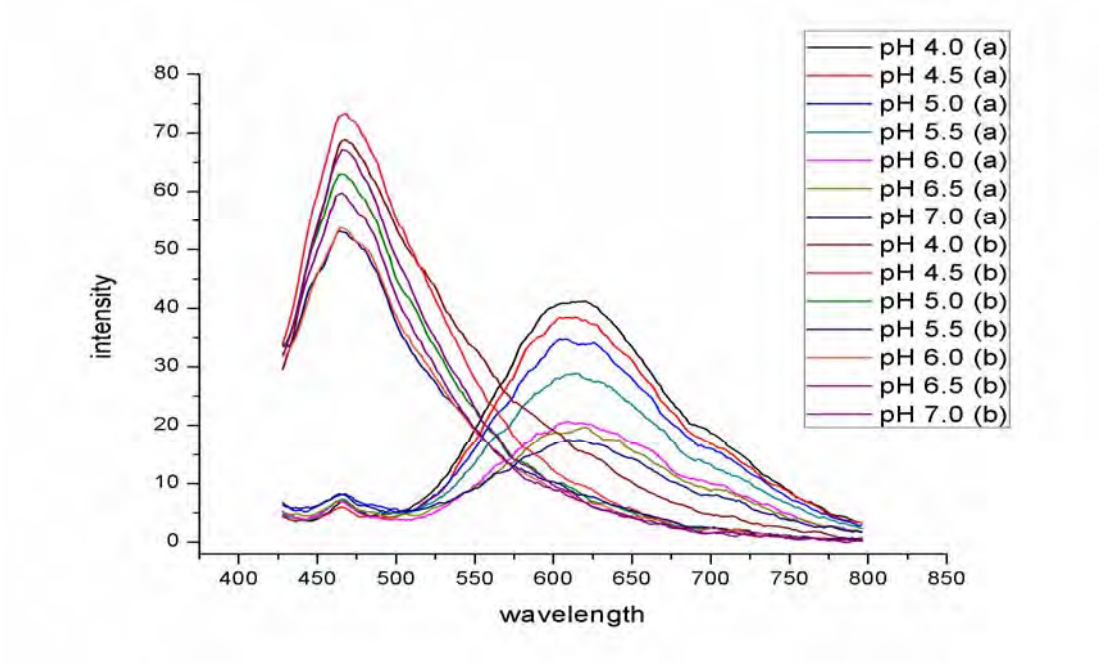

Figure A.43 The fluorescence spectra of **PAG** with various pH in enzymatic probe system (a) before enzyme adding (b) after added 5 minutes

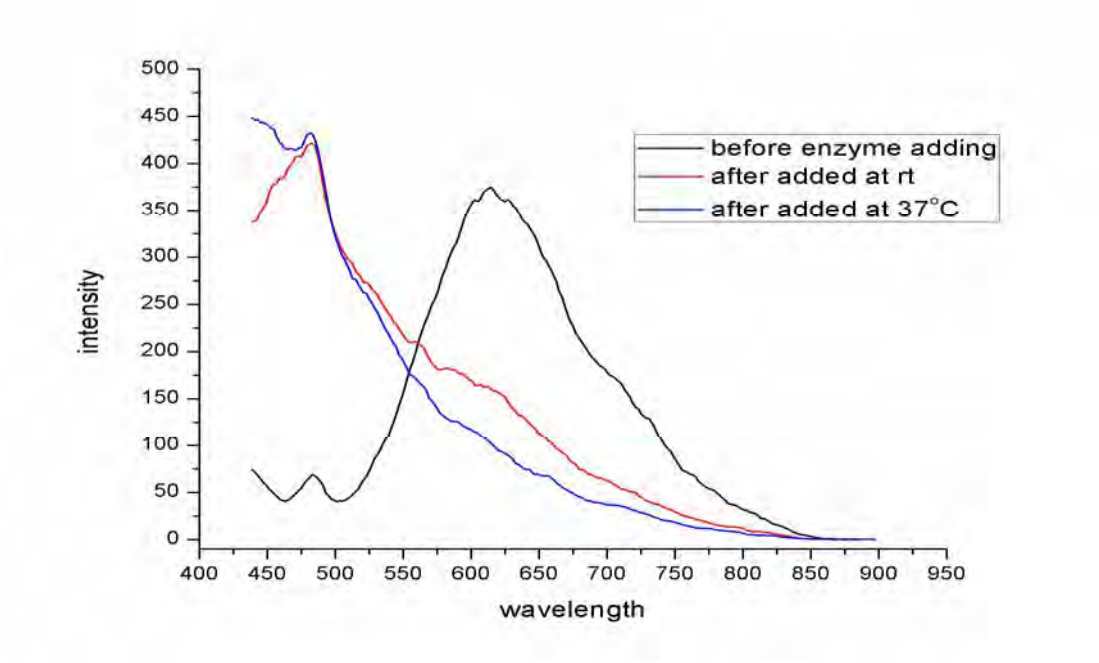

Figure A.44 The fluorescence spectra of **PAG** in various temperatures in enzymatic probe system

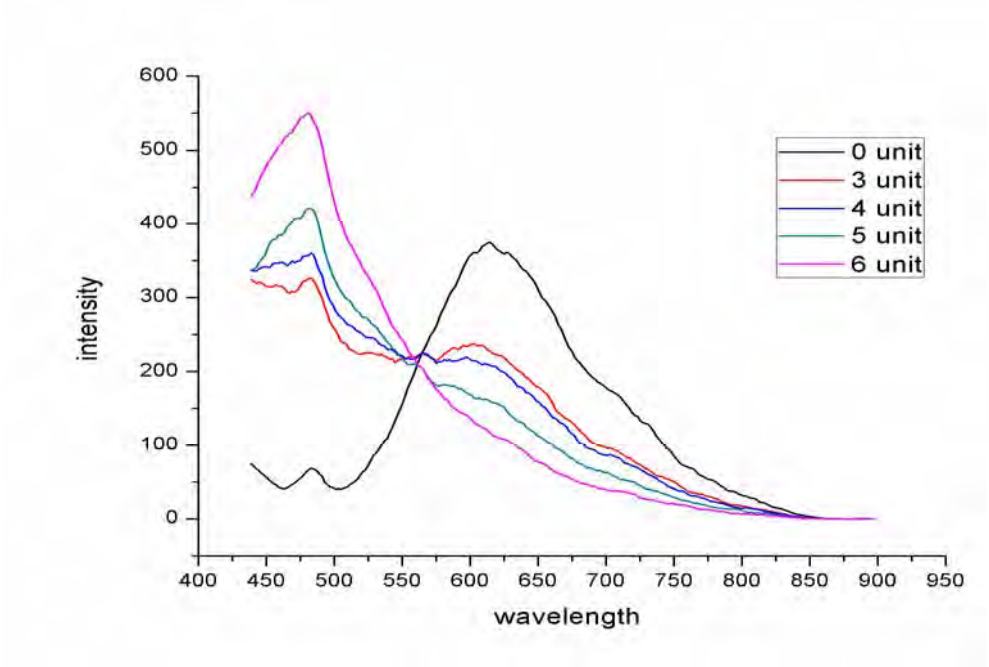

Figure A.45 The fluorescence spectra of **PAG** with various unit of *β*-glucosidase in enzymatic probe system

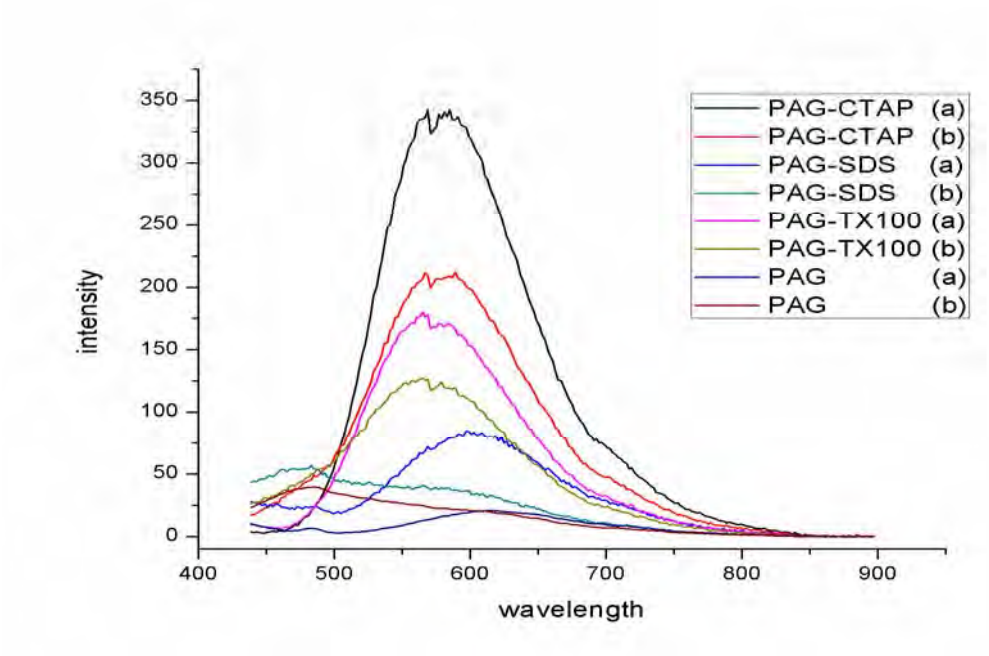

Figure A.46 The fluorescence spectra of **PAG** in enzymatic probe in various micelle systems. (a) before enzyme adding (b) after added 5 minutes

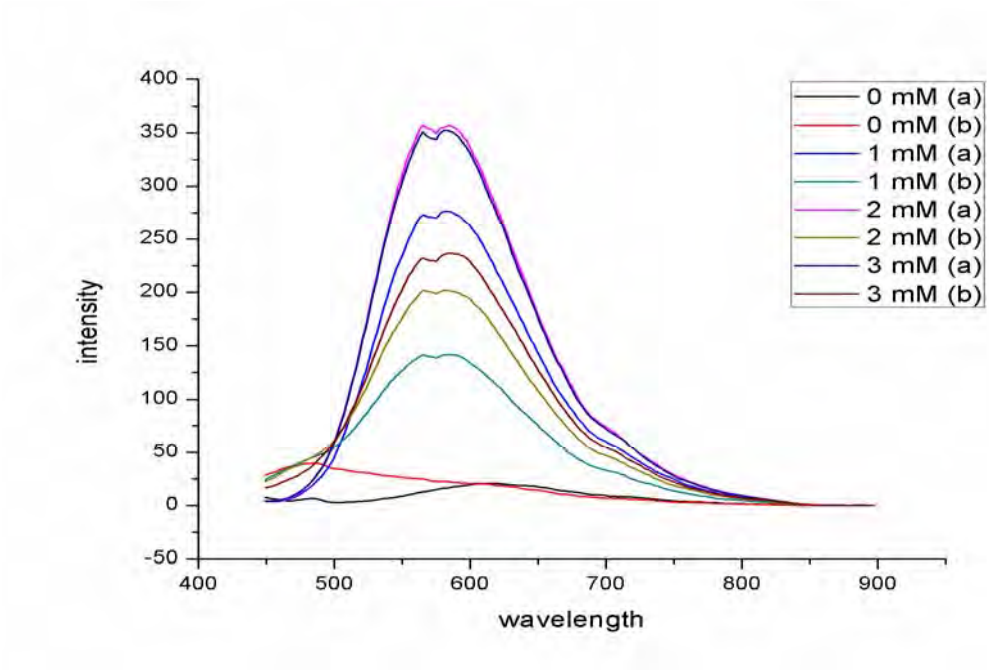

Figure A.47 The fluorescence spectra of **PAG** in enzymatic probe in various concentrations CTAB. (a) before enzyme adding (b) after added 5 minutes

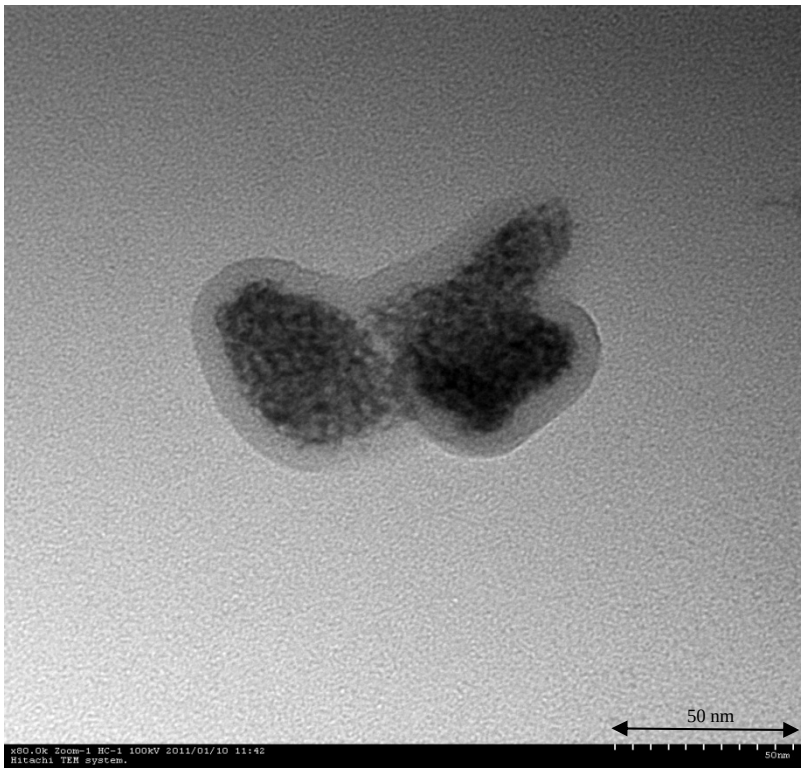

Figure A.48 The close-up TEM micrograph of sample SDS/Tb^{3+}

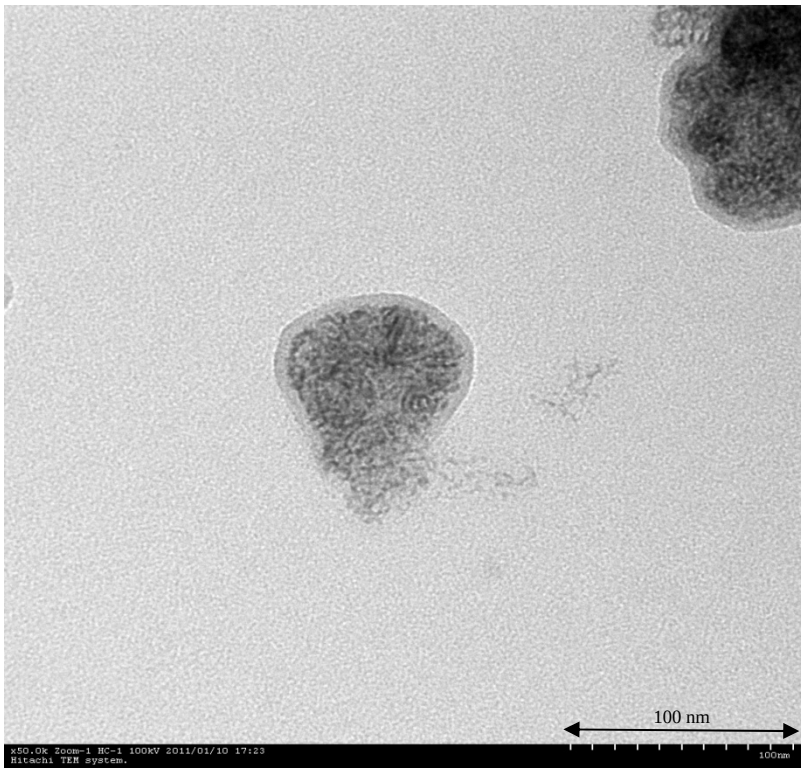

Figure A.49 The close-up TEM micrograph of sample SDS/Gd^{3+}

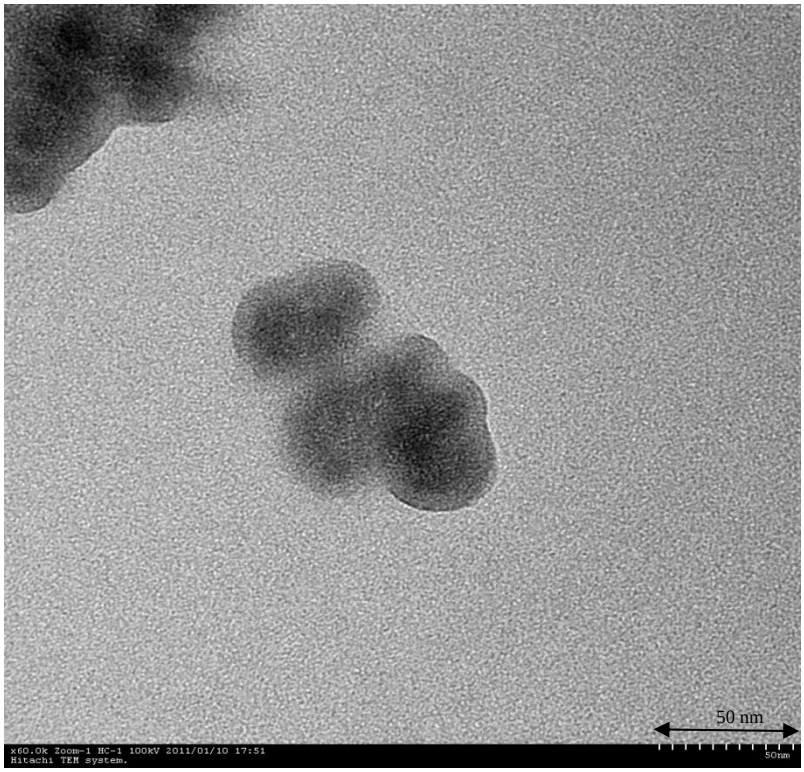

Figure A.50 The close-up TEM micrograph of sample SDS/La^{3+}

VITA

Mr. Krittithi Wannajuk was born on February 28, 1986 in Bangkok, Thailand. He received his Bachelor degree of science in chemistry from Chulalongkorn University in 2008. Since 2008, he has been a graduate student at the Department of Chemistry, Chulalongkorn University and become a member of Supramolecular Chemistry Research Unit under the supervision of Assistant Professor Dr. Boosayarat Tomapatanaget. He finished his Master's degree of Science in the academic year 2010.